Flexible Manufacture of Lightweight Frame Structures

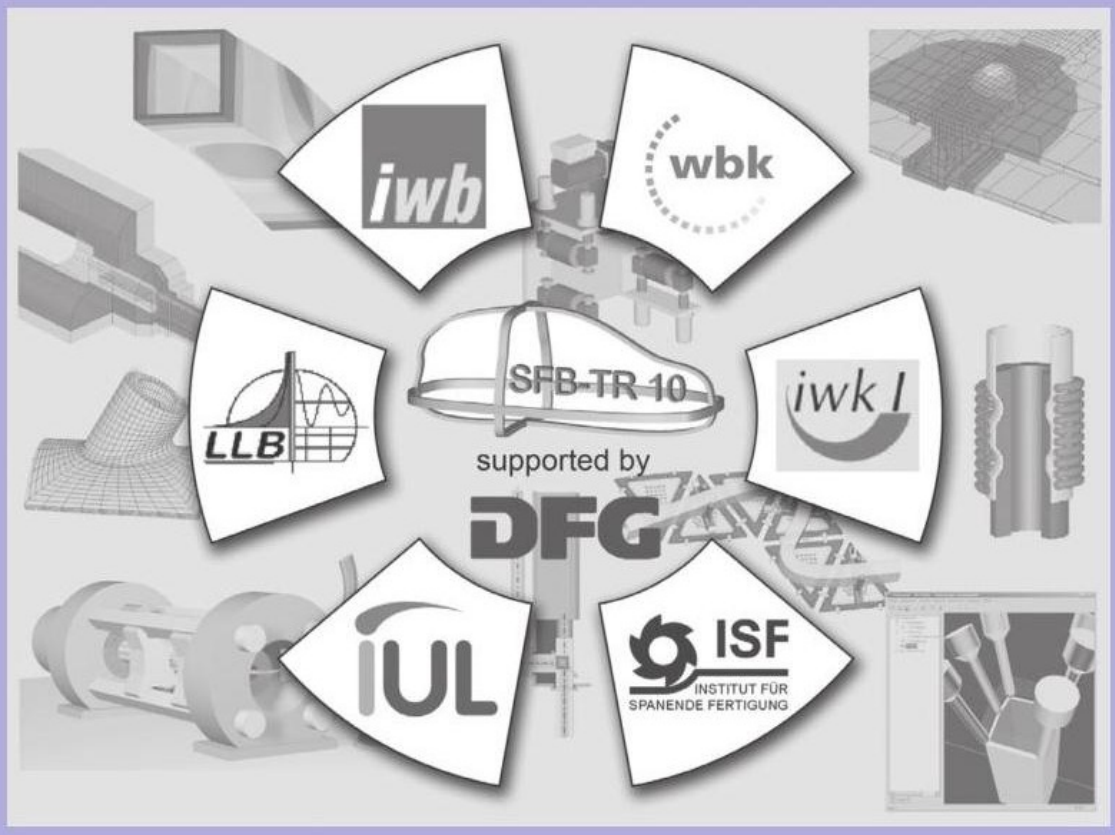

Edited by

Matthias Kleiner, Jürgen Fleischer, Michael Zäh and Marco Schikorra

ttp TRANS TECH PUBLICATIONS

Flexible Manufacture of Lightweight Frame Structures

Flexible Manufacture of Lightweight Frame Structures

Edited by

Matthias Kleiner, Jürgen Fleischer,
Michael Zäh and Marco Schikorra

TRANS TECH PUBLICATIONS LTD
Switzerland • UK • USA

Trans Tech Publications Ltd
Brandrain 6
CH-8707 Uetikon-Zuerich
Switzerland
http://www.ttp.net

Volume 10 of
Advanced Materials Research
ISSN 1022-6680

Full text available online at *http://www.scientific.net*

***Distributed** worldwide by*

Trans Tech Publications Ltd
Brandrain 6
CH-8707 Uetikon-Zuerich
Switzerland

Fax: +41 (44) 922 10 33
e-mail: sales@ttp.net

and in the Americas by

Trans Tech Publications Inc.
PO Box 699, May Street
Enfield, NH 03748
USA

Phone: +1 (603) 632-7377
Fax: +1 (603) 632-5611
e-mail: sales-usa@ttp.net

Preface

Integrated manufacturing for lightweight components is of increasing importance for production engineering today. Due to the market's need for high geometric flexibility in combination with small batch sizes and short production cycles the requirements of customers increase steadily. To handle this phenomenon in the field of production and manufacturing of profiles, the Transregional Collaborative Research Center / TR10 "Integration of forming, cutting, and joining for the flexible production of lightweight space structures" was set up by the German Research Foundation (DFG) at the Universities of Dortmund, Karlsruhe, and Munich in 2002. Back then, the ambitious aim of creating the scientific basis and methods for designing integrated process chains for an automated and flexible production of small batch sizes for lightweight structures was set. Within the scope of this research center an exemplary strategy for the combination of forming, cutting, and joining by an idealized process chain for a flexible production will be designed and set up. The chosen process chain is represented by production processes which additionally show a high potential to fulfill today's needs and also promise to improve product quality in future production.

The processes analyzed comprise as different aspects as:

- direct rounding during extrusion,
- extrusion of composite profiles,
- cutting on the fly,
- hybrid laser welding, and
- joining by electromagnetic high speed forming.

To support these projects, three consideration levels have been formed which deal with the development of the necessary technology, the numerical simulation and the integration of the processes analyzed. In this way, two process chains will be set up: a real one and a virtual one. This structure of technology development, simulation of production processes, and integrated consideration will also be found in the organization of the following peer-reviewed articles. It gives a review on certain aspects of theoretical and experimental projects while setting up the process chain.

Dortmund
January 2006

Matthias Kleiner
Marco Schikorra

Table of Contents

doi:10.4028/www.scientific.net/AMR.10.1

Research for a Flexible Production of Lightweight Space Frame Structures

Alexander Klaus[1,a], Matthias Kleiner[1,b]

[1]Institute of Forming Technology and Lightweight Construction,
Universität Dortmund, Baroper Str. 301, 44221 Dortmund, Germany

[a]alexander.klaus@iul.uni-dortmund.de, [b]matthias.kleiner@iul.uni-dortmund.de

Keywords: Lightweight construction, forming, cutting, joining, simulation, integration, space frame, flexible production

Abstract. This paper presents the focus of research and the structure of the Collaborative Research Centre SFB/TR10 „Integration of Forming, Cutting, and Joining for the Flexible Production of Lightweight Structures" funded in 2003 by the German Research Foundation (DFG). Driven by the demands of low volume production. The aim of the Research Centre is to investigate the scientific basis and methods to design integrated process chains for the flexible manufacture of space frame structures.

Introduction

The production of small batch sizes becomes increasingly important in the transportation sector. Rail vehicle and aircraft manufacturing have already adapted to this trend; the automobile industry is now subject to drastic changes. Due to a significant diversification as to the range of models, batch sizes for each individual vehicle decrease. This tendency is even more intensified by the introduction of niche and premium vehicles. Furthermore, the production time is significantly shortened by a more frequent alternation of models. This, of course, involves large-scale consequences for the production strategies to be applied.

Referring to car body manufacturing, this influence particularly affects the choice of materials. While steel offers economic advantages when producing large quantities due to low material costs, aluminium predominates in small batch size production. In contrast to steel, aluminium offers – apart from sheet metal – further semi-finished products as casts or extruded profiles. Especially extruded profiles are, compared to rolled steel profiles, much more economical with regard to small batch sizes owing to comparatively low tool costs. At the same time, they offer the chance of highly complex cross-sections for an integration of functions. The share of sheet metal, casts, and profiles varies according to the produced quantities. When producing medium quantities, sheet metal parts are still profitable. Complex cast parts reduce the number of components within the structure and can replace profiles. When producing very small quantities, a high share of extruded profiles is much more economical. The implementation of curved profiles is to be favoured due to design,

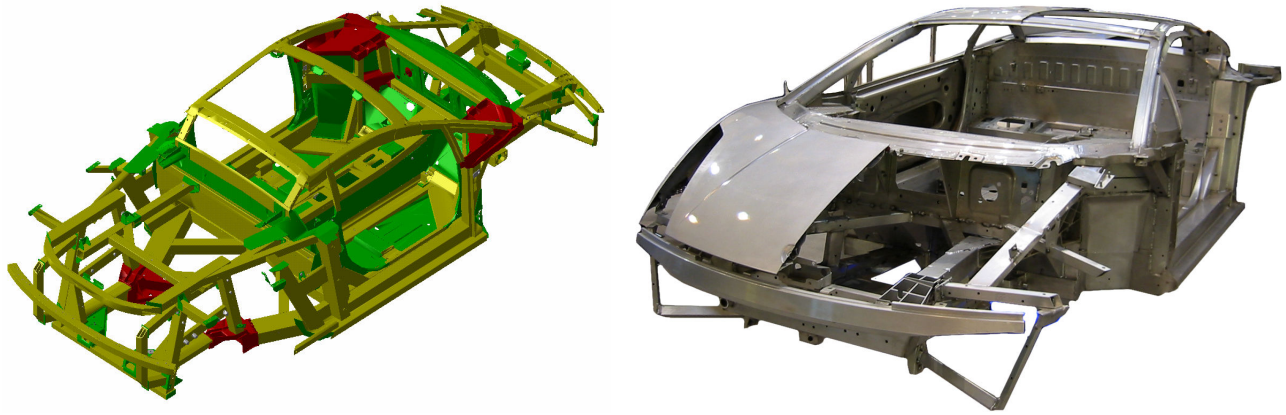

Fig. 1: The space frame of the Lamborghini Gallardo (source: Audi).

structural characteristics, and aerodynamics. Based on existing manufacturing processes and their economic restrictions, straight profiles, which then need to be joined to complex structures, are increasingly applied in small batch size production, involving high costs and little automation (Fig. 1).

The tendency to produce space frame structures in ever smaller quantities which, at the same time, have to be ever lighter and better leads to growing demands on a flexible production which can not be sufficiently met by existing production chains. This demand for flexibility refers to

- applicability with regard to different quantities,
- applicability with regard to a large type variety, and
- short-term producibility.

Particularly manufacturing procedures from the field of forming technology have always been characterised by excellent cost effectiveness in connection with rather large quantities. While in mass production short production times are the most decisive factor, small batch sizes, involving even single-part production, require short production preparation times which mainly consist of tool manufacturing, set-up time, and setting period. In order to transfer a comparable productivity and cost effectiveness of mass production to flexible low volume production, innovative production processes need to be modified and interlinked. This is the target of the Transregional Collaborative Research Centre SFB/TR10, established in 2003 and funded by the German Research Foundation (DFG) for a period of four years in the first instance. Located at three universities throughout Germany (Dortmund, Karlsruhe, München), involving six chairs and institutes, scientists work on the common objective of acquiring the scientific fundamentals and methods for the design of integrated process chains for an automated and product-flexible batch production of light space

Location	Institute	Director	Projects
Dortmund	Institut für Umformtechnik und Leichtbau (IUL)	Prof. Matthias Kleiner	A1, A2, A10, B1
Dortmund	Institut für Spanende Fertigung (ISF)	Prof. Klaus Weinert	A6, B2, B3
Karlsruhe	Institut für Produktionstechnik (wbk)	Prof. Jürgen Fleischer	A4, C3, C4
Karlsruhe	Institut für Werkstoffkunde I (iwk1)	Prof. Detlef Löhe	A3, A9
Munich	Institut für Werkzeugmaschinen und Betriebswissenschaften (iwb)	Prof. Michael Zäh	A7, B4
Munich	Lehrstuhl für Leichtbau (llb)	Prof. Horst Baier	C1

Table 1 Institutes involved in the SFB/TR10.

Project	Title
A1	Three-dimensional Curved Profile Extrusion
A2	Composite Extrusion
A3	Material Systems for Reinforced Lightweight Profiles
A4	Flying Cutting
A6	Drilling of Lightweight Frame Structures
A7	Process-reliable Joining of Aluminum Structures by Means of a Hybrid Bifocal Laser
A9	Relation of Structure and Properties of Joints
A10	Joining by Forming
B1	Simulation of Composite Extrusion
B2	Simulation of 5-Axes Milling
B3	FEM-Analysis of Workpiece Interference by Machining
B4	Simulation of Hybrid Bifocal Laser Welding to Optimise Process and Workpiece Properties
C1	Design Optimisation
C3	Flexible and Intelligent Gripping Technology
C4	Combined Kinematics for Handling and Machining Technology

Table 2 Projects involved in the SFB/TR10.

frame structures (s. Table 1). Here, a scenario including batch sizes from 1 to 10 structures is considered since traditional process chains tend to fail economically in this particular batch size range. A total of 15 SFB/TR10 subprojects investigate in the fields of technology (project range A), simulation (project range B), and integration (project range C).

Especially in the field of production process technology there is an urgent need for research. Processes involving shape-bound design are quite uneconomical for small batch sizes and a large type variety. Apart from high costs for individual tools, according handling times and setting periods for tool changes are also critical. Choosing and, if necessary, advancing as well as qualifying processes which include kinematic design should be a major objective (A1). Furthermore, process safety of production processes needs to be enhanced. In order to accomplish process preparation times as short as possible, forming, cutting, and joining processes need to produce components within close tolerances and structures without any handling times (A1, A4, A6, A7, A9, A10). This is only possible by an extensive production process control regarding tool selection and production as well as process parameters and machining strategies. Here, an increased and inter-process application of simulation techniques is an absolutely crucial aspect in order to eliminate handling times and to avoid waste parts by an extensive process comprehension, on the one hand, and by an exact process prediction, on the other hand (B1, B2, B3, B4). (s. Table 2)

Finally, all sub-processes need to be sensibly interlinked and integrated within the production chain with regard to the small batch sizes. To reduce the number of process and component related interfaces between each production step, the vertical range of manufacture needs to be minimised by technological integration, i.e. by replacing various simple processes by few, but much more complex processes. At the same time, the simulations of the production steps need to be interlinked in order to enhance the prediction quality by a virtual integration of software and model interfaces and to enable shorter calculation times.

Lastly, the modified workpiece flow within the production plant causes a logistical integration. Since there are normally more processing steps than individual components of one and the same order in very small series, conventional concepts for series production and stocking between each interstation are no longer functional. An integrated solution for handling and processing problems, including an appropriate and flexible gripping technology, can lead to the necessary productivity, though (C3, C4).

The degree of lightweight construction of space frame structures can be economically increased for small series as well if design, production, and material choice are considered as a whole. Thus, the space frame structure design needs to be optimised, taking into consideration production restrictions and material characteristics (C1). At the same time, production processes need to eliminate restrictions obstructing lightweight construction and, simultaneously, introduce new lightweight options. New materials and hybrid material combinations need to be qualified and made

Fig. 2: The BMW C1 and its lightweight space frame structure.

applicable for the production processes (A3). The production processes, in turn, need to be adequately adapted to these new materials and the limits of applicability need to be determined, thus defining a certain design policy. (A2).

A close cooperation of the subprojects is, despite separate locations throughout Germany, absolutely essential. The BMW C1 space frame was chosen as demonstrator for the intersection of common achievements. This light space frame structure should show exemplarily how the results accomplished within each sub-project can be implemented (Fig. 2). A continuous awareness of problems, as for example the design of a demonstrator plant and the simulation of process chains and quality, are regularly discussed in working groups on an inter-subproject basis.

A review of all subprojects of the Collaborative Research Centre SFB/TR10 is given in the following. All these publications are based on research activities within the SFB/TR10, funded by the German Research Foundation (DFG).

doi:10.4028/www.scientific.net/AMR.10.5

Three-Dimensional Curved Profile Extrusion – First Results on the Influence of Gravity

Alexander Klaus[1,a], Dirk Becker[1,b], Matthias Kleiner[1,c]

[1]Institute of Forming Technology and Lightweight Construction,
Universität Dortmund, Baroper Str. 301, 44221 Dortmund, Germany

[a]alexander.klaus@iul.uni-dortmund.de, [b]dirk.becker@iul.uni-dortmund.de,
[c]matthias.kleiner@iul.uni-dortmund.de

Keywords: Bar Extrusion, Lightweight Construction, Flexible Manufacture, Bending

Abstract. This paper presents and discusses the latest achievements in the manufacture of three-dimensionally curved aluminum profiles using an integrated bar extrusion process. While the conventional process chain lacks applicability and quality especially in low volume production, the new technology is promising, but still needs research to understand the correlation between the product to be manufactured and the contour accuracy to be achieved. This paper shows first results on the manufacture using a robot-guided second guiding tool and direct air quenching. The results will have an impact on further processing steps.

Introduction

Extruded profiles are widely used in transportation and civil engineering. Due to design, aerodynamics, or structural advantages, extruded profiles are often required in a curved shape. Conventional bending processes are feasible for mass as well as low volume production, but has many disadvantages which include springback, cross section deformation, and inhomogeneously decreased formability. An alternative technology invented in 1994 and developed since then at the Institute of Forming Technology and Lightweight Construction offers new possibilities in the manufacture of curved profiles.

The Curved Profile Extrusion (CPE) has been investigated by Arendes in order to describe the fundamental process principle [1]: The extruded strand is inserted into a guiding tool with a suitable shape according to the profile´s cross section. Three possibilities arise and have to be differentiated:

1. By adjusting the guiding tool to the center of the extrusion press, a *straight* profile is manufactured. Conventional pulling or stretching operations like in conventional extrusion plants are not necessary.
2. By adjusting the guiding tool laterally, the profile exits the die in a *constantly curved* shape. The radius of the profile is solely determined by the position of the guiding tool in relation to the die.
3. By adjusting the guiding tool to varying positions while extruding, a *variably curved* profile is manufactured. The movement of the guiding tool has to be precisely calculated according to the desired contour and also has to be synchronized to the motion of the extrudate. As long as the guiding tool only moves in one axis, the profile contour is two-dimensional (2D-CPE). With a more complex movement of the guiding tool, even three-dimensionally curved profiles can be manufactured (3D-CPE).

In contrast to conventional bending processes, the force applied to the strand by the guiding tool does not plasticize the material between die and guiding tool. In fact, the lateral force is transferred to the already plasticized region within the die where the material flow is slightly changed so that a curved profile exits the die (s. Fig. 1). Most notably, the radius manufacture by CPE is not influenced by process parameters such as temperature, velocity, or material which usually have an important impact on forming processes.

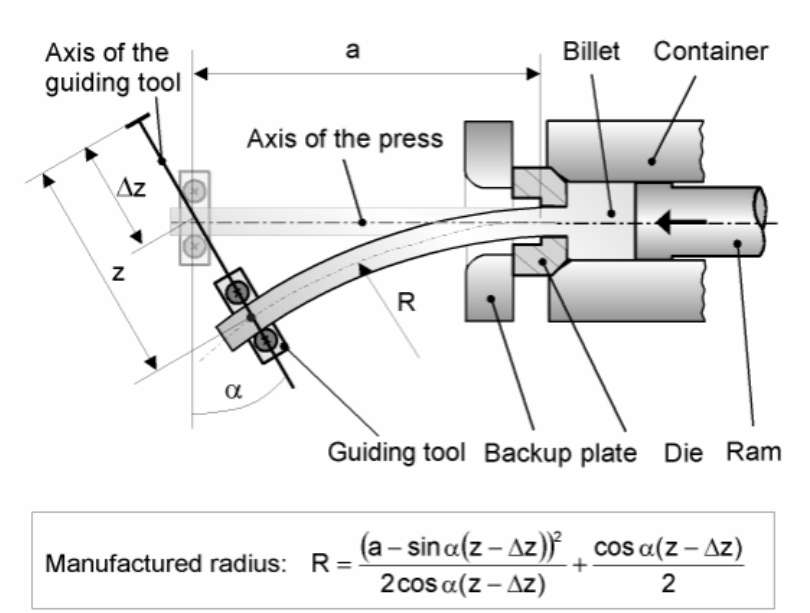

$$\text{Manufactured radius:} \quad R = \frac{(a - \sin\alpha(z - \Delta z))^2}{2\cos\alpha(z - \Delta z)} + \frac{\cos\alpha(z - \Delta z)}{2}$$

Fig. 1: Process principle of Curved Profile Extrusion (CPE).

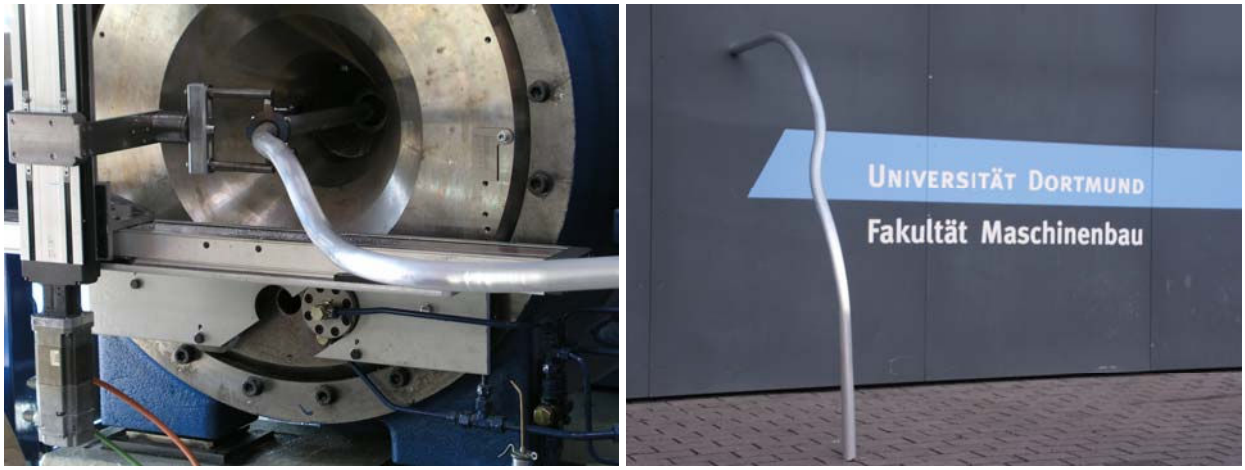

Fig. 2: Manufacture of three-dimensionally curved profile.

However, some process restrictions were found. As the curvature starts within the die, the curved profile collides with the backup plate if the radius of the profile contour is too small. The most important restriction is the minimum radius which is determined by the press geometry. A restriction of 1,500 mm had to be set up on a laboratory press. For a production press, that provided a smaller orifice in the backup plate, the minimum radius had to be restricted to 2,000 mm.

In addition to this, CPE was only investigated for the manufacture of two-dimensionally curved profiles. With a guiding tool mounted on a single linear axis, only profiles with a flat yet variable contour could be manufactured. Furthermore, this technology was still investigated on a laboratory scale. Continued research effort in cooperation with partners in the extrusion and press manufacturer industry led to an approach for a reliable environment regarding an industrial use of CPE. Moreover, an extrusion press was specifically designed for the technological needs of CPE which most importantly allowed for a minimum radius of 500 mm and less.

CPE has become a manufacturing process which is feasible especially in low volume production[2]. The Transregional Collaborative Research Centre SFB/TR10 (“Integration of forming, cutting and joining for the flexible production of light weight structures”) addresses this context.

From a general point of view, the manufacture of three-dimensionally curved profiles using CPE still needs to be researched.

Some progress has already been made:

- funded by the German Research Foundation (Deutsche Forschungsgemeinschaft, DFG), a 10 MN CPE press has been financed and installed at the IUL in Dortmund;
- the equipment necessary for 3D-CPE, e.g. linear axis and improved guiding tools, have been designed and installed at the extrusion press;
- the influence of gravity on the extrusion process has been investigated for initial cases of interest[3];
- first industrially relevant workpieces have been manufactured in close cooperation with automotive partners using 3D-CPE.

This paper will describe and discuss the latest advances made in understanding the ways in which gravity influences the 3D-CPE process and their implications on the complete process chain.

Influence of Gravity on CPE

The curvature in the profile is caused by the external force of the guiding tool on the material flow within the die. This force results from the position of the guiding tool in order to achieve the desired contour radius. Additional forces have to be suppressed since they might have a negative influence on the forming result. In the two-dimensional case, the lateral force of gravity on the profile is compensated by a run-out table that supports the extrudate vertically. In addition to this, axial and lateral forces caused by friction between run-out table and extrudate have to be minimized, e.g. by the use of a table surface made of graphite. Usually, a run-out table is no longer available in 3D-CPE since the profile has not necessarily a flat shape any more. The profile must be able to move freely in three dimensions. Gravity acts on the profile and undesirably changes the material flow, therefore the aim of the current research is to determine the kind and amount of influence gravity has on the extrudate.

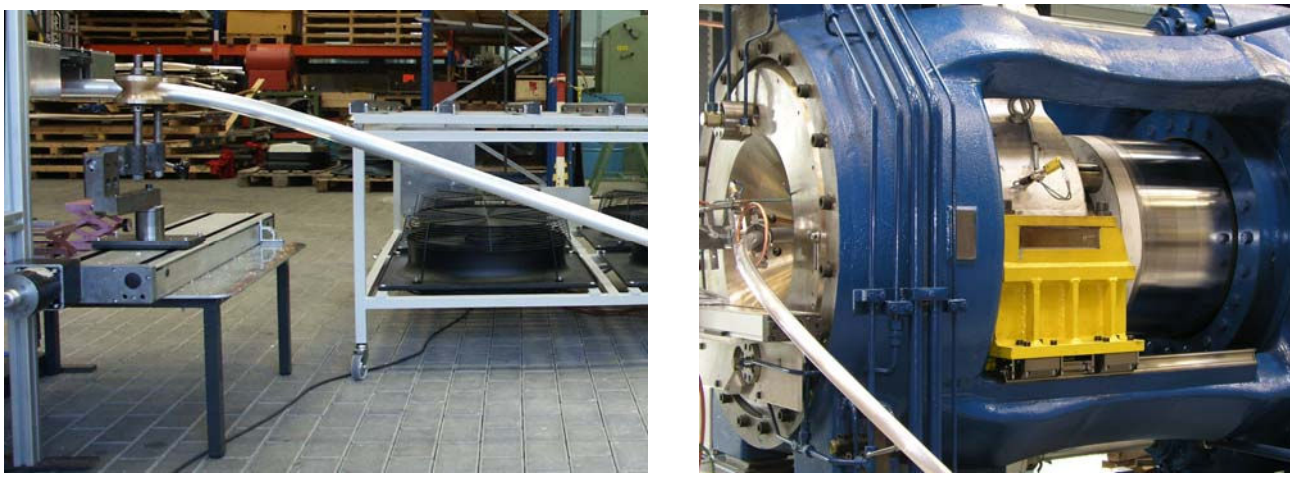

Fig. 3: Influence type 2 (left) and 3 (right) of gravity on CPE.

Basically, three types of influences of lateral forces on the extruded profile can be differentiated:

1. *CPE-effect.* The force is transferred to the forming zone where the material is already plasticized. This relates to the basic process principle of CPE. Additional forces like those of gravity (or of the cutting process, ref. A4) will directly affect the manufactured radius.
2. *Bending.* The force causes bending moments throughout the profile. The moment features maximum values at the guiding tool. When the bending stresses exceed the yield stress, a plastic bending takes place and undesirably affects the profile contour subsequent to the extrusion process. This applies e.g. when profiles with large radii or ultimately straight

profiles are manufactured (Fig. 3 left). This effect has been investigated on straight profiles in [4].

3. *Torsion.* When the centre of gravity is located off-axis from the profile, gravity additionally acts as a torsion moment throughout the profile and leads to a twist in the profile (Fig. 3 right).

All three types can appear in a combined way. The aim is to understand and suppress their negative influence on the contour accuracy.

For 2D-CPE, only a single guiding tool is required to determine the profile contour. 3D curvatures can also be principally achieved when this single guiding tool is moved along two axe but due to the influence mentioned above, gravity changes the profile contour. However, this influence can be avoided or at least significantly reduced by using a second guiding tool instead of the run-out table of the 2D case. In contrast to the first guiding tool that only has to move along two axes in front of the backup-plate of the extrusion press, the second guiding tool must be able to move in three dimensions in order

- not to increase the minimum radius,
- to allow for arbitrary 3D contours, and
- to perform different strategies of moving the second guiding tool.

Experimental Set-up

The 10 MN CPE front loading short stroke press installed at the IUL provides a container diameter of 146 mm and can extrude profiles with a circumscribing circle of up to 130 mm. The billets (EN-AW 6060) are heated in a chamber oven to 550°C and are fed into the press. The ram speed is set to 1 and 2 mm/s and 70 and 140 mm/s profile speed respectively. Funded by the DFG, an industrial robot (Kuka KR 150-2) with a reach of 2.7 m was financed and installed at the extrusion press to carry the second guiding tool. Both guiding tools are made of graphite discs with a round opening to fit the 40x2 mm round tube that is extruded. A simple pressure air quench made from a copper ring with punched holes is used directly after the die and at the first guiding tool. Additionally, the run-out table equipped with 4 axial blowers was used to further cool down the profiles for manual handling. However, the table did not protect the profile against gravity. (Fig. 4)

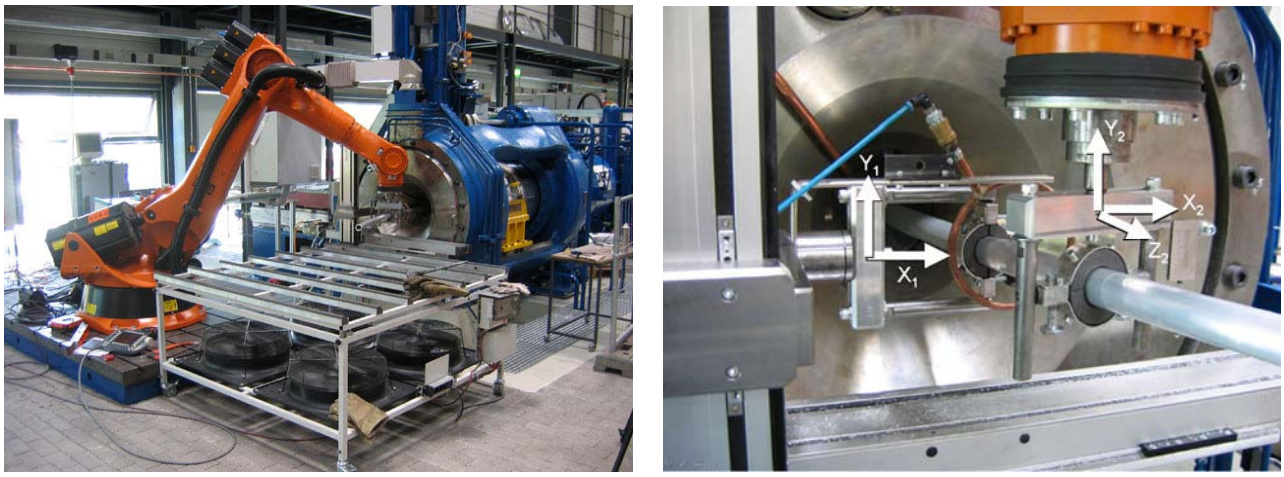

Fig. 4: Extrusion press with Kuka robot (left). Close-up view on first and second guiding tool (right).

For the experiments, a workpiece length of 2,300mm and different contours with a constant radius of 800mm as well as 3,000mm were chosen. In this paper, only the experiments with the 800mm radius are discussed as an example because this two-dimensional profile represents a worst case scenario for the manufacture of three-dimensional profiles:

1. As a two-dimensionally curved profile is being deflected horizontally, the torsion moment is at its maximum. In case of a vertical deflection, gravity would result in bending stresses instead of torsion stresses.
2. A radius of 800 mm is very small, resulting to a high displacement of the center of gravity. Thus, the torsion moment is high compared to larger radii. Additionally, a length of 2,300 mm can be manufactured which would not be possible if the radius was smaller.
3. Using a round tube, the individual guiding tool cannot act against torsion, thus the effect of the torsion moment caused by gravity is at its maximum.

Therefore, this set-up is best suited to investigate the effect of torsion on the contour accuracy of 3D-CPE. Further work focused on profiles with a radius of 3,000 mm. Here, the bending stresses are expected to be significantly higher.

The two-dimensional profile is a worst-case for 3D-CPE but it is very easy to evaluate. Ideally, the profile should be horizontally flat. Due to gravity, the profile will bend downwards. Using a laser-assisted spirit level, even a slight lowering off the horizontal axis can be measured when the press is stopped after a length of 2,300 mm is reached behind the second guiding tool and while the profile is still connected to the extruded strand. Once the profile is cut off, it is put on a flat table. Here, the contour accuracy or flatness of the profile is measured using a feeler gage. (Fig. 5)

The position of the first guiding tool is determined by the desired profile contour and calculated by different specific software solutions [5, 6]. The motion of the second guiding tool must be synchronized with the strand so that no additional forces are induced into the profile. In contrast to the first guiding tool, the second guiding tool can basically support the profile at an arbitrary position. Due to this and the possibilities of the robot, different guiding strategies can be implemented, this includes guiding at

- the end of the profile,
- the center of gravity, or
- a constant distance from the first guiding tool.

When the profile is guided at the end or at the center of gravity, the profile will be cut off between the first and the second guiding tool. As a consequence, the separated profile must be disconnected from the second guiding tool and the new profile has to be reinserted. Although technologically promising, this is not possible with the current type of guiding tool – but under investigation [7]. Therefore, the results presented were obtained with a second guiding tool supporting the strand at a constant distance (200 and 1,000 mm) to the first guiding tool. For both ram speeds and both guiding tool distances, three profiles were manufactured and tested for lowering and contour accuracy.

Results

Guiding tool distance and extrusion speed have a significant influence on how gravity downgrades the contour accuracy given the set-up described above (Table 1). A long guiding tool distance of 1,000 mm and low extrusion speed lead to considerably less lowering and better flatness than the short distance and the higher speed. Apparently, the longer distance of both guiding tools the beeter the moment induced by gravity is compensated. However, a smaller distance would be preferable to save space in front of the press.

Furthermore, the quenching rate increases at lower speeds since the air stream is constant, thus the profile cools down to a lower temperature resulting in higher yield stresses, and therefore it does not deform as fast as at higher temperatures, given the same load. A maximum flatness of -0+1 mm can be considered to be acceptable for applications in low volume production, taking into account the workpiece length. This deviation from a flat, round arc can be compared to the quality of a straight profile that may exhibit a deviation from an ideal straight line up to 1 mm at a length of

2,000 mm according to DIN 1748. Only the profiles manufactured with the long guiding tool distance and at the lower extrusion speed meet these requirements (Fig. 5, thick, solid line).

However, the lowering measured by the laser-assisted spirit level shows remarkably high values. For profiles with comparable contour accuracy, the lowering can also vary significantly, here by 270 and 485 mm. Even for the profiles with the best contour accuracy of -0+0.6 mm, the lowering of 60 mm must be taken into account for further processing.

The contour accuracy or flatness alone, as measured, do not fully represent the quality of the profiles. The torsion of the round tube is not directly visible and irrelevant in this particular case. However, this torsion can be measured and will be of interest as soon as cross sections which are not rotationally symmetric are extruded. Here, profiles extruded at the long guiding tool distance and low extrusion speed exhibit a torsion between 3° and 4° on a length of 2,300 mm. Given the set-up described above, this torsion theoretically accounts for a lowering of 55 to 80 mm. An elastic lowering might as well be possible, but calculations and experiments show that this amount is negligible.

Profile Speed (v)	Guiding Tool Distance (GTD)	Mean Lowering	Mean Contour Accuracy
70 mm/s	200 mm	270 mm	-0+3.5 mm
140 mm/s	200 mm	485 mm	-0+3.2 mm
70 mm/s	1.000 mm	60 mm	-0+0,6 mm
140 mm/s	1.000 mm	87 mm	-0+1.9 mm

Table 1: Measurement of the profile´s lowering and contour accuracy (at a workpiece length of 2.000 mm).

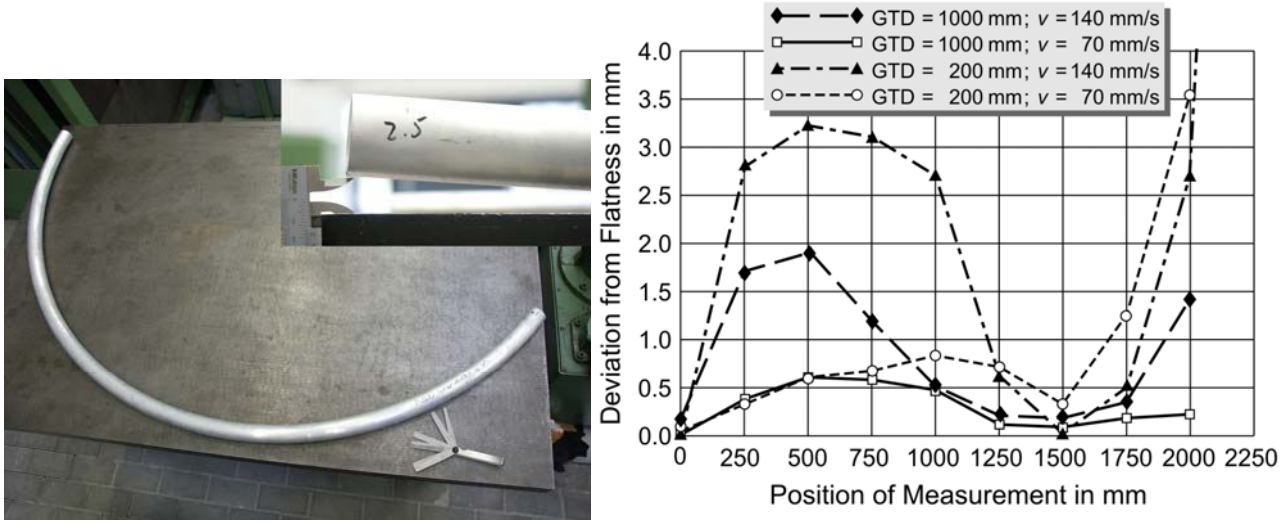

Fig. 5: Contour accuracy measured over the profile length for different guiding tool distances and extrusion speeds.

Discussion

The quenching within the process chain has multiple effects on the usability of 3D-CPE. Firstly, moderate quenching is sufficient for alloys like EN-AW6060 (AlMgSi0.5). For harder alloys, like 6005 (AlMgSi0.7) or 6082 (AlMgSi1), rapid quenching is essential in order to establish the required mechanical properties during the subsequent aging process. Thick walled profiles made of harder alloys might not even be press-quenchable so that a separate solution heating and *water* quenching is necessary. This would not be feasible within the context of the SFB/TR10, though. Secondly, rapid quenching of asymmetric profiles or inhomogeneous quenching leads to distortion

and, thus, to a loss in contour accuracy. However, rapid *air* quenching is possible without distortion, even with 2024 and 7075 alloys[8], but was not included in the extrusion process.

Thirdly, higher quench rates applied directly after the die would also lead to significantly lower profil temperatures in the area between die and guiding tools. The gravity-influenced lowering and torsion would be minimized. Therefore, improvements regarding the quench rate directly improve the contour accuracy.

Fourthly, the available quench rate limits the extrusion speed, given the required contour accuracy at the cross section and the desired contour geometry. A high moment of area inertia per weight per meter, as given in structural application, is ideal for 3D-CPE. But a higher speed decreases the quenching efficiency and therefore decreases the contour accuracy. However, the extrusion speed considerably determines the economical feasibility of the extrusion process. This circumstance is lessened as the added value of 3D profiles is very high compared to simple straight profiles. Yet, the extrusion speed will be an important parameter for the acceptance of this technology. Improvements of the quench rate will increase the possible extrusion speed. As a consequence, the applicability of 3D-CPE will increase.

All four implications have to be observed. The press quenching must be as high as possible in order to achieve the mechanical properties, to improve the contour accuracy, and to maximize the possible extrusion speed. At the same time, the quenching must not be very high in order to avoid distortion.

Although the 3D-CPE process shows good workpiece results at low extrusion speeds with the current quenching setup, the profile lowering must be considered in follow-up processes. The investigations discussed in this paper concern the 3D-CPE process itself, delivering curved profiles. However, these profiles have to be cut off in-process by a circular saw mounted on a second robot and synchronized to the profile position and speed (project A4). Additionally, the profile has to be gripped before it is cut off for subsequent handling operations (project C3). Both operations have to take into account the real profile position in order not to cut and to grip at the wrong position. Moreover, as the lowering can vary significantly, the correct profile position will not be properly predictable at a tolerance of a few mm. Therefore, the cutting and gripping process must, at any rate, approach and additionally support the profile as soon as possible, ideally directly after the second guiding tool. This would increase the complexity of 3D-CPE because up to four actuators (2 guiding tools, cutting support, and gripping) have to be synchronized to the extrusion speed. But on the other hand, this would also increase the contour accuracy as the lowering will be reduced to zero at the cutting and at the gripping location. Potentially, the second guiding tool and the cutting device can be integrated into one single actuator. This will be the focus of continued collaborative research effort in the SFB/TR10.

Summary

Curved extruded profiles are important components in transportation and civil engineering. The conventional process chain implies disadvantages, especially for low volume production. Curved Profile Extrusion is an alternative technology that produces curved instead of straight profiles in the extrusion process. Currently, this technology is industrially feasible only for 2D applications. In 3D-CPE, gravity influences the manufacture as the conventional support by a run-out table is no longer available.

The experiments using a worst case scenario show that a second guiding tool is essential. At low extrusion speeds and a large guiding tool distance, the best results are achieved. Flat profiles with a radius of 800 mm and a length of 2,300 mm were manufactured at a contour accuracy that outperforms the dimensional tolerance of straight profiles. Only the torsion of 4° is a drawback that has to be further investigated. Rapid air quenching will help to increase accuracy as well as productivity.

The in-process lowering of the profile has to be considered. Subsequent cutting and handling operations must ideally approach and additionally guide the profile as soon as possible after the second guiding tool.

Acknowledgement

This paper is based on investigations of the collaborative research centre SFB/TR10 which is kindly supported by the German Research Foundation (DFG).

References

[1] D. Arendes: *Direct Manufacturing of Rounded Aluminium Profiles During Extrusion.* PhD-Thesis (in German), University of Dortmund, Shaker, Aachen, 1999.

[2] A. Klaus, M. Kleiner: *Developments in the Manufacture of Curved Extruded Profiles – Past, Present, and Future.* Light Metal Age, August (2004), p. 22-32.

[3] D. Becker, M. Schomäcker, A. Klaus, M. Kleiner: *Alternative Manufacture of Curved Profiles for Automotive and Railway Lightweight Constructions.* Proceedings of the Int. Conference Aluminium in Transport, 27.-29.04.2005, Moscow, Russia

[4] M. Kleiner, A. Klaus, D. Becker: *Mehrachsiges Runden beim Strangpressen.* Aluminium, International Journal for Industrie, Research and Application, Volume 80 12/December 2004, pp. 1366-1370

[5] J. Bickendorf and A. Birkenstock: *Roboter als Schlüsselkomponente für das "Runden beim Strangpressen"*. Robotik 2004, München

[6] J. Fleischer and G. Stengel: *Bahngenerierung für eine robotergeführte Abtrenneinheit für räumlich gekrümmte Strangpressprofile - Einsatz eines CAD-Systems zur Programmierung einer fliegenden Säge*. wt Werkstattstechnik online Jahrgang 94 (2004) Issue 9

[7] J. Fleischer, C. Munzinger, S. Kies, J.P. Schmidt-Ewig, and D. Ruch: *Flexible Profilbearbeitung im Leichtbau - Neuartiges Maschinenkonzept zur flexiblen Handhabung und Bearbeitung räumlich gerundeter Profile.* wt Werkstattstechnik Jahrgang 94 (2004), Issue 9, pp. 422-425

[8] A. Irretier, O. Kassler, F. Hoffmann, P. Mayr: *Dry and clean age hardening of aluminum alloys by high-pressure gas quenching.* Journal of Materials Engineering and Performance, Vol. 13 (2004) Issue 5, pp. 530-536

doi:10.4028/www.scientific.net/AMR.10.13

Composite Extrusion – Determination of the Influencing Factors on the Positioning of the Reinforcing Elements

Matthias Kleiner[1, a], Alexander Klaus[1,b], and Michael Schomäcker [1,c]

[1]Institute of Forming Technology and Lightweight Construction,
University of Dortmund, Baroper Str. 301, 44221 Dortmund, Germany

[a]matthias.kleiner@iul.uni-dortmund.de, [b]alexander.klaus@iul.uni-dortmund.de,
[c]michael.schomaecker@iul.uni-dortmund.de

Keywords: Composite Extrusion, Influencing Parameters, Element Positioning

Abstract. In order to manufacture a workpiece fulfilling specified requirements with the lowest possible weight, it is crucial to be able to work with a variety of materials and to combine them accordingly. The production of profiles based on hybrid materials demonstrates such an approach. The continuous and selective reinforcement of aluminum profiles with metallic elements like steel wire and steel wire ropes by composite extrusion is being investigated within the scope of research of the Transregional Collaborative Research Center (SFB/TR10). A stable production process for composite profiles with embedded continuous reinforcing elements was developed during the research work. In this paper, the process principle is shown and an overview of the special tools is given. Furthermore, the temperature and the strand speed as influencing factors on the final state of the composite are analyzed, based on real size experiments using a 2.5MN and a 10 MN extrusion press.

Introduction

Conventional particle or short fibre reinforced profiles are manufactured by extruding accordingly reinforced billets. The extrusion of composite billets, however, is associated with a number of disadvantages. The reinforcement of the billets leads to significantly higher extrusion forces compared to the use of regular billets which, again, leads to an increase in the minimum wall thicknesses that can be manufactured. Further significant disadvantages are the increased tool wear and the higher costs for reinforced billets than for regular billets. [1, 2]

In contrast to this, composite extrusion of regular billets is an interesting alternative. In an innovative process for the manufacturing of composite profiles regular billets are extruded and the composite is formed by feeding the reinforcing material in form of continuous elements during the extrusion process. Research on composite extrusion at the Institute of Forming Technology and Lightweight Construction (IUL), University of Dortmund, Germany, is an essential part of the Transregional Collaborative Research Center (SFB/TR10: "Integration of forming, cutting, and joining for the flexible production of lightweight structures") funded by the DFG. [1, 2]

Research on Composite Extrusion Using Regular Billets

Process Principle. In this process, a homogenous billet is used and the hybrid is formed inside a special die by feeding a secondary material into the metal flow during the extrusion. In front of the sealing element the billet material splits into an upper and a lower partial strand which join again in the welding chamber. In the meantime, the reinforcing elements are fed into the tool from the sides where they are redirected into the press direction within a cartridge with milled channels and merged again with the billet material in the welding chamber; see also fig. 2 in paragraph *tool design*. [3, 4]

This process has been similarly used in industrial applications for some time, e.g. for the production of steel-aluminum bus conductors [5] or steel-magnesium sacrificial anodes. Yet, using

this process for lightweight construction purposes, currently no application is currently known to the authors.

Aims of Research. The fundamentals of the composite extrusion of continuously and selectively reinforced aluminum profiles are being investigated within the scope of research activities of the project A2 of the Transregional Collaborative Research Center (SFB/TR 10). The main objective of project A2 is the characterization of the manufacturing process with regards to process stability and element positioning, including the analysis of main influencing parameters and the development of special tools. The process results depend on an alternating correlation between the parameters cross-section geometry, reinforcing elements, and the pressing tool. To characterize the process parameters, the complexity of the manufacturing process is enhanced stepwise, meaning a gradual increase of the cross-section complexity and a rise in the number of reinforcing elements while at the same time reducing the wall thickness. The current focus concerning reinforcing elements lies on metallic elements like high-strength steel wires and steel wire ropes. In future the investigations should be extended to non-metallic elements like carbon fibres [6].

Experimental Equipment. The first experiments were carried out on a modified 2.5 MN extrusion press which was originally constructed for lead alloys and subsequently adjusted to the extrusion of aluminum alloys. It was possible to manufacture profiles up to a circumscribing circle of 40 mm with the matching tool for this press which has a maximum die diameter of 125 mm. An additional press with a maximum pressing force of 10 MN is available for experimental investigations since July 2004. The tool for the 10 MN press has a maximum die diameter of 400 mm and can manufacture profiles up to a circumscribing circle of 130 mm.

Cross-section Geometries and Reinforcing Elements. The complexity of the cross-sections is enhanced stepwise within the scope of research activities. Currently, the basic research mainly focuses on solid bar profiles. However, a round hollow cross-section was also successfully manufactured with four embedded wires. Fig. 1 shows the cross-sections of the experimental investigations. As billet material the aluminum alloy EN AW 6060 (AlMgSi0.5) was used. Initially, metallic reinforcing elements (RE) like wires and ropes were examined within the scope of experimental research of the SFB/TR10. The research focused on high strength steel wires and steel wire ropes with a tensile strength of about 2000 N/mm^2, but also wires of nickel and cobalt-based alloys were successfully embedded. During the research concerning interface optimization, which was carried out in cooperation with the iwk1 in Karlsruhe, the wires were partially coated or surface-treated by grinding and etching [7].

The experiments showed that the process is more stable the smaller the number of single wires within a given rope diameter. A 1x7 (7 single wires) construction displays a significantly higher process stability than a 7x7 (49 single wires) construction [8]. The most stable process can be reached by use of full wires. Using wires, continuously reinforced profiles from a number of subsequently extruded billets could be manufactured without failure. But not only the structure of the reinforcing elements has an influence on the process stability. To improve the interface between the wires and the billet material, they were coated with zinc, nickel, and AlSi12 [9]. The coatings partially peeled off during the feeding and plugged up the feeding bores, which lead to tearing of the wires.

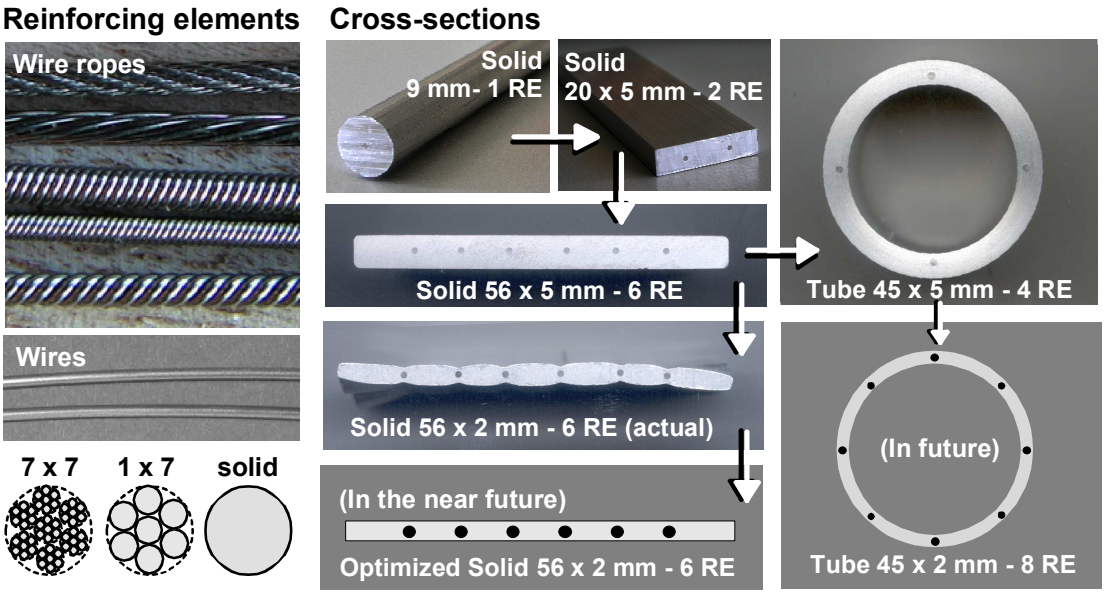

Fig.1: Reinforcing elements and tool design

Tool Design. Depending on the construction of the extrusion press and the accessibility from outside, the elements can be fed into the tool either from the side or from the front plate. A deflection of 180° is necessary, however, if the tool stack is only accessible from the front plate. The 2.5 MN press used for the first experiments required a 180° turn with a very small radius due to its small die. This inhibited the use of wires as they would be deformed plastically and which would exit the die in a narrow circle. As a consequence, only wire ropes were initially used because they provided a much easier deflection within the die. The 10 MN press, on the other hand, allows a 90° turn with a significantly larger deflection radius due to its larger tool stack. Here, solid wires can be incorporated.

Fig. 2 shows the tool design for composite extrusion. The pictured tool, as designed for the 10 MN press, is used to embed six reinforcing elements into a 56 x 5 mm solid profile with a rectangular cross-section. Taking into consideration the high stress level in the welding chamber, it is possible to reduce the strain on the reinforcing elements by feeding them after the primary forming of the matrix material is finished [4]. Therefore, a two-stage process is favorable, inserting the reinforcing elements after the primary forming, but when the remaining degree of deformation is still sufficient to ensure an adequate forming of the composite. The total press ratio of the pressing tool displayed in fig. 2 is 60:1, while the ratio after insertion of the elements is 6:1.

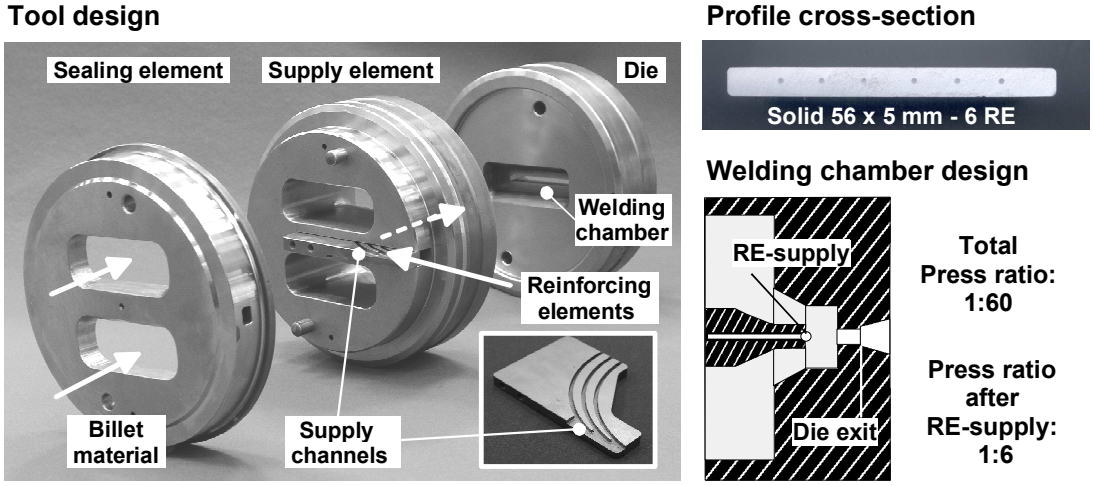

Fig. 2: Tool design

Influencing Factors on the Positioning of the Reinforcing Elements

Embedding of the Reinforcing Elements. After the feeding process, the reinforcing elements merge with the billet material within the longitudinal weld seam and follow the material flow towards the die exit. Therefore, the material flow plays an important role. Its characteristics during and after the feeding determines the position of the reinforcing elements in the extruded profile. A deflection of the position of the reinforcing elements in the manufactured profile concerning the supply position in the welding chamber can be divided into two cases:

- A displacement of the longitudinal weld seam (vertical deflection) and
- a deflection along the longitudinal weld seam level (horizontal deflection).

Fig. 3 shows the etched cross-sections of solid rectangular profiles with embedded reinforcing elements of earlier experiments. When using a tool with symmetrically designed material inlets and welding chamber, it can be expected that the longitudinal weld seam is located in the centre line of the manufactured profile. Especially for the 20x5 mm profile, however, a deviation of the longitudinal weld seam is clearly visible. The comparison of the longitudinal welding seams of reinforced and non-reinforced profile samples does not show a great influence on the run of the welding seam.

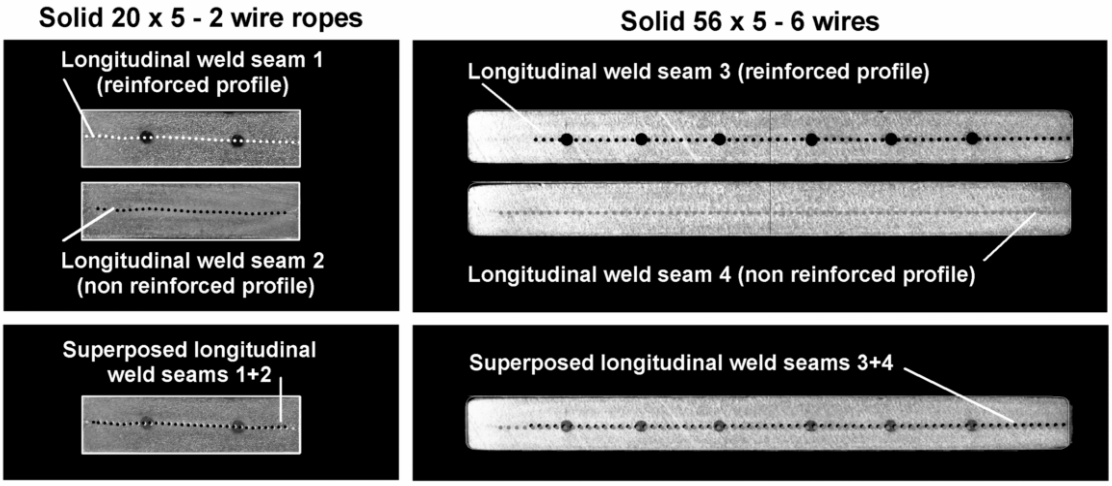

Fig. 3: Ground and etched cross-sections of reinforced and non-reinforced profiles

Influencing Factors on the Material Flow. The positions of the reinforcing elements in the manufactured profile depend most likely on the geometric tool parameters like

- the design of the material inlets,
- the supply position,
- the height of the welding chamber,
- the reduction of the cross-section,
- manufacturing tolerances

and last but not least on the process-related influences like

- the billet material,
- the reinforcing element,
- the temperatures of billet, container-liner, and tool.

Sheppard investigated the influence of the billet temperature on the material flow in a conventional extrusion process [10]. The material flow inside the tool can be characterized by the following aspects: As known from literature, the material flows faster towards the press axis than in the peripheral zone due to the shear friction at the wall and the velocity profile which depends on

the billet temperatures. In composite extrusion, these characteristics will certainly influence the position of the reinforcing element in the manufactured profile cross-section.

Furthermore, it has to be considered that temperature fluctuations may have effects on the positioning of the reinforcing elements in the manufactured profile. There are a number of reasons for temperature fluctuations which can also superpose each other, for example

- drain of billet heat into the colder container liner,
- drain of billet heat into the tool,
- drain of heat from the tool into the backup plate, and
- heating of the tool caused by forming energy.

Apart from these fluctuations, local deviations, which lead to different flow stresses in the material, can influence the material flow, too. When multi-hole dies are used, an inhomogeneous temperature allocation can cause the strands to exit the die at different speeds. This behavior was visible during the experiment displayed in fig. 4. The same sealing plate and supply element were used with the multi-hole die as with the tool shown in fig. 1 that is used for the extrusion of the reinforced solid 56x5 mm profile. Only the die was exchanged for a three-hole die. During this pressing the middle exit was consciously blocked so that only the upper and the lower strand were exiting.

A temperature measurement at the front surface showed an inhomogeneous temperature allocation. In order to determine the exact distribution, an additional video thermographical picture was taken, see Fig. 4. The measured temperature difference between the upper and the lower die opening was 25°C, which is very likely to be the reason for the upper strand having a higher exiting speed than the lower strand at the beginning of the pressing. During the course of extrusion, the discrepancy in length, and therefore the exiting speed, decreased, which could be an indication for the different exiting speeds being caused by thermal effects. Transferred to the process of composite extrusion, this means that a temperature gradient can shift the longitudinal weld seam, thus influencing the position of the reinforcing elements.

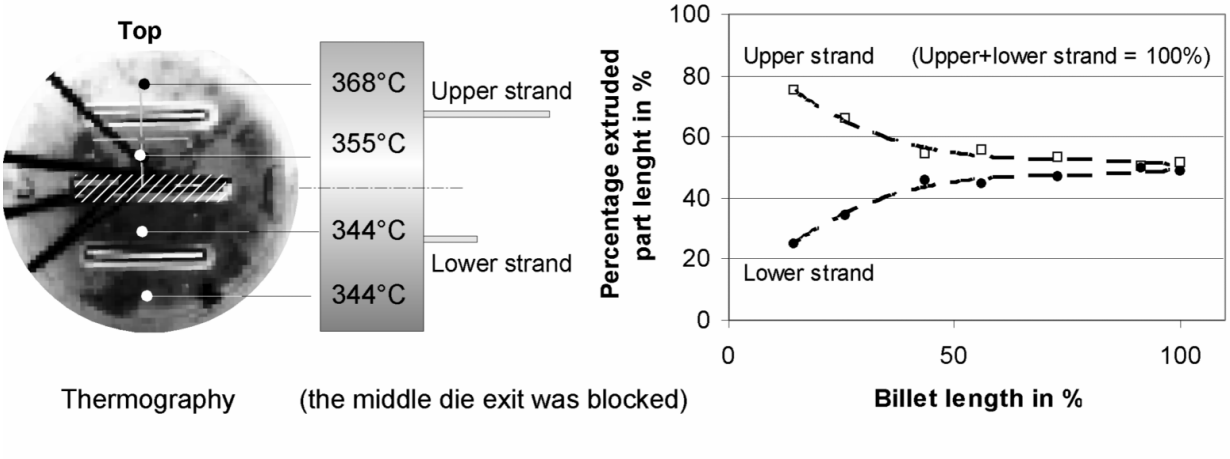

Fig. 4: Different exiting speeds in dual-strand extrusion

Experimental Set-up and Proceedings

Concerning a precise positioning, it is necessary to investigate the possible temperature influence on the positioning of the reinforcing elements. As further possible influencing parameter, the effect of the extrusion speed on composite extrusion is examined.

Experimental set-up. Fig. 5 shows the geometry of the tool which was used for conducting a large part of the experimental investigations concerning RE-positioning. The experimental cross-section is the 56x5 mm solid profile with six wires, which have a diameter of 1 mm (picture of tool design, see fig. 2). The supply bores have a diameter of about 2 mm. To eliminate a possible

influence of geometrical tool inaccuracies, as for example an offset between the supply-bores and the die exit, the assembled tool was measured for reference. Only slight deviations of approximately 0.05 mm could be determined. In the supply bores, between the wire and the wall, the tolerance is about 0.5 mm, however. For the experiments described in the following, the billet temperature at the start was 550 °C and the container liner temperature was 450 °C. The die holder of the pressing tool is equipped with a heating device that can pre-heat the tool up to 370 °C in the "warm position" of the press. For this purpose, the tool is pulled back from the backup plate by a special device so that the heat transfer between the hot tool and the container liner is inhibited.

The extrusion press is specially constructed to hold the target ram speed with high precision, so a defined extrusion speed with very low fluctuations can be achieved.

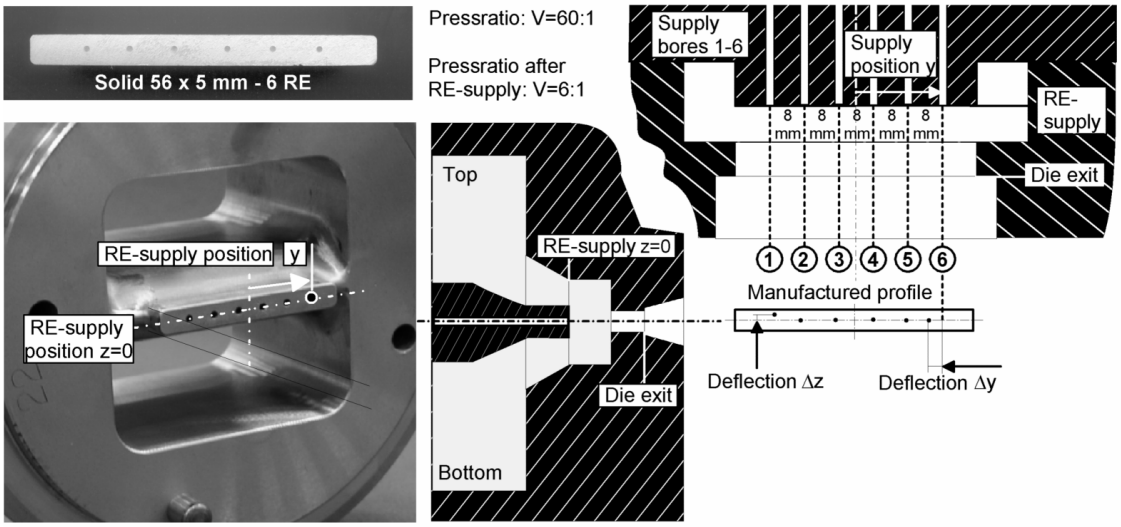

Fig. 5: Geometry of the welding chamber

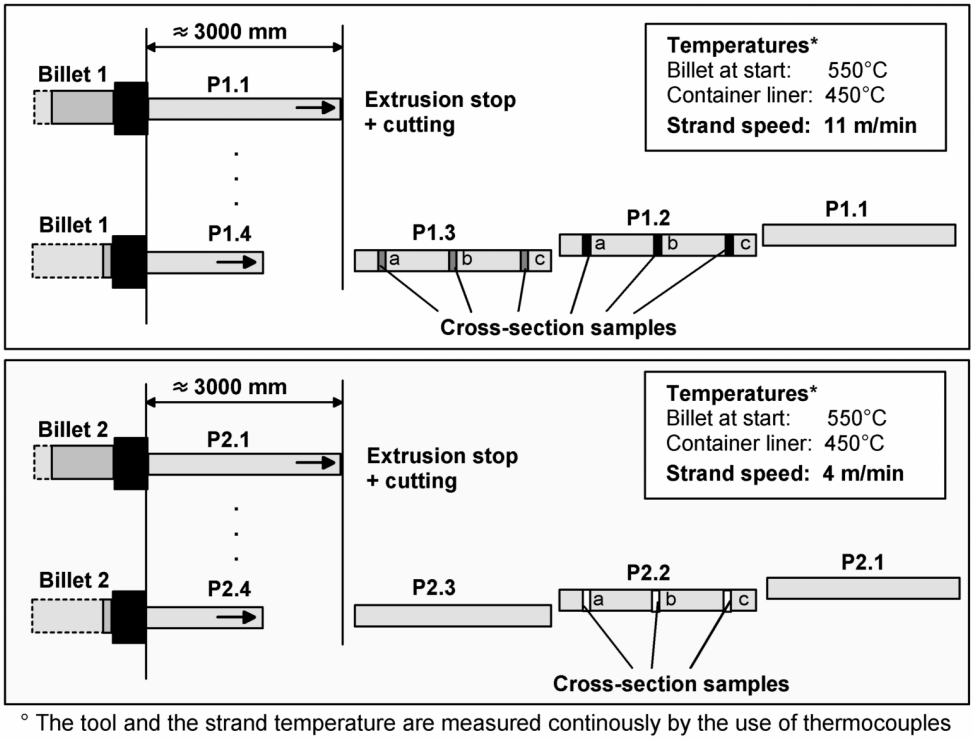

° The tool and the strand temperature are measured continously by the use of thermocouples

Fig. 6: Experimental procedures

To determine the influence of the tool temperature in composite extrusion, the tool used was equipped with two thermocouples (TC) on the front side of the exit. The strand temperature was measured by a sliding thermocouple, about 250 mm behind the die exit. Fig. 6 shows the experimental procedures concerning the determination of the temperature influence on the positioning of the reinforcing elements. During the manufacturing of the profiles a continuous length of about 3000 mm was extruded, then the press was stopped and the strand was cut. In order to investigate the influence of the extrusion speed in addition to the temperature influence, experiments with extrusion speeds of 4 and 11 m/min were carried out. To acquire the quantitative effects of the temperature differences and the extrusion speeds on the element positioning, cross-section samples (*CS*) were taken from the beginning (*a*), the middle (*b*), and the end (*c*) of the manufactured strands. The deflections of the reinforcing elements were analyzed by an optical measurement system (Optomess).

Experimental Results

Temperature Developments During Extrusion. Before starting the pressing, the temperature difference between thermocouple 1 and thermocouple 2 was about 25°C. Additionally, a video thermografical photograph was taken before the experimental pressing. The results of the thermografical photograph were in compliance with the measurements of the two thermocouples.

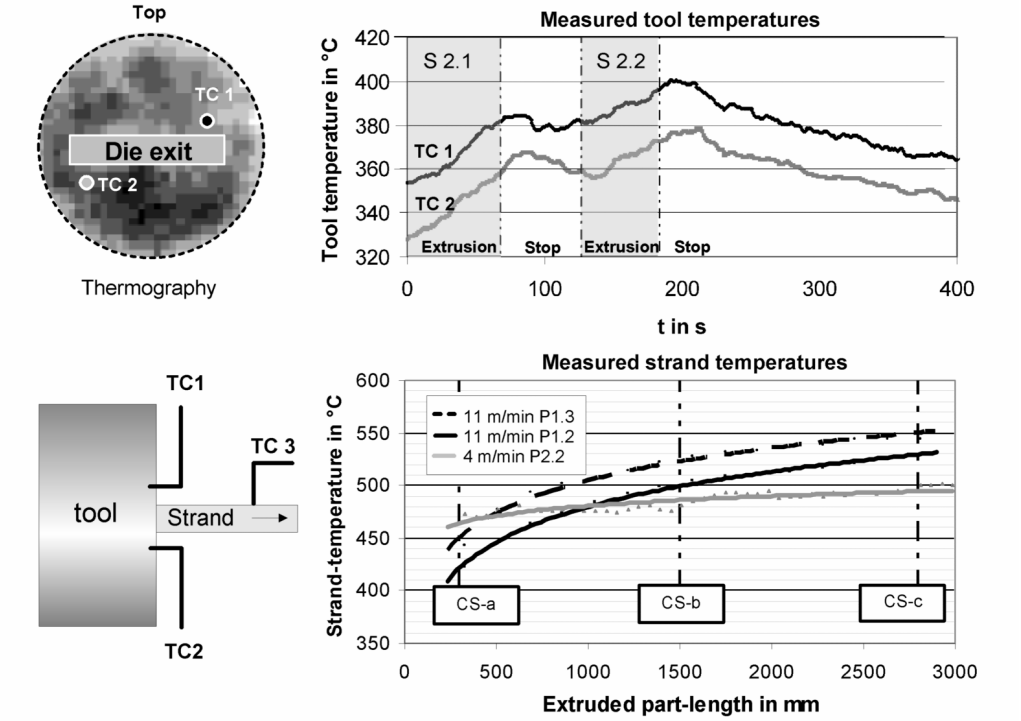

Fig. 7: Measured tool and strand temperatures

The tool temperature increases during extrusion, which can be attributed to the induced forming energy and to the hotter billet material that is pushed into the forming area. Further, it was recorded that the tool temperature decreases while the press is stopped, see fig. 7. This can be explained by the heat drain from the tool into the cold backup plate. The initial tool temperature increase after stopping the press could likely be attributed to a delayed heating behavior of the tool. During the process the absolute temperature level changes significantly, but the relative difference between the measurements of thermocouple 1 and thermocouple 2 remains basically constant. The reasons for the temperature differences in the tool will be subject of further investigations.

The strand temperature increases with the extruded length. As a result of the inserted forming energies, the temperature increase is steeper at a higher extrusion speed than at a low extrusion speed, see fig. 7. Table 1 shows the measured temperatures at the beginning and after the manufacture of the profile segments.

Part	Place of measurement	Measured temperatures in °C		
		Beginning	End	Temp.-rise
1.2	Tool upper TC	392	404	12
(11 m/min)	Tool lower TC	370	384	14
	Difference upper/lower TC	22	20	
	Strand	420	520	100
1.3	Tool upper TC	404	414	10
(11 m/min)	Tool lower TC	382	394	12
	Difference upper/lower TC	22	20	
	Strand	450	543	93
2.2	Tool upper TC	383	400	17
(4 m/min)	Tool lower TC	357	378	21
	Difference upper/lower TC	26	22	
	Strand	465	501	36

Table 1: Measured temperatures at the beginning and after the part manufacture

Cross-Section Analysis. Fig. 8 shows the deflections Δy and Δz of the reinforcing elements in dependency of the supply position y. As determined in the temperature measurements, the absolute temperature level of the tool changes significantly during extrusion, but the relative difference between the measurements of thermocouple 1 and thermocouple 2 remains basically constant. Under the constraint that such a temperature difference of the tool causes a temperature difference of the billet material in the inlets and the welding chamber, varying flow stresses of the forming material would result. Varying flow stresses, in turn, would lead to an inhomogeneous velocity allocation. As a result, a downward offset of the longitudinal weld seam as well as of the wire positions can be expected. The expected offset is confirmed by the analysis of the cross-sections. The measured values vary up to +/- 0.1 mm around an average value of about 0.3 mm, see fig. 8. The difference in the tool temperatures is a likely reason for this fact, but effects of other influencing factors, which are still unidentified, cannot be excluded.

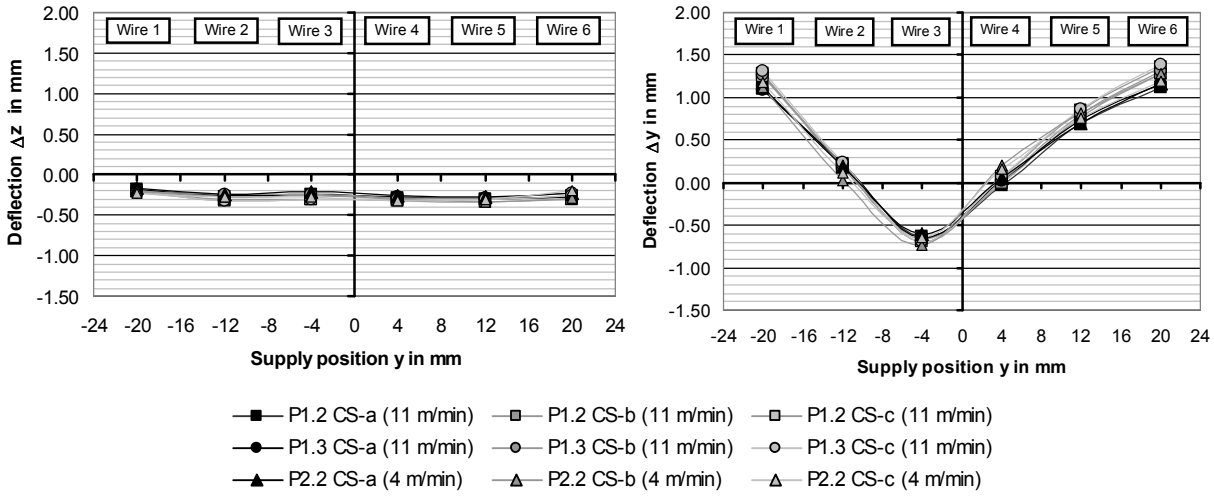

Fig. 8: Measured deflections

However, the asymmetric characteristics in vertical direction are not clearly explainable, but the tolerances of the supply bores have to be taken into account.

The measured deflections vary within a range of 0.3 mm. To investigate the influence of the temperature on the element position, fig. 9 shows the horizontal deflection of the wires 1-6 in dependency on the measured temperatures. Especially concerning the outer wires 1, 5, and 6, a definite correlation between the temperature and the deflection could be noted. The deflections increase with rising temperatures. Under the test conditions, a temperature difference of about 100 °C leads to a change of the deflections of about 0.3 mm. The influence of the strand speed appears to be of marginal importance. Concerning the same strand temperature, a three times higher extrusion speed only causes a positioning difference of about 0.1 mm in the experiments.

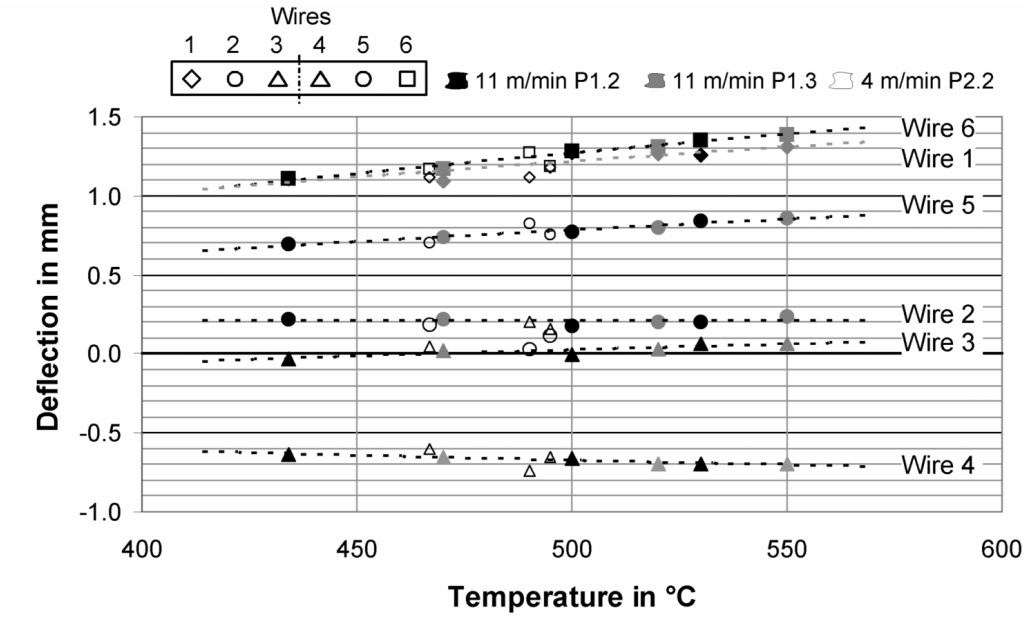

Fig. 9: Horizontal deflections in dependency on the strand temperature

Conclusions and Outlook

The experimental results show that the supply position and the forming temperature have a direct influence on the positioning of the elements in the manufactured composite profile. The effects of the temperature can be divided into two different cases. Firstly, a constant temperature gradient of the pressing tool likely leads to a constant average deflection of the longitudinal weld seam and the embedded reinforcing elements. Presumably, it is possible to compensate this effect by corresponding tool modifications, for example calculated offsets of the supply bores and an adjusted design of the material inlets, respectively. A more flexible option is the use of gradually heated pressing tools, particularly with regard to the second case of temperature influence, i.e. the deviations in the positioning, which are caused by fluctuations of the temperature during the extrusion process. The experiments showed that an increase in the temperature during the extrusion process leads to a deviation concerning the horizontal positioning of the reinforcing elements. This effect could be compensated by a continuous and isothermal extrusion process, which requires the use of tapered billets, i.e. with a gradual temperature allocation. Recapitulating, a defined temperature control appears to be necessary for composite extrusion, if a precise positioning is demanded. A temperature control to achieve a high positioning accuracy will be examined more closely within the scope of further research on composite extrusion.

Acknowledgement

This paper is based on investigations of the Transregional Collaborative Research Centre SFB/TR10 which is kindly supported by the German Research Foundation (DFG).

References

[1] Klaus, A.; Schomäcker, M.; Kleiner, M.: *First Advances in the Manufacture of Composite Extrusions for Lightweight Constructions*. Light Metal Age Vol. 62 (2004), No. 8. pp. 12-21

[2] Kleiner, M.; Klaus, A.; Schomäcker, M.: *Verbundstrangpressen.* Aluminium, International Journal for Industrie, Research and Application, Vol. 80/ 12 (2004), pp. 1370-1374

[3] Aluminium Walzwerke Singen: *Verfahren zur Herstellung von Verbundprofilen sowie Vorrichtung zu dessen Durchführung*, German Patent Application Publication DT 2414178 A1, 23.3.1974

[4] Kleiner, M.; Schomäcker, M.; Schikorra, M.; Klaus, A.: *Manufacture of Continuously Reinforced Profiles Using Standard 6060 Billets.* Extrusion Technology 2004, Orlando, USA

[5] Mier, G.: *Composite bus conductors aluminium-steel for metropolitan railways and underground trains (in German).* Schweizer Aluminium Rundschau, Vol. 37 (1987) Issue 5, pp. 12-17

[6] Weidenmann, K.; Schomäcker, M.; Kerscher, E.; Löhe, D. ; Kleiner, M.: *Composite extrusion of aluminium matrix specimens reinforced with continuous ceramic fibres*. Light Metal Age, October 2005, pp. 6-10

[7] Weidenmann, K.; Kerscher, E.; Schulze, V.; Löhe, D.: *Grenzflächen in Verbundstrangpress-profilen auf Aluminiumbasis mit verschiedenen Verstärkungselementen*. Prakt. Met. Sonderband 37, 2005, pp. 131-136

[8] Kleiner, M.; Schomäcker, M.; Schikorra, M.; Klaus, A.: *Herstellung verbundverstärkter Aluminiumprofile für ultraleichte Tragwerke durch Strangpressen*, Materialwissenschaft und Werkstofftechnik 35 No.7, 2004, pp. 431-439

[9] Tillmann, W.; Vogli, E; Weidenmann, K.; Fleck, C.: *Reinforced lightweight composite materials*. Proc. of ITSC 2005, Basel

[10] Flitta, I.; Sheppard, T.: *Nature of friction in extrusion process and its effect on material flow.* Materials Science and Technology, Vol. 19, July 2003, pp. 837-846

doi:10.4028/www.scientific.net/AMR.10.23

Mechanical properties of compound-extruded aluminum-matrix profiles under quasi-static loading conditions

Kay André Weidenmann[1,a], Eberhard Kerscher[1,b], Volker Schulze[1,c] and Detlef Löhe[1,d]

[1]Institut für Werkstoffkunde I, Universität Karlsruhe (TH), Kaiserstr. 12, 76131 Karlsruhe, Germany

[a]weidenmann@iwk1.uka.de, [b]kerscher@iwk1.uka.de,
[c]schulze@iwk1.uka.de, [d]loehe@iwk1.uka.de

Keywords: Structural materials, Compound extrusion, Mechanical properties, Tensile tests, Compression tests

Abstract. Compound-extruded unidirectionally reinforced lightweight profiles are a novel class of materials for the realisation of load-bearing structures. They may be fabricated in a flexible and rapid near-net-shape process. The authors present investigations of the reinforcing effect of wires in compound-extruded aluminum profiles under quasi-static tension and compression. In particular, the compounds were characterized by metallographic examinations focusing on the fracture morphology. Furthermore, specimens subject to compression tests were examined using micro computer tomography (μ-CT) and light microscopy (LM). It is shown, that the mechanical properties of wire-reinforced profiles are improved under both positive and negative quasi-static loads in comparison to non-reinforced profiles.

Introduction

Light-metal matrix compounds are considered to be an innovative material for lightweight structures for different applications such as aircraft and vehicle space-frames, railway carriages and ropeway cars. Compound extrusion is a recently rediscovered process representing a flexible technique for rapid in-line production of unidirectionally reinforced lightweight profiles [1]. The compound extrusion technology was originally developed in the 1970s in order to facilitate the production of compound conductor rails for subway systems combining the functional properties of the individual components, such as electric conductivity and wear resistance [2-4]. The investigation of mechanical properties focused primarily on the adhesive strength of the cladded steel ribbon, as the mechanical reinforcing effect under tensile or compressive load played a minor role for the aspired application. Therefore, no further investigations on the mechanical properties of compound-extruded compounds under quasi-static loading conditions, which may be used for predicting the functionality of weight-bearing structures composed of compound-extruded profiles, were done. A systematic materials selection process was performed by the present authors to provide a list of preferable material combinations suitable for the compound extrusion process and, additionally, featuring good mechanical properties [5]. In addition to ropes, reinforcing wires made from stainless spring steels as well as nickel- and cobalt-based alloys were embedded in an aluminum alloy having a prominent extrudability turned out to be a promising solution.

Model for the Mechanical Behavior of Composites

Kelly [6] proposed a model to describe the reinforcement of light metals by reinforcing elements of high strength. This model is based on the parallel orientation of continuous fibres in a surrounding matrix. It is only adaptive for uniaxial stress states because the external load is supposed to be applied in the fibres' direction. While these demands are met by the specimen geometry, the

investigated samples represent a composite's unit cell with only one reinforcement surrounded by matrix material and so there is no regular distribution of the reinforcing elements. Hence, the composite's stress state is extremely inhomogeneous. Nevertheless, Kelly's model is used for the calculation of the expected mechanical behaviour of the compound from the data of the matrix and the reinforcement, though the internal stress state of the tensile specimen is homogenised and the model is rather simplified. The resulting strains for matrix, reinforcing element, and compound are assumed to be the same and the stress on the compound consists of the average stress on the matrix and the reinforcing elements, according to the volume fraction of matrix and reinforcement, V_M and V_F

$$\sigma_C = \sigma_F V_F + \sigma_M V_M \,. \tag{1}$$

In this correlation, σ_C, σ_F and σ_M represent the stresses in the compound, the reinforcing elements, e.g. fibres, and the matrix material, respectively, disregarding inhomogeneities of the internal stress distribution inside the matrix and the reinforcement. The corresponding stress-strain-diagram of the compound is characterized by four distinct regions [7] (see Fig. 1, left).

- Matrix and reinforcing elements are stressed elastically.
- The matrix material is deformed plastically while the deformation of the reinforcing elements is still elastic.
- Matrix and reinforcing elements are plastically deformed.
- The reinforcing elements are broken and the specimen fails after reaching the failure strain of the remaining matrix [8].

Regarding structural applications under tensile load, the first two stages are all dominant. The third stage degenerates, if the reinforcing elements remain predominantly elastic and break in a brittle manner.

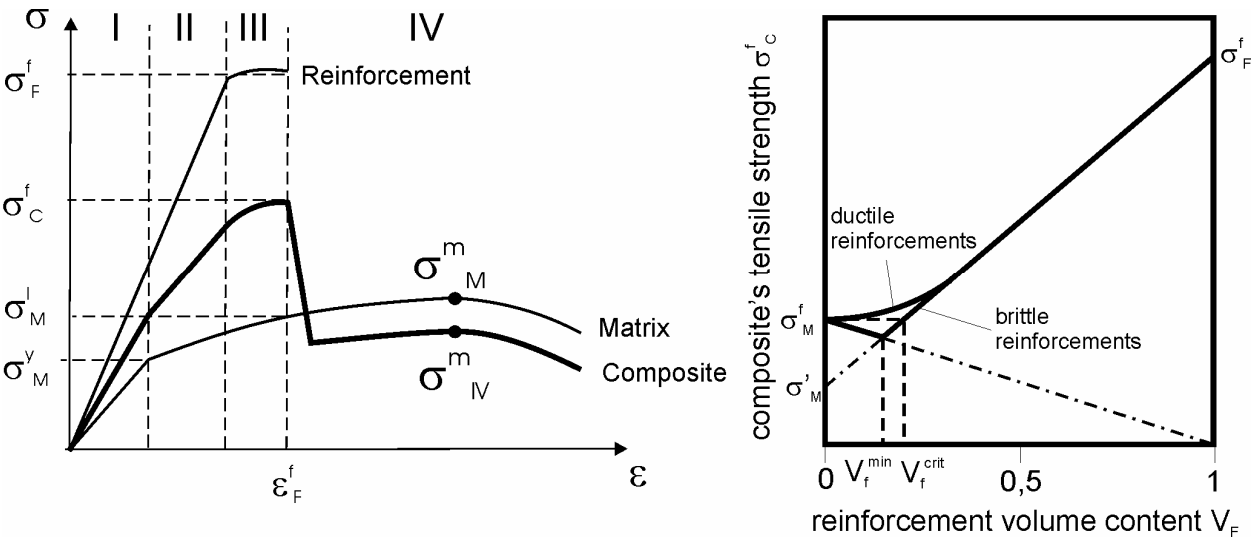

Fig. 1: Schematic stress-strain diagram for a compound owing a ductile matrix and reinforcements calculated from the mechanical behaviour of its components (left), correlation between reinforcement volume content and compound's tensile strength (schematic) revealing the difference between brittle and ductile reinforcing elements (right).

The model also allows the calculation of the elastic modulus of the compound in stage 1 using

$$E_C^I = E_F V_F + E_M V_M . \quad (2)$$

In spite of the plastic deformation of the matrix, the compound can also be used in stage 2 for structural applications. After releasing the external load, the reinforcing element is unloaded elastically with the matrix being compressed plastically. Hence the mechanical behaviour is referred to as quasi-elastic. This state occupies most of the curve in real stress-strain diagrams of composites. Within this stage the modulus of the composite is given by

$$E_C^{II} = E_F V_F + \left(d\sigma_M / d\varepsilon\right)_\varepsilon V_M . \quad (3)$$

The differential coefficient describes the slope of the stress-strain curve and is smaller than 1% of E_M for most matrix materials. If the reinforcement shows significant plastic deformation, this stage is followed by stage 3 with the matrix and the reinforcement deforming plastically.
The transition from stage 2 or 3, respectively, to stage 4 is marked by the tensile strength of the compound

$$\sigma_C^f = \sigma_F^f V_F + \sigma_M^I V_M , \quad (4)$$

which is of vital importance. σ^f_F is the fracture strength of the reinforcing elements, σ^I_M indicates the stress in the matrix material at the strain, at which the reinforcing elements break. This relation allows the assessment of the compound's ultimate tensile strength, even if the reinforcement shows some degree of plastic deformation. A minimum volume content of the reinforcing elements restricts the validity of Eq. 4. However, the minimum fiber content in aluminum matrix compounds is generally well below 10 % [7]. As this study concentrates on compounds with fibre contents of approx. 11 %, this presents no serious limitation and the data experimentally acquired may be compared with Kelly's model.

Fig. 1 (right) shows the relationship between content of reinforcing elements and the ultimate tensile strength of the compound using Kelly's model. The schematic curve progression for compounds using ductile reinforcing elements, e.g. metal ropes or wires, is depicted. As Kelly's model disregards stress states perpendicular to the fibre axis, the mechanical interaction between matrix and reinforcing elements is not accounted for. This may cause an underestimation of the effective compound's tensile strength. On the contrary, relaxation processes taking part in the reinforcing element may mar its mechanical behaviour. In this regard, the loss of strength due to the formation of interfacial phases affecting the adhesion or degrading the fibre have to be kept in mind.

Material and Experimental Setup

First investigations of the mechanical properties of compound-extruded reinforced aluminum matrix compounds focus on the behavior at quasi-static loading. The matrix material was the aluminum alloy 6060 (AlMgSi0,5), which is a state-of-the-art material for extrusions used in automotive space frames. The incorporated reinforcing wires were made from the nickel-base alloy Inconel 718 (2.4668), austenitic spring steel X10CrNi18-8 (1.4310) and cobalt-base alloy Haynes 25 (2.4964). Additionally, a rope in 1x7-construction made from X10CrNi18-8 was also incorporated. All reinforcements had a diameter of 1 mm. Previous investigations on wire-reinforced profiles have shown that various surface treatments of the reinforcements have major influence on the interfacial debonding shear strength [9]. Therefore, all the reinforcements' surfaces

were cleaned with acetone (initial state) and some of the reinforcing wires were pickled or ground in addition to cleaning prior to the extrusion process. The compound-extruded profiles with a rectangular cross-section of 56x5 mm^2 containing 6 wires regularly distributed along the longitudinal weld seam were produced on a 10 MN extrusion press at a billet temperature of 550 °C and a total press ratio of 60:1 [10]. Furthermore, non-reinforced profiles were extruded, which is referred to as sample state M1. All profiles were quenched with compressed air as well as fan-cooled on cooling tables and subsequently naturally aged resulting in a T4 heat treatment state. Table 1 gives an overview on the materials combinations and the reinforcements' surface states.

sample type	reinforcement type and material	reinforcement pre-treatment
S1	austenitic spring steel wire, 1.4310	ground
S2	austenitic spring steel wire, 1.4310	initial state
S3	austenitic spring steel wire, 1.4310	pickled (stainless steel pickle)
C1	cobalt-base alloy wire, Haynes 25	ground
C2	cobalt-base alloy wire, Haynes 25	initial state
N1	nickel-base alloy wire, Inconel 718	ground
R2	austenitic spring steel rope, 1x7 1.4310	initial state
M1	-	-

Table 1: Overview on the specimen types investigated, including the reinforcements and their pre-treatment

The present stage of compound extrusion technology only allows for the production of profiles having a reinforcement content significantly below 10 %, which shall be deemed to be a realistic research objective. Therefore, the reinforcement content was increased by turning the specimen to a gauge diameter of 3 mm containing one reinforcing element at its centre. In doing so, the effective reinforcement content in the gauge was 11 %. Fig. 2 shows the specimen geometry for the tensile and compression tests.

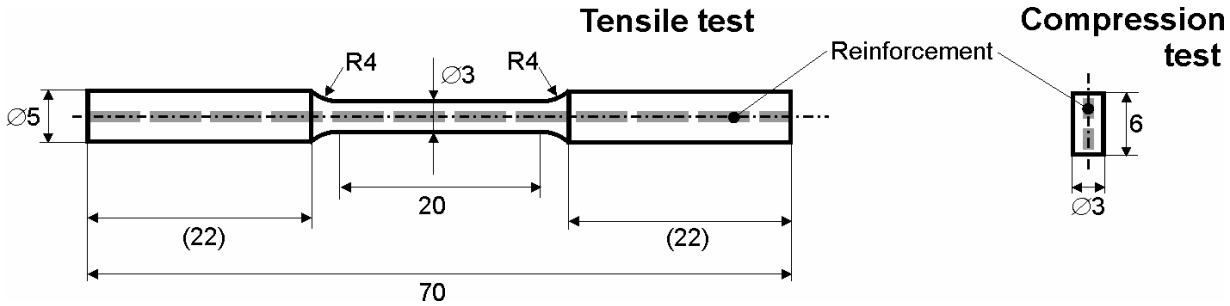

Fig. 2: Specimen geometry for tensile (left) and compression tests (right) with dimensions in mm.

The tensile tests were carried out on a universal testing machine with a maximum load of 200 kN. The samples were clamped by mechanical grips. The deformation was registered with a strain gauge up to a total strain of 2 % and simultaneously determined from the crosshead displacement. The compression tests were carried out on a universal testing machine with a maximum load of 500 kN using a capacitative extensometer for strain registration. Starting from an initial sample height of about 6 mm, the samples were unloaded after reaching a total strain of 33 %. Both mechanical tests were traverse path controlled at a constant strain-rate of $d\varepsilon/dt = 0.05\ min^{-1}$ ($8 \cdot 10^{-4}\ s^{-1}$).

The mechanical characterization was complemented by SEM investigations of broken specimens, focusing on the fracture surfaces and the reinforcement-matrix interface. Investigations of the deformation behaviour under compressive stress were carried out on a X-ray µ-CT in cooperation with RJL Micro and Analytics GmbH, Karlsdorf-Neuthard. The maximum resolution

was 2x2x2 μm^3. Additionally, non-reinforced compression samples were subject to metallographic examination using light microscopy.

Results and Discussion

Tensile tests on reinforced compound-extruded specimens. Fig. 3 shows the stress strain curves for the spring steel reinforced specimens with different reinforcement geometries and pre-treatments in comparison to the non-reinforced specimen type M1. Table 2 summarizes the mechanical properties of the different sample types.

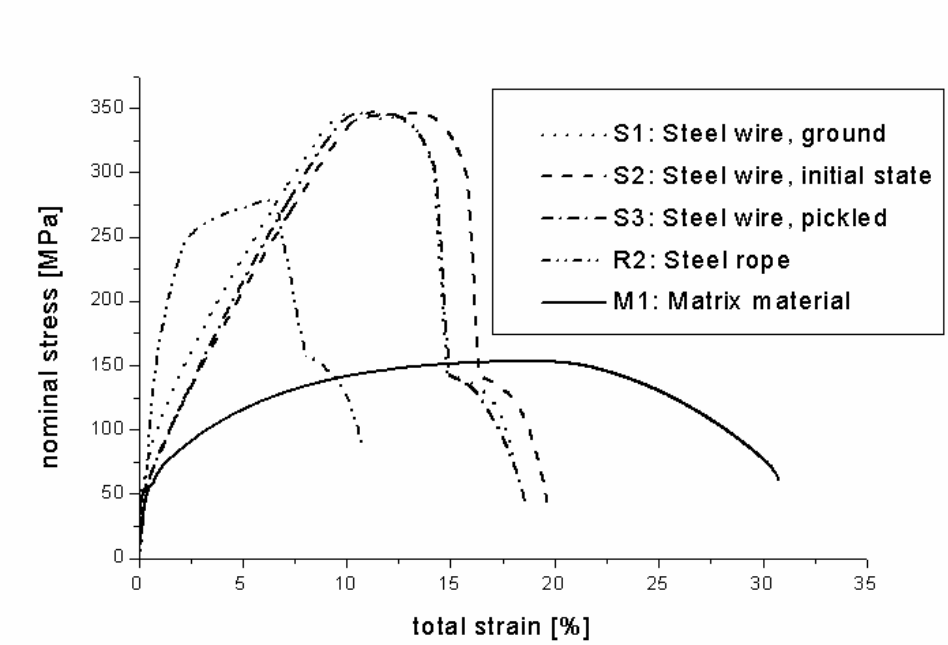

Fig. 3: Stress strain curves for the spring steel-reinforced specimens featuring different reinforcement geometries and pre-treatments in comparison to the matrix material.

state	Young's modulus E^I_C [GPa]	Modulus E^{II}_C [GPa]	σ^f_C [MPa]	total strain at fracture of the reinforcement [%]	total strain at fracture of the compound [%]
S1	83	26,5	342	14,8	18
S2	83	26,5	346	16,0	19
S3	81	26,2	345	15,4	18
R2	77	-	278	6,6	11
M1	72	-	157	-	31

Table 2: Mechanical properties of the spring steel reinforced specimens with different reinforcement geometries and pre-treatments in comparison to the properties of the matrix material

As expected the Young's modulus of the matrix material is about 70 MPa. The modulus of the compound is increased when using reinforcements made from austenitic spring steel with a Young's modulus of approximately 185 GPa. For the wire reinforced specimens, the compounds' moduli E^I_C are in good accordance with the value calculated from Eq. 2 as presented in table 3. For the rope reinforced sample, the Young's modulus is significantly lower by reason of the rope construction with the reinforcing wires not being parallel to the loading direction. On the other hand, the expected stiffness loss in stage 2 is by far less pronounced for R2 in comparison to the wire-reinforced materials but successively increasing. This may be due to the fact that continuously enhancing the load applied on the compound and the reinforcing element, respectively, leads to

twisting effects in the rope and therefore to a multiaxial stress state, which significantly influence the deformation behaviour of the compound. In contrary, for the wire-reinforced sample types, the modulus E^{II}_C is again in good accordance with Kelly's model (see table 3). Regarding the ultimate tensile strength of the compound σ^f_C which is marked by a sudden stress drop due to fracture of the incorporated reinforcement, the overall increase is about 120 % for the wire-reinforced specimens and 77 % for the rope-reinforced specimen in comparison to the ultimate tensile strength of the matrix material. The difference is due to the filling grade of the 1x7 rope, which is about 76 % compared with 100 % for the wire. The calculated values for σ^f_C based on an ultimate tensile strength of 1340 MPa for the rope and of 2000 MPa for the spring steel wire.

state	Young's modulus E^I_C [GPa]	theor. value acc. to Eq. 2 $E^I_{C,theo.}$ [GPa]	Modulus E^{II}_C [GPa]	theor. value acc. to Eq. 3 $E^{II}_{C,theo.}$ [GPa]	σ^f_C [MPa]	theor. value acc. to Eq. 4 $\sigma^f_{C,theo.}$ [MPa]
S1	83	82,7	26,5	20,4	342	345
S2	83	82,7	26,5	20,4	346	345
S3	81	82,7	26,2	20,4	345	345
C1	80	87,1	25,2	24,8	317	312
N1	85	84,3	29,1	22,0	293	279
R2	77	82,7	-	-	278	284
M1	72 (E)	-	-	-	157 (R_m)	-

Table 3: Mechanical properties of the reinforced specimens with different reinforcement geometries and pre-treatments in comparison to the calculated values using Kelly's model

Considering the weight increase of the reinforced specimens of 20 %, the increase of the specific ultimate tensile strength of the compounds is about 48 % (R2) and 80 % (S1, S2 and S3), respectively. Due to comparable specific Young's moduli for spring steel and aluminum both wire- and rope-reinforced compounds show no increase in specific Young's modulus E/ρ. In comparison to the matrix material and in contrast to the prediction according to Kelly's model, the total strain at fracture of the reinforced specimens is significantly reduced. This reduction has already been investigated by the present authors [11] and is due to the strain localisation after the fracture of the reinforcement for specimens containing one single reinforcing element. Furthermore, comparing the total strains at fracture of the reinforcement for S1, S2 and S3, it is evident, that S2 shows a higher value than the types S1 and S3 both bearing a mechanically or chemically pre-treated reinforcement. Investigations of the interfacial properties [9] have revealed that ground or pickled spring steel wires offer an increase in the debonding shear strength. Hence, the debonding process taking place in stage 3 of the stress-strain curve parallel to the plastic deformation of the wire should be more localised for S2 and S3 leading to a decrease of the total strain at fracture of the reinforcement. Admittedly, the changes are rather qualitative than quantitative as both pre-treatments grinding and pickling lead to the same debonding strength increase of approximately 50 % in comparison to the ground state and should therefore lead to the same decrease in total strain reduction at the fracture of the reinforcement, which is only tendentiously the case. This effect is also evident for the sample states C1 and C2 presented in Fig. 4. The ground sample type C1 reveals a lower debonding shear strength in push-out-tests. Consequently, the total strain at fracture of the reinforcement is increased in comparison to C2 (initial state).

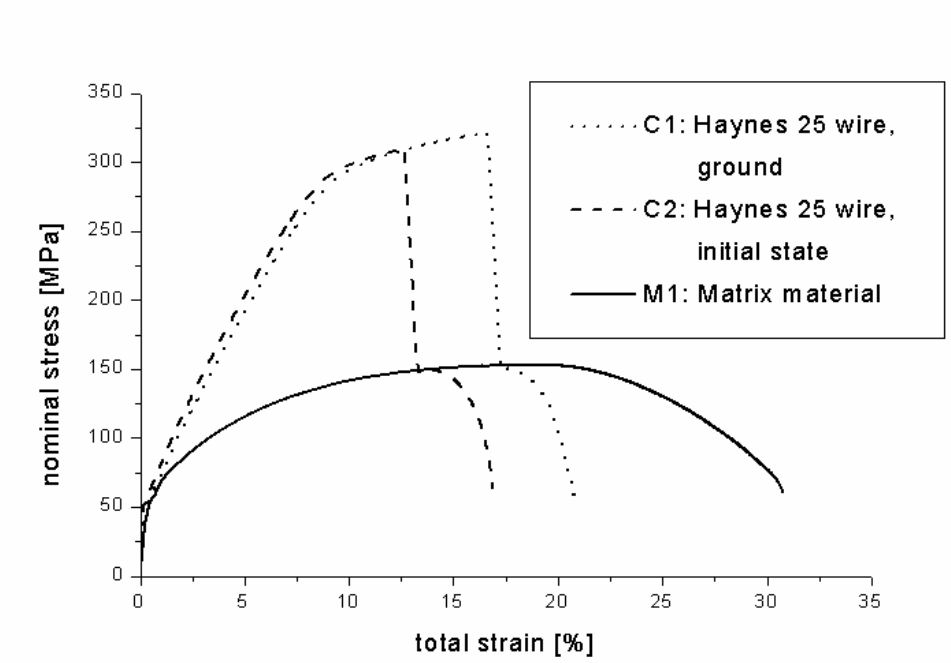

Fig. 4: Stress strain curves for the cobalt-base-wire-reinforced specimens featuring different reinforcement pre-treatments compared with to the non-reinforced specimen type M1.

Fig. 5 shows the stress-strain curves for the wire-reinforced specimens using different reinforcement materials in comparison to the non-reinforced specimen type M1.

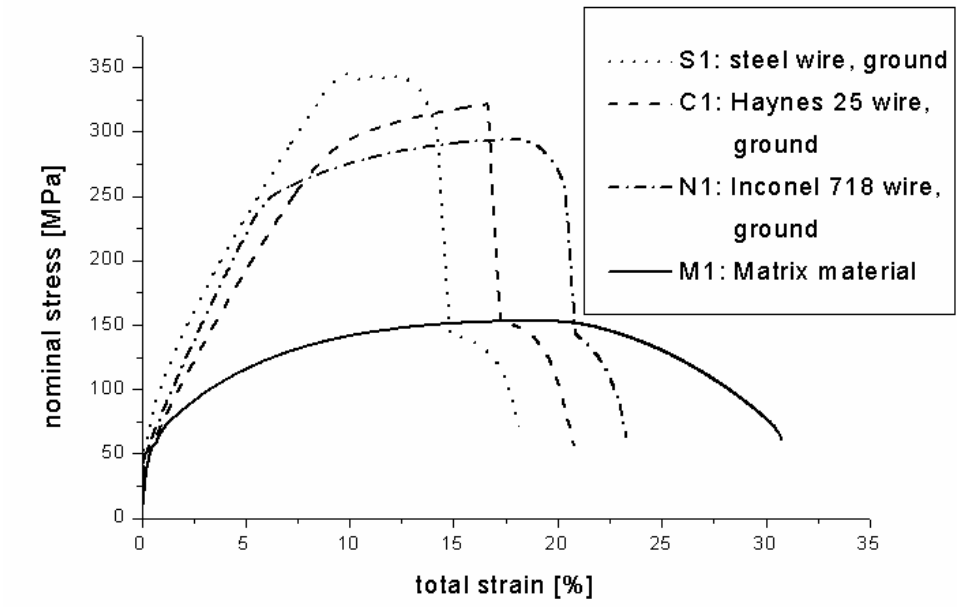

Fig. 5: Stress strain curves for the wire-reinforced specimens with different reinforcement materials compared with the matrix material M1.

All the compounds have the same curve progression mirroring the four stages according to Kelly's model except the above-mentioned effect of ultimate strain reduction. The sudden stress drop for sample type C1 without previous stress declination indicates a sudden fracture of the cobalt-base wire without necking. Table 4 summarizes the mechanical properties of the compounds S1, N1 and C1. For the sake of clarity, the properties of M1 are listed once again.

sample type	Young's modulus E^{I}_{C} [GPa]	Modulus E^{II}_{C} [GPa]	σ^{f}_{C} [MPa]	total strain at fracture of the reinforcement [%]	total strain at fracture of the compound [%]
S1	83	26,5	342	14,8	18
C1	80	25,2	317	15,5	20
N1	85	29,1	293	21,4	24
M1	72	-	157	-	31

Table 4: Mechanical properties of the spring steel reinforced specimens featuring different reinforcement geometries and pre-treatments in comparison to the properties of the matrix material

Young's moduli and ultimate tensile strengths are in good agreement with calculated values using Kelly's model again, which is shown in table 3. The theoretical values for σ^{f}_{C} for C1 and N1 with an assumed ultimate tensile strength of the reinforcing wires of 1700 MPa and 1400 MPa, respectively, are validated by the experimental results. Nevertheless, the calculation partially underestimates the measured values, which indicates the remarkable interference of debonding processes taking place at the wire-matrix interface, which is not considered in Kelly's model [7]. Compared with S1, the increases in specific strength are lower for C1 (68 %) and N1 (55 %).

For all tensile tests the measured total strain at fracture of the reinforcement is significantly higher in comparison to the total strain at fracture for the non-embedded reinforcements being far below 10 %. Investigations on the residual stress state in rope-reinforced profiles have revealed that the matrix material underlies tensile stresses in longitudinal direction, i.e. parallel to the reinforcements, and compressive stresses in radial directions around the cross-section of the reinforcement [12]. Since the reinforcement has to compensate this residual stress state, compressive stresses in longitudinal direction and tensile stresses in radial direction are expected. This multi-axial stress state obviously influences the deformation behaviour of embedded reinforcements and leads to an increase of the total strain at fracture.

Investigations on fractured specimens. The above discussed interfacial effects were investigated by analysing the fracture surface of the tested specimens using SEM. Fig. 6 presents exemplary micrographs of fracture surfaces for different types of wire-reinforced compounds.

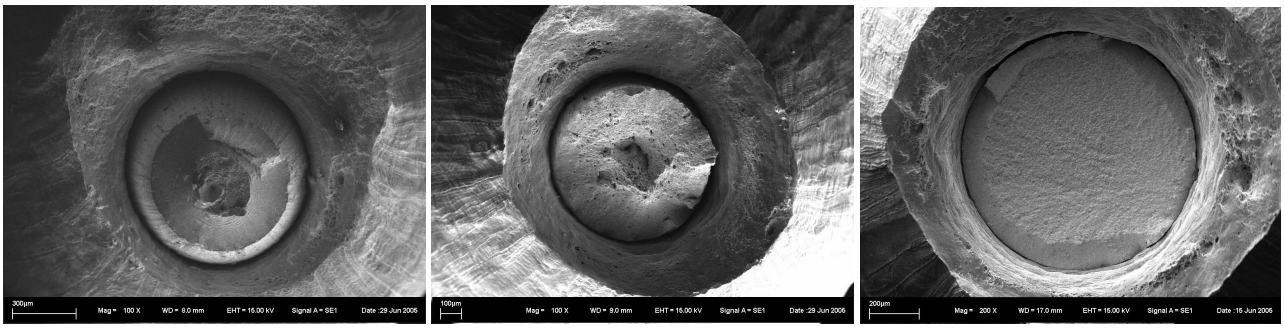

Fig. 6: SEM micrographs of fractured tensile specimens for the sample states S1 (left), N1 (centre) and C1 (right)

The micrographs reveal the differences in deformation behaviour of the reinforcements. While the steel wire shows a pronounced (S1) and the nickel-base wire at least a significant necking (N1), the cobalt-base wire shows no necking at all (C1). Looking at the gap between reinforcing wire and matrix material at a higher magnification (see Fig. 7), it is obvious that aluminum is bonded on the wire surface (S1) and the matrix extrusions at the interface have been formed during the debonding process.

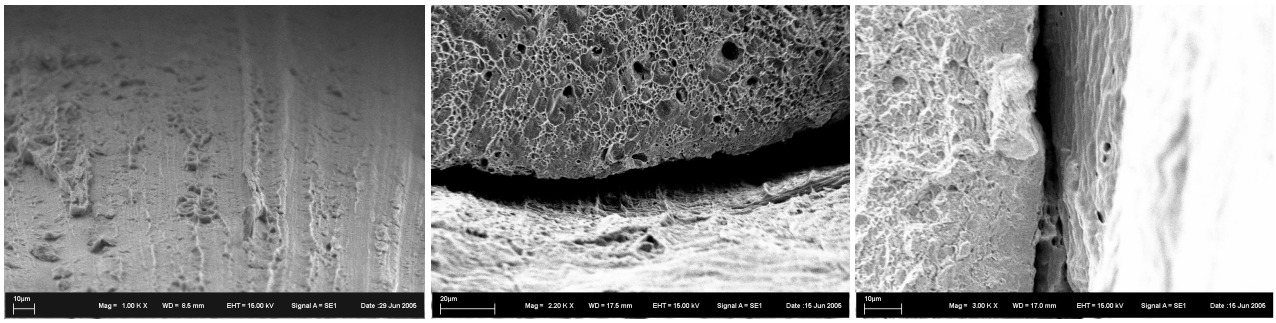

Fig. 7: SEM micrographs of fractured tensile specimens for the sample states S1 (left), N1 (centre) and C1 (right), focusing on the wire's surface (S1) and the gap between matrix material and wire (N1, C1).

The formation of such artefacts during the debonding verifies the excellent wire-matrix bonding, which the authors have already investigated and quantitatively measured in push-out-tests for incorporated wires having been subject to the same pre-treatments [9], although wires do not provide a form fit. The existence of a metallurgical bond additionally to a form fit for rope-reinforced compounds has also been accounted for [11,12]. The restriction of the debonding processes taking place in the compounds is responsible for the discrepancies between the experimental stress strain curves of the compounds and the theoretical curve progression predicted by Kelly.

Compression tests on reinforced compound-extruded specimens. For the sake of comparing the deformation behaviour of rope-reinforced as well as wire-reinforced samples with the matrix material under compressive load, compression tests using specimen type S2, R2 and M1 were carried out. Fig. 8 presents the compressive stress-strain curves. The curve progression is different to that obtained in tensile tests. Compared with the stress-strain curves determined from tensile tests showing a significant stiffness lost in stage 2 – at least for S2 – at stresses above approx. 70 GPa, all reinforced samples reveal a 0.2 % compressive yield strength above approx. 200 GPa. Furthermore, only M1 shows the well-known curve progression with a steady stress increase while the compressive stress strain curves of both reinforced samples exhibit a local stress maximum.

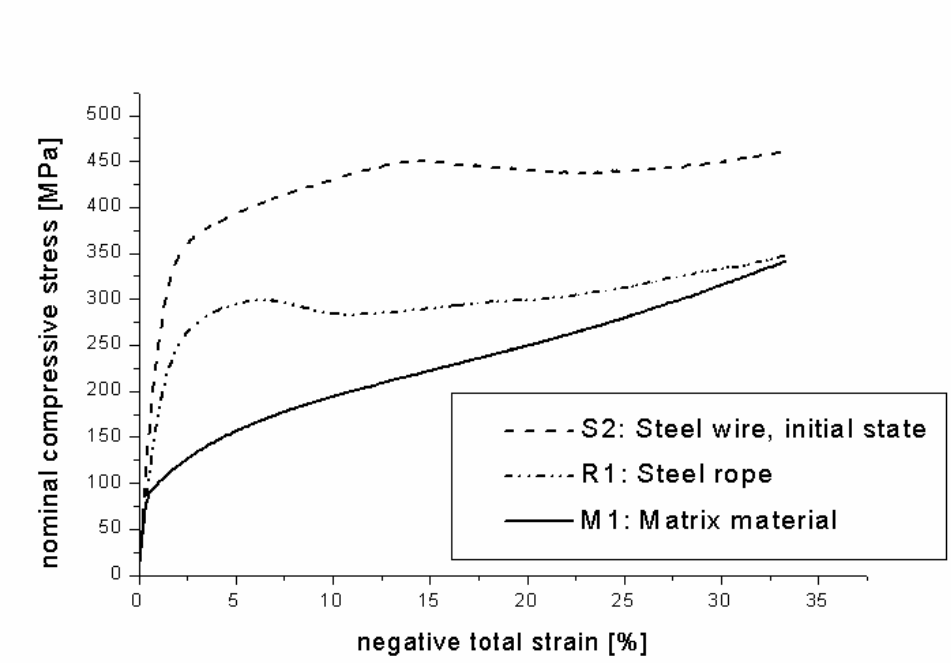

Fig. 8: Exemplary compressive stress-strain curves for the spring steel-reinforced specimens featuring different reinforcement geometries compared with the matrix material M1.

For M1 the 0.2 % compressive yield strength $\sigma_{0.2,comp}$ is 75 MPa. For S2, $\sigma_{0.2,comp}$ is about 219 MPa. For R2, the value averages out to 134 MPa. The local maxima in the stress-strain curves appear at 454 MPa (S1) and 284 MPA (R2), respectively. Correlating these stresses with the ultimate tensile strengths obtained from tensile tests results in an increase by 33 % and 2 %, respectively. The reasons for this local maximum and the consequential deformation behaviour are given below.

Metallographic examination of compression samples. Observing the in-situ sample deformation indicated that the local maximum in the stress-strain curve is a sign of failure of the reinforcement. In fact, this was verified by µ-CT examinations prior to and after deformation of the samples (see Fig. 9).

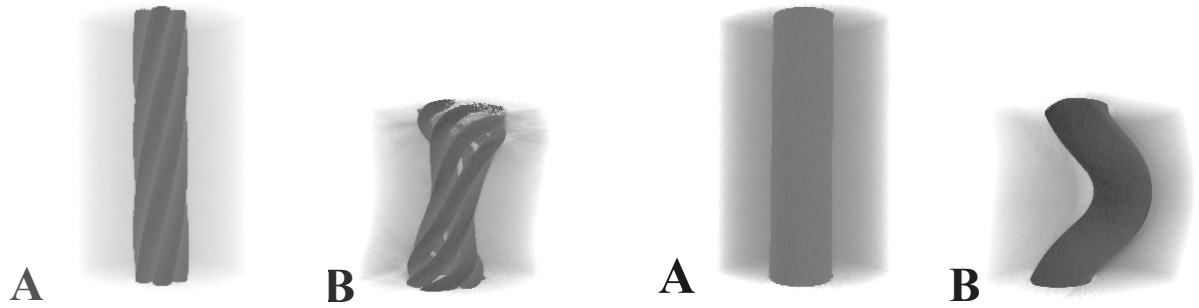

Fig. 9: Micro-computer tomographs of rope-reinforced (left) and wire-reinforced specimens (right) prior to (A) and after (B) the compression test

The deformation behaviour of the reinforcements depends on their geometry. Ropes fail by untwisting whereas the centre wire is loosened and falls out after the test. Thereby, the untwisting process is more pronounced at the end planes. In contrary, wires start bulging in the centre of the specimens prior to buckling, which can be seen from Fig. 9. Compression of the originally cylindric specimen of type M1 leads to an oval shape while normally the initial geometry should persist. Fig. 10 shows a micrograph of an etched specimen M1 after the deformation, which reveals the reason for this extraordinary deformation behaviour: The longitudinal weld seam in the centre of the sample has a hardening effect and constrains therefore the plastic flow of the material in one direction.

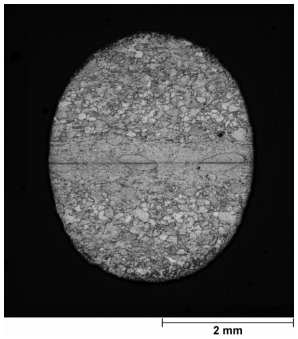

Fig. 10: LM-micrograph of a non-reinforced specimen M1 after the compression test. The specimen was etched using 1 % HF.

Summary and Conclusions

Reinforced aluminum matrix compounds and non-reinforced samples have been investigated regarding their mechanical properties and fracture surfaces. Considering the mechanical properties, both ropes and wires emerged to be a promising approach for compound-extruded profiles under

tensile load. Ropes or wires at a volume content of 11 % increase the ultimate tensile strength substantially when compared with non-reinforced specimens. Moreover, the specimens also showed good results under compressive loads. Correlating the experimentally determined compound tensile strength with calculations based on a simple model presented by Kelly [6] good coincidence could be shown; differences may be based on debonding processes at the reinforcement-matrix interface or are due to the specimens containing only one single reinforcement. Under compression, the failure stress for both rope- and wire-reinforced samples is higher than under tensile loads. Thereby, the increase in failure stress is more pronounced for wire-reinforced compounds. Nevertheless, neither ropes nor wires made from the chosen materials significantly increase the specific stiffness of the compounds. The existence of a metallurgical bond between reinforcement and matrix for compound extrusions has already been stated [9,11,12] and can be confirmed by the present results. Further investigations ought to focus on ceramic fiber-reinforced compounds, which are supposed to provide a substantial increase of specific stiffness.

Acknowledgements

This paper is based on investigations of the Transregional Collaborative Research Centre SFB/TR10, which is kindly supported by the German Research Foundation (DFG).

References

[1] M. Kleiner, M. Schomäcker, M. Schikorra, A. Klaus: Materialwissenschaft und Werkstofftechnik Vol. 35 [7] (2004), p. 431.

[2] A. Wagner, U. Hodel, in: *Neue Verfahren der Massivumformung*, Symp. der DGM, Bad Nauheim (1983)

[3] P. Furrer, R. Gitter, J. Maier, in: *Verbundwerkstoffe*, DGM-Verlag, Oberursel (1991)

[4] J.J. Theler, A. Wagner, A. Ames: Metall Vol. 30 [3] (1997), p. 223

[5] K.A. Weidenmann, C. Fleck, V. Schulze, D. Löhe: accepted for publication in Adv. Eng. Mat.

[6] A. Kelly: Metal. Rev. Vol. 10 [37] (1965), p. 1

[7] K.E. Saeger: Aluminum Vol. 46 [10] (1970), p. 681

[8] T.H. Courtney: Mechanical Behavior of Materials (McGraw-Hill, USA 1990)

[9] K.A. Weidenmann, C. Fleck, V. Schulze, D. Löhe, in: *Verbundwerkstoffe und Werkstoffverbunde*, edited by M. Schlimmer, DGM-Matinfo-Verlag (2005)

[10] M. Kleiner, A. Klaus, M. Schomäcker: Adv. Mater. Res. Vol. 1 (2006)

[11] K.A. Weidenmann, C. Fleck, V. Schulze, D. Löhe: submitted to Z. Metallkunde

[12] K.A. Weidenmann, C. Fleck, V. Schulze, D. Löhe: Materialwissenschaft und Werkstofftechnik Vol. 36 [5] (2005), p. 307

doi:10.4028/www.scientific.net/AMR.10.35

Flying Cutting of Spatially Curved Extrusion Profiles

J. Fleischer[1, a], C. Munzinger[1,b], G. Stengel[1,c]

[1]wbk Institute of Production Science, Universität Karlsruhe (TH),
Kaiserstraße 12, 76128 Karlsruhe, Germany

[a]fleischer@wbk.uka.de, [b]munzinger@wbk.uka.de, [c]stengel@wbk.uka.de

Keywords: Production Process, Control, Robot

Abstract The innovative process of curved profile extrusion facilitates the cost-effective production of lightweight structures with spatially curved profiles even for small series. Due to the extrusion process a continuous flow of material is unavoidable. The profiles have to be separated reactionlessly during the extrusion following the complex trajectory of the cut-off point in space. This paper discusses the challenges for a flying cut-off device. In addition to a concept to generate the trajectories and control the movements, the main parameters for dimensioning a cut-off device are presented. A specially designed clamping device permits to generate high accelerations. Further on, cutting results are shown especially for extruded sections with continuous reinforcing elements of steel.

Introduction

Applying the innovative process of "multiaxial curved profile extrusion" for the production of lightweight structures, some disadvantages of the conventional process chain including straight profile extrusion and subsequent bending, can be avoided [1]. The outline of the profiles is defined strictly kinematically and can be modified for each of them to achieve a high flexibility. Within the new process chain, the devices for the "Flying Cutting" work as link between the extrusion press and the following drilling and end machining processes. Two major tasks must be taken in consideration: During the curved profile extrusion the influences of the gravitational force and the mass inertia while accelerating have to be compensated. The second task is to separate the profiles and to transfer the cut-off parts to the following machining.

In [2] a process to cut off plane rounded profiles is introduced. Thereby, the cut-off point moves on a planar trajectory. In the case of spatially curved extruded profiles the end of the profile describes a complex trajectory in a stereoscopic space to be followed by the cut-off device. The overlaying profile has to be guided additionally against the influence of the gravitational force and the mass inertia during acceleration. One of the difficulties lies in avoiding reactions to the rounding process, e.g., by cutting forces. This would influence the contour accuracy of the profile severely. Furthermore, it must be pointed out that the extrusion press velocity is not accurately constant even if the ram velocity of the press can be controlled. This is essentially due to the elastic deformation of the press rack actuated through the non-constant backpressure, especially at the beginning and the end of the billet.

Cutting in the Context of the Process Chain

The considered profiles have a wall thickness up to 5 mm, a diameter of maximum 100 mm and length up to 2 m. The used materials are aluminum and magnesium alloys with endless reinforcing in form of wires and cords made of steel (e.g., 1.4310) to increase the tensile strength [3]. During the cutting it must be taken into consideration that the temperature of the strand is approximately 200 degree Celsius. As a requirement arising from the movement of the cut-off point of the profiles to be extruded, a relatively large workspace results for the kinematics of the cut-off device in the range of some cubic meters. For the support of the profile at a defined place the link of six degrees

of freedom is necessary. Since the profile must be clamped during the cutting process, all six degrees of freedom must be driven. It has been determined in the analysis phase that a six-axis vertical articulated robot is most suitable for the kinematics used for cutting and guiding [4]. The entire concept for the cutting of the profiles is shown in fig. 1 and fig. 2:

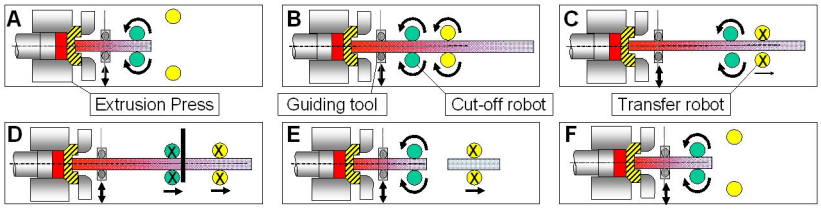

Fig. 1: Scheme of the extrusion line

As shown in fig. 1A, at the beginning of the extrusion process, the profile leaving the guiding tool is threaded automatically to the clamping devices by the cut-off robot and the transfer robot. During the rounding process a relative movement arises between strand and guiding tool. Before reaching the cut-off point, the strand moves through the cut-off robot's clamping system (enlargement in fig. 2). Meanwhile, the profile moves through the transfer robot's gripping device (fig. 1B) until the centre of the new profile is reached. The device then synchronizes and clamps the profile (fig. 1C). Subsequently, the cut-off robot moves synchronously to the cut-off point, clamps the profile completely and separates it (fig. 1D). Having separated the profile, the cut-off robot opens the clamping device. The transfer robot transfers the separated profile to the subsequent machining (fig. 1E), while the cut-off robot is moved back to the next cut-off point along the new profile contour, which still has to be supported against gravity and acceleration forces (fig. 1F). The transfer robot threads the new profile (fig. 1B) and synchronizes to the new profile center (fig. 1C), while the cut-off robot is moving synchronously to the cut-off point (fig. 1D).

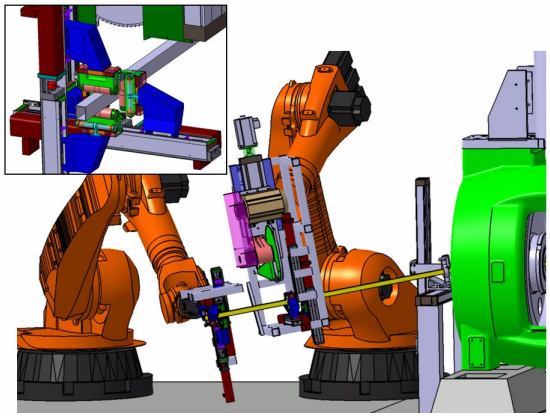

Fig. 2: Extrusion line

Cutting-off Processes

The cutting-off process for the process-chain described above has to fulfill the following requirements. Depending on the profile cross section and length, a maximal time between 3 to 10 seconds remains for cutting-off. The cutting figure should be good and the process cost effective and safe for workers in the proximity of the extrusion press. Irrespective of the kind of guiding kinematics, one main requirement regarding the cut-off device is a low inertia. Possible cutting-off processes are amongst others torch-cutting, plasma cutting, abrasive water-jet cutting, laser cutting,

adiabatic cutting or sawing. Using torch or plasma cutting results in the deformations at the section ends caused by high temperature being very distinctive. Since the input of heat is not highly concentrated and the temperature transmission coefficient of aluminum is high, the width of these deformations is within centimeter range. Experiments concerning abrasive water-jet and laser cutting effected positive results in cutting flat profiles, reinforced with steel-wires [5]. Higher and in particular star shaped cross sections would lead to high separation times. Furthermore, high expenditures for safety engineering are required. The influence of temperature has been determined as insignificant in tests with profiles scalded in a hardening furnace. Higher temperatures tend to result in higher cutting depth. At very high temperatures the profiles burst (fig. 3). Adiabatic cutting is a kind of shearing with a very high shear rate (>>3m/s) [6]. This results in nearly the entire kinetic energy being used as cutting energy. Caused by the huge requirements of stiffness and power, the inertia of devices for adiabatic cutting is too high for mounting on a robot. Reducing the mass results in low shear rates, e.g., used for hydraulic shears, and therefore compressed section ends.

Buzz sawing with a high cutting output and moderate weight proved to be an optimum for the overhung cutting off. First experiments suggest that aluminum profiles, reinforced with steel cords (1.4310), can be cut off with good cutting results. For this, the common parameters for usual aluminum alloys have proved to be suitable. Concerning the dimensioning of the saw, the maximum requirements regarding the cutting-off time have been set to approximately 3 s for a curved profile with a diameter of 100 mm and a wall thickness of 5 mm. As for a saw blade with a diameter of 350 mm and a coaxial saw blade contact, the cutting forces or rather normal feed forces and feed forces were calculated according to [7] and [8] on the basis of the cutting force formulae of Kienzle and Victor. Since the used parameters were to be partly extrapolated and the calculation only refers to unreinforced profiles, saw experiments were conducted in parallel on a high speed machining center (Heller MC16). In conjunction with a saw blade retainer for the main spindle and a clamping device with 3-axial piezo force sensor the machining forces have been determined. It has been shown that the measured cutting forces or rather the normal feed forces corresponded widely with the calculated ones. The measured feed forces were noticeably smaller than the calculated ones, in which according to [9] the results of the feed force calculation are only to be regarded as reference values. As for the dimensioning of the saw unit, the calculated (higher) forces have been used.

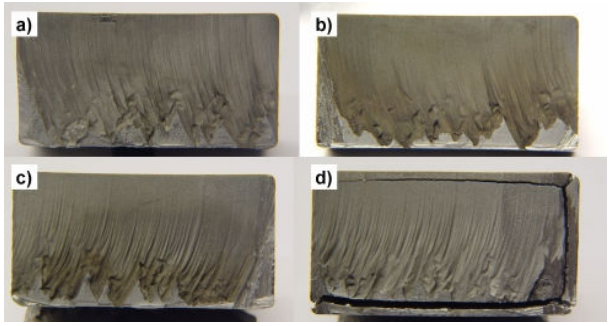

Fig. 3: Abrasiv water-jet cutting: a) 25°, b) 214° before- 107° after cutting, c) 305°-153°, d) 492°-267°

Challenges for the Movement of the Cut-off Device

Fig. 4 shows a typical path and velocity profile for the x- and y-direction of the tool center point of the cut-off robot. A comparatively simple spatial profile which shows different radii merging tangentially was designed.

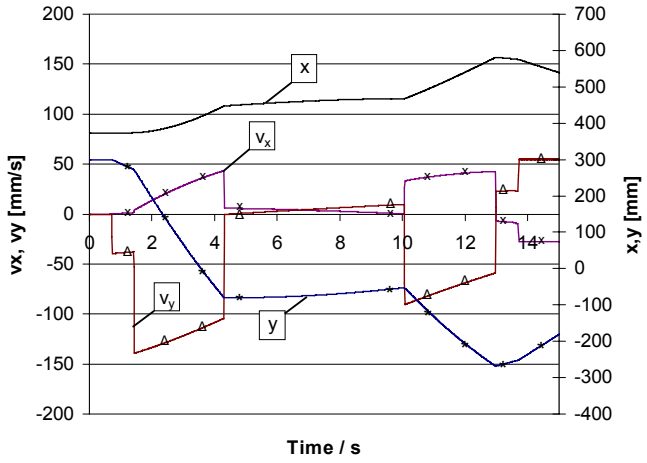

Fig. 4: Path and velocity for a profile with radii merging tangentially

For geometric reasons the profile shows points of discontinuity regarding velocity if two radii merge in the die. In order to avoid this, the profile has been approximated by splines, effecting minor deviations from the set contour. Thus, the robot suites the acceleration requirements (fig. 5), so that no relevant reactions via the cut-off kinematics have to be considered. In the case of the used profile the deviation from the set contour caused by the approximation of the spline is about 0.1 mm, which is tolerable. With an increasing length of the profile and therefore a bigger distance to the press, decreasing radii and increasing extrusion velocity deviations arise. Due to the limited dynamics of the robot, this suggests thinking about an additional kinematic structure for the increase of accuracy and acceleration.

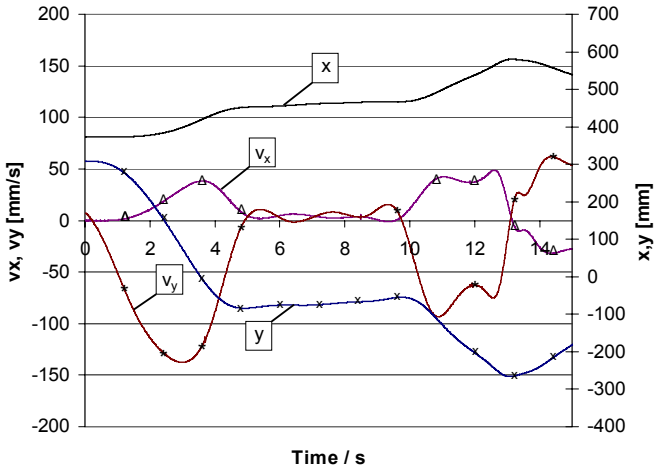

Fig. 5: Path and velocity for a spline-approximated profile

Besides the dynamic requirements on the kinematic structure the trajectories for robots and guiding tool have to be generated. Therefore the kinematic conditions of rounding were implemented in a CATIA module, as described in [4]. Thereby, it is very important to consider that the profile extends out of the die tangentially. It is possible to control the cell configuration, especially the placing of the robots. In order to also generate the trajectories for robots and guiding tools on this basis, adequate formulae have been implemented. These formulae describe the behavior of the grip technique, the saw feed and steer the phases during which the cut-off robot runs synchronously to the cut-off point or rather along the profile of the new cut-off point. In order to automatize the generation of trajectory it is possible to access CATIA via Visual Basic in batch

mode. The disadvantage of this process has to be seen in the comparatively high computation time and the fact that the dynamic behaviour of the robots can not be taken directly into consideration. This is to be optimized in following studies. Subsequent to the generation of the trajectory, the recurrent accelerations are to be controlled.

To realize the calculated trajectories, a special control loop is necessary. For the closed-loop control of the entire system the velocity of the extrusion press, which is approximately constant, is decisive. Nevertheless, in order to achieve a sufficient geometric accuracy of the profiles, the guiding tool, the cut-off robot and at times the transfer robot have to be controlled synchronously with the velocity of the extrusion press. Also the clamping actuators must be controlled synchronously in order to increase dynamics and accuracy by using these clamping actuators in a manner described later on in this article. Therefore, the aim is to use the extrusion press as a virtual master axis, which is linked electronically with all drives serving as slave axes, similar to an electronic gear.

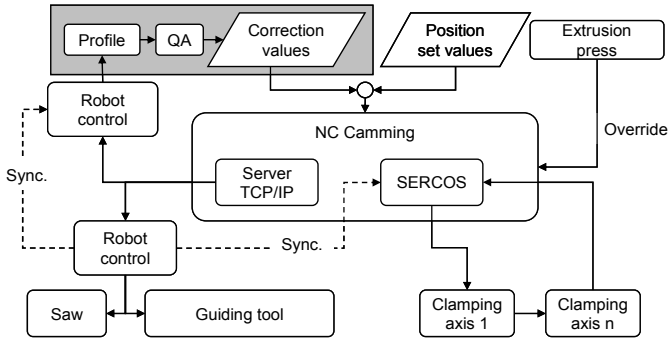

Fig. 6: Control design

The result of the generation of path data is a list of set values, which is read by the camming module of a numerical control and distributed to the motors of the clamping devices and the robot controls in accordance to the signal of the velocity of the extrusion press (fig. 6). The use of a SERCOS-Ring is intended for the communication with the clamping devices. So alternatively torque set values or position set values can be provided with short cycle times (2 ms and less) to achieve the actuators' full dynamics. During the cut-off process the profiles must be clamped tightly. Therefore, at any time two drives are joined electronically, with one drive being position controlled and the second one being force controlled. The position controlled drives get new position set values every interpolation cycle, whereas the force controlled drives get their feedback from strain gages. After the cut-off process it is switched over from force control to position control. During their interpolation cycle (12 ms), the robot controls require position set values, via TCP/IP, of a server which runs on NC. The synchronization of both processes is to be run via a hardware clock-pulse generator of a robot which leads to fine interpolation also within the robot. The signal is used in the second robot control and utilized as a trigger by the SERCOS-master.

Implementation of the Cut-off Device

After the description of the requirements and challenges of the cycle of the rounding process, the following demonstrates the concept for the flying cut-off device and status quo realization. Besides the intrinsic cutting-process, the design should provide an accurate and dynamic guiding of the profile. On the basis of the predefined sawing experiments a saw concept was developed and rated accordingly. To get low gyroscopic moment, the smallest possible saw blade in conjunction with a belt drive was selected. The system for the automatic clamping of the profiles mentioned at the beginning of this text is shown in fig. 2. In addition, the clamping device is shown in detail in fig. 7. On one side of the saw blade two pairs of rolls turned about 90 degree are located. Each roll can be

moved over a linear axis. To thread the profile, the rolls open wide and are subsequently closed until they lie against the profile and the return spring is low compressed (see fig. 7). In this condition it is possible to move the profile through the clamping device because of the pivoted rolls. By moving along the linear axes the left friction lining is relocated in the positive X-direction and the right friction lining in the negative X-direction. Thus, the return springs are compressed insofar as the rolls lie against the friction lining making twisting impossible. A safe clamping is guaranteed while sawing.

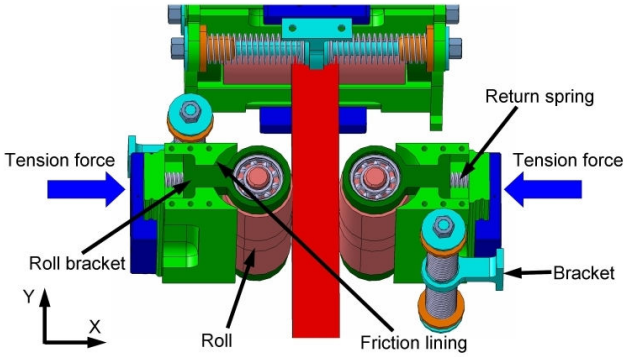

Fig. 7: Function principle of the clamping device

In the shown square profile there is a line contact between profile and rolls. In pre-testing, no plastic deformations induced through the clamping forces appeared. If a rounded profile is used instead of a square profile, a point contact between rolls and profile results. The method of Finite Elements was used in order to check that no remaining deformations of the profile sections occur for the regarded spectrum of profiles, in spite of the clamping forces and the temperature of about 200 degree Celsius. The calculations showed that on the surface there are only small local plastic deformations in form of pressings. These dents were classified as irrelevant after pre-tests were carried out. For optically critical units a special roll, aligned to the outline of the profile, can be used. The linear axes are powered by servo motors facilitating the control of the clamping force even in acceleration phases or if the cross section varies because of the profile curvature. On the other hand, the acceleration of the profile can be augmented using the method described in [4]. For this purpose, two opposing rolls can be driven in the same direction by the servo axes in order to change the profile position on the cut-off device (fig. 2). This motion can be superposed with the robot motion and therefore increase the absolute acceleration in two dimensions up to 20 m/s². The third dimension can be achieved by powering the rolls. There is no need of more degrees of freedom, since roll systems are not able to transfer moments. Thus, accuracy and dynamics can be increased noticeably during the extrusion via the constructive design of the gripping and clamping system.

Cutting Results

Based on the tests for dimensioning, further cutting experiments have been carried out. For these experiments, the cut-off device has been implemented with a lightweight manual clamping system and a 3-axial piezo force sensor. The speed of the asynchronous motor is about 2850 rpm and the cutting speed is 3000 m/min.

Tests with a saw feed rate up to 6 m/min for non-reinforced aluminum ENAW 6060 were carried out and showed good results. The optimal feed rate of 2 m/min was kept for all further experiments. After approximate 200 experiments with non-reinforced profiles, no wear could be detected at the saw blade. The surface finish Rz (ISO 4287) at the maximum cross section (100 mm diameter x 5 mm thickness) is between 18 µm and 35 µm with a rate of feed of 2 m/min (fig. 8).

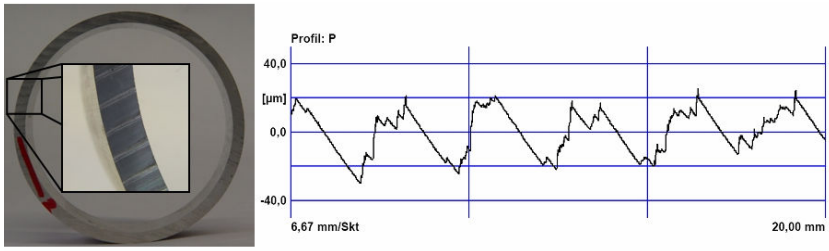

Fig. 8: Cut-off rounded profile with Rz=28.9 µm (Ø100x5; 2m/min)

Reinforced samples with a cross section of 56 x 5 mm² and 6 reinforcing elements made of steel wires (1.4310; Ø 1 mm) were also cut with a good cut surface. In contrast to the pre-tests mentioned with steel cords, the experiments showed that steel wires are a big challenge for tool life.

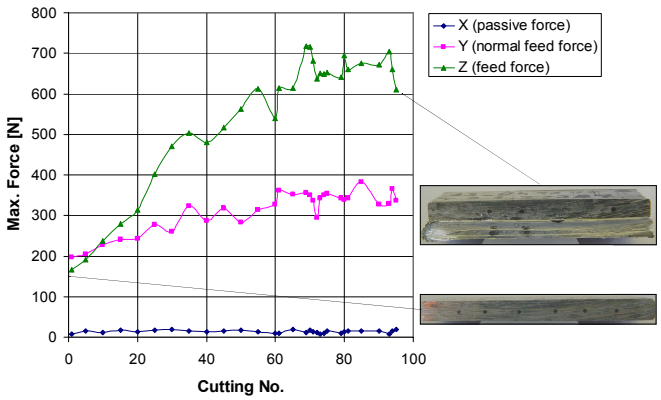

Fig. 9: Cutting forces: 56x5 mm² ENAW6060, reinforced with 1.4310

In fig. 9 the progression of the cutting forces is shown for 95 cuts in steel-wire reinforced aluminum. The enormous growth of the feed forces is caused by disruptions and beveling of the cutting edges due to the hardness of the reinforcing elements. This results in built-up edges (fig. 10). Besides the fact that the occurring increased wear is not tolerable for economic reasons, the cutting surfaces and the burr formations are not a problem due to the subsequent end machining which is necessary at any rate.

Parallel experiments on an automatic circular saw confirmed the result that the reinforcing elements cause increased wear in combination with a normal cutting edge geometry for aluminum. Reducing the cutting speed resulted in a low improvement of tool live. In further experiments the behavior with low cutting speed in combination with cutting edge geometry for steel will be analyzed prior to the variation of cutting materials and coatings.

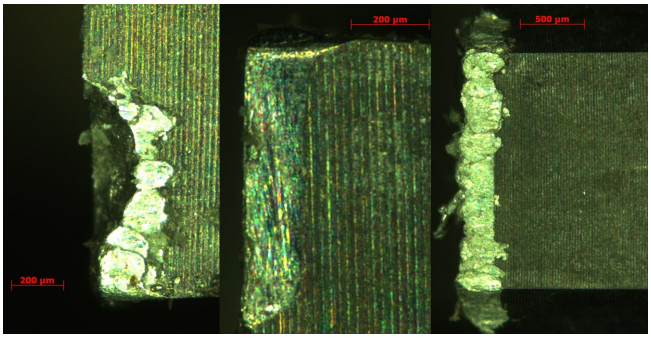

Fig. 10: Wear of the saw blade after 100 cuttings

Summary

Based on an innovative process to produce spatially curved reinforced extruded profiles, this paper discusses the resulting requirements for flying cutting of the profiles. Besides the elaboration of the cutting process, the main focuses are on the clamping and guiding of the profiles as well as experiences in cutting continuous reinforced profiles. For the guiding and clamping of the profiles an industrial robot in connection with a special clamping device is used. This device takes over the real clamping and allows an increasing dynamic which heightens the outline accuracy of the profiles and the production speed. A method for generating the needed trajectories with the kinematic modul of a CAD-System and controlling of the plant is shown. This facilitates cutting-off the profiles without reactions to the extrusion process.

For the cutting process a buzz saw was chosen and a prototype for cutting experiments was implemented. Extruded profiles can be cut with a good cutting figure, both with reinforcing elements and without these elements. In further studies, the increased wear of the cutting edge caused by reinforcing elements will be analyzed. Simultaneously, the automatic clamping device and the control system will be implemented. A challenge will be the re-calibration of the installations during the operation by using the corresponding information of the measuring of the profile. As a result of the press and profile temperature, comparatively high influences of thermal fluctuations on the profile precision must be dealt with.

Acknowledgment

This paper is based on investigations of the collaborative research centre SFB/TR10 which is kindly supported by the German Research Foundation (DFG).

References

[1] Klaus, A.; Kleiner, M.: Developments in the Manufacture of Curved Extruded Profiles – Past, Present, and Future. Light Metal Age (2004) 8, pp.22-32

[2] Bickendorf, J.; Birkenstock, A.: Roboter als Schlüsselkomponente für das „Runden beim Strangpressen“. In: VDI/VDE-GMA: Robotik 2004 VDI-Berichte 1841 VDI Verlag, Düsseldorf 2004, pp. 195-202

[3] Kleiner, M.; Klaus, A.; Schomäcker, M.: Verbundstrangpressen. Aluminium Vol. 80 (2004) 12, pp. 1370-1374

[4] Fleischer, J.; Stengel, G.: Bahngenerierung für eine robotergeführte Abtrenneinheit für räumlich gekrümmte Strangpressprofile. wt Werkstattstechnik 94 (2004) 9, pp. 457-461

[5] Fleischer, J.; Kies, S., Stengel, G.: Fliegendes Abtrennen. Aluminium Vol. 80 (2004) 12, pp. 1378-1382

[6] Leßle, P.; Böning, M.: Built-in-tools High Speed Impact Cutting HSIC. Fraunhofer TEG annual report 2003, Stuttgart 2004

[7] König, W., Essel, K., Witte., L.: Spezifische Schnittkraftwerte für die Zerspanung metallischer Werkstoffe. Verlag Stahleisen MBH, Düsseldorf 1982

[8] Maulhardt, U.: Dynamisches Verhalten von Kreissägen. Dissertation Technische Universität München, Springer, Berlin Heidelberg New York 1991

[9] Paucksch, E.: Zerspantechnik. Vieweg Verlag, Braunschweig/ Wiesbaden 1996

doi:10.4028/www.scientific.net/AMR.10.43

3D-Laser Processing of Spatially Curved Profiles

J. Fleischer[1,a], S. Kies [1,b], C. Munzinger[1,c], R. Rilli [1,d]

[1]wbk Institute of Production Science, Universität Karlsruhe (TH),

Kaiserstraße 12, 76128 Karlsruhe, Germany

[a]fleischer@wbk.uka.de, [b]kies@wbk.uka.de, [c]munzinger@wbk.uka.de, [d]rilli@wbk.uka.de

Keywords: Laser cutting, CO_2 laser, Solid-state laser, Latching elements

Abstract. Due to economical, ecological and functional reasons, lightweight-construction is continuously gaining importance. Therefore, lightweight space frames made of pipe profiles are subsequently of higher importance in today's technology. Today, the lower limits of the production range of lightweight space frames are set by joining processes that require jigs. For a flexible variation in a small-scale production, the use of latching elements for the pre-attachment in the jig-free assembly of frame structures serves as a good approach. In consideration of the analysis of the actual situation this article takes up this approach and points out the potential enabled by latching elements. Subsequently, the implementation of laser cutting will be motivated and the results of the first experiments on reinforced and unreinforced profiles will be discussed. To conclude this article, the challenges and approaches for the integration of this procedure to an existing handling and machining kinematics will be pointed out, and finally the implementation potentials of the procedure within an entire process-chain will also be mentioned.

Introduction

Due to economical, ecological and functional reasons, lightweight construction continuously gains importance [1]. Especially in the domain of traffic engineering, the application of optimized construction as well as the use of new and composite materials enables the reduction of air pollution and fuel consumption [2]. Lightweight space frames made of pipe profiles are therefore of importance in the domain of traffic engineering. In the manufacture of lightweight space frames, different established as well as research based attaching methods could be used to join the profiles of a frame structure. Thus, new joining methods are being investigated for mixed joints consisting of aluminum and steel [3,4,5,6,7]. A high quality manufacture of frame structures however requires alignment of the joint-partner to each other. Modern jigging techniques involve the use of product-customized jigs. They reduce accessibility to the joints and are also time and cost-intensive to manufacture. Especially the cost of the jigs, restrict their implementation field, thereby making their application only for large-scale production profitable. Due to decreasing in batch sizes and increasing product varieties, there is a need for a method and a concept of manufacturing techniques with which the flexible variation demand in the small-scale production can be achieved. The aim is to achieve a jig-free assembly of frame structures or a jig-free adjustment of the individual profiles of a frame structure, respectively.

Conceptional Approach and Evaluation of the Technological Demands for Manufacture

This article is mainly focused on developing the pre-conditions of the fabrication techniques for the processing of round and rectangular profiles made of light metal and composite materials of light metal matrix. In this case, flat, round and rectangular light metal profiles such as aluminum and composite materials of light metal matrix reinforced with long fibers, with wall thicknesses of two to five millimeters are of interest. Challenging factors to jig-free assemblies e.g. the highest possible

accessibility to the joints, the maintenance of a once achieved state of order in the entire process-chain as well as the reduction of the assembly complexity [8] will be discussed.

The conceptional approach implemented by the Institute of Production Science (wbk) for this task include the use of the smartly constructed three-dimensional latching elements situated at the ends of the profiles, as described by Kristensen in [9] for two-dimensional components. Based on the possibilities of joining sheet metals as pointed out by Kristensen, a further development is consequently necessary in the domain of spatially curved pipe profiles. The construction of complex contours at the end of the profiles enables the latching of the profiles onto each other during the assembly process. This form-closure connection permits the erection of a preliminary fixed frame structure, and thereby facilitating the adhesive bonding of the joints, due to the accurate alignment of the profiles. Figure 1 shows a possible exemplarily selected latch of two rectangular profiles for a frame structure.

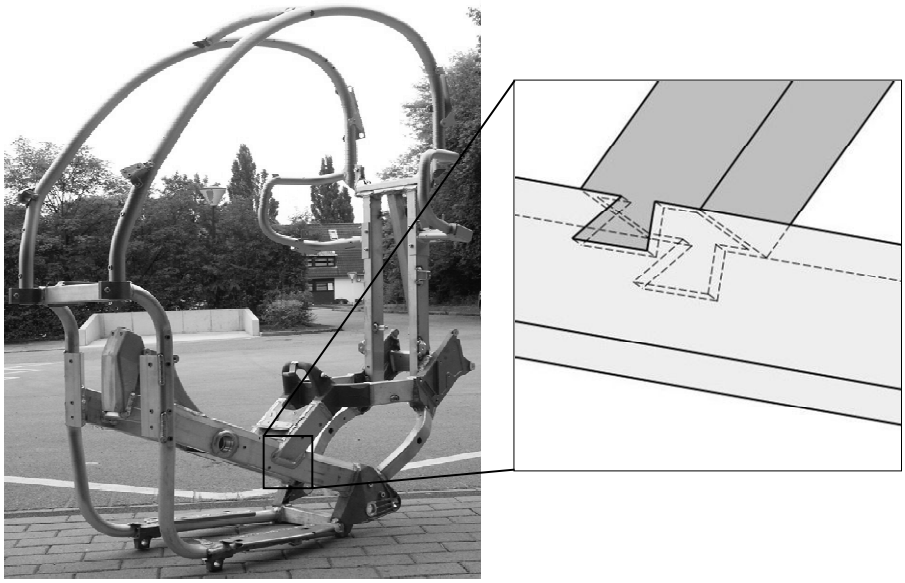

Fig. 1: Possible latch in the frame of the BMW C1

It is immediately plausible that there is practically an unlimited variety of latching elements. In order to determine the essential structural features of the conceivable latching element, an analysis of the joints as well as the number and types of defined degrees of freedom involved should be performed. As far as the types of joints are concerned, T and I joints as well as their derivates are of high importance. The types and number of degrees of freedom, the order of assembly and the associated demands regarding the compensation of a tolerance are significant. Also of high significance are latches that enable the compensation of length or angles within close tolerance. This is illustrated in figure 2 with the aid of exemplarily selected latches for identical and unidentical cross-sections. Figure 2a shows the latching of a round and a rectangular profile. Figures 2b, 2c and 2d show the latching of two rectangular profiles. The latch in figure 2b allows a slight sideways displacement, which could possibly compensate tolerances due to the manufacturing process of the profile. With the aid of an adapted shape the latch in figure 2c could enable a slight movement around the center of the sector.

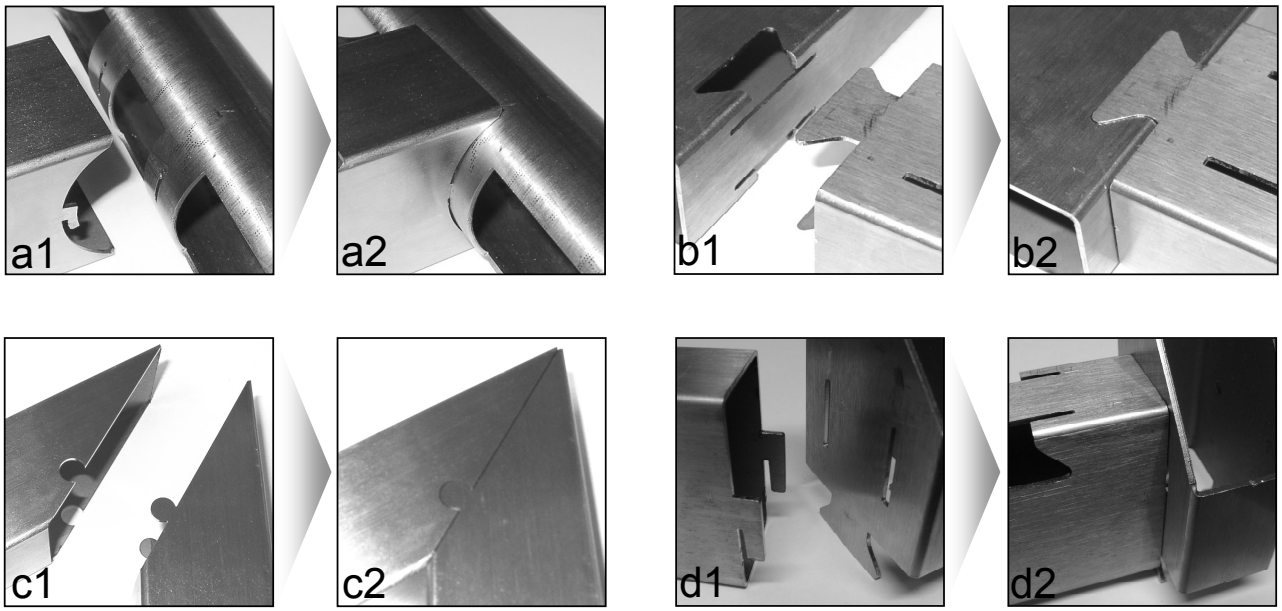

Fig. 2: Compensation possibilities of production tolerances provided through latching (1: Latches before the joining process; 2: Latches after the joining process)

Besides the types and shapes of the latching elements, the economical aspect of the chosen production technique is also essential, whereby the choice is based on the analysis of established, innovative as well as new process-chains. Within an established process-chain for the production of lightweight space frames, the pipe profiles are first of all sawed to an end-length and then brought to the right shapes using a suitable forming technique. The cutting of the ends is usually done after the forming process. The transregional collaborative research center SFB/TR10 presents a new method contrary to the above described. Due to a circular form bending in the rod extrusion process, the profiles are produced in spatially curved near-net-shapes. Due to the near-net-shape manufacturing the profiles are separated directly after the extrusion machine by flying circular saws controlled by an industrial-robot. The ends of the profiles are now evenly cut and analogically to the established process-chain, require further treatments before joining. Considering the current observation, emphasis will be laid on the milling process as a means of cutting for the further treatments.

Techniques such as milling, laser, plasma and jet cutting can be applied for the necessary processing of the ends. Before laying emphasis on the stroven jig-free assembly, the special boundary conditions of the fabrication of latching elements should be discussed. The fabrication of latching elements demands a technology that can produce almost any contour on a profile. At the same time, structural sizes within the range of one and two millimeters should be feasible. The technology should be capable of cutting light metal and composite materials of light metal matrix with wall thicknesses of up to five millimeters. The produced structure must have very close tolerances, in order to ensure a proper laser welding process.

Due to the cycle time and the feasible structural sizes, milling and laser cutting are most promising. Research was performed on both cutting techniques to find out further limiting factors for profile processing. In both cases round and rectangular unreinforced aluminum profiles and a flat aluminum profile reinforced with six steel wires (1.4310) with equal diameters of 1 mm (see figure 3) were treated.

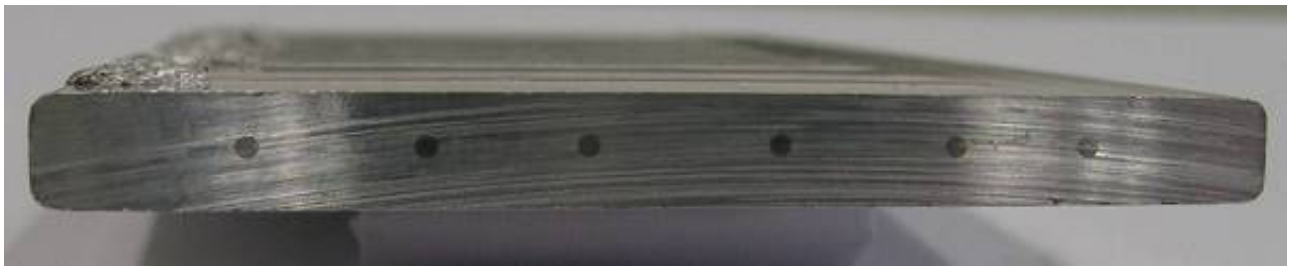

Fig. 3: Flat profiles with reinforcement elements; 56 x 5 millimeters

The result of the research showed that milling is the more convenient for the manufacturing of profile ends without latches and is therefore to be favored. Reasons such as the need for small structural sizes in the manufacturing of latches, the tool to be charged and the set-up time associated with tool changing classify milling as a laborious process for the manufacturing of latching elements. On the other hand, the research shows that the application of laser has substantial production potentials in this domain. Besides low set-up time, the advantages of laser cutting include high process dynamics and constant quality of the cutting surface, due to the lack of "tool" wearing. The application of laser brings along a further spectrum of profile processing. For example, if heated with a laser beam a profile can be bent a few tenths of a degree along the longitudinal axis [10,11,12,13], this means a geometrical correction of the profile (figure 4). Due to the above mentioned advantages, laser cutting is therefore favored for the fabrication of latching elements.

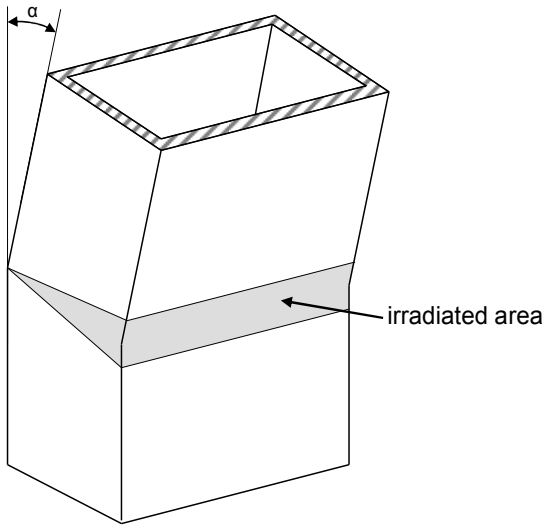

Fig. 4: Bent rectangular profile

Selection of Laser Source

Based on the chosen procedure, the next step is focused on choosing a suitable fabrication technique. Since the processing of reinforced and unreinforced aluminum profiles is primary, the selection of a convenient laser source for their machining should be aimed at.

Due to aluminum's high heat conductivity and the high melting point of the passivating oxide film, the cutting of aluminum requires a high concentration of heat supply despite its low melting point. Therefore, only CO_2 lasers, Nd:YAG lasers or Ytterbium fiber lasers can be applied in the cutting process. The power of these laser types ranges within kilowatts and as a result, they assure effective and high quality cutting for materials that are less than five millimeters thick. Table 1 shows the lasers in question and their application domains.

Table 1: Lasers suitable for profile processing [14-16]

	Wave length	Power	Mode of Operation	Application domains
Solid-state laser				
Nd:YAG laser	1.06 µm	Up to a few kW	continuous and pulsed mode	material processing, measuring technology, medicine
Ytterbium fiber laser	1.07–1.08 µm	1-50 kW	continuous and pulsed mode	material processing
Gas laser				
CO_2 laser	10.6 µm	1-40 kW (100 MW in pulsed mode)	continuous and pulsed mode	material processing, medicine, separation of isotopes

Within the scope of the first experiments conducted in collaboration with a manufacturer of laser cutting machines, round and rectangular unreinforced as well as flat reinforced aluminum profiles were processed using a CO_2 lasers in cw mode (cw = continuous wave) (see figure 5). The applications of lamp-pumped and diode-pumped solid-state lasers were examined in further experiments, using the above mentioned flat reinforced aluminum profile. Parameters such as gas pressure, laser power, focal diameter, cutting speed, nozzle diameter, nozzle distance and focusing positions were varied in order to obtain an optimal result. Figure 6 shows the basic set-up of experiment.

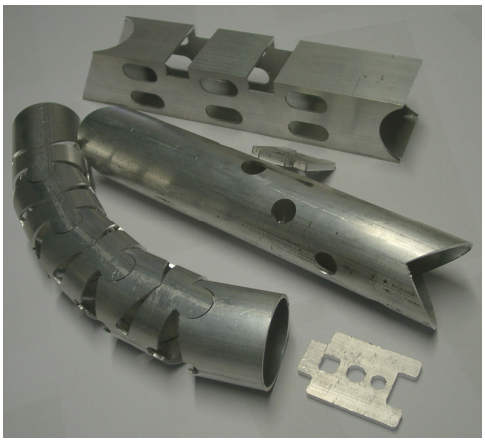

Fig. 5: Experimental samples of reinforced and unreinforced profiles processed with CO_2 laser.

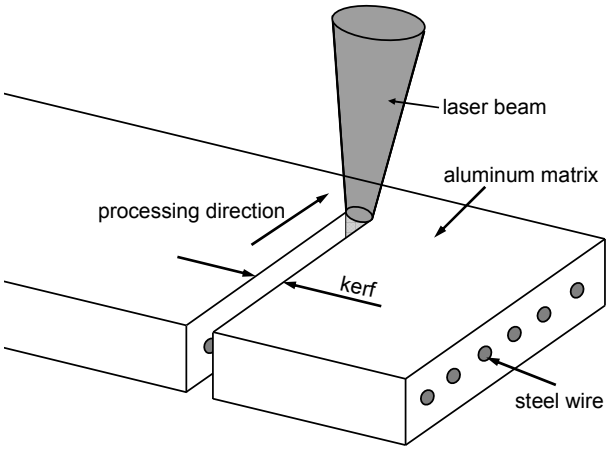

Fig. 6: Basic set-up of experiment.

The qualitatively best cutting result of each laser type is shown in figure 7. The reinforcement steel wire is found in the middle of each sample. All three samples were processed from left to right, with the laser beam pointed from above. Due to a better laser beam absorption by the steel wires, there is a high heat intake and hence a strongly melted area below the steel wires. The kerf also gets wider in this area. Figure 8 and 9 show an EDX-analysis (Energy Dispersive X-ray Analysis) and the analyzed areas of samples cut with CO_2 laser. The analysis shows that aluminum, iron and other composite materials of alloys such as Chrome and Nickel are found in the area below the steel wires. Samples that were cut with solid-state lasers only made prove of aluminum and iron in this area. Further experiments will determine the impact of this heat intake on the subsequent joining process. The analysis of all three samples also showed that the area above the steel wires purely

consists of aluminum. SEM micrographs of the samples (figure 10) show that the steel wires can locally be disintegrated from the aluminum matrix. Further researches will have to show if this could significantly affect the subsequent processes. Furthermore, aluminum melts can be observed over the right side of the steel wires. This is because the steel wires melt stronger than aluminum, thereby causing a recess, which due to the left to right processing is situated on the right side and is partially filled with aluminum.

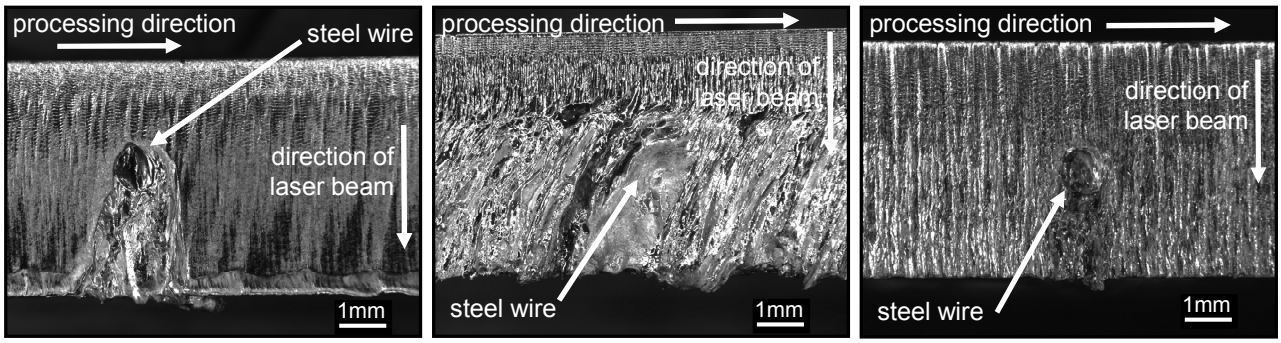

Fig. 7: Cutting surface of steel reinforced aluminum profile, Left: Lamp-pumped solid-state laser 4 kW; Middle: Diode-pumped solid-state laser 4 kW; Right: CO_2 laser 3.2 kW.

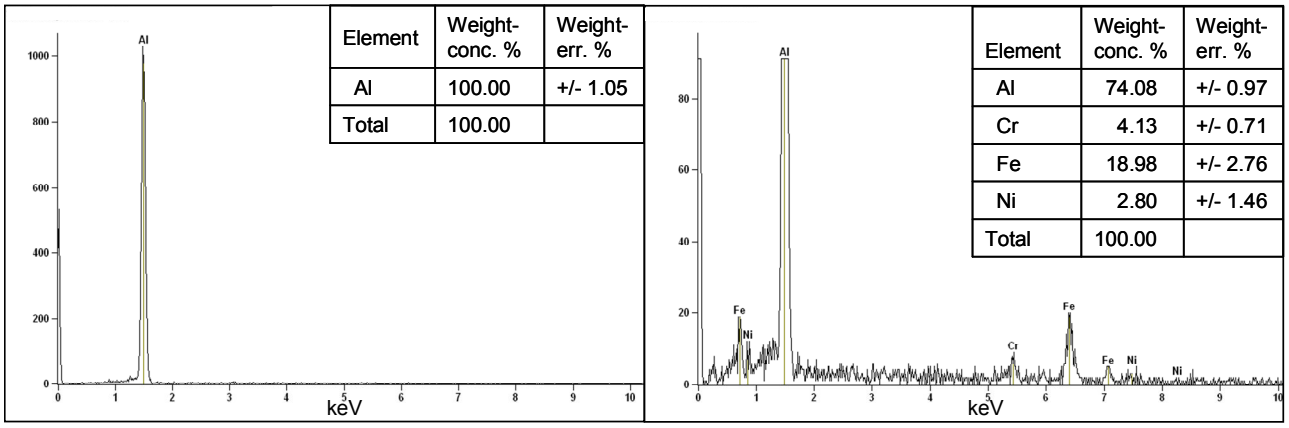

Fig. 8: EDX-analysis of a reinforced aluminum sample cut with CO_2 laser; Left: Analysis of the steel wires, Right: Analysis of the area below the steel wires.

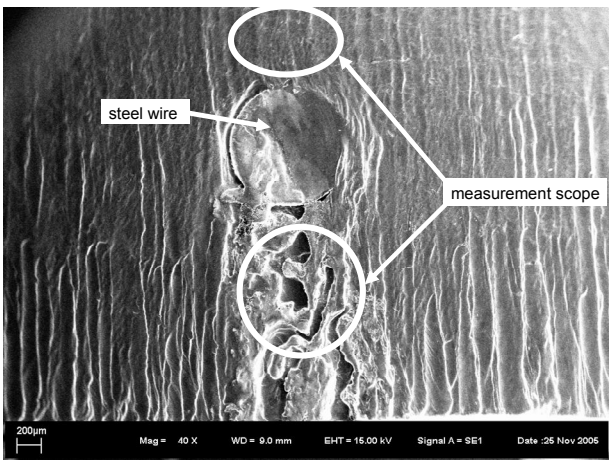

Fig. 9: Range of measurements for the EDX-analysis of the sample cut with CO_2 laser

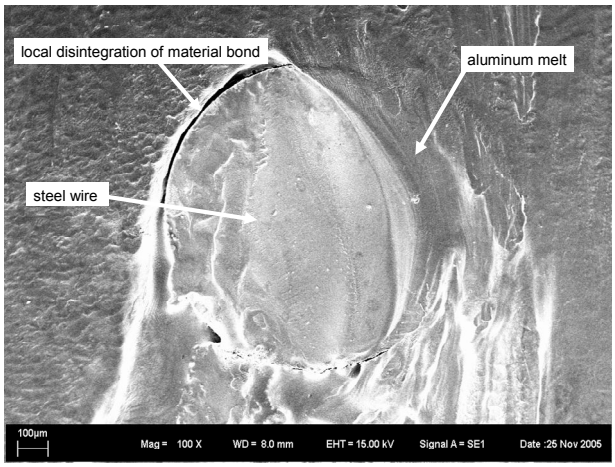

Fig. 10: SEM micrograph of a sample cut with lamp-pumped solid-state laser

The applied cutting speed, power, beam quality and the obtained surface roughness (surface finish Rz (ISO 4287)) are listed in Table 2. Since the steel tends to couple laser better than aluminum, samples cut with a lamp-pumped laser (figure 7, left) have a significantly rougher surface below the steel wires compared to that of the rest of the cutting surface. The quality of the cutting surface of the profile cut with diode-pumped solid-state laser worsens as the cutting depth increases (figure 7, middle). Due to the narrowness of the kerf, molten mass cannot be sufficiently blown out. The obstruction of this flow leads to a turbulence, hence the molten mass is conveyed back into the kerf and eventually leading to rewelding of the kerf. The burr formation on the lower edge of the cutting surface of the samples cut with solid-state laser amounts to a height of up to one millimeter. The formation of burr is associated with the high melting point of the passivating oxide film. Similar to the narrow kerfs, the oxide film obstructs the blowing of the molten mass out of the kerf. This could lead to the formation of a pointed adhesive burr at the lower edge of the cutting surface [17]. A nearly constant cutting result over the entire cutting surface was obtained using the CO_2 laser. In this case, the maximum height of the burr was 0.2 millimeters and is clearly smaller than that of the samples cut with solid-state lasers.

Table 2: Results of experiments

Laser	**Parameter**	**Rz-value (ISO 4287)**
Diode-pumped solid-state laser (HLD4002)	Cutting speed 4 m/min Laser power 4 kW Beam quality 8 mm•mrad	6.6 µm upper half of the cutting surface 90 µm lower half of the cutting surface
Lamp-pumped solid-state laser (HL4006D)	Cutting speed 3 m/min Laser power 4 kW Beam quality 25 mm•mrad	18 µm above and next to the steel wires 80 µm below the steel wires
CO_2 laser (TLF 3200)	Cutting speed 0.8 m/min Laser power 3.2 kW Beam quality K: 0.6 ±5% (reference ISO 11146)	30 µm over the entire surface

Regarding the processing abilities, all three types of laser sources can be applied for the manufacturing of latching elements. However, the cutting results differ regarding the quality of the cutting surface and are in favor of the application of a CO_2 laser. Additional to the obtained cutting results, safety-related aspects have to be considered in the selection of a laser source. Due to the high power and energy density of the laser beam, an encapsulation from the environment is necessary in order to avoid damages. Solid-state lasers need to be enclosed within massive walls. On the other hand, the encasement of gas-lasers within sheet metal or polycarbonate-plates is sufficient. Based on the present state of knowledge and reasons that include good cutting results and the easy encasement, the application of a CO_2 laser is more convenient then that of solid-state lasers in this case. It is also to be mentioned, that so far the application of fiber laser could not be examined in the research, due to availability reasons. The required experiments, required laser power, achievable cutting speed and the quality of the cutting surface will however be the subject of further researches.

Challenges and Approach to the Integration into a Process Chain

The process-prove application of the CO_2 laser for the processing of unreinforced aluminum assures a reliable process, it is a state-of-the-art technology with low improvement potentials. On the contrary, the processing of composite materials of light metal matrix as well as the previously mentioned flat reinforced aluminum profiles need to be further investigated, in order to evaluate the influence of the reinforcement elements on the entire process and on the quality of the cutting surface. Process parameters that assure the required quality of the cutting surface for a fit joining have to be determined. In order to assure that the joints fit, the dimensions of the profile especially

those of the ends are bound to have close tolerances. The process accuracy and the achievable structural shapes and sizes have to be examined in order to assure the required tolerances.
The molten mass blown out of the kerfs, the so called melting loss mostly, remains in the inner space of the profile, and could later lead to undesirable noise, once the framework is put into use (figure 11). In order to solve this problem, a concept that will help fetch out melting losses from the inner space of the profile has to be developed. Flexibility is a challenge to such a system, since the profiles are three-dimensionally curved. An already existing system is shown in figure 12. The new system is to be provided with a catcher that is flexible along the longitudinal axis, thus being capable of reaching every position of the inner space of the profiles.

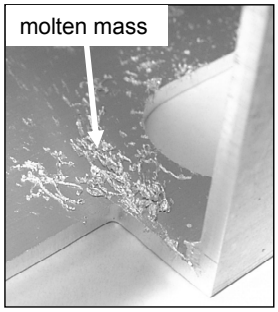

Fig. 11: Molten mass in the inner space of the profile

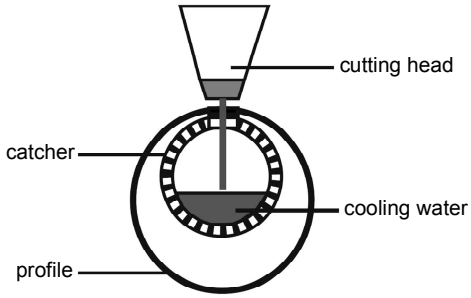

Fig. 12: Catcher to avoid melting loss in the inner space of the profile [18]

Processing a profile with laser requires that either the profile or laser beam or both have to be moved. Due to specific qualities regarding machining techniques, the combined handling and machining kinematics developed in the transregional collaborative research center SFB/TR10 is suitable for this process. It can basically assume the guidance of the processing head as well as that of the beam [19,20]. The machining kinematics, which is a parallel kinematics (figure 13) developed by the Institute of Production Science (wbk) is suitable for the integration of a laser, due to its high dynamics and accuracy. However, this kinematics demands a flexible beam guidance form the laser source to the processing head. The beam guidance of a CO_2 laser is only feasible with the aid of a laser arm, since beams of CO_2 lasers cannot be transmitted through glass fiber, because of their wave lengths. The laser arm is free-moving and its joints are equipped with mirrors that enable beam delivery through the inner space of the arm (figure 14). The high dynamics of the parallel kinematics require an adjustment of the laser arm, since the beam delivery takes place in the laser arm, the high accelerations of the arm could cause the laser beam to stagger and thereby not assuring a stable process. The integration of a solid-state laser in a parallel kinematics presents no difficulties, since the beams of solid-state lasers can be transmitted through glass fiber.

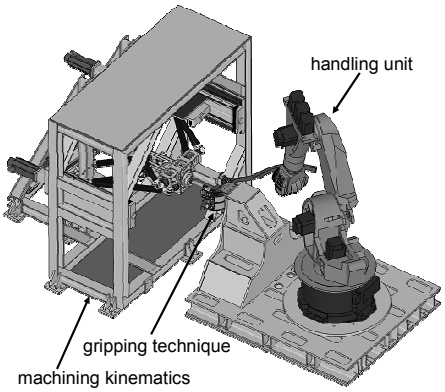

Fig. 13: Combined handling and machining kinematics

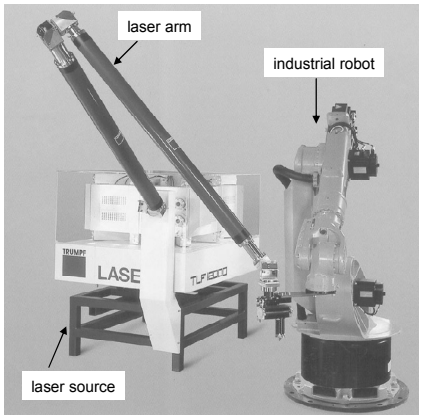

Fig. 14: Laser arm in connection with an industrial robot. Source: Trumpf

The existing machining kinematics allows at least 3+2-axial manufacturing of latching elements on spatially curved pipe profiles. The highly flexible gripping and clamping techniques of the handling unit additionally promises an economical assembly of frame structures, using the processed profiles. Even when the general approach of a jig-free assembly is still to be validated in further works, the introduced approach clearly shows that the application of latching elements will help eliminate boundaries regarding batch production and enable the achievement of an economical small-scale production.

Summary

The automated small-scale production of lightweight frame structures requires new possibilities to achieve jig-free assembly. Latching elements situated at the ends of profiles enable positioning and fixation, therefore can potentially enable the achievement of jig-free assemblies. Further works on this subject need a structural analysis of the feasible latching elements in consideration of joints types as well as types and number of degrees of freedom. The almost unlimited possibility of producing geometrical shapes and the short set-up time of laser machines, makes laser cutting very suitable for the manufacturing of latching elements. The first experiments on reinforced and unreinforced aluminum profiles showed that CO_2 lasers have the highest potentials. Using reinforced profiles it was possible to obtain surface qualities with Rz-values of 30 µm. Although laser cutting is classified as profoundly researched, detailed studies concerning the fabrication of latching elements should first of all be carried out, in order to determine the process parameters and the achievable structural sizes.

As concerns the integration of a laser source into an existing handling and machining kinematics, the development of the entire approach to suit a jig-free assembly is to be examined in further works. Within the scope of this work, the interaction between beam guidance and kinematical structures needed special attention.

Acknowledgment

This paper is based on researches of the collaborative research center SFB/TR10 which is supported by the German Research Foundation (DFG).

References

[1] Kleiner, M.: Leichtbaustrategien; in: Karlsruher Arbeitsgespräche 2002, Forschung für die Produktion von morgen, pp. 177-178, 2002

[2] Bleck, W.; Blümel, K.; Prange, W.: Leichtbau mit intelligenten Stahllösungen. Konferenz-Einzelbericht; VDI-Berichte, Band 1080 Düsseldorf; in: VDI (1994), pp. 25-34

[3] Haferkamp, H.; Ostendorf, A.; Bunte, J.; Engelbrecht, L.: Modern Laser Beam Brazing of Thin Sheets; in: Joining in Traffic and Transportation Industry, Processes, Progress, Applications; 9. International Aachen Welding Conference (2004), pp. 395-405

[4] Vollertsen, F.; Sepold, G.; Seefeld, T.; Kreimeyer, M.; Wagner, F.: New Laser Joining Processes for Aluminium-Steel Joints; in: Joining in Traffic and Transportation Industry, Processes, Progress, Applications; 9. International Aachen Welding Conference (2004), pp. 367-376

[5] Brucker, J.; Himmelbauer, K.; Schmaranzer, C.: Application Possibilities of the CMT – Process, with Particular Emphasis on the Joining of Steel with Aluminium; in: Joining in

Traffic and Transportation Industry, Processes, Progress, Applications; 9. International Aachen Welding Conference (2004), pp. 97-106

[6] Kleiner, M; Klaus, A.: Flexible Fertigung leichter Tragwerkstrukturen – der neue SFB/TR10, in: Geiger, M.; Ehrenstein, G. W. (Hrsg.): Robuste, verkürzte Prozessketten für flächige Leichtbauteile. Tagungsband zum Industriekolloquium 2003 des SFB 396. Bamberg: Meisenbach-Verlag (2003)

[7] Kreimeyer, M.; Wagner, F.; Vollertsen, F.: Properties of Laser Joined Aluminum/Steel Sheets; in: Proceedings of the Second International WLT-Conference on Lasers in Manufacturing 2003, Munich, June 2003

[8] Fleischer, J.; Kies, S.; Ruch, D.: Flexible und intelligente Greiftechnik, in: Aluminium, Vol. 80/12, Giesel Verlag GmbH Isernhagen (2004), pp. 1421-1424

[9] Kristensen, T.; Olsen, F.; Alting, L.: Increasing the potential of laser welding using self fixturing weld parts, in: Laser Assisted Net shape Engineering, Proceeding of the CIRP Seminars, manufacturing systems, Vol. 24 (1995), No. 2, pp. 105-109

[10] Dietz, C.:Laserstrahl biegt auch komplexe Geomerien, Neue Perspektiven beim berührungslosen Blechteilefertigen; in: Industrieanzeiger, Band 119, Heft 20 (1997), p. 48

[11] Geiger, M.; Kraus, J.; Vollertsen, F.: Laserstrahlumformen räumlicher Bauteile; in: Bänder Bleche Rohre, Band 35, Heft 11 (1994), pp. 26-37

[12] Beckmann, M.; Vollertsen, F.: Methoden der lokalen Kurzzeitwärmebehandlung bei 6000er Aluminiumlegierungen; in: Metall, Vol. 7-8 (2002), pp. 462-467

[13] Vollertsen, F.: Laserstrahlumformen, Lasergestützte Formgebung: Verfahren, Mechanismen, Modellierung; Meisenbach Verlag Bamberg (1996), pp. 193-197

[14] Poprawe, R.: Lasertechnik für die Fertigung, Grundlagen, Perspektiven und Beispiele für den innovativen Ingenieur, Springer Verlag Berlin, Heidelberg (2005)

[15] Vollrath, K.: Kilowatt-Leistungen aus dünnen Glasfasern; MM Maschinenmarkt Sonderausgabe 12/2005; pp. 28-31

[16] Morgenthal, L.: Cutting with Fiber Lasers; 1st International Fraunhofer Workshop on Fiber Lasers; 11/2005

[17] VDI Technologiezentrum – Physikalische Technologien: Schneiden mit CO2–Lasern, Laser in der Materialbearbeitung Band 1; VDI-Verlag (1993)

[18] TRUMPF Systemtechnik GmbH: Laserschneidanlagen für Rundrohre; 12/2005, p. 3

[19] Fleischer, J.; Schmidt-Ewig, J. P.: Innovative Machine Kinematics for Combined Handling and Machining of Three-Dimensional Curved Lightweight Extrusion Structures, in: Annals of the CIRP Volume 54/1, pp. 317-320, 2005

[20] Fleischer, J.; Kies, S.; Munzinger, C.; Troendle, M.; Schmidt-Ewig, J. P.: Berechnung und Optimierung eines neuartigen Werkzeugmaschinenkonzepts zur Bearbeitung dreidimensional gerundeter Profile; in: ZWF 9 (2005)

doi:10.4028/www.scientific.net/AMR.10.53

Analysis and Simulation of Cutting Technologies for Lightweight Frame Components

K. Weinert[a], N. Hammer[b], J. Rautenberg[c]

[1]Department of Machining Technology, University of Dortmund,

Baroper Str. 301, 44227 Dortmund, Germany

[a]weinert@isf.de, [b]hammer@isf.de, [c]rautenberg@isf.de

Keywords: cutting technology, lightweight components, drilling, milling, reinforced aluminium

Abstract. Innovative composite extrusions consisting of an aluminium matrix material with steel fibres for reinforced lightweight constructions require adapted cutting technologies. Due to the resulting tool wear when machining such composite materials, new tools and processes have to be developed. The following article describes experimental investigations concerning conventional drilling operations in comparison to helix milling operations for the manufacturing of holes in these materials. Therefore especially wear and quality aspects are discussed. Furthermore a flexible cutting process for thin walled lightweight frame connector elements to combine profiles is described. To obtain detailed process knowledge also FEA-Simulations of the thermo-mechanical loads affecting the workpiece during the process are performed.

Introduction

Lightweight frame constructions are essential construction elements for road-, railway and water vehicles as well as for aviation. As an innovative material, extruded composite light metal profiles with different reinforcement fibres are newly available [1, 2]. Today reinforcing elements like steel cables or wires can be joined with aluminium in the extrusion process under reliable process conditions.

Machining thin-walled, reinforced, and non-reinforced extruded light metal profiles and their resulting framework structures is often regarded as critical because of manifold factors influencing the machining process. Particularly the drilling of holes within satisfactory quality specifications using conventional twist drills in arched, inclined, but also straight component surfaces often leads to considerable burr formation at the bore edge. In addition, process related workpiece deformations result to deviations of shape and position [3]. Furthermore, the ductile wrought alloys, which are usually used for extrusions, facilitate early tool wear through intense material disposal at the rake faces and the flutes of the tools. When machining, an appropriate process design is necessary to get reliable cutting conditions. Especially the varying machining conditions resulting from different composite materials (aluminium and steel) make a well adjusted tool design indispensable [4].

In comparison to the conventional drilling process using twist drills, the machining of holes by circular milling offers numerous advantages. In contrast to drilling processes with twist drills in which the diameter of the bore hole is defined by the tool diameter, the circular milling and thus the milling along a helix path, offers the possibility of machining different bore hole diameters or other milling operations with the same tool. In comparative studies a considerable increase in process quality can be observed [5]. Both the discontinuous cut with its resulting favourable chip formation and chip removal and considerably less burr formation at the edge of the drill hole, predestine circular milling to be used for machining thin-walled space frame structures.

The machining of highly stressed lightweight products such as connectors for aluminium profiles require adequately adapted manufacturing processes. The adaptation of various profiles with different surface qualities to varying joining methods leads to complex workpiece structures. Today, an economic production often makes use of five-axis milling machines and modern cutting-simulation technologies. Algorithms from computer graphics allow the description of highly

accurate cutting chip geometries needing only NC-files, cutter data and the dimensions of the raw material. Efficient techniques allow not only to estimate the process forces related to tool deviations but also to generate optimised NC-paths that avoid contour faults and collisions between workpiece and tool. The use of FEA supports the consideration of additional stress and temperature conditions of the workpiece. These data are the basis for the selection of improved cutting strategies for various machining concepts. This article focuses on the practical analysis of the process chain from the NC-path generation via the milling simulation to the machining of lightweight aluminium nodes.

Manufacturing and application of extruded composite profiles

With a modified extrusion method, developed by the Institute of Forming Technology and Lightweight Construction at the University of Dortmund, the continuous extrusion of endless reinforced aluminium steel composites profiles becomes possible. Due to this innovative technology cable structures as well as solid wires can be joined to aluminium material. For the experimental investigations presented below, the composite extrusion profiles consist of common aluminium wrought alloy (AlMgSi0.5) as matrix material and high strength steel alloy (X12CrNi17-7) with good mechanical properties at elevated temperatures as reinforcement material. The shape of the reinforcing elements used are on the one hand flexible cables with a diameter of approximately d = 1 mm and on the other hand solid wires with a diameter of d =1 mm. The dimensions of the cross-section of the cable reinforced profiles are 20 x 5 mm with two fibres embedded in the aluminium matrix. The dimensions of the wire reinforced profiles are 56 x 5 mm with six reinforcing elements embedded, parallel to the extruding direction. Fig. 1 exemplarily depicts the extrusion process as well as the microstructure surrounding an embedded reinforcing cable.

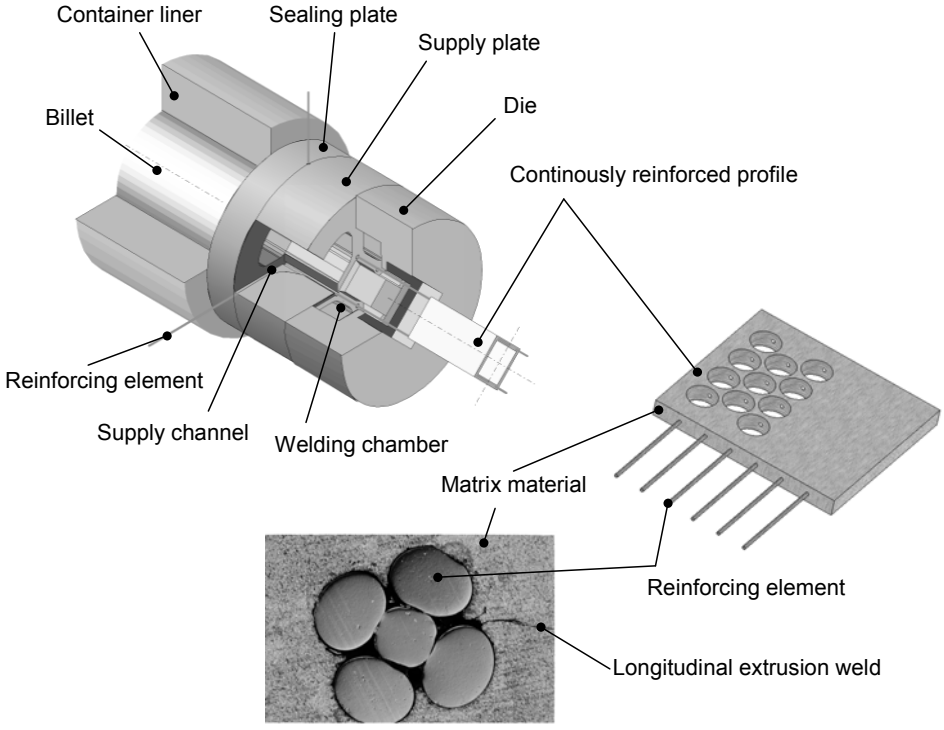

Fig. 1: Extrusion process and workpiece microstructure

Concerning the application of such composite profiles different fields of use can be derived. Especially due to specific properties like increased strength and restricted crack growth these

materials are predestined for security relevant components that need an overload protection. Beside a lot of imaginable applications for sports equipment, emergency equipment (lightweight rescue and recovery devices) etc, first concrete applications appear. For example reinforced profiles are used as security relevant stringer within aircraft construction and as side impact protection system for passenger cars or as wear resistant, lightweight conductor rail for crane constructions.

Cutting tools and test procedure

For the comparison of conventional drilling and helix milling for the manufacturing of holes in the continuously reinforced profiles different processes and tool concepts were analysed. Concerning the conventional drilling operation three standard drills with various designs as well as one chisel edge modified drill were applied under minimum quantity lubrication conditions for the machining of reinforced materials. The design of the used twist drills with a diameter of d = 8.5 mm can be seen in fig. 2. All drilling investigations were performed on a flexible machining centre Grob BZ600. The process related machining loads were recorded with a special measurement assembly consisting of a force plate for feed force and drilling torque detection, a signal conditioner to amplify the signals and a PC for signal analysis.

For the investigations of helix milling in reinforced aluminium, special single tooth milling cutters with diameters of d = 5 mm and d =12 mm were used. Previous investigations in conventional thin-walled aluminium profiles showed that especially the adhesive behaviour of the aluminium and the resulting disposal of workpiece material on the rake faces and in the flutes of multi fluted end mills lead to rapid tool failure [6]. Thus especially for relatively small tool diameters single fluted end mills with well dimensioned and polished flutes showed the best results. Furthermore all helix milling investigations were performed under dry cutting conditions.

To compare the process behaviour of different tool concepts, beside the cemented carbide end mills also a milling cutter d = 12 mm with cemented carbide inserts was applied. In this context fig. 2 shows the differences between the conventional drilling operation and the helix milling as well as their specific tool concepts. Also a process scheme and some tools for both operations can be seen in fig. 2.

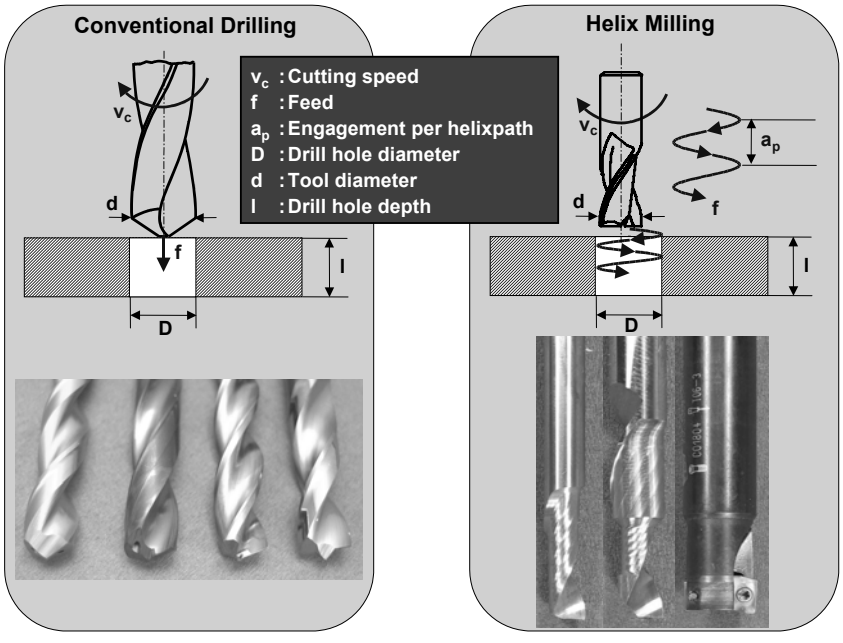

Fig. 2: Comparison of cutting operations for the machining of continuously reinforced extrusions

To realise adequate cutting speeds and feed rates for the helix milling operations these investigations were performed on a flexible machining centre Grob BZ40CS, which is specially designed for the machining of lightweight materials like aluminium or magnesium. With its spindle speed of n_{max} = 24.000 rpm it is able to realise a maximum cutting speed of v_c = 375 m/min while using end mills with a diameter of d = 5 mm.

Cutting behaviour while machining extruded composite profiles

The drilling of the reinforced aluminium profiles generates different feed forces and torques depending on the tool type and the adjustment of the machining parameters. The values of feed force and torque are measured during the machining process. The analysis of the recorded characteristics contributes to the basic understanding of the work process and helps to uncover differences particularly with the use of different tools.

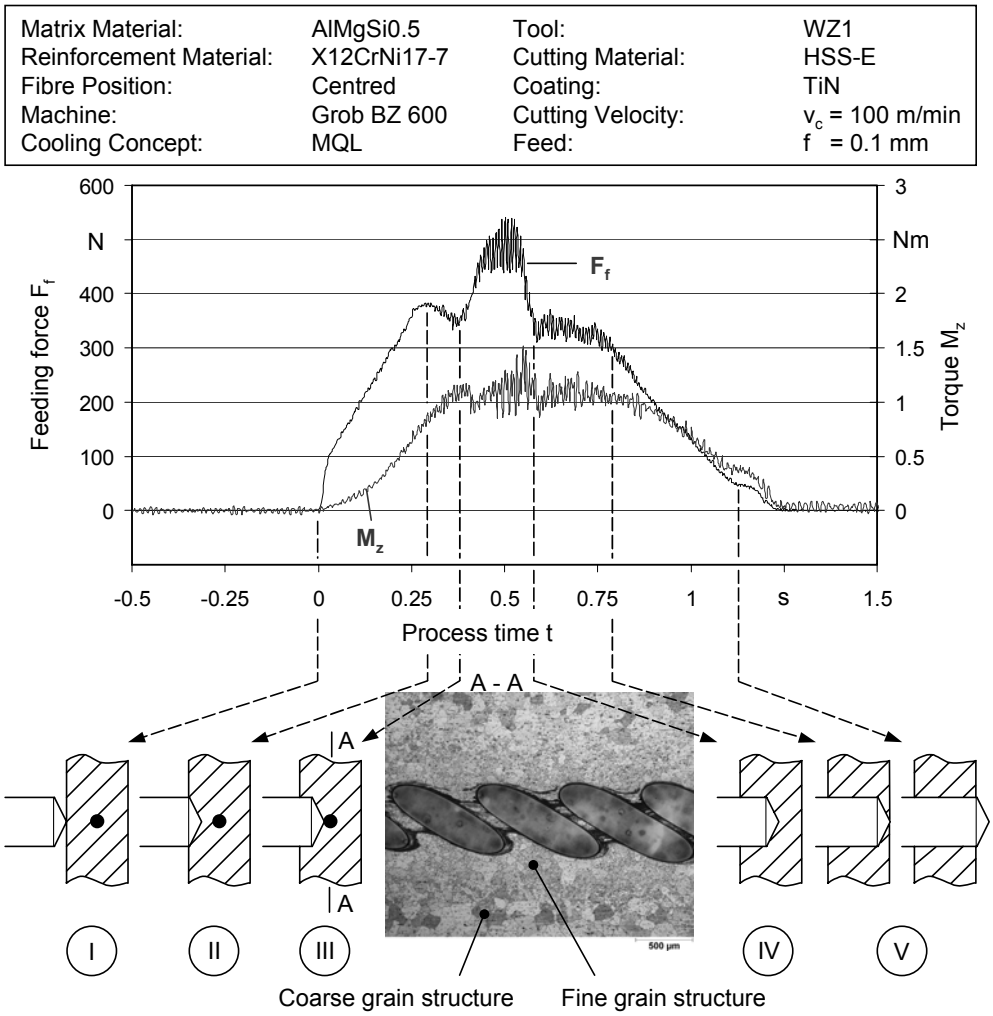

Fig. 3: Force progression while drilling cable reinforced Profiles

The machining process of the reinforced profiles can be divided into five phases:

I. Admission Phase: The tool touches the aluminium profile and starts the machining process. The drill enters the profile; aluminium is machined exclusively. Feed force and torque rise steadily till a first local maximum is reached. At this time the drill top has completely penetrated into the material, the work is continued with the full tool diameter.

II. Machining of Aluminium: Aluminium which is in work order in front of the reinforcement fibre is machined with the full tool diameter in this phase. The feed force remains almost unchanged; the torque rises slightly due to the increased friction with increasing drilling depth. Prior to the machining of the reinforcement fibre, the formation of a local minimum in the course of the feed force and the torque can be obtained frequently. The cause for this is a difference in the microstructure of the aluminium alloy in the surrounding of the reinforcement fibre.

III. Fibre cutting: The tool machines the reinforcement element. As a consequence the feed force increases to an absolute maximum in the temporal course. The torque course usually shows a typical frequency pattern in the area of the fibre if a tool with two cutting edges is in use.

IV. Machining of Aluminium: Aluminium which is in the work order behind the reinforcement fibre is machined with the full diameter of the tool. After the reinforcement element is cut, the feed force declines and similar to phase II., local minima in the course of the feed force and the torque can occur.

V. Exiting Phase: The tool reaches the back of the profile. The drill top exits the material before the tool protrudes from the workpiece in full diameter. The feed force and the torque decrease correspondingly. The work process is completed.

Besides the determination of process related machining forces, also measuring of tool wear and workpiece quality show interesting results that should be considered for process design. Especially the cutting edge design of the drills is important for the quality and the process reliability. While tools with sharp cutting edges and positive rake face angles showed the best cutting results when machining non-reinforced aluminium, this tool design is not convenient for cutting steel fibres in the composite material (see fig. 4).

The high strength properties of the steel fibres lead to significant tool wear when drilling these fibres. The reinforcing elements produce fractured cutting edges and spalling on the rake faces, so that an insufficient drill hole quality as well as an early tool failure results. Fig. 4 shows scanning microscopy images of a sharp and worn twist drill as well as the produced drill hole quality of this tool. At the first drill hole the cutting edge does not cut the material exactly in the area of the reinforcing fibre and already after 15 drill holes the tool produces unacceptable burrs. A conventional drill operation with the tested tool is therefore not appropriate for machining reinforced material. Also other tested twist drills react with insufficient tool life due to significant wear when machining the reinforced material.

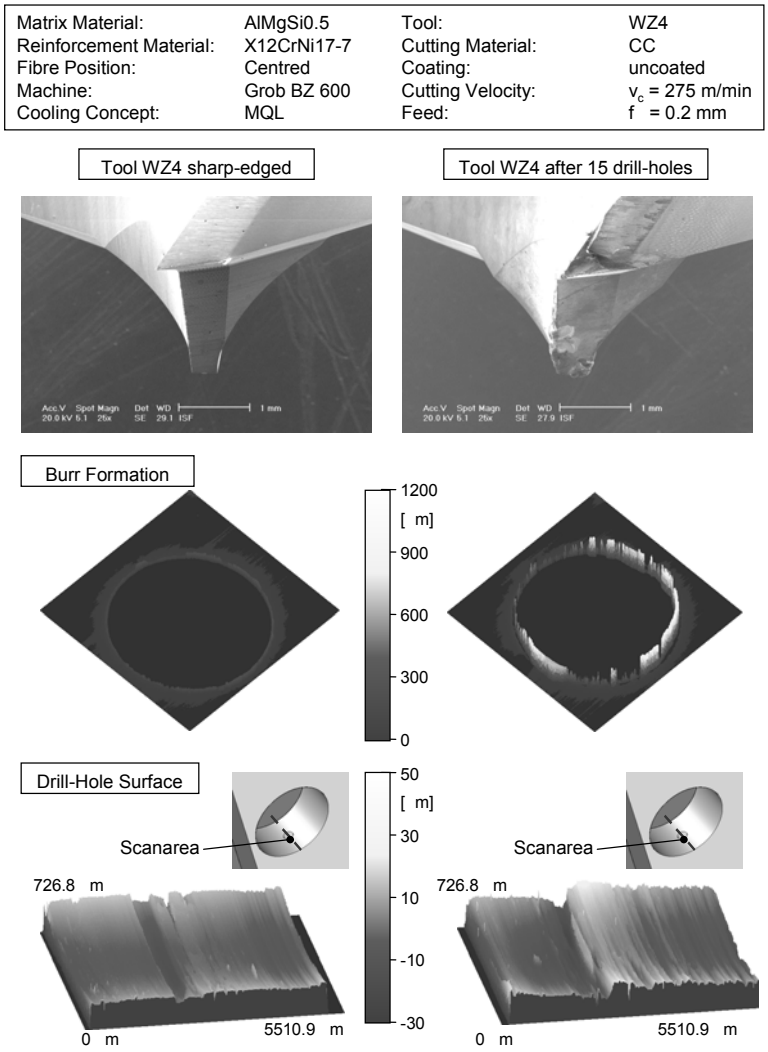

Fig. 4: Influence of wear development and machining quality

Against the background of insufficient surface quality and the significant burr formation when using conventional drilling processes to produce holes, the alternative helix milling operation showed promising results on the quality aspects. Furthermore with the aid of the helix milling an improved lifetime of the tools could be realised. However an increased machining time has to be considered.

With a modified cutting edge corner at the single tooth end mills, the wear behaviour as well as the cutting time can be improved, as it can be seen in fig. 5. Besides an increased engagement per helix path, reduced wear behaviour could also be realised due to a chamfer of 0.2 mm x 45° at the cutting edge corner. Because of this chamfer the most stressed part of the tool gets stabilised. Moreover it indicates, that in comparison to peripheral milling operations the wear development of the both cutting edges are of interest. Corresponding to the selected engagement per helix path the minor cutting edge is stressed and the loads at the major cutting edge are primary induced by the feed, so that the tool life depends basically on the material removal rate. Similar to the conventional drilling operation also at the helix milling the alternating cutting conditions of ductile matrix material and high strength reinforcing fibres leads to rapid tool wear. But the surface quality of the bore holes and the burr formation are clearly better.

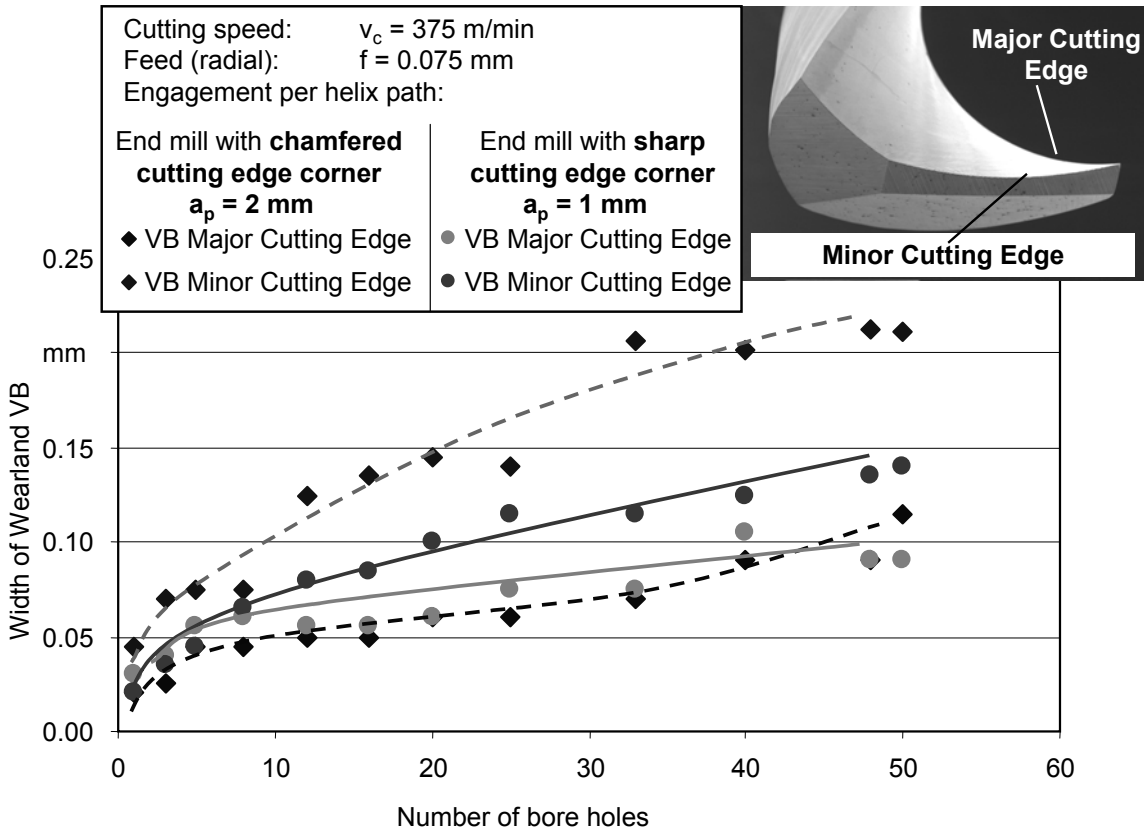

Fig 5: Wear development for a conventional and a modified end mill

Simultaneous 5-axis milling of aluminium nodes

Stable and safe processes are required for the milling production of complex lightweight adapted and load optimised nodes. Producing the geometrical accuracy and surface quality of mainly highly stressed parts is a task which is too complex to be designed and controlled manually, so that the demand for flexible computer-based simulations to support, control, and optimise the milling process is inevitable.

The types of nodes which are needed to combine profiles in lightweight structures are different, according to the method by which they should be connected. Depending on the intended purpose, these components can be connected by welding, adhering methods, through inductive magnetic energies [7] or through expansion with the help of rolling tools [8]. Besides manufacturing restrictions, constructive requirements, and demands to sustain stresses in the later product, the different joining methods lead to different shapes to be considered. Nodes for welding need an appropriate opportunity to connect the profile, drain the heat during the welding process, and specially designed grooves for the weld metal. Nodes for electromagnetical forming require different surface structures for different loads like torsion, tensile, or compressive stresses [9]. The general geometry varies, according to the type of the used profiles (round or square, opened or closed, tube or solid).

Different machine concepts lead to different constraints to be considered. The range of possible movements depends on the used machining concepts. Machines with a serial kinematic structure, e.g. allow a rotational movement of the tool holder with a fork head, parallel kinematics allow rotational and longitudinal movements through struts where each single strut is changeable in its length and carries its own actuation. A parallel kinematics machine (PKM) requires a different treatment than a machine with serial adapted axes and also allows other choices of cutting strategies. Therefore, it is necessary, not only to be aware of constant engagement conditions between cutting edge and material, but also to be conscious of the kinematic restrictions of the

machines used. Not every desired angle of the tool can be realized and not every needed rotational movement for positioning the tool or the workpiece can be accomplished in the way and the sequence it would be necessary.

Recent CAM-modules try a machine-neutral planning of the tool-paths in a first step and an additional consideration of dynamic and geometric restrictions through machine-specific postprocessors in a second step to generate the NC-data, but a preceding consideration of the chosen machine is not possible. Recent milling simulations offer a chance to consider the cut material for each single tool rotation as well as the synchronous movement of all machine axes [10]. The use of Finite Element Analysis (FEA) is another simulation method for analysing segmented chip formations for high speed cutting processes [11]. It can be also a helpful tool for the estimation of temperatures, structural deformations, strains, and stresses resulting from an external load acting on a respective part [12].

Multi-axis tool path strategies are often designed as an addition to existing three-axis strategies. The paths are planned as a three-axis movement with an additional two-axis movement to change the orientation of the tool to the workpiece. This additional rotational movement often requires extensive programming experiences to design expedient and efficient tool paths which are free of collisions between tools or tool holders and the workpiece. A few software tools in modern CAM-systems deliver some kind of collision detection, but they are often restricted to three-axis milling or to collision detection against the final geometry only and not against the current process geometry of the free-formed surface. In order to obtain stable and safe processes, solutions are required which provide a generation of collision-free multi-axis tool paths as well as a consideration of machine-specific dynamic restrictions and opportunities to gain constant engagement conditions.

An important aspect is the generation of adequate NC-paths which on one hand allow constant cutting forces and on the other hand provide a collision-free milling process. Therefore it is necessary to choose the right strategies according to the used machine concept. The second aspect is that different machine concepts lead to different constraints to consider, so that not only the variation of the aluminium structures needs to be considered but also the behaviours and restrictions of the machines used. A third aspect is given by the form of the connector itself. Different joining methods like welding or electromagnetic forming require different forms and also different surface qualities or a special design of the surface to provide a maximum of stiffness and load capacity. The idea of including the possibility for an adaptation of different aluminium profiles enlarges the range of constraints to be considered.

Simulation and practise

A software library, which was developed at the Department Of Machining Technology (ISF) at the University of Dortmund, offers the opportunity to increase the potentials of five-axis milling. The oscillations of long tools can be noticably reduced, the cutting conditions can be adapted to the recent engagement conditions and an accompanying harmonisation of the tool movements and process safe collision detection and avoidance can be accomplished. This library is based on a rotationally symetric model for the tool and the tool holder and a multidexel volume model for the workpiece. The combination of this two models allows a fast, flexible and precise calculation of single process steps and the resulting process forces [13].

The use of the simulation is following directly after the CAM-based generating of NC-files (s. fig. 6). In case of a possible failure (e.g. a collision), which does not only lead to high tool costs and waste of workpieces but also can affect parts of the machine, the riscs can be detected and avoided during the planning phase.

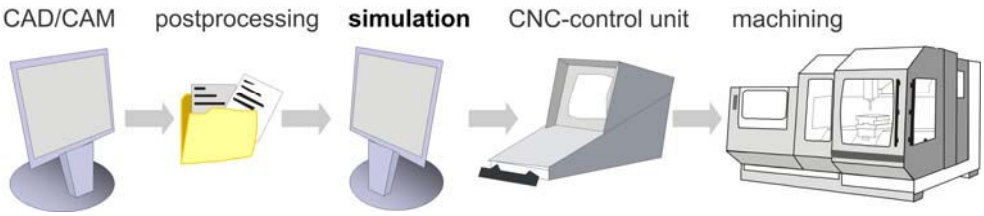

Fig. 6: Description of manufacturing the node

The difficulties of milling the nodes is shown in fig. 7. Whereas the roughing process in area A, where one part of a profile will be attached later on, is possible with a 3-axis process (endmill with inserts, d = 16 mm) unto the full depth of 78 mm, the semi-finishing (spherical mill, d = 6 mm) and the finishing process (spherical mill, d = 3 mm) is only possible with a simultaneous 5-axis movement to avoid collisions between the tool holder and the workpiece to optain the desired geometry. A 3-axis movement unto the depth of 78 millimeters would requiere long and thin tools. The use of these tools would lead to unwanted oscillations and, due to the thin tools, to an unreliable process.

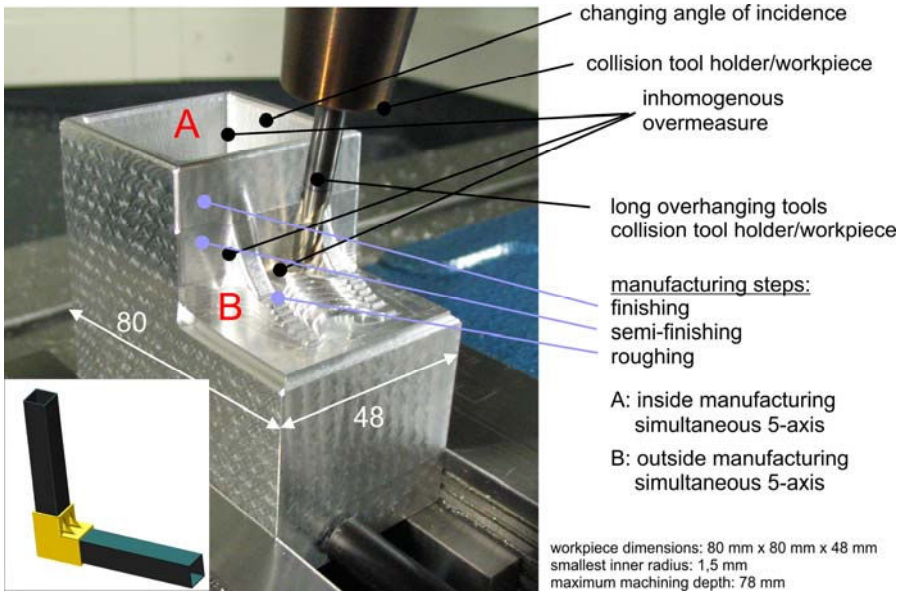

Fig. 7: Description of manufacturing the node

Area B shows the three different manufacturing steps from the bottom of the rips to the top of the part. The semi-finishing and the finishing processes also require a simultaneous 5-axis movement of the tool. On the one hand to avoid long clamped tools or collisions and on the other hand, to react to the constantly changing engeagement conditions when manufacturing the rips. Because of the higher overmeasure in the corners between the rips and the main part after roughing, the enlacement of the material around the tool increases. This leads to higher process forces and force peaks which are often stressing the tool more than needed for a reliable process. The developed simulation tool is able to calculate these engagement conditions and the existing process forces before the manufacturing process and is able to recalculate the toolpaths and feedrates to set a maximum force level to reduce this tool stress and to avoid oscillations.

Fig. 8 shows a graph of measured and simulated process forces during the semi-finishing milling with a titanium-nitride coated spherical cutting tool (d = 6 mm) along the rips.The calculated forces have a maximum difference of 2 N according to the simulated forces for the time of one single chip removal. It has turned out to be enough for a precalculation. The higher the resultion of the simluation is, the more accurate are the results.

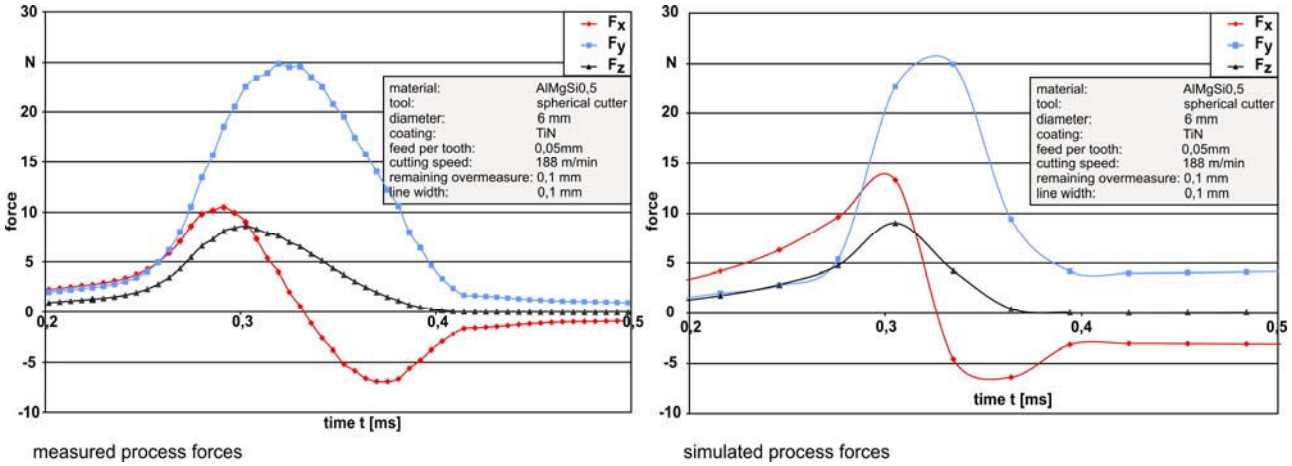

Fig. 8: Measured and simulated process forces during the manufacturing process of an aluminium node

The visual part of the simulation contains all the necessary information to analyse the different steps of the milling process (fig. 9). The geometry of the tool and the tool holder have to be set, the geometry of the workpiece its self is according to the milling paths which should be shown. From the dimensions of a raw part of the roughing process to the finishing process, the workpiece can be shown in its different manufacturing steps. In this picture, the semi-finishing process (1) along the rips and the following finishing step (2) can be seen as well as chamfering (3) and finishing (4) the intake (A in fig. 7). Besides that (on the left), the recently calculated cutting volumina are shown and according to those volumina, a graph shows the according process forces. The real picture on the upper left shows a part of a surface which was not optimised through the simluation. High peaks of process forces lead to oscillations which can be seen as marks on the surface.

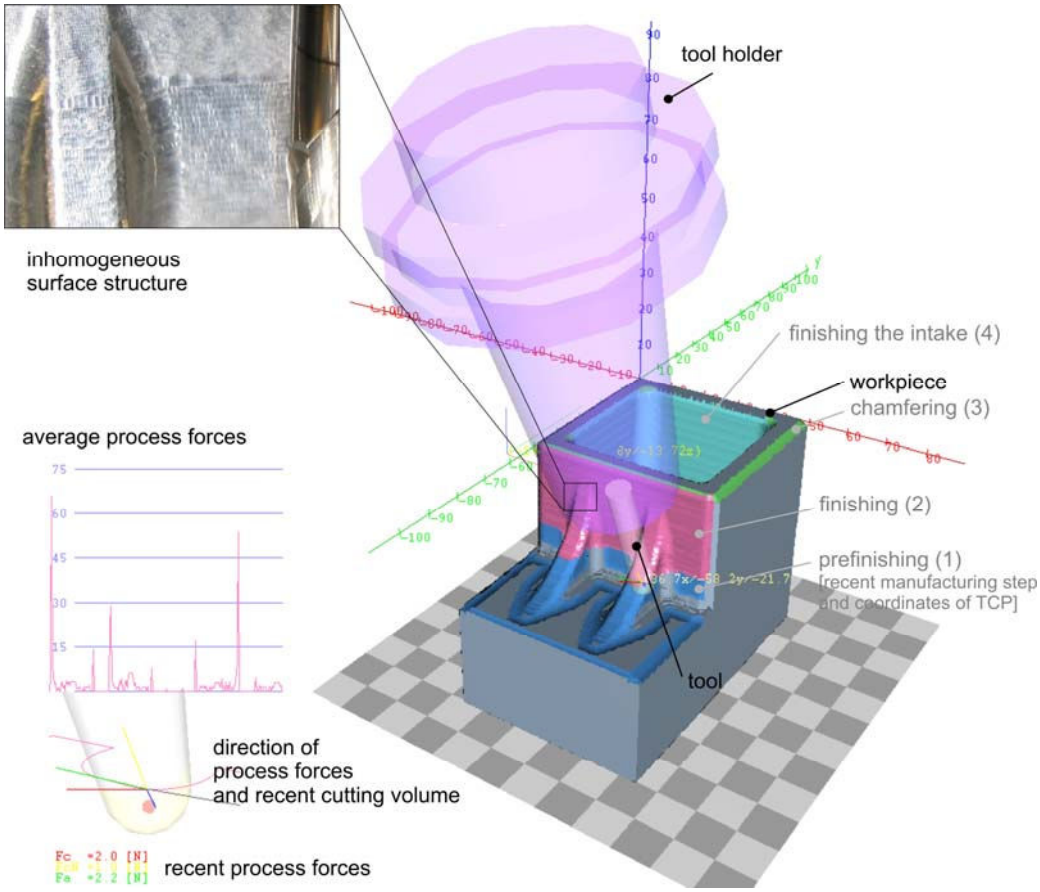

Fig. 9: simulation of manufacturing the node

A further problem in manufacturing aluminium lightweight components is given through the generated process temperatures. A high level of reliability in later apllications is only possible, when high temperatures, which could influence the stability of the components, can been avoided. This is another aspect which will be included in the simulation.

Summary

The conducted investigations show that the machining of the aluminium and steel composite material makes adapted cutting tools as well as adapted processes necessary. While the conventional drilling operation provides a short essential operating time, the helix milling leads to excellent surface qualities and little burr formation. Especially the combination of two different material related cutting behaviours lead to increased mechanical tool loads which result in rapid tool wear. Due to a modified cutting tool design a first solution which considers different cutting demands in one tool could be developed.

For both operations further investigations have to show, how to reduce the tool wear by using tool coatings, further tool geometries and cutting materials. Also investigations concerning the machining related material and workpiece changes have to be carried out.

Concerning the simultaneous 5-axis milling of the lightweight aluminium nodes, an interaction of the single components is necessary. The basic aim of the milling process has to be the conversion of the existing tool paths into an accurate workpiece. Besides the geometrical accuracy of the machining concept, the dynamic behaviour along the feed direction has to be implemented precisely. Importing all the necessary information for reliable process conditions into the described simulation allows to control the tool paths and to optimise them in terms of a harmonic and collision free movement of the tool. Considering the process temperatures fullfills the opportunity to increase the process reliability and the quality of the produced parts with just a small intermediate step in the process chain between CAD and production.

Acknowledgement

This paper is based on investigations of the collaborative research centre SFB/TR10 which is kindly supported by the German Research Foundation (DFG).

References

[1] M. Kleiner, M. Schomäcker, A. Klaus: Verbundstrangpressen In: Aluminium, International Journal for Industrie, Research and Application, Volume 80 (2004) 12, S. 1370-1374

[2] M. Kleiner, M. Schomäcker, M. Schikorra, A. Klaus: Herstellung verbundverstärkter Aluminiumprofile für ultraleichte Tragwerke durch Strangpressen In: Materialwissenschaft und Werkstofftechnik 2004, 35 , Nr. 7, S. 431-439

[3] K. Weinert, N. Hammer: Analyse der spanenden Bohrbearbeitung an Space-Frame-Strukturen. Aluminium, International Journal for Industry, Research and Application, 80 (2004) 12, S. 1382-1387

[4] K. Weinert, S. Gruenert, M. Kersting, N. Hammer: Analysis of Circular Milling Processes for Thin-Walled Space-Frame-Structures Applying FEA-Simulation. Production Engineering – Research and Development, Annals of the German Academic Society for Production Engineering, XIII (2005) 2

[5] R. Janssen: Bohren und Zirkularfräsen von Schichtverbunden aus Aluminium, CFK und Titanlegierungen. Dissertation Universität Bremen, Shaker Verlag, 2003

[6] K. Weinert, N. Hammer: Zirkularfräsen von Bohrungen im Leichtbau. In: WB Werkstatt und Betrieb, Industrielle Metallbearbeitung 137 (2004) 10

[7] Homberg, W.; Marré, M.; Kleiner, M.: Umformtechnisches Fügen leichter Tragwerkstrukturen. Aluminium, International Journal for Industrie, Research and Application, Volume 80 (2004) 12, S. 1396-1400.

[8] J. Mehnen, J. Rautenberg, M. Hagedorn, J. Schaefer: Fertigung von Leichtbaustrukturen. In: Spanende Fertigung, 4. Ausgabe, Hrsg. K. Weinert, Vulkan Verlag, Essen, 2005, ISBN 3-8027-2935-8, S. 403-410.

[9] E. v. Finckenstein, H. Bühler: Fügen durch Magnetumformung – Lösekräfte von Sickenverbindungen aus Stahl. WB Werkstatt und Betrieb, 101 (1968) 11, pp. 671-675

[10] P. Damm: Strategien zur 5-achsigen Hochgeschwindigkeitsbear-beitung von Freiformflächen. In: Proceedings of Intelligente Leichtbau Systeme ILS 2003, NMN e.V., Hannover, 2003

[11] Behrens, A.; Westhoff, B.: Numerical Simulation of Chip Formation Processes. Production Engineering – Research and Development IX (2002) 1, pp. 13-16

[12] K. Weinert, M. Stautner, C. Peters, J. Mehnen: Combining Finite Element Analysis and Simulation of Cutting Engagement Conditions. Production Engineering, X (2003) 2, pp. 47-51

[13] A. Zabel, M. Stautner. Einsatzfelder der mehrachsigen Frässimulation. wt Werkstattstechnik online, 95 (2005) 1-2, S. 56-61

doi:10.4028/www.scientific.net/AMR.10.65

Laser Bifocal Hybrid Welding of Aluminum

Trautmann, A. [1, a], Zaeh, M. F.[1, b]

[1]Institute for Machine Tools Industrial Management,

Technical University of Munich, Boltzmannstr. 15, 85748 Garching, Germany

[a]andreas.trautmann@iwb.tum.de, [b]michael.zaeh@iwb.tum.de

Keywords: Laser welding, hybrid, bifocal, aluminum, EN AW-6060, filler wire, finish crater.

Abstract. This paper renders research into the fundamentals governing the melt pool dynamics of a hybrid bifocal laser welding system consisting of an Nd:YAG and a high power diode laser (HPDL). The resulting superposition of keyhole by heat conduction mode welding is assayed for extruded aluminum. In particular the diffusion of the surface oxygen layer is considered. By comparing the results attainable by bifocal laser hybrid welding to the constituent laser processes synergetic effects of the laser hybrid can be demonstrated. These are namely the doubling of the welding speed from 2.0 min^{-1} to 4.0 m min^{-1}, the reduction of the roughness of the weld surface from 60 µm to approximately 10 µm and an increase in energy transfer efficiency. The experimental investigations verifying these synergies are outlined and discussed.

Introduction

The experimental setup of the bifocal hybrid laser system consists of an Nd:YAG laser (transmitted by optical fiber) and a high power diode laser (transmitted directly), both of 3 kW maximum output power. The beam parameter product (BPP) of the Nd:YAG laser of 25 mm*mrad translates with an optical system of focal length f = 150 mm into a circular focus of diameter 0.45 mm whereas the BBP of the HPDL of 85 x 200 mm*mrad can achieve a rectangular focus of 0.9 mm x 3.7 mm. Both lasers act within the same process zone and can be focused independently on their respective focal plane either coinciding with the work pieces' surface or on a plane within the work piece. However the system is not limited to variations of focal plane in z-direction. In addition the foci can be moved against each other in the x-y plane. The aluminum alloy considered is EN AW-6060 (AlMgSi0,5) temper T66 without and with filler wire Al4047 A (SG-AlSi12). Specimens were received extruded and of 2 mm thickness.

Welding Technology of Aluminum

Motivation. Forecasts suggest that Europe and the North America will at least until 2011 retain the biggest shares of the automotive market worldwide. Thus, most car manufacturers try to satisfy the demands of both markets to maximize the number of potential customers. Most European car producers are meanwhile as much dependent on their American as on their home markets.

In late 2004 the U.S. Secretary of Transportation proposed a major regulatory upgrade in side-impact crash protection for all passenger vehicles. Federal Motor Vehicle Safety Standard 214 is about to be accordingly strengthened and the requirements for crashworthiness will follow. Passive security systems will not be able to satisfy those regulations on their own. So surely the space frame and body shell have to be toughened to absorb the additional distortional energies. Henceforth it would seem inevitable for the car chassis to have its weight increased.

Europe obliged itself to reduce overall CO_2-emissions to counteract climate change. Although the Kyoto protocol might never be enacted worldwide, the pressure from environmentalists is still considerable. On the other hand costumers seek more saving vehicles, since oil is on a decade high and petroleum tax adds to gas prices.

To met these demands the automotive industry has to satisfy two diametrically opposed aims. In the USA vehicles need to be much tougher, meaning heavier, and in Europe lighter in order to consume less fuel [1].

Light weight design and further application of light weight alloys can overcome this predicament by reducing weight as well as increasing strength. Hence joining techniques are needed which satisfy the requirements of modern vehicles manufacturing [2]. In production they need to be reliable, robust and produce repeatable results which can be quality controlled by sensor systems [3]. For their economic case they need to be profitable and moreover the expectations of the costumer need to be fulfilled. Thus such new technologies are under the scrutiny of manufacturing, economics and sales [4].

Arc-Welding of Aluminum. Classical fusion welding techniques, such as MIG, TIG and other arc and plasma utilizing processes can achieve satisfactory welds, however cracks, pores, inclusions and other defects in the fusion zone are to be heeded [5]. The welding process itself induces a heat affected zone (HAZ) in the material. In classical welding this zone is considerably enlarged compared to laser welding thus leading to an increase in distortion of the structure [6]. In case of heat tempered material those advantageous effects are lost in the HAZ.

However welding with laser reduces the size of the HAZ as well as overall heat input into the structure. Several techniques have been developed to preserve this advantage as well as simultaneously to counteract the arise of cracks, pores and other defects.

Arc-Augmented Laser Welding. There have been a number of industrial developments, where the laser beam has been combined with the arc from a conventional welding power source. Currently, several laser/MIG welding heads are commercially available and the process has been able to produce the “sturdiest vehicles doors in the world” [7]. MIG, TIG and plasma-arc processes have been adapted, enabling higher welding speeds, particularly in thin sheet automotive industry. In addition to higher speeds the enhancement of the laser beam allows greater variations in fit-up to be tolerated. Penetration is increased and the change in shape of the weld pool assists in allowing hydrogen to diffuse out of the joint, reducing porosity [8]. This hybrid process has been implemented into production lines and will gain a widening field of application, where welding speed and penetration depth of the constituting arc process has reached its limits.

However the physical phenomena and the mechanisms influencing penetration are yet not fully understood, e.g. the absorption mechanism are different for radiation mediated energy input of a laser compared to matter, i.e. electron, mediated energy transfer of an arc welding process. Experience in research as well as industrial development showed that the adjustment of the process’ parameters is complex and elaborate [9]. The interplay of arc and laser process does not allow for one to be independently varied of the other. The process gas, which has been demonstrated to have a meliorating effect on penetration and porosity, can not be freely chosen in its composition without repercussions on the arc welding process.

Multiple Spot Laser Welding. Since laser welds in aluminum are prone to porosity several techniques utilizing multiple focal spots to influence keyhole geometry during welding have been devised. The low viscosity of molten aluminum and its alloys compared to iron in steels causes the keyhole to easily close up at the orifice. Up to three multiple beams at a time can significantly influence the keyhole’s geometry. Moreover, they fail to generate pore free fusion zones. [10]

The so called twin spot uses two laser beams. One of which is focused onto the plates surface to enable keyhole welding whereas the other is defocused to create a broader intensity distribution to act as an extended heat source. As an effect the orifice of the keyhole opens up and facilitates diffusion of gas entrapments as well as stabilizing the overall welding process. The success of this method has been demonstrated [11], and optical systems for twin spot welding are commercially purchasable. However the corresponding optic splits a single beam emerging from an Nd:YAG laser source. Thus the power which can be attributed to each of the two beam profiles is limited by the nominal output power of the Nd:YAG laser source used. Nd:YAG lasers are readily

commercially available up to 4.5 kW nominal output power for a buffered 6 kW system. Assuming that the heat loss due to the optical system is approximately 0.5 kW, an even beam splitter thus provides max. 2 kW for deep penetration welding and 2 kW for the heat source acting at the surface. By reducing of the power share of one beam part in favor of the other it seems difficult to sustain their respective favorable effects during welding. Hence, such systems are not flexible with regards to the adjustment of the secondary laser beam independently of the primary beam, i.e. neither power nor independent control of both laser sources. The independency of control is however a critical enabling factor for the prevention of finish craters of aluminum fusion weld seam, as described below.

Fundamentals and Constituent Processes of Hybrid Bifocal Laser Welding

In contrast to the laser/MIG hybrid process the bifocal hybrid is a combination of two laser sources, namely an Nd:YAG laser and a high power diode laser (HPDL) [12]. The two beams are superimposed in the process zone and thus interact to beget several synergetic effects. The welding results of each laser source, which they achieve independently, are outlined in the following. In specific cases the designation as synergy will be justified by experiment.

Heat Conduction Mode Welding with HPDL. In aluminum alloys such as EN AW-6060 the HPDL can merely initiate heat conduction mode welding. The characteristic weld pools have an aspect ratio. i.e. width over depth of the fusion zone, ≥1. Fig. 1 displays the widths of the overbeads achieved in EN AW-6060 for varying HPDL powers and feed speeds. For steels the HPDL enables the transition from heat conduction mode welding to deep penetration welding. Since the reflectivity of aluminum is up to 87 % (cf. steel: 58 %) and its thermal conductivity is considerably higher than for iron, the threshold for keyhole welding can not be reached [13].

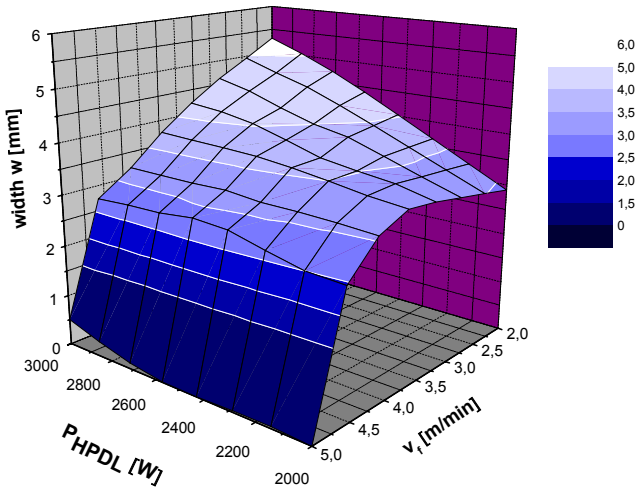

Fig.1: HPDL power and v_f versus width

Yet deep penetration welding is a critical deciding factor to avoid the ‘kissing bond’ phenomenon in aluminum welds. Without special pre-process treatment such as pickling or in-process removal of the surface oxide layer, heat conduction mode welds lack coalescing fusion of the alloy’s matrix. On the contrary, butt joints show the former divide. The surface oxide layer on the edges can not be dispersed by convectional fluid flow throughout the melt pool. Moreover the vaporization temperature of aluminum is practically coinciding with the melting point of aluminum oxide. See Table 1.

Material Property	*Al*	*Al_2O_3*
Melting Temperature [°C]	660	2054
Vaporisation Temperature [°C]	2060	·/·
Thermal Conductivity [W m^{-1} K^{-1}]	230	6.3 - 30
Density [g cm^{-3}]	2.7	3.9

Table 1: Material Properties

In addition the thermal conductivity of Al_2O_3 is below that of pure aluminum. Thus excess heat energy is accumulated in the aluminum oxide layer until its phase transition from solid to melt. Concomitantly, the evaporating base aluminum causes characteristic voids. The evaporating aluminum can be seen to bubble through the Al_2O_3 on the perimeter of the weld pool in fig. 2. The HPDL can therefore not satisfactorily join aluminum alloys.

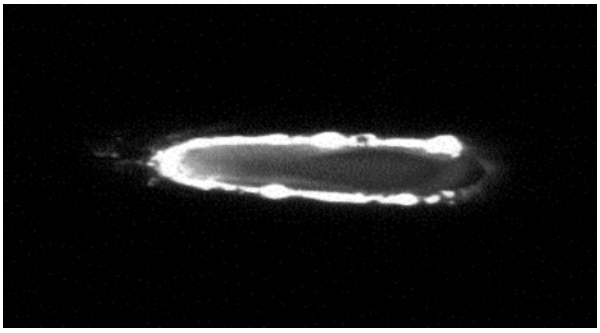

Fig.2: High speed photograph of weld pool perimeter

P_{HPDL}= 3 kW; 10000 fps; f = 150 mm; φ = 20°; Lasgon 25 l min^{-1};
v_w= 2 m min^{-1}; bead on plate EN AW-6082

Besides all these drawbacks the HPDL induces several advantageous effects when welding aluminum alloys. Heat conduction welding causes the characteristic sedation of the melt pool dynamics by convectional fluid flow. The oxide layer breaks up upon welding on the upper side of work piece. Pure aluminum melts at a much lower melting point temperature asAl_2O_3 as can be seen in table 1. Hence, the heat gradient induced in the work piece by a discrete heat source explains why solid aluminum oxide initially floats on the molten base metal until it melts down or more likely submerges as its density well is above that of aluminum. The dissolving oxide film can be seen in fig. 3 appearing dark on the melt pool's surface.

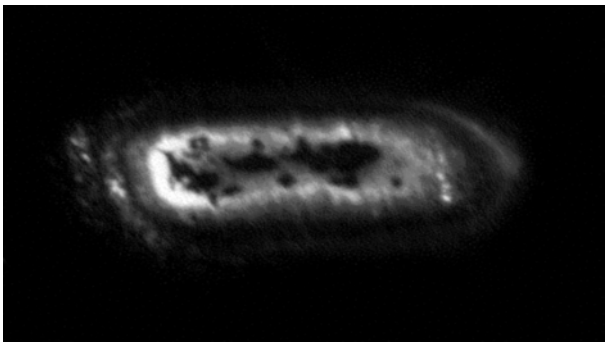

Fig. 3: High speed photograph of surface oxide

P_{HPDL}= 3 kW; 10000 fps; f = 150 mm; φ = 20°; Lasgon 25 l min^{-1};
v_w= 1 m min^{-1}; bead on plate EN AW-5754

Deep Penetration Welding with an Nd:YAG Laser. The energy density within the focal spot of the described hybrid system is well above the threshold to vaporize aluminum, since the Nd:YAG laser supplies 3 kW to the fusion zone. Hence, keyhole welding is achieved, the fluid dynamics of which exhibits vigorous fluid flow within the thermal capillary. Welding by avail of a keyhole accomplishes the dispersion of the oxide layer on the surface and more importantly on the edges of work pieces throughout the fusion zone.

Notwithstanding these advantages of the process the size of the Nd:YAG laser's focal spot necessitates precise positioning of the work pieces. Gaps in the order of magnitude of the beam waist in the focal plane result in the laser beam not to be obstructed by the work piece. Then the beam is not absorbed but transmitted and melting of the work pieces can not be achieved. Although laser welds in aluminum are less prone to porosity than laser/MIG welds, pores still exit in Nd:YAG laser welds [8]. In the following it will be shown the by using the hybrid welding technique the porosity in EN AW-6060 can further be reduced. This process result has to be considered in the context of ISO 10042 [14], which deals with arc-welded joints in aluminium and its alloys and defines auality levels for imperfections and ISO 13919-2 [15] on electron and laser beam welded joints providing guidance on quality levels for imperfections. Part 2 of ISO 13919 is specifically on aluminium and its weldable alloys.

In both standards quality level B imposes the strictest requirements yet allowing some pores. In arc-welded joints however more porosity is permissible than in laser welds. A quality level free of pores for which quality level A was obviously saved is not standardized, which is due to the fact that porosity in aluminium alloys can practically not be overcome in fusion weld joining.

Synergetic Effects in Hybrid Bifocal Welding Technology

According to definition a *hybrid* process is a functional unit in which two or more different technologies are combined, i.e. deep penetration welding of an Nd:YAG laser together with conduction mode welding of a HPDL. Since both lasers are focused on the surface of the work piece the process is termed '*bifocal'*. For a synergy two propositions have to be fulfilled:

1. The interaction of two or more processes so that their combined effect is greater than the sum of their individual effect.
2. Moreover the behavior of whole system is not predictable from the behavior of separate parts.

The first proposition requires *quantitative* analysis of each of the contributing process as a prerequisite to demonstrate a synergy. The second proposition calls for *theoretical* analysis, as one can only speak of a synergy if experimental results are well beyond what could be induced and expected form already known data.

Welding Defects and Porosity. Porosity is detriment to the mechanical properties of the seam in quasi-static tensile as well as dynamical loading. Macroporosity denoting pores which can be resolved by the naked eye, i.e. as small as 0.1 mm in diameter, are well reported in fusion welding of aluminum alloys. The pores seen in extruded EN AW-6060 have the following major causes:

1. The extrusion process gives rise to contaminations of the base metal as well as the surface. Upon fusion welding *contamination* pores arise.
2. The solubility of hydrogen in the aluminum melt of 6.5 10^{-3} ml g^{-1} drops to 0.34 10^{-3} ml g^{-1} upon solidification. *Hydrogen* pores precipitate in the fusion zone close to free surfaces.
3. The instability of the thermal capillary causes entrapment of gas bubbles during keyhole welding. These artifacts of the employed welding technique will subsequently be called *process* pores.

Contamination pores are randomly distributed throughout the base metal and should be rather small for quality controlled aluminum profiles. Hydrogen can enter the fusion zone via free surfaces, as it is a constituent of the ambient atmosphere. Proper shielding of these surfaces by hydrogen free gas can counteract their formation. However contaminations of the edges of the work piece with organic material can release hydrogen upon sublimation during welding. Fig. 4 shows pores located in the vicinity of the former dividing edge and close to the lower free surface, since the root was not protected by shielding gas. Proper cleaning and degreasing can prevent these pores.

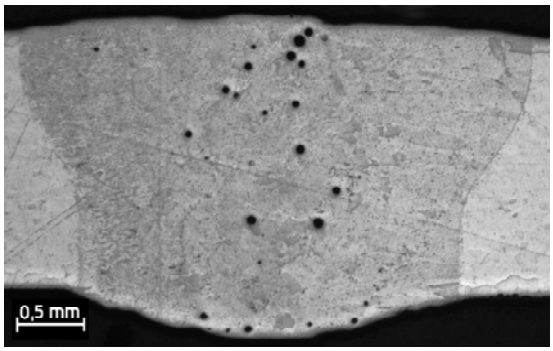

Fig. 4: Hydrogen pores

P_{hybrid} = 3 kW + 3 kW; f = 150 mm; φ = 20°; Argon 25 l min^{-1};
v_w= 3.75 m min^{-1}; butt joint EN AW-6060

Process pores in aluminum are due to the fact that the orifice of keyhole apperiodically closes up, as can be seen in high speed photography. The resultant entrapments within the solidification front of the thermal capillary form characteristically extended pores, as can be seen in fig. 5.

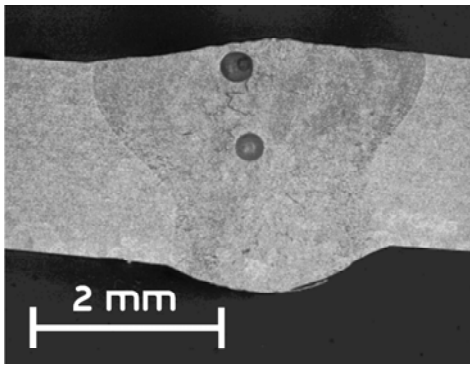

Fig. 5: Process pores

P_{hybrid} = 3 kW + 3 kW; f = 150 mm; φ = 20°; Argon 25 l min^{-1};
v_w= 4.0 m min^{-1}; butt joint EN AW-6060

The variables of welding of the bifocal laser hybrid process are not affected by a change in gas composition, as is a hybrid based on an arc technique deploying the voltage to ionize the gases used. Thus the specific influence of different gas mixtures on porosity can be studied by a laser process, since the welding parameters remain unchanged. For EN AW-6060 porosity is significantly reduced by using hybrid bifocal welding compared to the Nd:YAG laser alone, irrespective of gas. Yet mixtures of argon and helium considerable reduce porosity as can be seen in fig. 6 and 7. Contamination pores are also visible. The HPDL stabilizes the keyhole, thereby reducing process pores.

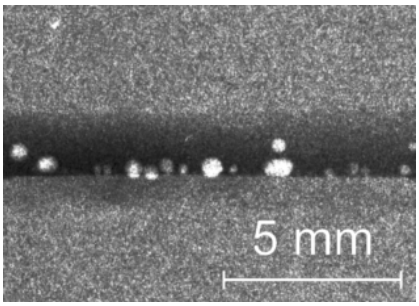

Fig. 6: Shielding gas 100 %,argon, top view X-ray of porosity

P_{hybrid}= 3 kW + 3 kW; f = 150 mm; φ = 20°; Argon 11 l min^{-1};
v_w= 3.0 m min^{-1}; v_f = 1.7 m min^{-1}; butt joint EN AW-6060

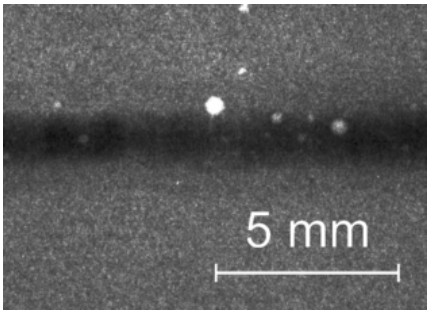

Fig. 7: Shielding gas mixture He 50 % + Ar 50 %, top view X-ray of porosity

P_{hybrid}= 3 kW + 3 kW; f = 150 mm; φ = 20°; He/Ar 40 l min^{-1};
v_w= 3.0 m min^{-1}; v_f = 1.7 m min^{-1}; butt joint EN AW-6060

Surface Quality and Roughness. For automotive shell bodies which are to be ready for immediate lacquering subsequent to welding the beads should be smooth and free of spatter. Generally, the usage of filler wire decreases surface roughness. So for these experiments the amount of Al 4047 A was normalized with respect to the welding speed. The surface roughness determined according to ISO 4287 [fehlt noch] of beads welded with Nd:YAG laser is R_t= 60.3 µm. Although heat conduction mode welding with the HPDL could not create a stable coalescence of the work pieces it sets the benchmark for surface roughness. Bead on plate welds exhibited R_t= 9.8 µm. Butt joints showed R_t= 19.3 µm, because the oxide layer on the edges could not be dispersed by the HPDL. The bifocal butt weld had a surface roughness of as small as R_t= 6.3 µm, thus obviously making full use of the sedation of the weld pool surface by the convectional fluid flow within the train of the melt pool subsequent to the keyhole.

Process Efficiency and Welding Speed. Figures of merit such as the energy transfer efficiency η_{ET} or the melting efficiency η_M which is correlated to the process efficiency η_P characterize a given laser process. These quantities are defined as follows [16]:

$$\eta_{ET} \equiv \frac{E_a}{E_L} \tag{1}$$

$$\eta_M \equiv \frac{E_m}{E_a} \tag{2}$$

$$\eta_P \equiv \frac{A \cdot v_w \cdot \rho \cdot \left[c_o\left(T_m - T_0\right) + h_m\right]}{P_{laser}} \tag{3}$$

E_L is the energy irradiated by the laser onto the surface, E_a is the energy absorbed by the workpiece and E_m is the energy necessary just to melt the base metal. A is the cross sectional area of the fusion zone, v_w the speed of welding, ρ the density, c_0 the specific melting energy, T_0 the initial temperature, h_m the specific melting energy and P_{laser} the power of the laser.
Measurements were made with the calorimetric method of both the power of the laser and the energy absorbed within the work piece. For HPDL η_{ET} was experimentally determined to be 0.37. This is almost three times as high as the reflectivity of 0.87 would allow for. However, η_{ET} is increased by the absorptive layer of Al_2O_3. For the Nd:YAG laser η_{ET} is 0.55 and thus greatly increased then the reflectivity of 0.93 would suggest. Multiple reflections on the wall within the keyhole can account for this result. The theoretical combination of these figures renders a nominal value for η_{ET} of 0.45 for bifocal welding.
The synergy is obvious from the experimentally determined value of 0.55 being 20 % above the calculated efficiency. These results were normalized to a specific v_w. Unsurprisingly the speed of welding still enabling root fusion rises from the benchmark set by the Nd:YAG laser of 2.0 m min^{-1} to 4.0 m min^{-1} for the hybrid process. Penetration depth versus variation of laser powers is shown in fig. 8.

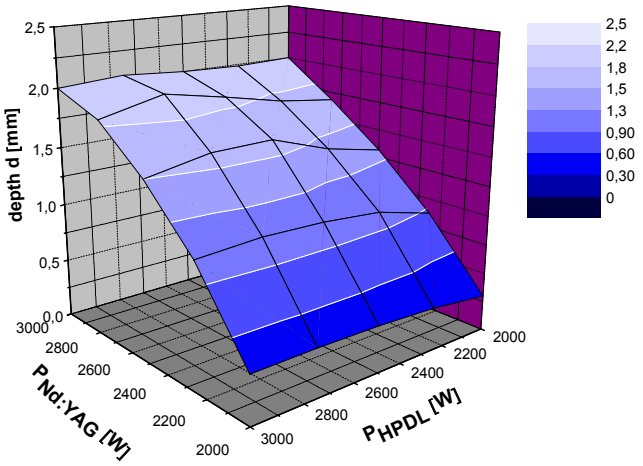

Fig. 8: Hybrid laser power of Nd:YAG and HPDL versus depth

The doubling can be contributed to the increased energy transfer due to the stabilization of the keyhole or the break up of the oxide surface layer in the zone before the keyhole. These intuitive explanations however have to be treated with care. The melting efficiency η_M is connected to the Rykalin number [17]:

$$Ry = \frac{E_a v_w}{\alpha^2 \Delta H_m} \tag{4}$$

Here α is the thermal diffusivity of the workpiece at the liquidus temperature and ΔH_m the enthalpy of melting. These are constant for EN AW-6060, as is E_a for the given surface and geometry of the samples used.
Although Ry predicts that the melting efficiency rises upon increasing v_w the doubling of η_P however, which is observed for the hybrid system, must be a synergetic effect.

Process Optimization of Hybrid Bifocal Welding

The hot crack susceptibility of aluminum alloys is dependent on their silicon content. This function has a maximum for a silicon content of 0.5 %. Thus, EN AW-6060 forms hot cracks in laser beam welding. The hot crack susceptibility is altogether reduced in laser beam welding compared to MIG or TIG welding. The range of crack susceptibility is limited to a smaller alloying interval. Yet filler wire has to be supplied to the weld metal to alloy it exceed 1.5 % silicon content in order to avoid hot cracks.

The filler wire has to be homogeneously distributed to secure the continuous Si-alloying throughout the weld metal. Whether the filler wire is supplied leading or trailing the Nd:YAG laser's focus with respect to the welding direction significantly influences the dilution and distribution of the filler material [18]. In fig. 9 and 10 the difference between leading and trailing filler wire position can be seen.

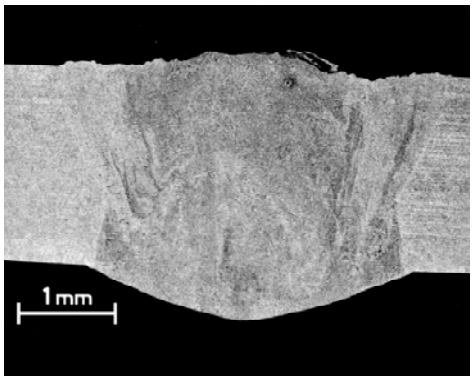

Fig. 9: Dilution of filler material, trailing position

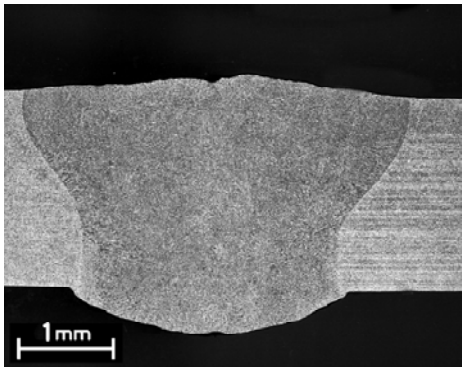

Fig. 10: Dilution of filler material, leading position

P_{hybrid} = 3 kW + 3 kW; f = 150 mm; φ = 20°; Argon 25 l min^{-1};
v_w= 4.0 m min^{-1}; v_f = 3.0 m min^{-1}; $Ø_f$= 1 mm; butt joint EN AW-6060

When laser beam welding is integrated into a production line, e.g. in the automotive industry, the welding process should be able to tolerate misalignment between the edges of the pieces to be joined. The addition of filler wire combined with the extended spot of the HPDL measuring 2 mm across enables the bridging of wider gaps than could be tolerated by the Nd:YAG laser on its own. The twin spot technology allowed 0.4 mm [11] whereas the bifocal hybrid permits 1.0 mm without the welding parameters and the tensile strength being considerably affected. Cf. fig. 11.

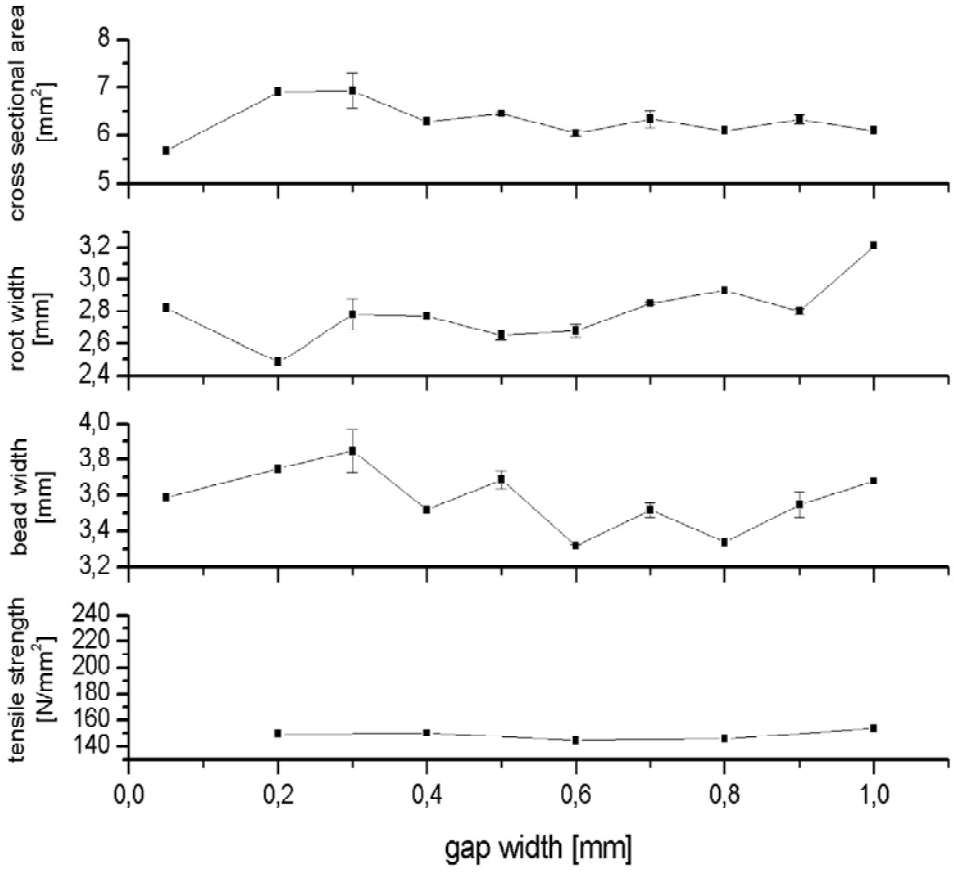

Fig. 11: Gap width vs. cross sectional area, root width, bead width and tensile strength, leading position

P_{hybrid} = 3 kW + 3 kW; f = 150 mm; φ = 20°; Argon 25 l min^{-1}; v_w= 4.0 m min^{-1}; $Ø_f$= 1 mm; v_f was adjusted to fill the gap

Customary filler wires are available of 1 mm or 0.8 mm in diameter. The focal spot generated by the Nd:YAG laser has a diameter of 0.45 mm for a focal length f = 150 mm. The positioning of the filler wire with respect to the focal spot is cumbersome and the supply can not be robustly maintained. For the bifocal hybrid however, the wire can be stuck into the rectangular focal spot of the HPDL, measuring 2 mm along its fast and 4 mm along its slow axis.

For all the techniques discussed herein only the weld seams were considered. However an often overlooked issue for application of laser beam welding to production is the start and end point where singularities form, e.g. craters. The onset of the bead is generally well behaved as it is formed by successive solidification fronts. The end point however is correlated to the shape of the weld pool since it develops upon solidification of the weld pool stopping to further move through the plate. Fig. 12 and 13 show the top and bottom view of the end point. A small offset from line of the divide was intentionally introduced to clearly demonstrate that the longitudinal crack originates from the finish crater and is not a continuation of the edges into the fusion zone.

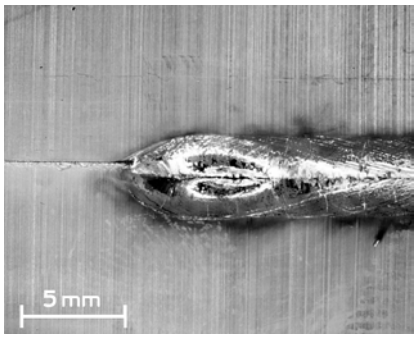

Fig. 12: Finish crater, top surface view

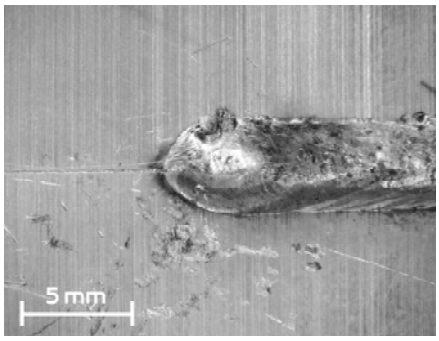

Fig. 13: Optimized finish crater, top surface view

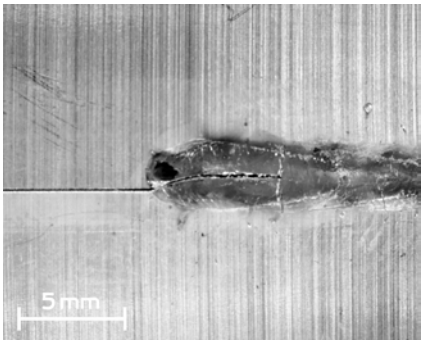

Fig. 13: Finish crater, bottom surface view

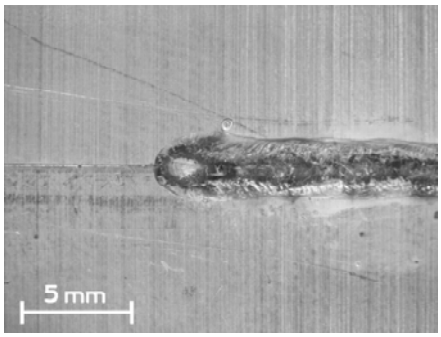

Fig. 15: Optimized finish crater, bottom surface view

P_{hybrid} = 3 kW + 3 kW; f = 150 mm; φ = 20°; Argon 25 l min^{-1}; v_w = 4.0 m min^{-1}; v_f = 3.0 m min^{-1}; $Ø_f$ = 1 mm

P_{hybrid} = 3 kW + 3 kW; f = 150 mm; φ = 20°; Argon 25 l min^{-1}; $Ø_f$ = 1 mm

The bifocal hybrid system can make full use of the independent triggering of the two separate laser sources. Several strategies were devised and experimentally compared. It proved to be best practice to avoid finish craters and their associated cracks to switch off the Nd:YAG laser just before the end of the seam. Subsequently letting the HPDL act until the crater is filled up by wire before pulling back the wire. The results are shown in fig. 13 top view and fig. 14 displaying the bottom view.

Discussion and Summary

The bifocal hybrid technology being a combination of two independent laser sources facilitates several synergies to be employed to advance laser welding of aluminum alloys. In comparison to other established technologies such as twin spot or laser/MIG hybrid welding it allows for any gas mixture according to weld pool requirements. Thus further reduction of porosity is facilitated than was attainable by the stabilization of the keyhole solely by the HPDL. The superior surface qualities and an overall improved energy transfer efficiency or process efficiency respectively clearly demonstrate the synergies between these two laser sources. Under production circumstances the avoidance of longitudinal cracks originating from the finish crater is to be noted as well as the more robust supply of filler wire and improved misalignment tolerance of the bifocal hybrid process.

Conclusion

Production in industrialized countries is under great cost pressure, as labor is cheaper in developing countries. Only if innovation takes place and a viable economic case exists for these new technologies research and development can be retained in industrialized countries. As laser sources necessitate substantial investments, laser joining technology is very dependent on the cost structure [19]. By topping up a possibly depreciated conventional Nd:YAG laser system by a comparably cheap HPDL a new joining technology is created to take on new challenges that new materials and designs may pose in the future.

References

[1] M.F. Zäh, A. Trautmann, A. et al.: Forschung als Motor der Leichtbau-Fügetechnik, in: Blech in Form, Vol. 2 (2004), p. 32-34

[2] M.F. Zäh, A. Trautmann, et al.: Den Vorsprung sichern, in: Blech in Form, Vol. 5 (2004), p. 23-27

[3] H. Zhao, D.R. White, T. DebRoy: Current issues and problems in laser welding of automotive aluminium alloys, in: Int. Mat. Rev., Vol. 44, No. 6 (1990), p. 238-266

[4] M.F. Zäh, A. Trautmann, D. Eireiner, S. Roeren: 19. Deutscher Montagekongress, München. Landsberg: Moderne Industrie 2005, p. 3.1-28

[5] G. Mathers: The welding of aluminium and its alloys, Woodhead Publishing Ltd. Cambridge, UK (2002)

[6] S. Roeren, A. Trautmann, M.F. Zaeh: Modelling of Transient Clamping Conditions during Laser Beam Welding, in: Proceedings of the Third International WLT-Conference on Lasers in Manufacturing 2005, Munich, Germany (2005), p. 95-100

[7] T. Graf, H. Staufer: LaserHybrid at Volkswagen, IIW-Doc. XII-1730-02

[8] S. Katayama, Y. Naito, S. Uchiumi, M. Mizutani: Penetration and Porosity Prevention Mechanism in Laser-Arc Hybrid Welding, in: Proceedings of the Third International WLT-Conference on Lasers in Manufacturing 2005, Munich, Germany (2005), p.193-198

[9] M.F. Zäh, A. Trautmann: Vergleich des hybriden, bifokalen Laserschutzgasschweißens mit Laser-MIG-Hybridverfahren, in: Aluminium 80, Vol. 12 (2005), p. 1387-1391

[10] M. Leimser, F. Dausinger, H. Hügel: Melt pool dynamics and element distribution in laser welding of aluminium alloys with wire, in: Proceedings of the Third International WLT-Conference on Lasers in Manufacturing 2005, Munich, Germany (2005), p. 61-66

[11] C. Schinzel: Nd:YAG-Laserstrahlschweißen von Aluminiumwerkstoffen für Anwendungen im Automobilbau, Laser in der Materialbearbeitung, University of Stuttgart, Germany (2002)

[12] A. Trautmann, S. Roeren, M.F. Zaeh: Welding of Extruded Aluminium Profiles by a Hybrid Bifocal Laser System, in: Proc. of 4th LANE 2004, Erlangen, Germany, p.169-180

[13] N.N. Rykalin, A. Ugalov, I. Zuev, A. Kokara: Laser and electron beam material processing: handbook, Mir Publishers, Moscow (1988), p. 358-418

[14] ISO 10042:1992: Arc-welded joints in aluminium and its weldable alloys - Guidance on quality levels for imperfections

[15] ISO 13919-2:2001: Welding - Electron and laser beam welded joints - Guidance on quality levels for imperfections - Part 2: Aluminium and its weldable alloys

[16] F. Dausinger: Strahlwerkzeug Laser: Energiekopplung und Prozesseffektivität. Laser in der Materialbearbeitung, Stuttgart, Germany (1995), p. 50-83

[17] P.W. Fuerschbach: Welding Efficiency: Calorimetric and Temperature Field Measurements, in: Welding Journal (Miami), Vol. 75 (1996), p. 24-32

[18] J. Berkmanns: (1998) Steigerung der Prozeßstabilität beim Laserstrahlschweißen von Aluminiumwerkstoffen mit Strahlleistungen bis 6 kW und Tragverhalten der Verbindungen, Berichte aus der Lasertechnik, University of Aachen, Germany

[19] C. Ulrich, A. Trautmann: Methodische Wissensaufbereitung zur Planung von Fügeaufgaben, in Industriekolloquium Sonderforschungsbereich 582, Munich, Germany (2004), p. 11.1-10

doi:10.4028/www.scientific.net/AMR.10.79

Investigation of the Influence of Process Parameters on the Structure and the Mechanical Properties of Joints Produced by Electromagnetic Compression

V. Schulze[1], P. Barreiro[1], D. Löhe[1].

[1]Institute of Materials Science and Engineering 1, University of Karlsruhe,

Kaiserstr. 12, Karlsruhe 76131, Germany.

pablo.barreiro@mach.uni-karlsruhe.de, volker.schulze@mach.uni-karlsruhe.de, detlef.loehe@mach.uni-karlsruhe.de

Keywords: electromagnetic forming, pull out force, residual stresses, joining by forming, assembly.

Abstract

Electromagnetic Compression of tubular profiles with high electrical conductivity is an innovative joining process for light weight structures. The components are joined using pulsed magnetic fields which apply radial pressures of up to 200 MPa to tubular work pieces causing a symmetric reduction of the diameter with typical strain rates of about 10^4 sec^{-1}. This process avoids any surface's damage of the workpiece because there is no contact between the components and the forming tool. The load, which the joints can transmit, strongly depends on the process parameters. Of them, the charging energy and initial gap between components are the most important. In the present article, the influence of these two parameters on the joint's characteristics, material's microstructure and the mechanical properties is analyzed. The strength of the joint is determined by tensile tests and by measurements of the residual stresses. Finally, conclusions for the joint design are given.

Introduction

The reduction of weight of motor vehicle body components is commonly reached by introducing lightweight materials in the automotive industry. In addition, there is a requirement of several joining technologies which provide high strength joints for the main structure of automobile vehicles. A vast experience is available for conventional joining processes like laser-welding, screwing, clinching, riveting and gluing, but they require a complex preparation of the joint before the joining process takes place. That is a reason why joining by forming processes like electromagnetic forming is feasible to fulfil the requirement of strength while allowing an easy preparation process. Another benefit of the process is the absence of contact to a forming tool. As a consequence there are no tool marks on the workpiece surface, avoiding any damage of the component after forming. Besides this, composite materials or two non-weldable alloys can be joined. However, the influence of process parameters on the performance of the joints is hardly investigated. A deeper knowledge about this is necessary to establish electromagnetic forming in industrial production [1, 2, 3, 4].

Process principle and characteristic of force fit joints

Fig. 1 shows a scheme of the joining process that concerns an electromagnetic tube compression. A tubular workpiece is placed coaxially inside a forming coil *L*. The coil is connected with a capacitor *C* and a switch, forming an RLC circuit.

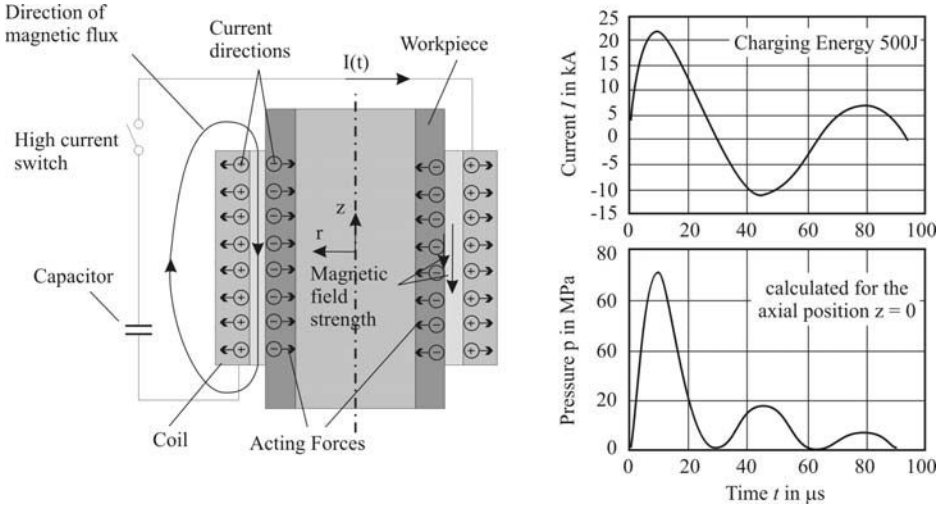

Fig. 1: Schemetic representation of the process [2, 9].

Lenz's Law is the physical effect which govern the electromagnetic forming process. First of all the capacitor must be charged. When the switch is closed the capacitor discharges a sinusoidal current which generates an alternating magnetic field in the coil. This field induces an eddy current in the workpiece which flows near the outer surface of the workpiece. Due to the skin effect, the magnetic field penetrates the work piece wall. Both currents (in the coil and in the workpiece) flow in opposite directions, hence, they repel each other. The Lorentz's force will compress and deform the tubular piece, if the induced stresses are higher than its yield strength. The deformation process is completed within a few microseconds [1, 2, 3, 4, 5, 6, 7].

The pressure can be calculated using the following expression [8, 9, 10]:

$$p(r,t,z) = \frac{1}{2} \cdot \mu_0 \cdot \left(H_o^2(r,t,z) - H_i^2(r,t,z) \right)$$

It is possible to simplify the equation by assuming a very low magnetic field on the inner side ($H_i(r,t,z)$). Then the pressure can be calculated using the magnetic field on the outside ($H_o(r,t,z)$) which is like the one from the coil.

In the electromagnetic forming process the forming velocity plays a decisive role. [9] measured the radial displacement of the tubular component during the deformation by the light shadowing method. They found that the necking velocity during the deformation process shows an acceleration and deceleration part. As a consequence, an increase of the charging energy by keeping the same arrangement of pulse generator, coil and workpiece, means an augmentation of the maximal pressure without increasing the pulse duration. It is possible to restrict the radial displacement by placing a mandrel into the tube. The velocity of the tube being compressed as well as its mass determinine the kinetic energy at the time of impact and the force which takes effect on the mandrel is a result of the kinetic energy. Thus the tube will impact the mandrel, for a particular charging energy, with a certain acceleration [9].

Materials and testing method

For the present work aluminum tubes were compressed together with aluminum mandrels in Institut für Umformtechnik und Leichtbau, Dortmund (Germany). The alloy of both components was AA6060. The tubular components were 170 mm long, with 40 mm as outer diameter and 36 mm as interior diameter. The mandrels were 180 mm long and had three different diameters: 34, 33 and 32 mm. Thus the initial gap between tube and mandrel was varied three times: 1, 1,5 and 2 mm. The joining process was made with three different charging energies, 10%, 15% and 20% of the maximum energy of the device (32 kJ).

Due to the prescence of tangential tensile residual stresses on the tubular component, the length of the joining zone could not be defined by fully cutting a test tube along its main axis because of the distortions due to cutting. In order to avoid this only some of the tubular components were millcut like shown in Fig. 2.

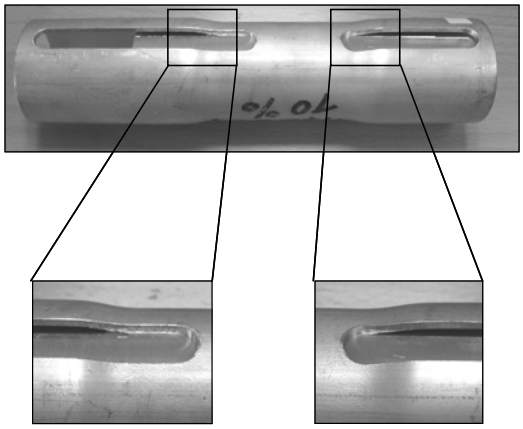

Fig. 2: Millcut sections of test tubes.

A quarter was cut from each test tube in order to extract a piece of both components for metallographical investigations. A piece of the quarter for each test tube was embedded and etched. All metallography cuts were etched with Keller's reagent to reveal the grain structure. The thickness of the tubular component was measured with a macroscope and an image analysis software. Microhardness (Vickers 10) measurements were carried out at the same specimens. They were performed along the tubular piece from the middle point of the joining zone and in the middle layer between the inner and outer surface.

A 10 mm thick plate was cut from each test tube perpendicular to the test tube's main axis, in such a way, that one of its surfaces was exactly in the middle layer of the joining zone. Micrographs were taken to analyse the contact zone between the different components.

The tensile tests were carried out in a 200 kN Zwick machine with a crosshead velocity of 4 mm/min to assure an approximate strain rate ($\dot{\varepsilon}$) of 3.10^{-3} 1/s.

The determination of residual stresses was made by x-ray with the $\sin^2\psi$ method. Because the grain structure of the aluminum tubes produced by extrusion is not fine enough, specific equipment and measurement method was necessary in order to irradiate enough grains. Fig. 3 shows a scheme of the measurement method. The same 10 mm thick plate used to acquire micrographs was used for these measurements. The plate was placed in the device so that this surface was irradiated. The axis of the plate was positioned in the rotational axis of the equipment. By rotating the equipment it was possible to irradiate the complete surface of the tubular component. Finally, an average of the radial residual stresses on the surface of the tubular component was measured by tilting the plate as illustrated in Fig. 3.

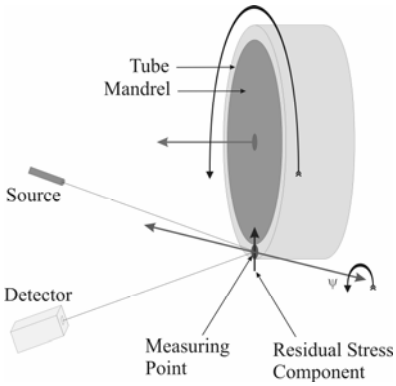

Fig. 3: Schematic representation of measuring device.

Experimental results

Influence of the process parameters on the joining zone

Fig. 4 shows the influence of the charging energy and the width of the initial gap on the thickness of the deformed zone. Increasing initial gap widths lead to increasing reductions of diameter causing increasing thickness due to the constancy of volume during plastic deformation.

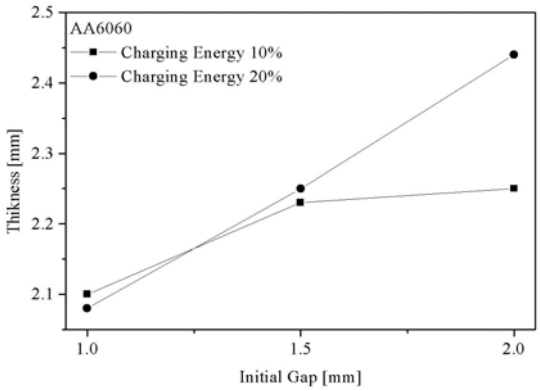

Fig. 4: Results of thickness measurements.

For an initial gap of 2.0 mm this augmentation of the thickness is a bit lower for a charging energy of 10%. This indicates that the pressure force of the joining process was in this case not high enough to reach a complete constriction of the tubular component, since the deformation occurs at constant volume.

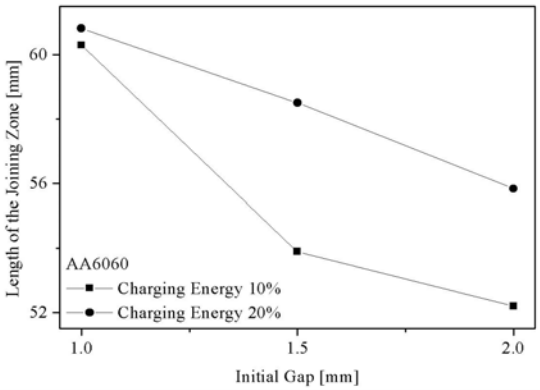

Fig. 5: Results of measurements.

The lenght of the joining zone is plotted in Fig. 5. As expected, the joining zone is the longer the higher the charging energy of the joining process. In addition the curves indicate that by increasing the initial gap between the components the length of the joining zone decreases. As more energy is neded for the constriction of the tubular component, less energy is left for the further deformation upon the surface of the mandrel.

Figure 6 shows several micrographs of the joining zone for an initial gap of 1.5 mm and a charging energy of 10 %. It can be seen that a gap remains and that its size severely varies between 7.5 and 95 µm. Only in few points direct contact could be determined.

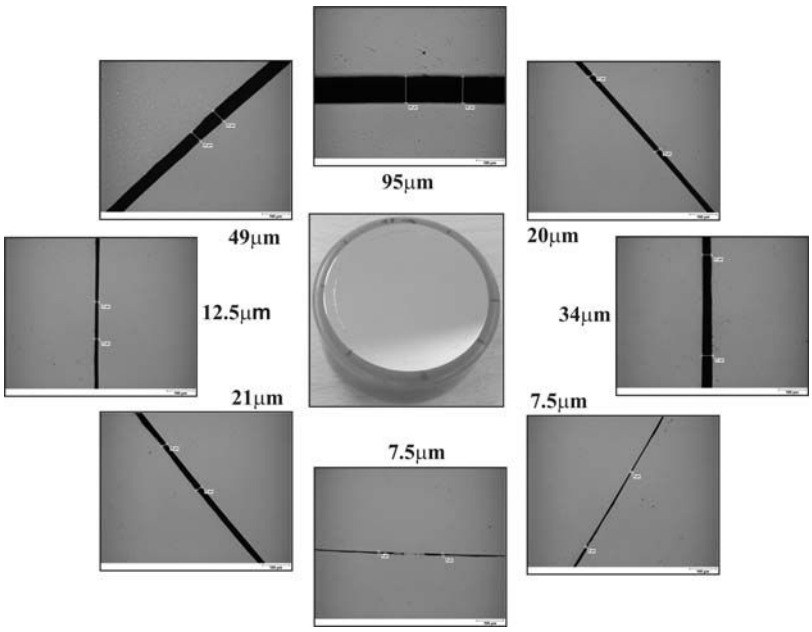

Fig. 6: Contact zone between tube (outside) and aluminum mandrel (inner side) in a cut perpendicular to test tube axis.

This result was also found for other process parameters as shown in Fig 7. In total the remaining gap seems to be decreasing with decreasing initial gap and increasing charging energy. The changes of the remaining gap size along the joining zone may be caused by two effects: First, the large deformation of the tube leads to a roughness increase of its internal surface, allowing only for micro contacts instead of full contact. Second, there is an inherent inhomogeneity of the magnetic field leading to fluctuations in the acceleration of the tube.

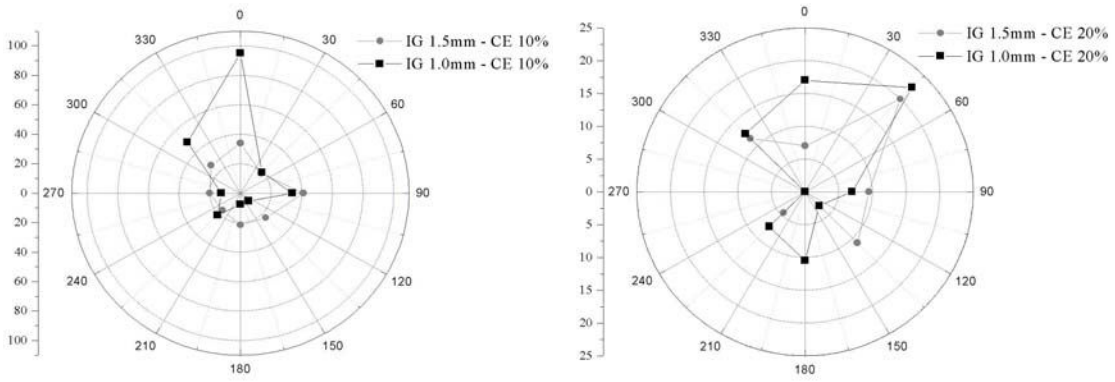

Fig. 7: Polar representation of the reamining gap between tube and mandrel for initial gaps of 2 and 2.5 mm and a charging energy of 10 % (left) and 20 % (right).

Besides the geometrical aspects, the forming process leads to workhardening effects which can be seen from hardness tests representatively shown in Fig. 8 left. An average of the hardness of the workhardened zone was used for the further analysis. Fig. 8 right shows the

dependence of the results on the process parameters. The maximum microhardness increases with growing initial gap and charging energy due to the higher plastic deformation.

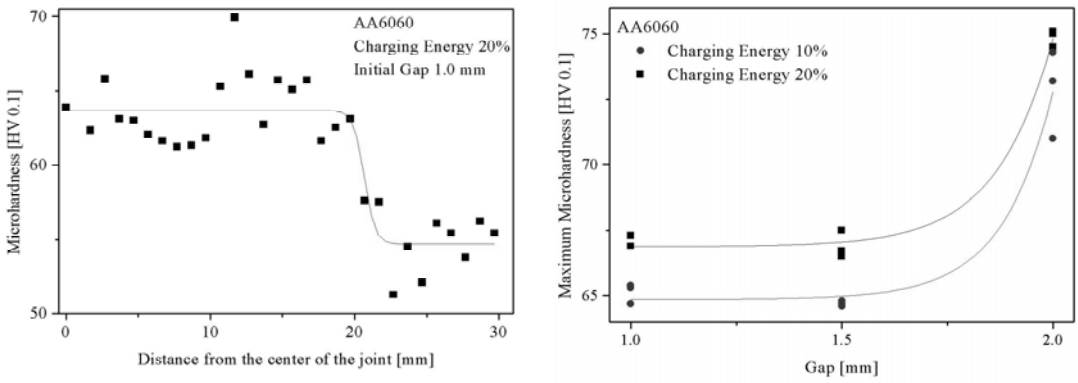

Fig. 8: left: Distribution of hardness, right: Results of microhardness measurements.

Because the strain rate is extremely high during electromagnetic deformation, a microstructure showing twins was expected. Such a configuration would have explained the augmentation of the microhardness in the joining zone. Micrographs were acquired in order to identify any change in the microstructure due to the joining process. Fig. 9 shows two micrographs made of the same piece of a tubular component. The left one was taken in the base material. It shows the typical grain structure of aluminum alloys, with a grain size between 100 and 200 μm. The figure on the right side was taken from the joining zone. There is no observable difference between the microstructure of the joining zone and the initial one of the tube. It can be concluded that the strain rate may be lower than necessary for twin formation and that the hardness increase should be fully caused by dislocation hardening.

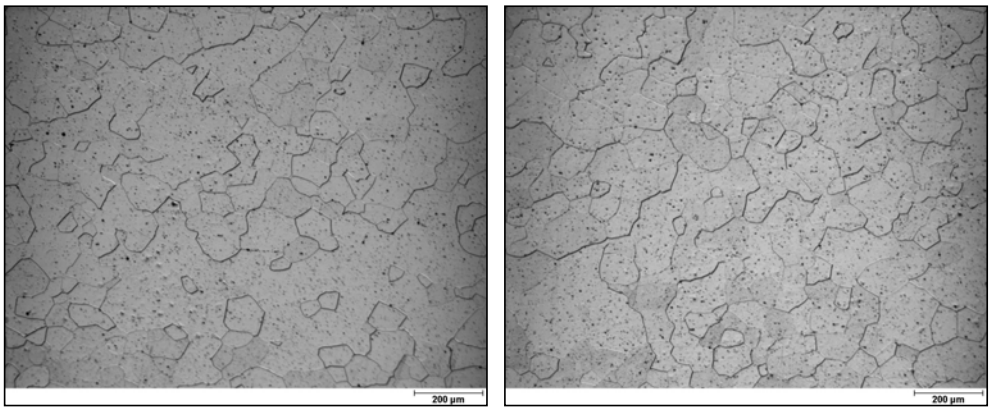

Fig. 9: left: Initial microstructure. Right: Microstructure of the joining zone.

Influence of the process parameters on the mechanical properties

Tensile tests were carried out in order to determine the influence of the process parameters on the pullout load. Fig. 10 left shows a diagram of one tensile test which is representative for all other tests. The pullout load of about 6.9 kN is easy to observe. At this point, both parts (mandrel and tube) start to glide on each other. Ideally the further behavior would show a continuous glide at an initially constant and then decreasing load. Indeed, mandrel and tube glide on each other, but their behavior presents a “seizing effect”. This can be seen from the mandrel’s surface after testing shown in Fig. 10 right. The tube takes off some material from the mandrel and increases the contact surface between tube and mandrel. As a consequence, a continuous increase of the total contact surface is observed. In all cases it was possible to detect this seizing effect, which may be quite important with regard to safety measures because a further failure can be optically identified in time since the ultimate failure does not

occur abruptly. However, the exact behaviour of the joint during seizing is stochastical and therefore shows a large scatter.

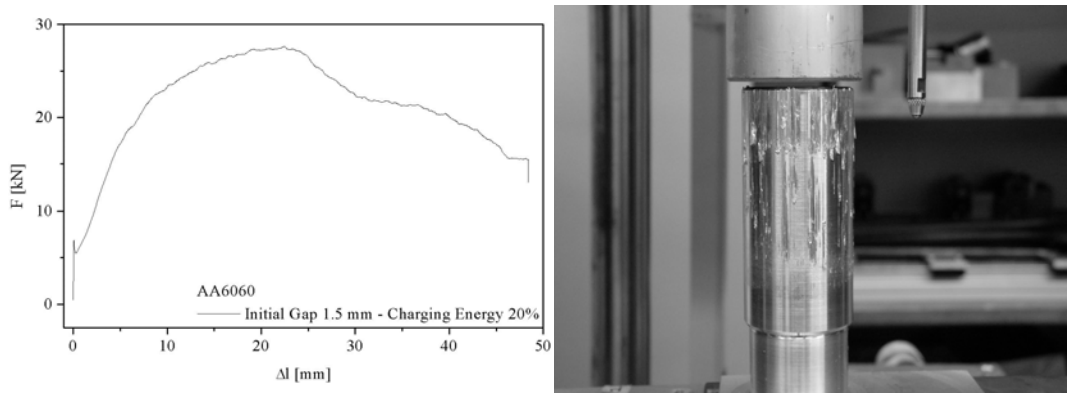

Fig. 10: left: Tensile test diagrams of specimens joined with the same parameters. Right: Mandrel's surface after testing.

The pullout loads for different initial gaps and charging energies are presented in Fig. 11 left. The curve for a charging energy of 10 % shows a continuous decrease of the pullout load by increasing the initial gap between tube and mandrel. The pullout load seems to be maximal for a 1.0 mm initial gap. The other two curves show an increase of the pullout load by increasing the initial gap between tube and mandel.

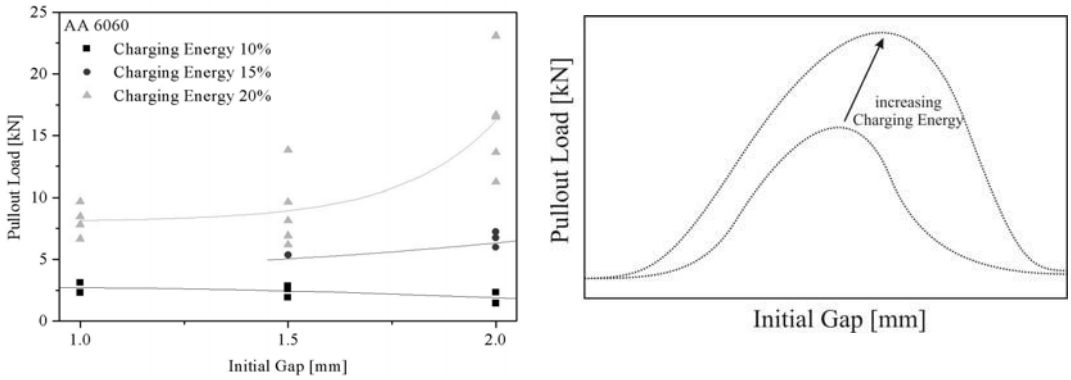

Fig. 11: Results of pullout-tests (left) and Schematically representation of the expected results (right).

A schematical representation of the expected influence of process parameters on the mechanical properties of electromagnetically formed joints is shown in Fig. 11 right. It can be suggested that an increase of the charging energy in the joining process leads to a higher impact force when the tube hits the mandrel, which causes a higher compression of the mandrel. As a consequence, the normal force which holds both components together will be higher as well. Besides there is an increase of the maximum pullout force with increasing charging energy. This new maximum is placed at higher initial gaps. At high initial gaps the tube already decelerated significantly when the mandrel is hit. Therefore the normal force also decreases in this region [11].

Influence of the process parameters on the residual stresses

Fig. 12 shows the results of all residual stresses measurements performed. The curve for a charging energy of 10 % shows the same non-linear behaviour for the contraction speed as found by [9]. The residual stresses reach a maximum value for an initial gap of 1.5 mm, and then they decline. Such a maximum value was not observed in the case of a charging energy

of 20 %. By comparing both curves it is possible to determine that an increase of the charging energy yields an augmentation of the compressive residual stresses. This can be ascribed, in the same way as for pull-out loads, to the contraction speed of the tube when the mandrel is hit. By increasing the charging energy at the same initial gap, the tubular component hits the mandrel with a higher velocity. That generates a higher compression of the mandrel, which increases the radial reaction force of the mandrel as well. These results mainly agree with the results of the tensile tests shown in Fig. 11.

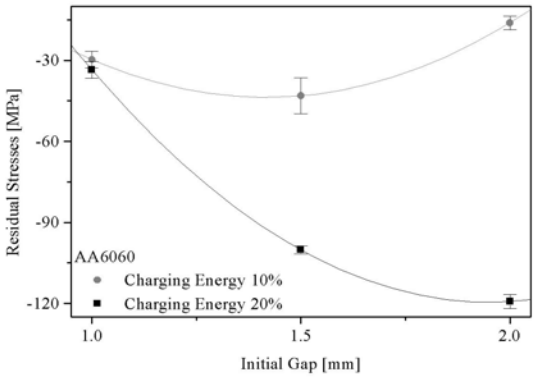

Fig. 12: Results of residual stresses measurements.

The pullout force expected from the residual stresses assumig Coulomb friction can be calculated as follows:

$$F = -\pi \cdot d \cdot l \cdot \sigma_{rad}^{ES} \cdot \mu$$

where d is the mandrel's diameter, l is the joining zone's length, σ_{rad}^{ES} are the radial residual stresses and μ (assumed equal to 0.1) is the friction coefficient. Fig. 13 shows the expected pullout load using all results obtained in the present work.

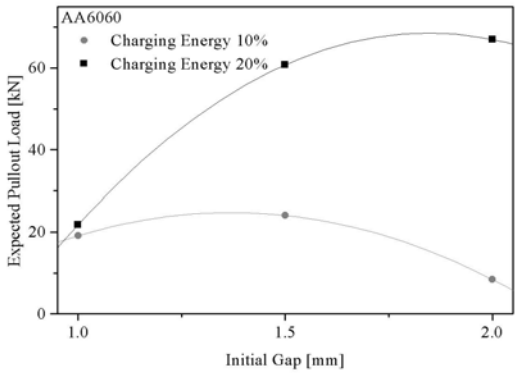

Fig. 13: Expected pullout loads.

All the expected pullout loads are much higher than the measured ones. That is because the calculation was made assumig an ideal contact between tube and mandrel. But the micrographs showed that the components have a kind of micro contact which reduces the real joinig surface significantly. Since the real contact is also dependent on the charging energy and the initial gap, it is also possible to explain that the difference between expected and measured pullout load is not always the same.

Conclusions

In the present paper electromagnetically joined tubes and mandrels of AA 6060 were investigated. Because of the joining process, there is a change in the characteristics of the tubular component. An increase of the thickness in the joining zone was measured. This consequence is independent of the charging energy, but only if the charging energy is sufficient to completely constrict the tubular component. Besides, the joining zone becomes longer by increasing the charging energy.

According to literature, the contact surface between both components should be ideal. But the observations made using light microscopy showed that mandrel and tube stay in contact only in points or small regions of the joining zone. In addition, it was appreciated that the inherent inhomogeneity of the magnetic field contributes to an inhomogeneous deformation of the tubular component as well.

A work hardening of the tubular component during the joining process was identified as well. The work hardening is higher by increasing both the charging energy and the initial gap before the joining process. In spite of the high strain rate deformation of the tubular component twins were not identified in the microstructure.

The tensile tests showed a seizing effect which could be quite significant with regard to safety measures because a failure in a structure may be optically identified in time since the ultimate failure does not occur abruptly.

The pullout load of the joint can be increased by increasing the “contraction speed” using a higher energy in the joining process and an adapted initial gap width. The explanation is that the tubular component hits the mandrel with a higher velocity if the charging energy is increased. This leads to a higher compression of the mandrel. As a consequence the radial reaction force of the mandrel is higher as well.

The measurement of the residual stresses allowed the direct determination of the radial force which holds both components together. According to the results of tensile tests the radial compression force is higher when the charging energy increases. The difference between the expected and the measured pullout forces may be caused to the remaining gap between tube and mandrel.

Acknowledgements

This paper is based on investigations of the Transregional Collaborative Research Centre SFB/TR10, which is kindly supported by the German Research Foundation (DFG).

References

1. *M. Kleiner, D. Löhe, M. Marré, Ch. Beerwald, P. Barreiro, V. Schulze, W. Homberg:* Investigation of force-fit joints produced by electromagnetic tube compression. Submitted by WGP-Annuals.
2. *Mamalis, D. Manolakos, A. Kladas, A. Koumoutsos*: Electromagnetic forming and powder processing: Trends and developments. Applied Mechanics Reviews (2004) 57, pp. 299-324.
3. *F. Bach, A. Rossberg, M. Schäperkötter, M. Schaper, L. Walden, J. Weber*: The sheet metal materials aluminum, magnesium, steel and also titanium and their forming properties.
4. *F. Bach, M. Rodman, A. Rossberg, J. Weber, L. Walden*: Verhalten von Aluminumwerkstoffen bei der elektromagnetischen Blechumformung. Proc. 2. Kolloq. Elektromagnetische Umformung, 28. Mai 2003, Dortmund, S. 11–18.

5. *H. Bühler, E. Finkenstein*: Hochsgeschwindigkeitsumformung rohrförmige Werkstücke durch magnetische Kräfte. Bänder, Bleche und Rohre (1966) 3, pp 115-123.
6. *H. Bühler, E. Finkenstein*: Ein Beitrag zur Magnetumformung rohrförmige Werkstücke. Werkstatt und Betrieb (1968) 9, pp. 513-516.
7. *H. Dietz, H. Lippman, H. Schenk*: Theorie des Magnetforms-Verfaren: die Bewegung des Werkstückes. Elektronische Zeitschrift Ausgabe (1967), 12, pp. 273-278.
8. *Beerwald*: Grundlagen der Prozessauslegung und –gestaltung bei der elektromagnetischen Umformung. Universität Dortmund 2004.
9. *Beerwald, W. Brosius, M. Kleiner*: Determination of flow stress at very high strain rates by a combination of magnetic forming and FEM calculation. Lehrstuhl für Umformtechnik (LFU) der Universität Dortmund.
10. *H. Dietz, H. Lippman, H. Schenk*: Theorie des Magnetforms-Verfaren: Erreichbarer Druck. Elektronische Zeitschrift Ausgabe (1967), 9, pp. 217-222.
11. *Beerwald, W. Homberg, M. Kleiner, M. Marré, V. Psyk*: Einfluss der Umformgeschwindigkeit beim kraftschlüssigen Fügen rohrförmiger Werkstücke durch elektromagnetische Kompression , Symposium Fügetechnik 2004 Universität Paderborn, November.

doi:10.4028/www.scientific.net/AMR.10.89

Joining by Forming of Lightweight Frame Structures

Homberg, W [1, a], Marré, M. [1, b], Beerwald, C. [1,c], Kleiner, M.[1,d]

[1]Institute of Forming Technology and Lightweight Construction,
University of Dortmund, Baroper Str. 301, 44221 Dortmund, Germany

[a]werner.homberg@iul.uni-dortmund.de, [b]michael.marre@iul.uni-dortmund.de,
[c]charlotte.beerwald@iul.uni-dortmund.de, [d]matthias.kleiner@iul.uni-dortmund.de

Keywords: Joining by forming, frame structures, aluminum, magnesium, manufacturing of joints, electromagnetic forming, hydroforming, rolling-in

Abstract Joining of lightweight frame structures in small quantities is subject to specific conditions, which are exemplarily determined for joining by forming processes. Experimental investigations have been carried out to evaluate both feasibility and capability of joining by forming processes. Joining has been accomplished by compressing or expanding cylindrical profiles using rigid tools for rolling-in processes, fluid active medium for hydro-forming as well as active energy for electromagnetic forming.

Introduction

One major objective of the Collaborative Research Center SFB/TR10 is the flexible and competitive production of frame structures, which fulfill the condition of lightweight constructions as structural parts, cabins, or chassis frames. To achieve this common aim, the application of innovative joining technologies as well as joining strategies are necessary. Joining by forming as a cold joining procedure is an attractive alternative solution compared to welding processes. In this article, the feasibility of selected forming processes to join tubular workpieces in an aluminum structure by compression or expansion is examined.

Demands on the joint design

Special requirements on the joint design must be fulfilled to achieve the aim of the SFB/TR10, which is the low volume production of lightweight, highly stressable and stiff frame structures made of tubes or profiles. Therefore, a joint design must be developed taking into account holistic aspects to exclude suboptimal solutions. Furthermore, there are influencing, partially conflicting requirements in the field of *material characteristics*, *design* as well as *production engineering* which have to be considered, as indicated in fig. 1 [1]. As a designated target for the joint design, the according influencing factors as well as their influencing intersections on the joint design should lead to solutions considering the central aspects of joint quality, cost, and time.

In general, joints could be established by welding, or bonding, dominating form-fit, or dominating force-fit. Investigations on welding processes are currently carried out within an associated project [2]. Either a dominating form-fit or a dominating force-fit could be manufactured by joining by forming processes [3].

To identify influencing parameters of force-fit joints and to understand the mechanism of gripping we revert to interference-fits produced by shrink-on. Interference-fits produced in this way depend on the operational demands, categorized by the dominating strain in elastic, elastic-plastic, and full-plastic interference-fits [4]. A joint can be produced by compressing a tube on another joint partner or expanding a tube in a joint partner. The force which determines the forming of the tube leads to an elastic-plastic deformation of the tube and an ideally elastic deformation of the other joint partner. After this, the corresponding elastic recovery of both joint partners occurs. If a full

elastic relaxation of the joint partner is limited by the tube, a permanent radial pressure (interference stress) is established.

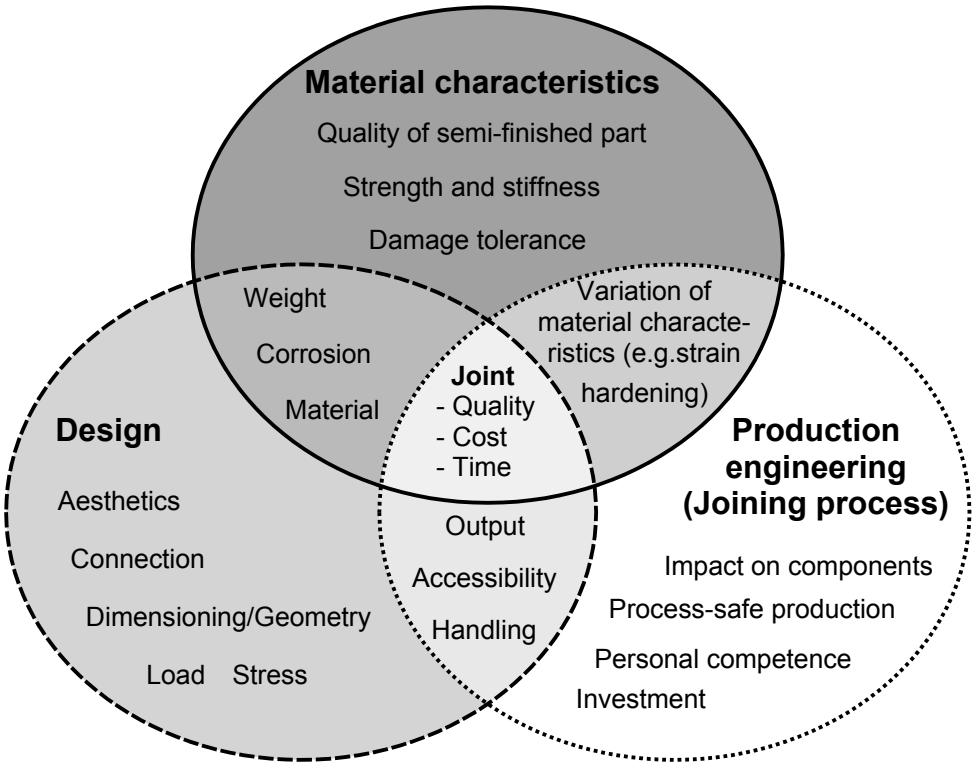

Fig. 1 Selected demands on the joint design [1]

This pressure is a balanced condition of the joint partners stress relief, on the one hand, and the subsequent resulting reinduced stress in the tube, on the other hand. The strength of interference-fits strongly depends on the area of the contact zone, the friction coefficient and the remaining interference stress within the contact zone. While the first two aspects directly influence the strength of the joint, irrespective of the material to be joined, the interference stress depends on material and process parameters, e.g. yield point, Young's modulus, and the geometrical stiffness of the parts [4,5,6]. To create the interference stress by expansion as well as compression the forming operations were carried out using rigid tools for rolling-in processes, fluid active media for hydro-bulging as well as active energy for electromagnetic forming.

Joining by Rolling

Recently, the manufacturing of tubular hybrid components was successfully accomplished in long-term researches in cooperation of IUL and ISF [7]. Joining by rolling-in was primarily used for joining of tubes in boiler and apparatus engineering. Water- and steam-tubes are, for instance joined into the bottom of heat exchangers, which are e.g. used in power plants. Further, quite new examples are the manufacturing of composite camshafts and gear shafts; they have already been successfully manufactured as demonstrators for the automotive industry, fig 2a-c [8, 9, 10].

The process of rolling-in of tubes is based on the principle of roller burnishing. As the only non-cutting fine forming process, the original application for rolling-in is burnishing as well as reeling of tubes. The burnishing technology principle is based on applying a force to a roller body which rolls on the workpieces surface. A plastic deformation is induced into its surface layer, resulting in a

leveling of the roughness [11, 12]. A higher rolling oversize is used for joining, unlike the surface finishing of cylindrical workpieces.

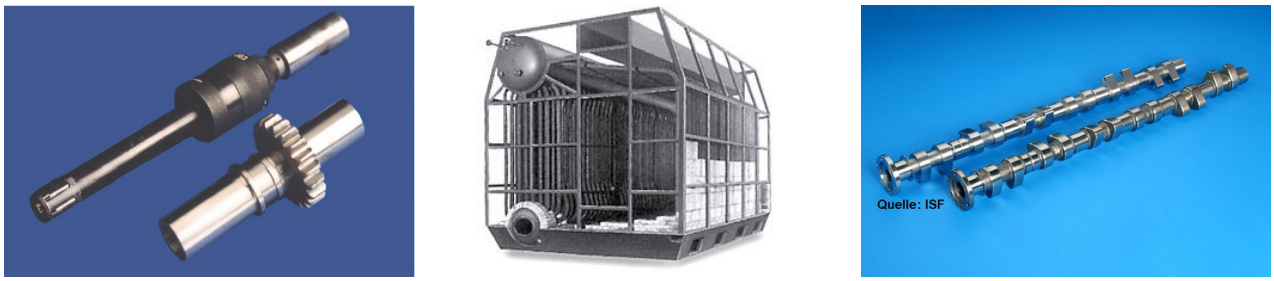

a) Rolling tool and gear shaft b) Heat exchanger c) Composite camshaft

Fig. 2 Applications of joining by rolling-in [8, 9, 10]

Joining by rolling-in is carried out by a special rolling tool. Rolls are driven by a conical mandrel and are positioned by a cage, as fig. 3 indicates. By pre-adjusting a rolling oversize the roller-bodies are radially pushed towards the tube. If the rolls are determining a pressure on the tube beyond the yield stress of the material, a plastic deformation occurs. The inner joint partner, mostly a cylindrical workpiece, is expanded by the rolling tool. If there is an appropriate outer joint partner with a small clearance between the internal tube, the outer joint partner will be elastically deformed by the expanded inner joint partner. The plastic deformation of the inner joint partner along with the elastic recovery of the outer joint partner leads to an interference fit between them [4,10,13].

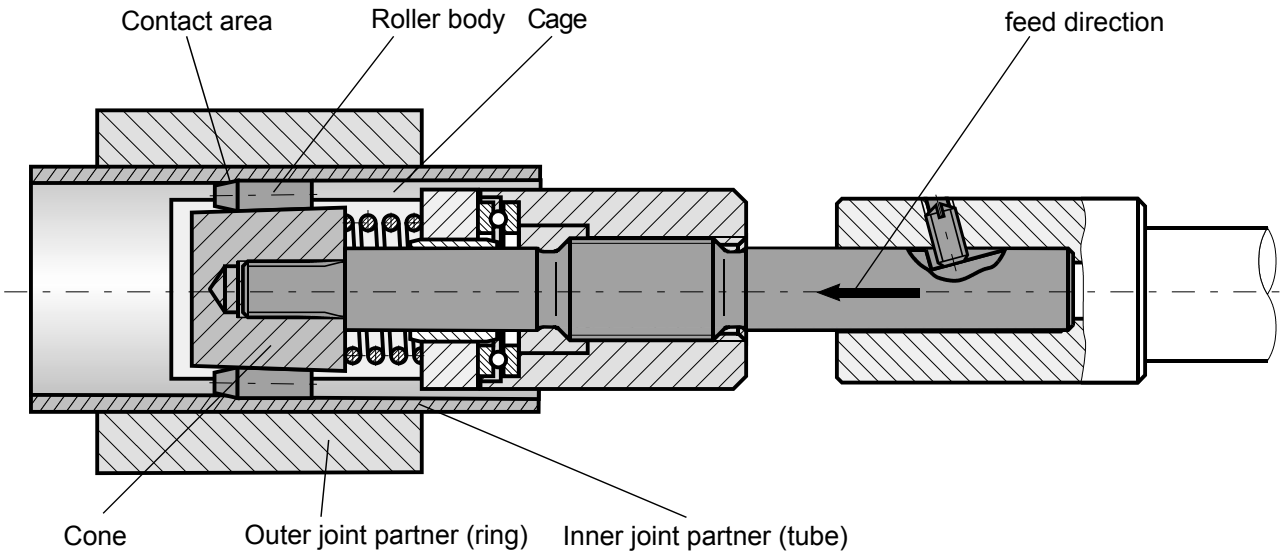

Fig. 3 Process principle of joining by rolling-in [13]

Experimental investigations on joints made of aluminum tubes (AA6060) and steel (C60) lead to the result that a transmission of axial forces and stresses respectively exceeds nearly 75% of the yield point of the weaker material [13]. In comparison to this, further investigations on joints made of equal materials (AA6060) lead to low interference-fits and, therefore, to low transmittable axial forces. Within these experimental investigations the following influencing factors on an interference-fit have been examined: length of the joining area, wall thickness of the outer joint partner as well as maximal expansion adjusted by the rolling oversize. Selected results are presented in fig. 4. As one result of these experimental investigations a maximal shear stress of 3.3 N/mm^2 could be determined by pull-out tests. This maximal shear stress occurred along with the largest wall thickness of the outer joint partner (18 mm), which was joined to a tube with an outer diameter of 60 mm and a wall thickness of 4 mm [14]. Instead of increasing the wall thickness a further option for increasing the transmittable axial forces with interference-fit is the increase of the

friction between the two joint partners. This could be accomplished by inserting e.g. corundum-hard material [13] or adhesive bonding in the joining area [14].

Therefore, experimental investigations were carried out with supporting adhesive, which was actually done using a two-component structural adhesive named DP490 manufactured by 3M. Assuming a hardening time of 72 hours, the adhesive resists a shear stress of more than 20 N/mm^2, handling operations are feasible after at least 3 hours of hardening. Without extensive preparations of the joining area shear stresses of up to 18 N/mm^2 could be determined with a combination of bonding and rolling-in. Both the potlife as well as the allocation of the adhesive are currently problematic with joints that are only bonded.

Hybrid joining, as a combination of joining by rolling-in and adhesive bonding, is a reasonable application for joining of equal aluminum material. On the one hand, the transmittable axial forces are larger in contrast to only rolled-in joints. On the other hand, the allocation of the adhesive is accomplished by the rolling tool as well as a resulting immediate pre-fixture for handling operations. Another option for increasing the transmittable axial forces is a dominating form-fit by inserting rectangular grooves in the outer joint partner [14].

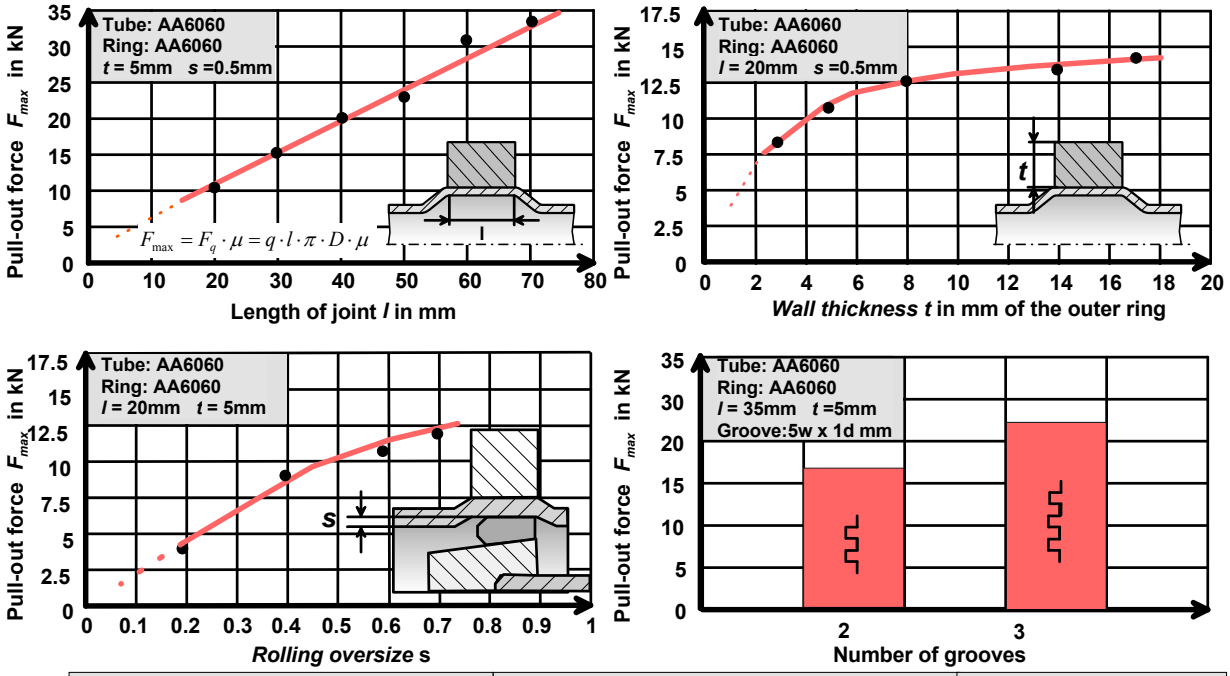

Tube:		Ring		Process parameters
Outer diameter: 60mm	Length: 450mm	Inner diameter: 60mm	Length: 20...70mm	Rotational speed: 210rpm
Wall thickness: 4mm	Material: AA6060	Wall thickness: 3...17mm	Material: AA6060	Feed: 4,8mm/r

Fig. 4 Selected results for joining by rolling-in [14]

Joining by rolling-in, as part of a hybrid joining process, is particularly interesting for the manufacturing of joints in light frame structures. Besides the achievable shear stresses it offers quite low tooling expenses, a feasible allocation of a supporting adhesive as well as comparably low demand on the joint preparation.

As another type of rolling-in process the use of external roller tools for compressing tubes onto a mandrel has been investigated. The external rolling or burnishing process is originally used as a surface finishing process of e.g. piston rods, thrust collars for rear axles, or cold rolling tools. To evaluate the feasibility of the external roller burnishing as joining operation, aluminum tubes have been compressed using a one-roller joining tool [15]. The specimens were rolled on a lathe by turning them fixed in a standard chuck and fixing the roller tool in a standard lathe tool holder. The

joining tool applies a radial incremental force of 0.5 to 1.5 kN on the tubes surface, which is probably not always enough to cause an elastic deformation of the massive mandrel.

In addition, a multi-roller tool was used for complementary tests. The multi-roller joining tool is equipped with a fixed conical bearing track and nine burnishing rolls. The pressure on the workpiece by the rolls is determined by the rolling oversize (cp. rolling-in with internal tool). The process principle of both tools is shown in fig 5. Regarding the results of joining by rolling-in as well as joining by electromagnetic forming (which is described in a following section) of primarily force-fit joints, experimental investigations were carried out joining tubes on massive cylindrical mandrels to be able to compare the different joining processes. However, it was impossible to produce strong interference-fits by using either the one or the multi-roller joining tool.

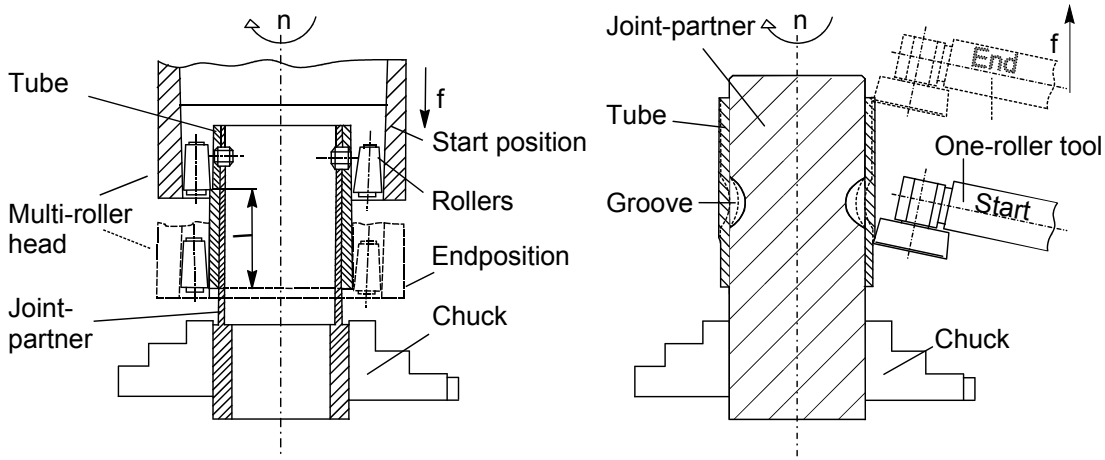

Fig. 5 Process principle of joining by external rolling-in using a multi roller as well as a one roller tool [15]

Consequently, further developments on both tool design and process control are necessary to establish dominating force-fits. Nevertheless, establishing joints with dominating form-fits as mentioned above is a further option. Therefore, the influence of the following factors has been exemplarily determined: shape of the insert contact surface (grooving and knurling), rolling parameters (cross rolling, straight rolling), supportive application of adhesive bonding in the joining area before rolling-in operation as well as type of tool (one-roller burnishing tool and multi-roller burnishing tool). Accordingly, grooves with a narrow width, but an upright flank resist higher axial forces than grooves with a wide width and flat flanks. The surface of the mandrel was joined, knurled as well as bonded with DP490. As a result, the knurled joint resists more than a blank surface, but less than the bonded ones, which were approximately resisting as much as those joints which were expanded by rolling and additionally bonded. Nevertheless, the most feasible joint was manufactured using a grooved mandrel (which allows an immediate pre-fixture) with narrow grooves and an additional adhesive [15].

Joining by Hydroforming

During the 1980´s joining by hydroforming was introduced into the manufacturing of heat exchangers for nuclear power plants. Economic reasons lead to a replacement of welding, resulting in the extensive control of the weld seams, which was mandatory for welded components in nuclear applications as well as the knowledgement about the corrosion behavior between the joint partners. New developments in the field of powertrain components introduced this joining process into the automotive industry [16]. Exemplary applications are e.g. composite camshafts, intermediate shafts, and countershafts as well as joining of cylinder liners, fig 6 displays two applications [17,18].

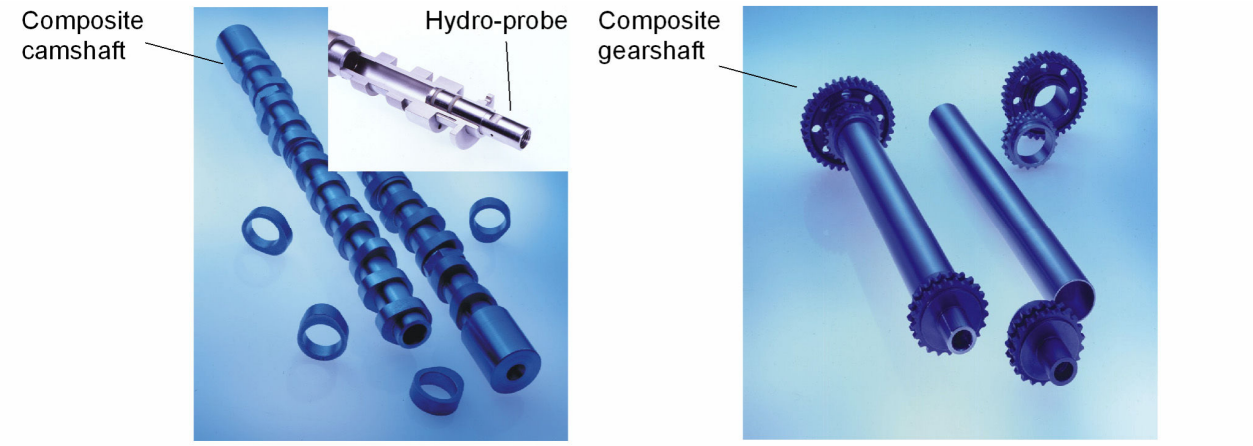

Fig. 6 Applications of joining by hydroforming [18]

Some characteristics of the joining by hydroforming process are joining of non-weldable alloys, short process time as well as a sufficient process controlling. The joining area is pressurized by a special joining tool, introducing it as hydro-probe. In case of joining by hydroforming with a hydro-probe, the pressure acts locally underneath a certain joining area instead of pressurizing a complete semi-finished part used in conventional hydroforming processes of tubes and sheet metal. The hydro-probe is inserted into the tube, and then the working medium is set under pressure after it filled the gap between the probe and the inner surface of the tube. A sealing limits the joining area in circumference as well as in longitudinal direction. The process of joining by hydroforming can be subdivided into three characteristic phases indicated in Fig 7.

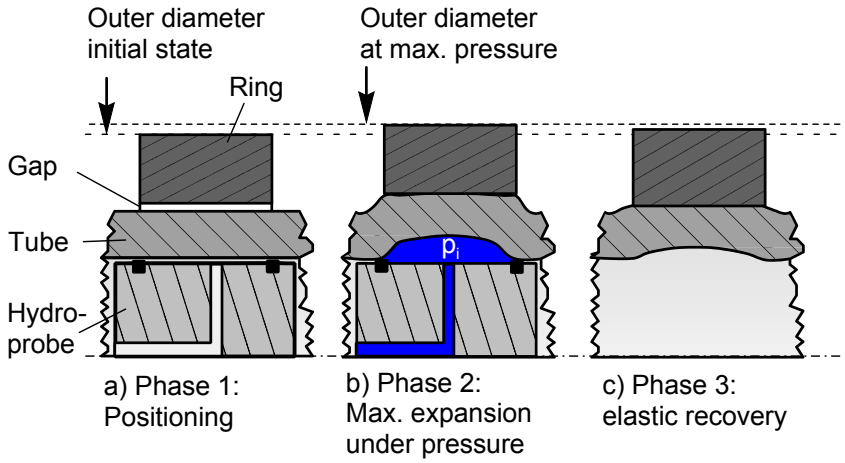

Fig. 7 Process principle of joining by hydro forming [16, 18]

In the first phase, the tube is expanded within the clearances (gap) limit. After this, both parts (tube-ring) expand together until a maximum radial displacement is reached, this is determined by a related joining pressure (Fig. 7 a-b). The pressure ideally determines an elastic-plastic deformation of the tube, but a straight elastic deformation of the ring. After releasing the pressure, the joint of tube and ring recovers elastically.The elastic recovery of the ring is prevented by the expanded tube (Fig. 7 c). Furthermore, the prevented elastic recovery of the ring results in an interference-fit between the joint partners (tube-ring). As known from the manufacturing of camshafts, the joint partners should be arranged with increasing yield points from the inner to the outer joint partner if both joint partners possess the same Young's modulus [16, 18, 19].

To compare the hydroforming with the joining by rolling-in, the quality of an interference-fit, which is influenced by the parameters material, thickness and length of the ring as well as expansion of the ring and assembly clearance has been tested by pull-out forces. Firstly, the

influence of the process parameters expansion as well as clearance was determined to manufacture the joints with optimized process parameters. Fig. 8 displays selected results of the experimental investigations. To provide comparability to the joining by rolling process, experimental investigations were carried out varying wall thickness and length. A maximal shear stress of 3.8 N/mm^2 could be determined as one result. Along with a wall thickness of 9.5 mm and a joint length of 32 mm the maximal shear stress occurred; concerning the tube's outer diameter of 40 mm and its wall thickness of 2 mm, joined at an expansion of approx. 0.4 mm.

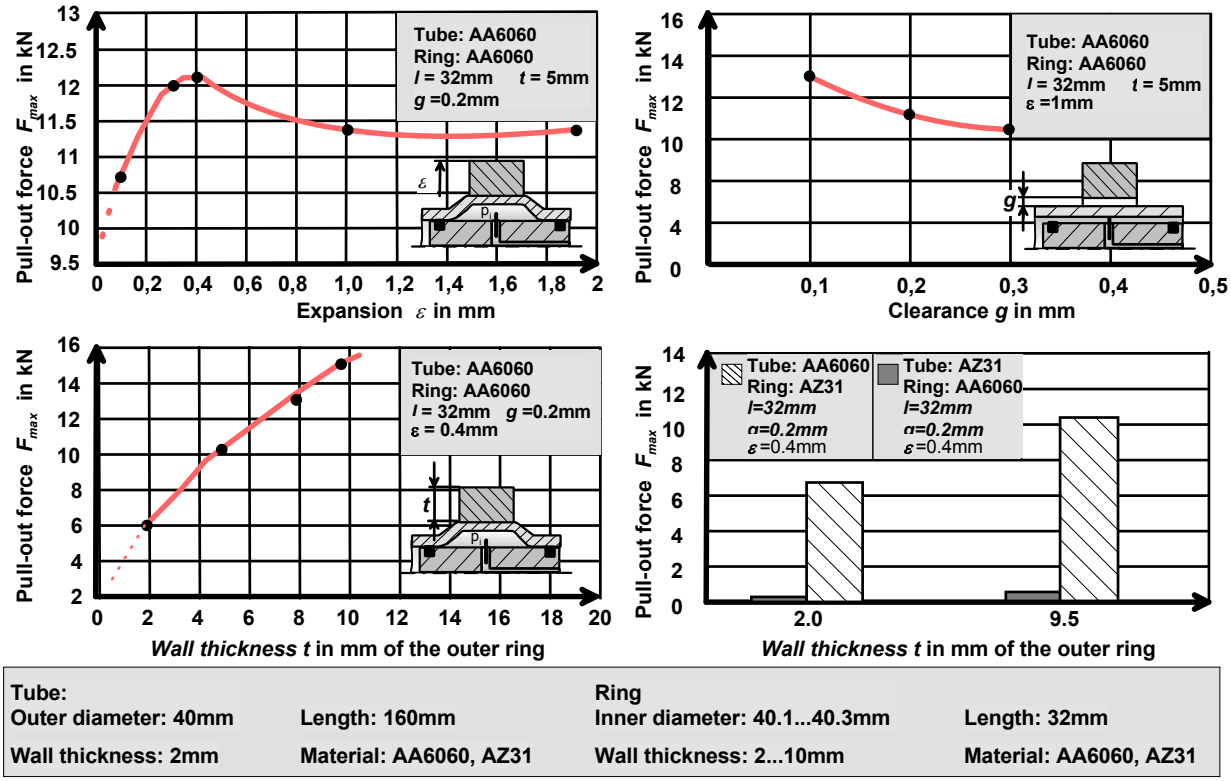

Fig. 8 Selected results for the joining by hydro forming [19]

Replacing the material of a lightweight structure by a material of a lower density reduces the weight, e.g. by replacing aluminum by magnesium. Therefore, joining of magnesium tubes to magnesium rings was done to evaluate the feasibility of the joining by hydroforming process for magnesium structures. Here, low interference-fits possibly caused by a low Young's modulus of magnesium could be observed. Furthermore, when producing joints made of different materials (of the tube and of the ring) it turns out that the joint of AA6060 (tube) and AZ31 (ring) is more resistant than the reversed assembly (AZ31-AA6060) [19].

Joining by hydro forming is particularly interesting for the manufacturing of joints in light frame structures. Besides the achievable shear stress features very low tooling costs and an elementary design of the hydro-probe, comparably low demands on the joint preparation as well as a sufficient process control. Currently it is only possible to establish joints in the way of shaft to collar connections with straight cylindrical profiles or at the end of a curved profile because of the current tool design. Further developments in the field of tool design are necessary to manufacture feasible joints in curved profiles except at its end.

Joining by Electromagnetic forming

Electromagnetic forming (EMF) is a high speed process using a pulsed magnetic field to form metals with high electrical conductivity such as aluminum. The energy density of a pulsed magnetic

field is used for the contactless forming of a workpiece. Joining is the most common industrial application of the EMF process. Due to the contactfree forming process the joining of coated fuel pipes is a feasible application. Furthermore, the joining of composite material as well as structural components is of increasing interest. Fig. 9 displays some exemplary applications.

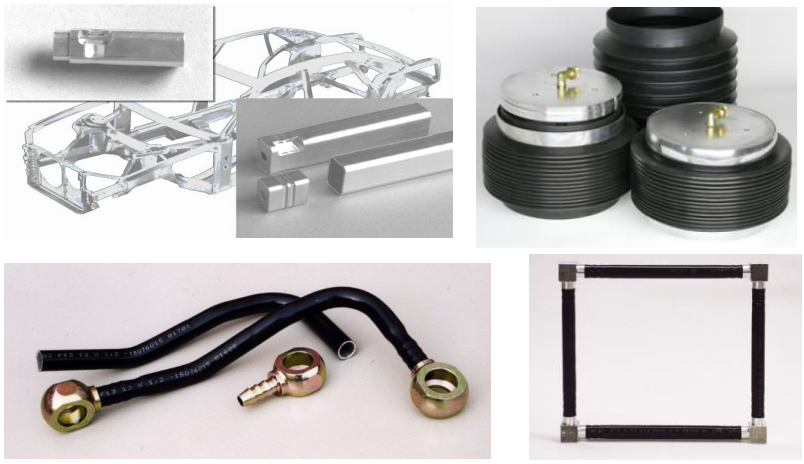

Fig. 9 Application of joining by electromagnetic forming [20,21]

Especially for structural components made of aluminum alloys (with good electrical conductivity) the EMF process is suitable and of increasing industrial interest. Assuming a good process design, the quality of these joints can satisfy the criteria of strength or impermeability even for the aerospace or automotive industry. New developments in the field of tool coil design allow forming and joining of non-cylindrical profiles as well as of completely closed frame structures. The forming process is closely related to electromagnetic issues. The process model (Fig. 10) can be described as an oscillating circuit which includes the capacitor C, the resistance R, and the inductance L of the pulse generator as well as the consumer load consisting of tool coil and the workpiece, here a solenoid and a tube. After the capacitor bank has been charged it is suddenly discharged by closing a high current switch. As a result, a damped oscillating current flows through the coil, generating a corresponding magnetic field. According to Lenz's law, a current in the workpiece will be induced flowing in the opposite direction to its cause. Due to the skin effect the current as well as the magnetic field penetrate the workpiece wall [25]. The resulting magnetic pressure p (t,r,z) is determined by the energy density of the magnetic field outside H_a and inside H_i of the workpiece and can be calculated on the basis of the measured coil current by p(t) [20].

$$p(t,r,z) = \frac{1}{2} \cdot \mu_0 \cdot \left(H_a^2(t,r,z) - H_i^2(t,r,z) \right)$$

The resulting pressure pulse acts vertically on both the field strength and the included induced current [22], this means in radial direction on tube and tool coil as, fig. 10 shows.

If the yield strength of the tube is exceeded, radial necking occurs. The velocity of the tube being compressed as well as its mass both determine the kinetic energy at the moment of impact, and therefore the force which takes effect on the mandrel [23].

To investigate the influence of the necking velocity, the radial displacement has been measured during the forming process without a mandrel by the light-shadowing method, as shown in fig 10. The characteristic shape of the necking velocity during this high speed process shows a characteristic acceleration and deceleration part. Fig. 11 shows such curves for different charging energies. The related velocity of the radial displacement of point A can be calculated by derivation of the measured and smoothed displacement curve.

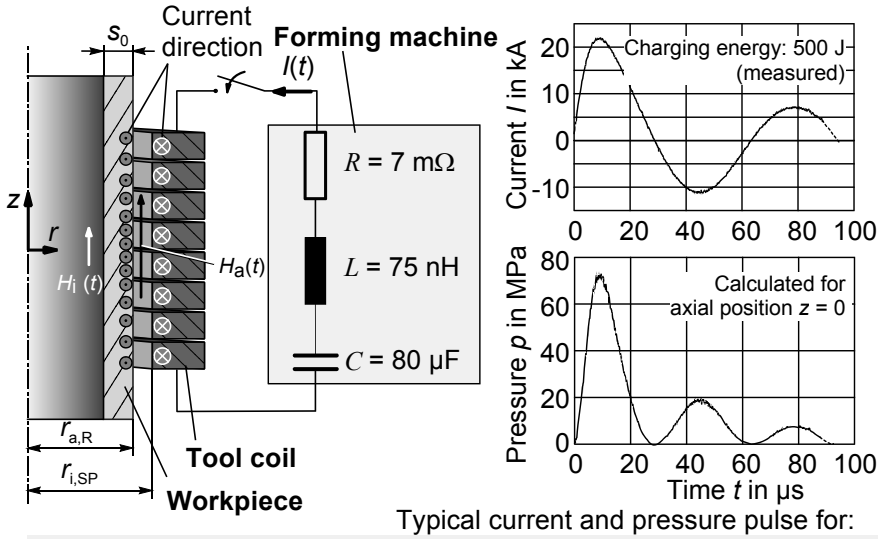

Typical current and pressure pulse for:

Workpiece		Tool coil	
Conductivity	κ = 26,5 MS/m	No. of turns	n = 14
Wall thickness	s_0 = 1,25 mm	Length of the winding	l_{Sp} = 27 mm
Outer radius	$r_{a,R}$ = 8.95 mm	Inner radius	$r_{i,Sp}$ = 9,6 mm

Fig. 10 Process principle of electromagnetic forming [24]

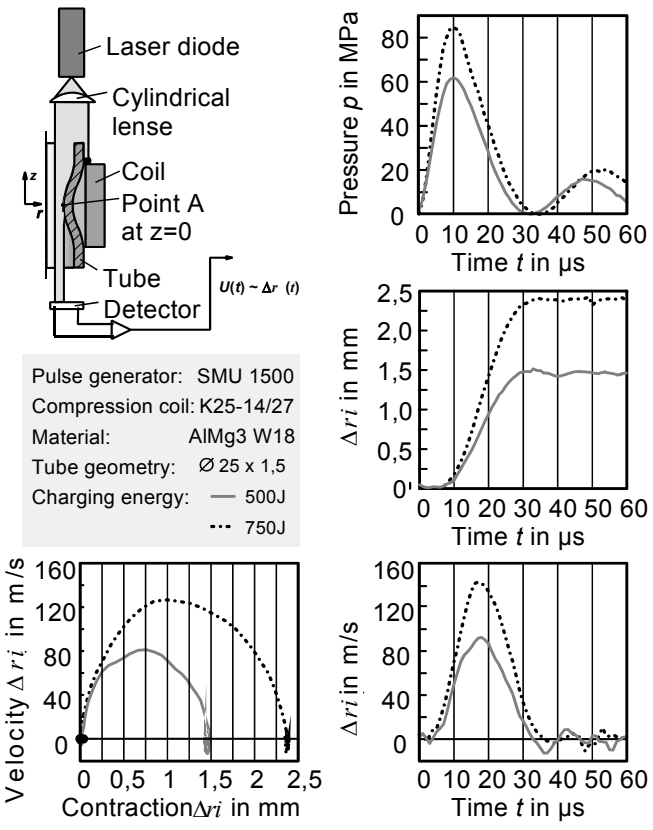

Fig. 11 Online measurement system and example of tube compression processes with different pressure rise time and forming velocity [24]

By increasing the charging energy and keeping the same arrangement of pulse generator, coil, and workpiece, the pressure maximum will be increased without increasing the pulse duration. This results in a larger deformation as well as in higher velocity, as the time curves of the radial displacement indicate. In addition to this, former experimental investigations led to the result that in the case of tube compression the deformation velocity can be influenced by the pressure rise time which, in turn, will be influenced by the characteristics of the above mentioned equivalent circuit of the process [24]. A mandrel or fitting inside

the tube limits the radial displacement. So, the gap a_0 between tube and mandrel is the distance which can be used for tube acceleration. On the one hand, it is possible to increase the velocity (and therefore the kinetic energy) of the tube at the moment of impact by increasing the charging energy, as fig. 12 indicates. On the other hand, the charging energy which is required for a particular velocity at the moment of impact can be reduced by an increase of the gap a_0. The resulting strength of the joint has been determined by pull-out tests. Fig. 12 indicates a close relationship between the impact velocity and the resulting pull-out force. Furthermore, the influence of different mandrel materials is shown in fig. 12.

The comparison of different aluminum alloys (Yield strength of AA6060 is 160-230 MPa, Yield strength of AA2007 370-470 MPa) shows higher pull-out forces in the case of AA2007. Therefore, it should be favorable to use a mandrel material of higher Yield strength than the tube material. To reduce the weight of a joint, a massive mandrel has been hollowed by drilling so that its wall thickness has been changed, which also results in a change of the mandrel's stiffness [25]. The influence of the ratio of diameter $Q=D_i/D_a$ has been examined by Bühler/von Finckenstein [6] for joining of a copper tube to a steel mandrel. Fig 12 verifies the results of Bühler/von Finckenstein for joints of aluminum tubes with steel mandrels and additionally shows the influence of the charging energy of the push-out force. In addition, tubes with an outer diameter of 40 mm and a wall-thickness of 2 mm made of aluminum (AA6060) as well as magnesium (AZ31) have been joined. As one result, the aluminum tubes could be joined by dominating force-fit to massive mandrels made of aluminum and magnesium respectively. Providing a joint length of 60 mm, push-out tests determine a failure of the aluminum tube by bulging instead of a failure of the joint.

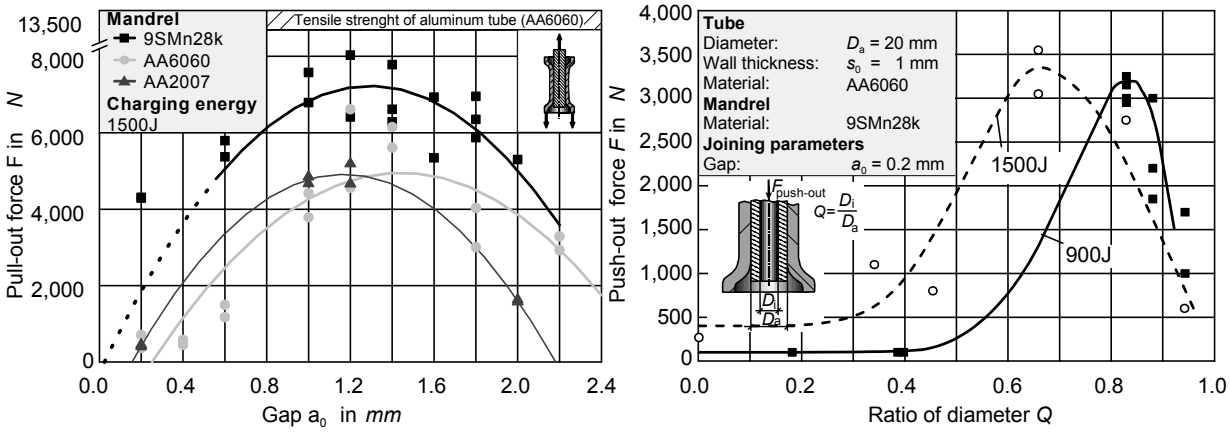

Fig. 12 Results of pull-out test [25]

However, joining of magnesium tubes by dominating force-fit was not feasible although using mandrels of different materials like aluminum, magnesium, and steel. Consequently, this will characterize further investigations to understand the mechanism for joining of magnesium. In order to achieve a good joining quality, the influence of geometrical parameters like gap width and mandrel stiffness, the mandrel material as well as process parameters like impact velocity and pressure pulse were examined.

Joining by EMF is especially interesting for the manufacturing of joints in light frame structures. The achievable shear stress with dominating force-fit joints could exceed the yield stress of the tested aluminum tubes (AA6060). Recent tool design allows the joining of non-cylindrical profiles and using separable tool coils allows the manufacturing of completely closed frame structures [26]. Further investigations should determine the feasibility of separable tool coils for the manufacturing of lightweight frame structures.

Conclusion

Joining by forming for the manufacturing of light weight frame structures is an attractive alternative to the thermal-based joining processes. Best potentialities to manufacture joints of high strength are provided by joining by rolling-in, by hydroforming and by electromagnetic forming. Further basic developments for the manufacturing of dominating form-fit joints by hydroforming as well as by electromagnetic forming are currently in the focus of investigations at the IUL.

Acknowledgement

This paper is based on investigations of the Collaborative Research Center SFB/TR10 which is kindly supported by the German Research Foundation (DFG).

References

[1] Homberg, W.; Marré, M.; Kleiner, M.: *Umformtechnisches Fügen leichter Tragwerkstrukturen*, in Aluminum, International Journal for Industrie, Research and Application, Volume 80 12 (2004), pp. 1396-1400

[2] Zäh, M.F.; Trautmann, A.: *Vergleich des hybriden, bifokalen Laserschutzgasschweißens mit Laser-MIG-Hybridverfahren*, in Aluminum, International Journal for Industrie, Research and Application, Volume 80 12 (2004), pp. 1387-1392

[3] Young-Bae Park, Heon-Young Kim, Soo-Ik Oh: *Design of axial/torque joint made by electromagnetic forming;* in Thin-Walled Structures 43 (2005)

[4] DIN 7190: 2001 - 02: *Interference-fits – Calculation and design rules.* Beuth Verlag GmbH, Berlin 2001

[5] Al-Ahmad, N.: *Das Fügen rotationssymmetrischer Formelemente durch Umformen mit Impulsmagnetfeldern*. Ph.D. Thesis Ingenieurhochschule Zwickau 1980

[6] Bühler, H.; von Finckenstein, E.: *Fügen durch Magnetumformung*. Werkstatt und Betrieb 101. Jahrg. (1968) 9, pp. 209-215

[7] Fuss, H.; Kleiner, M.: Zylindrische *Verbundwerkstücke herstellen im Aufweitverfahren*, Bänder Bleche Rohre 2 pp 43-46 (1992)

[8] Kleiner, M.; Weinert, K.; Hagedorn, M.; Krux, R.: *FEM-Analyse der Fügeverbindung beim Rohreinwalzen,* in UTF-Science III (2001), pp. 13-16

[9] Information on http://www.mausitalia.it (2005)

[10] Hagedorn, M.; Weinert, K.: *Manufacturing of composite workpieces with rolling tools*, in Journal of Material Processing Technology 153-154, pp. 323-329 (2004)

[11] Information on http://www.ecoroll.de (2005)

[12] Information on http://www.stecher.de (2005)

[13] Haase, V.: *Eigenspannungsermittlung an dünnwandigen Bauteilen und Schichtverbunden*. Ph.D. Thesis, University of Dortmund, Shaker Verlag Aachen, 1998

[14] Wojciechowski, J.; Klaus, A.; Hagedorn, M.; Przybylski, W.; Kleiner, M.: *Flexibles Fügen leichter Tragwerkstrukturen durch Einwalzen*; www.UTFscience.de I/2004

[15] Przybylski, W.; Wojciechowski, J.; Klaus, A.; Marré, M.; Kleiner, M.: *Manufacturing of Resistant Joints by Rolling*, submitted to The International Journal of Advanced Manufacturing Technology (2005)

[16] Garzke, M.: *Auslegung innenhochdruckgefügter Pressverbindungen unter Drehmoment-belastung*. Ph.D. Thesis. TU Clausthal, VDI Verlag Düsseldorf, 2001

[17] Rückert, F.; Stocker, P.: Patent DE 101 41 902 C1

[18] Information on http://www.mubea.com (2005)

[19] Przybylski, W.; Wojciechowski, J.: *Joining by hydro-bulging*, internal report of Institute of Forming Technology and Lightweight Construction, University of Dortmund (2005)

[20] Beerwald, C.: *Grundlagen der Prozessauslegung und –gestaltung bei der elektromagnetischen Umformung.* Ph.D. Thesis University of Dortmund (2004)

[21] Information on http:// www.poynting.de (2005)

[22] Winkler, R.: *Hochgeschwindigkeitsbearbeitung*, VEB Verlag Technik Berlin (1973)

[23] Wilson, W.: *High velocity forming of metals*, edited by American Society of Tool and Manufacturing Engineers (1964)

[24] Beerwald, C.; Homberg, W.; Marré, M.; Psyk, V.; Kleiner, M.: *Einfluss der Geschwindigkeit beim Kraftschlüssigen Fügen rohrförmiger Werkstücke durch elektromagnetische Kompression*, in Tagungsband 11. Paderborner Symposium Fügetechnik 2004

[25] Kleiner, M.; Marré, M.; Beerwald, C.; Homberg, W.; Löhe, D.; Barreiro, P.; Schulze, V.: *Investigation of force-fit joints produced by electromagnetic tube compression*, submitted to Production Engineering: Annals of the German Academic Society of Production Engineering XIII/1 (2006)

[26] Henselek, A.; Beerwald, M.; Beerwald, C.: *Design and Adaptation of EMF Equipment – From Direct Acting Multi-turn Coils to Separable Tool Coils for Electromagnetic Tube Compression,* in Conference Paper 1st International Conference on High Speed Forming 2004

doi:10.4028/www.scientific.net/AMR.10.101

Seam Weld Positioning for Composite Extrusion

Marco Schikorra[1, a], Matthias Kleiner[1, b]

[1]Institute of Forming Technology and Lightweight Construction,
Baroper Str. 301, 44227 Dortmund, Germany

[a]marco.schikorra@iul.uni-dortmund.de, [b]matthias.kleiner@iul.uni-dortund.de

Keywords: Extrusion; Seam Weld; FEM Simulation; Composite

Abstract. The production of continuously reinforced profiles by use of aluminium as base material and a reinforcement made of steel or carbon offers a great potential for modern lightweight constructions. Within this scope, they present the potential for an increase in usage of space frame constructions in automotive or aerospace engineering. But with the insertion of reinforcement in the material flow of the extrusion process some problems can occur that are negligible in thee conventional extrusion processes: in the composite development area a significant local perturbation of the material flow is induced that can lead to the induction of high tensile stresses into the reinforcement. Due to this, failures like cracking of the reinforcement elements during the extrusion process has been detected in experimental investigations. A second problem occurring is the necessity of prediction of the seam weld position and prediction of the seam weld quality. The reinforcement can only be induced by bridge dies between two strands and due to this it is always positioned in a seam weld. While in conventional extrusion the seam weld positions is often only an aesthetical problem, now this position mainly influences the extruded profiles properties like moment of inertia.

This paper deals with the problem of determination of seam weld position on the example of a double-t-profile extrusion. By use of a coupled thermo-mechanical finite element simulation with the commercial FE code HyperXtrude from Altair the velocity fields of an extrusion process with and without reinforcement were calculated and the resulting material flow was analysed. The numerical results went along with experimental investigations to verify the calculated results.

Introduction

In the field of transportation engineering, lightweight construction is of increasing importance, even will respect to decreasing quantities regarding the diversity of product variants. Parallel to this development, the need for profiles made of high strength materials with low density becomes more and more important. Due to this tendency, the use of extruded aluminum profiles increases caused by advantages like decreased weight and good formability. However, there are still many areas in extrusion research which are considered insufficient so far. One of these areas is the simulation of extrusion processes where research investigations are increasing since the 1990s. A reason for the late usage of simulations in general and simulations based on the Finite Element Method (FEM) in particular can be seen in problems like extreme deformation of the elements due to large strains, complex physics due to the thermal-mechanical coupling, or often complex geometry, especially when working in 3D. The lack of simulation led many investigations focusing on theoretical and visioplastic methods, but often geometry was kept simple and problems occurring in extrusions of complex or hollow profiles have not been analyzed [1,2]. With increasing use of simulation the determination of process parameters is now getting much easier, even for complex 3D geometries. Current research topics deal with material flow simulation even for hollow profiles and with the determination of the seam weld quality [3,4].

Within this trend of increasing use of simulation much effort in the field of extrusion has been spent on the development of special purpose FE codes and on clarifying the definition of boundary conditions [5,6]. One of these codes is the commercial program HyperXtrude which deals with an

Eulerian formulation and a space fixed mesh of Finite Elements. Due to this it is possible to simulate the material flow even for complex die geometries that occur, for example, in the analysis of composite extrusion processes when an endless steel wire reinforcement is inserted into the extrusion process of aluminum profiles [7,8]. For the insertion the material flow has to be split into at least two strands that build the upper and lower profile layer between whom the reinforcement will be placed. Due to the necessity of splitting the material flow an extrusion of this kind of composite profiles always needs a bridge die, making the tool construction and process analysis very time-consuming. Considering this, a large potential for the usage of these profiles can be seen. Depending on the choice of base and reinforcement material, advantages such as

- an increase in strength, stiffness, energy absorption, and safety against cracking,
- a reduction in the profile's weight with equal mechanical properties, and
- an integration of additional functions such as
  - a reduction in abrasion,
  - a control of electrochemical influenced procedures, and
  - an interruption of crack growing

can be achieved if a defined introduction of the reinforcement is possible [9]. But as shown in [7], the occurring stress level when introducing the reinforcement at an adverse position inside the die can lead to a cyclic cracking of the reinforcement. An explanation of this effect was found in the fact that the reinforcement has to flow through the die with the profile's exiting velocity when the compound is formed. Extreme stress concentration will occur when the fast moving reinforcement flows through areas of slow aluminum base material movement (fig 1.). This leads to a pulling of the reinforcement from the exiting profile and to clamping and braking inside the die.

In order to study this effect, investigations on a simplified 2-dimensional geometry of a welding chamber have been carried out with the Finite Element code HyperXtrude. The chosen materials were AA6060 aluminum for the base material and 1.4310 for the steel wire reinforcement. The velocity distribution shows the base material and reinforcement attending to leave the die with the same velocity. In contrast to this, in the composite development area the base material forms a dead zone that clamps the reinforcement. The concurrent pulling and clamping leads to the development of high tensile forces in X-direction. Additionally, the hydrostatic pressure is working orthogonally on the reinforcement and additional high stresses where induced into the elements. The combination of these high tensile and compressive stresses leads to a high equivalent stress level that will cause cracking of the reinforcement after a certain process time [8].

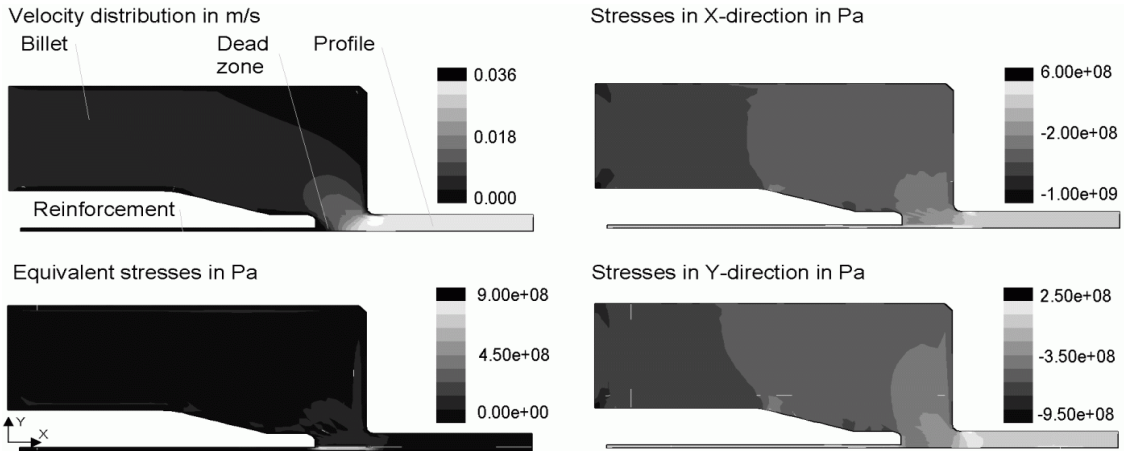

Fig. 1: Stress concentration in reinforcement elements caused by high velocity rates in the composite development area.

Conventional Extrusion Simulation for the Seam Weld Prediction using the Complete Model

In addition to the problem of occurring stresses in the reinforcement elements a further problem can be seen in their positioning. Due to the fact that the reinforcement will be introduced into the material flow via die bridges it is always placed in the seam weld of the profile and, thus, the composite profile's quality depends on the seam weld quality and position. A prediction of seam weld conditions and geometry becomes necessary for the process design. To analyze the influence parameters of this FE model for the simulation a complex shaped profile was set up. The geometry used for the analysis was a double symmetric profile with a double-T shape. Because of the symmetry, only a quarter of the whole system was considered in the simulation to reduce the calculation time. The chosen cross-section geometry and process parameters are shown in table 1.

Materials used:	
Base material	*AA 6060 / AlMgSi0.5*
Reinforcement material	*Steel 1.43.10*
	Wire Ø 1 mm
Temperatures:	
Die initial	*750 K*
Punch	*723 K*
Billet initial	*750 K*
Temperature air	*300 K*
Convection at free surfaces:	*50 W/(m²K)*
Heat flux at tool surfaces:	*0 W/m²*
Punch speed	*0.2 mm/s*

Profile cross-section and symmetry (in mm):

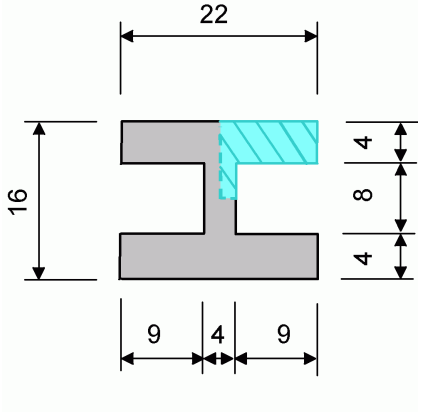

Table 1: Chosen boundary conditions and geometry of the double-T profile.

Due to the Eulerian formulation of the FE code the Finite Element mesh was treated as a room-fixed mesh with a material flow inside based on Navier-Stokes equations. The governing boundary conditions for metal extrusion cases are the material inflow that simulates the punch travel and the material outflow that represents the exiting profile. All other boundary definitions (solid wall, symmetry, die face, bearing) do not allow material flow through the outer elements` surface and consider only thermal and frictional boundary conditions. The first model analyzed was a model of the complete geometry including a billet of 175 mm length and 62.5 mm diameter. The complete model was meshed with 40140 hexaeder elements to ensure a high resolution to enable an accurate material flow simulation. The model including the chosen boundary conditions is shown in Fig. 2.

The initial analysis of the complete system - but without reinforcement elements - has been carried out to study the material flow including seam weld position and pressure distribution for the complete tool and conventional extrusion. To consider the decreasing container length, the effect of heating of the billet during the process time, and the change of the material flow due to this, the model was set up for a transient calculation run. During the simulation the FE mesh of the billet was adapted automatically regarding inflow speed and process time.

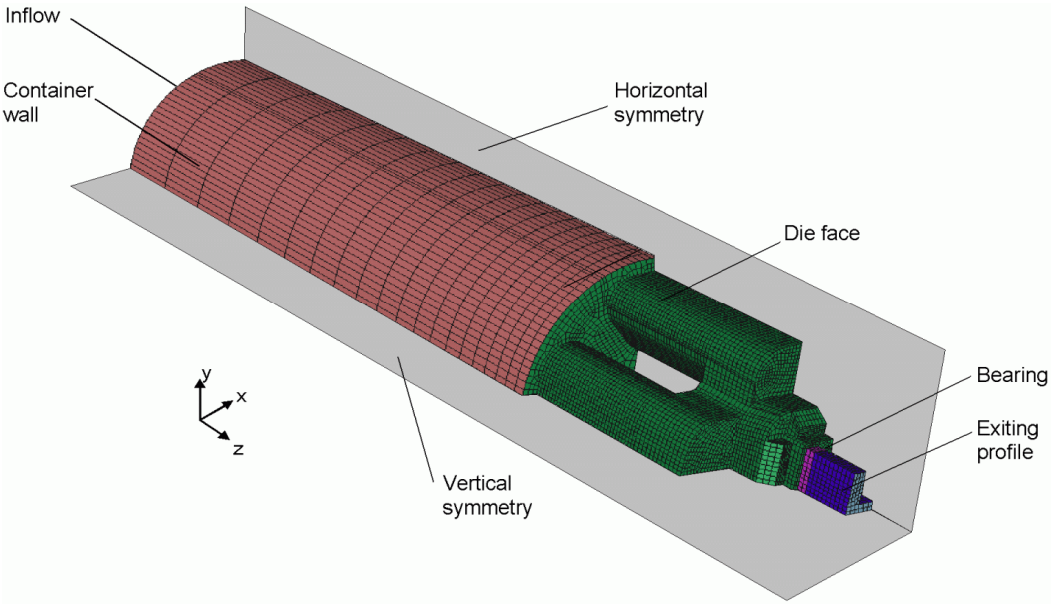

Fig. 2: FE mesh for extrusion simulation of the double-T-profile (press ratio: 18.37).

In order to analyze the material flow inside the die geometry, the occurring velocities and the pressure distribution are essential. Both are coupled by the materials viscosity that was considered by the use of a sine-hyperbolic material law based on the Zener-Holomon parameter [7]. They are directly connected to the material flow and useful for the interpretation of the predicted seam weld position.

As shown in Fig. 3, the material flowing through the chamber next to the horizontal symmetry plane has a slightly higher velocity ($v = 0{,}005$ m/s instead of $v = 0{,}004$ m/s) and needs a lower pressure level ($p \approx 7.9e{+}07$ Pa instead of $p \approx 8.3e{+}07$ Pa) to reach this speed. Considering the geometry the material is flowing through, this chamber shows less geometrical resistance concerning the material flow. Stream lines created by imaginary particles that flow through the volume are less curved and have larger radii in curved sections.

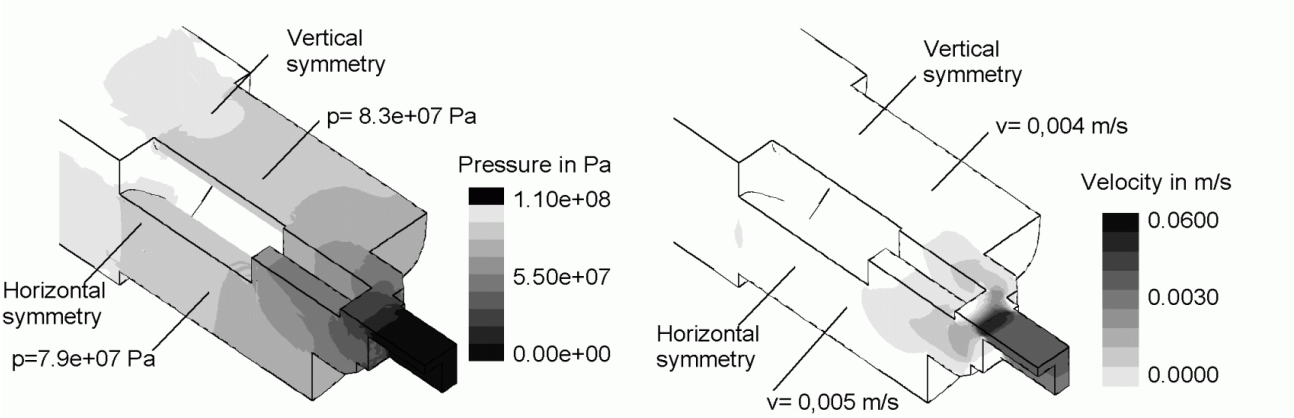

Fig. 3: Velocity and pressure distribution for transient simulation of double-T-profile extrusion.

The different velocities of the strands lead to more material flowing through the chamber next to the horizontal symmetry plane. In addition to this material from the channel next to the vertical symmetry plane flows near to the symmetry plane with a high velocity into the welding chamber. It can be assumed that this will result in a curved seam weld line instead of an initially planed straight line that divides the belts in the middle into two rectangular profile sections. The fast material flow next to the vertical symmetry plane will shift the seam weld line into the direction of the horizontal

symmetry plane whereas the material coming from the channel at horizontal symmetry plane will shift the seam weld line in general.

To visualize the seam weld, different possibilities are feasible. One is the visualization of the material flow tracing along the way particles would run through the extruded material. Thereby it is possible to choose the starting point of the traces, which is typically the midpoint of all elements that have inflow boundary conditions. The traces follow the material flow through the container material and divide into the two channels. Finally, they cross the welding chamber and end up at a point of the exiting profiles cross-section that defines the outflow conditions. By considering the division of the traces caused by the chambers it is possible to identify the way the streamlines took towards the outflow surface. In this way it is possible to find the seam weld based on line-search of the traces. Because the method is not automated the determination of the weld line position is mainly performed optically and thus implies a more qualitative character. Nevertheless a sufficient correlation between the experimentally determined seam weld position and the simulated one can be seen in Fig. 4.

A second method for the visualization of the seam weld line is an analysis of the effective or equivalent strain. In the area of seam weld formation higher effective strains usually occur than in neighboring regions. This way an analysis of the strains in the seam weld formation area indicates the merging of the two streams. For an analysis of the effective strain slices through the welding chamber have been plotted, which are also shown in Fig. 4. It can be seen that the slices through the extruded profile show a comparable distribution of high effective strains as the weld line in experiment and in the analysis of the particle tracking. For both simulated seam weld predictions the correlation is good and the comparison with the experimentally determined seam weld geometry is acceptable, too. But like the analysis of the particle tracking the effective strain analysis does not lead to precise geometric data. Both methods only give a qualitative assumption of the seam weld line geometry.

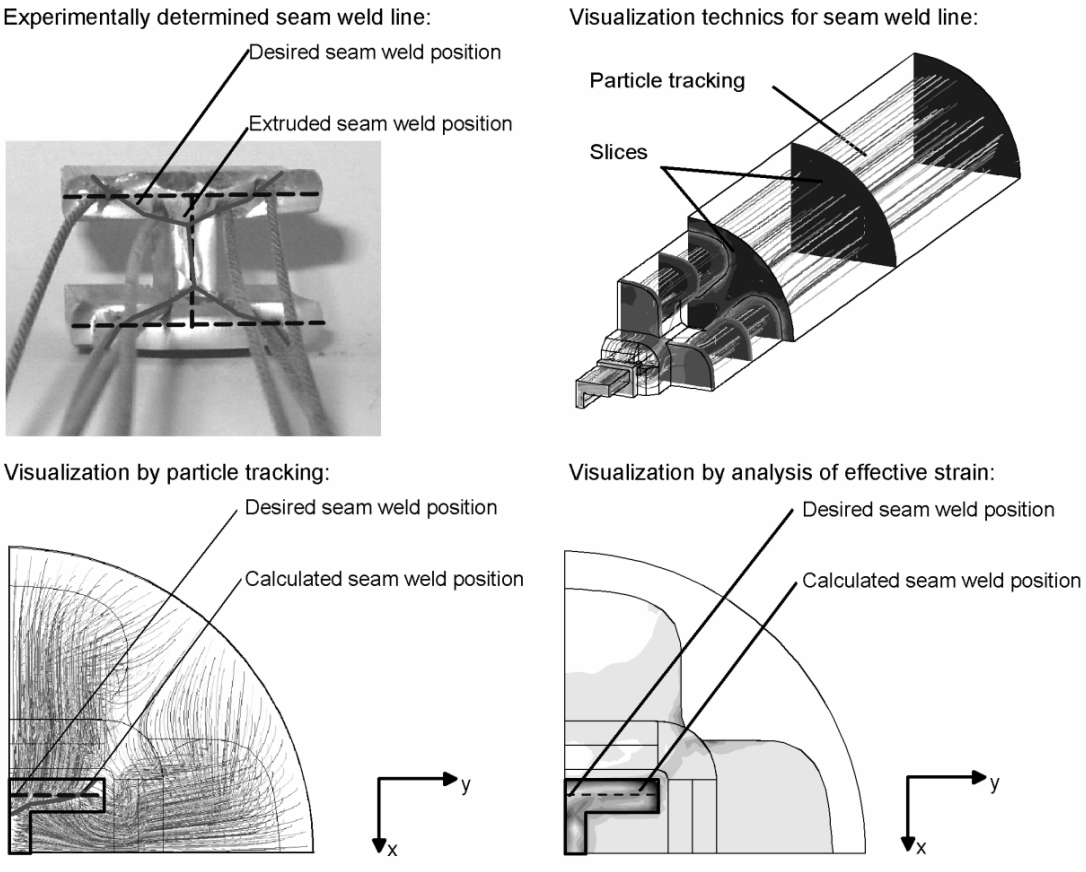

Fig. 4: Seam weld visualization and comparison between experimental and numerical result.

Conventional Extrusion Simulation for the Seam Weld Prediction using the Reduced Model

For the analysis of the influence parameters on the seam weld position the model has been modified in order to reduce the calculation time and to increase the flexibility for parameter variation. For further calculations the complete container and billet geometry will be neglected. On account of that the number of elements will be reduced from 40140 to 25460 hexaeder elements. Thus, the model has two inflow surfaces. Both of them were treated independently, so they offer the possibility of separate material inflow or temperature control. Additional small changes of the boundary definitions of the solid wall in the container area and the die face for die definition have been necessary, but friction, temperature, and heat flux have not been changed. The reduced model is shown in Fig. 5.

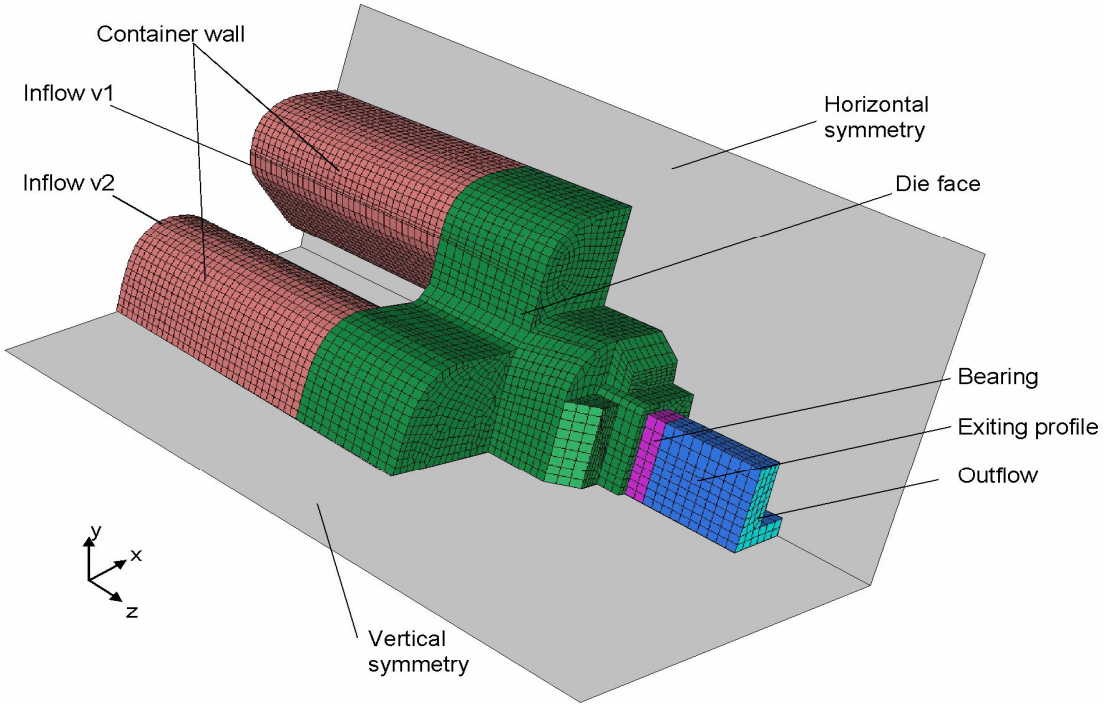

Fig. 5: Reduced Finite Element mesh for variation of channel inflow velocity (press ratio 8.2).

The model was set up to study the change of the seam weld position depending on the material flow of each channel. For the analysis of this reduced area the simulation mode was changed from a transient simulation, which includes a decreasing billet length, to steady state simulation. This assumes an infinite material flow for a constant FE mesh and solves the flow equations to calculate the velocities, temperatures, and stresses when equilibrium between inflow and outflow and temperature increase and decrease is reached. This is what usually happens in the die area when material from the container flows with constant speed into the channels for a long period of time and when the temperature rises due to heat dissipation.

For the analysis of the seam weld position three different inflow conditions assuming material flow control by different friction or different feeder port geometry have been simulated:

- constant inflow of 5 mm/s at both inflow surfaces (approximately equal to material velocity in the channels of the complete model).
- inflow of 8 mm/s at channel in horizontal symmetry plane and 2 mm/s at channel in vertical symmetry plane.
- inflow of 8 mm/s at channel in vertical symmetry plane and 2 mm/s at channel in horizontal symmetry plane.

All of them have a constant inflow of 2080 mm^3/s which is approximately equal to the inflow of the complete model. The resulting velocity and pressure distributions are shown in Fig. 6.

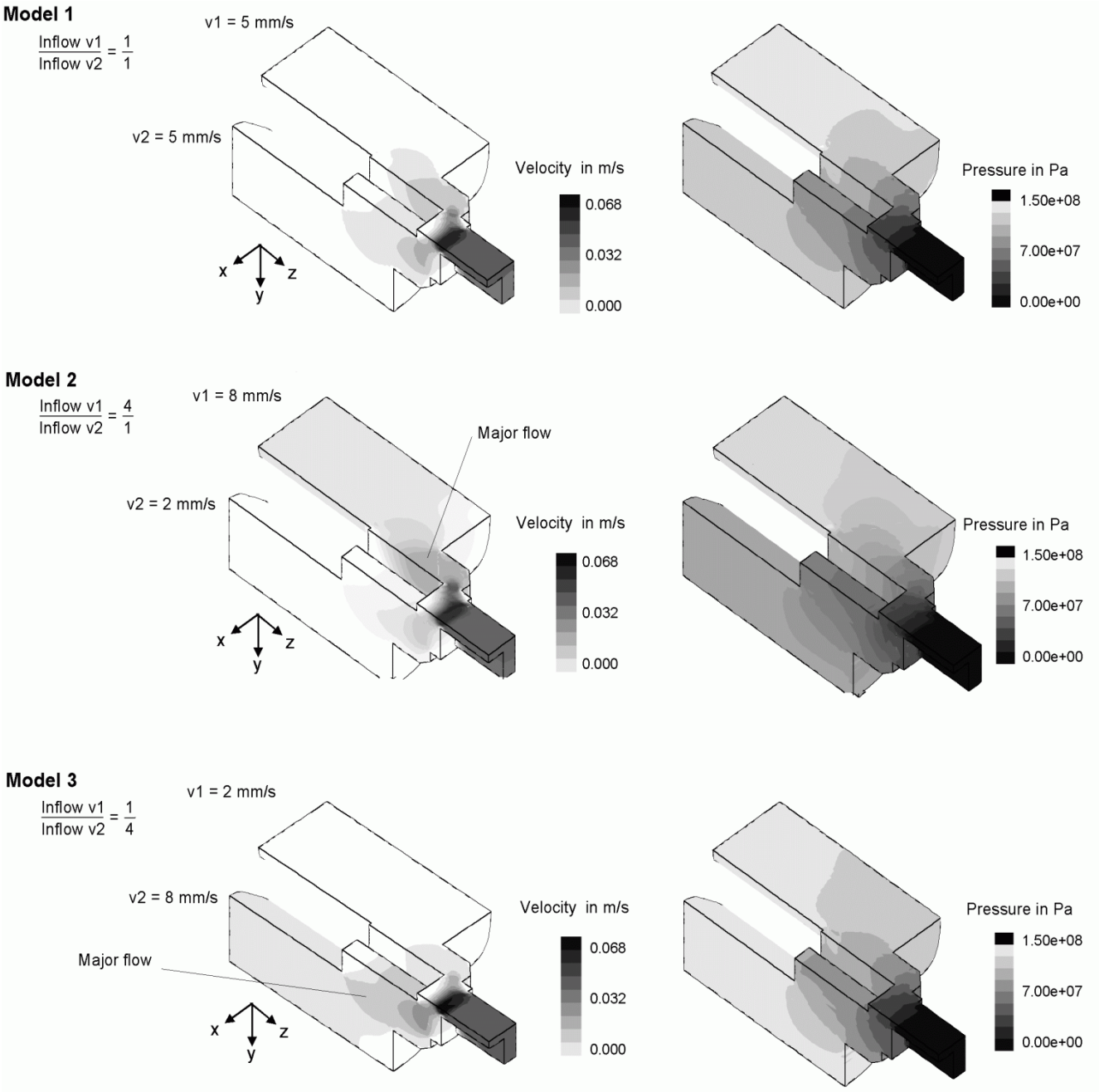

Fig. 6: Velocity and pressure distribution for different inflow velocities for the reduced FE mesh.

A comparison of the velocity distribution shows the relation of material inflow speed to material flowing in the welding chamber. In the case of equal inflow speed material from both channels flows with nearly the same velocity into the welding chamber. In cases of unequal material inflow the material flowing with higher speed dominates and suppresses the material flow from the slower channel. In model 2 (v1/v2 = 4/1) the material flow from the channel next to the vertical symmetry plane shows a much higher speed and pressure. This will lead to a shift of the seam weld line into the direction of the of the horizontal symmetry plane. In model 3 (v1/v2 = 1/4) the opposite can be expected. The stream of material from the horizontal symmetry plane leads to an increase in pressure in the channel that shifts the seam weld away from the horizontal symmetry plane. Model 3 is the only model where the pressure in the channel in horizontal symmetry plane is higher than in the channel next to vertical symmetry plane. However, due to the over all constant material inflow of the whole model the pressure distribution in the welding chamber stays approximately constant.

Considering the velocity and pressure distribution, the differences of the seam weld line positions can be explained easily (fig. 7). While the weld line of model 1 is quite similar to the weld line of the complete model, its position in model 2 and model 3 mainly shifts in x-direction. Comparing model 1 with the complete model it shows only a slight difference of the seam weld in the upper right corner of the profile. In that region the seam weld prediction with the reduced model for steady state analysis does not predict such a distinctive curvature. Compared with model 2 it can be shown, that the unequal material flow leads to a complete shift in positive x-direction. Considering the desired seam weld position the unequal material flow makes an embedding of reinforcement elements even worse. For model 2 it can be expected that the reinforcement will lay right at the profiles surface and no acceptable compound will be formed. This effect is not very problematical for model 3. The position of the seam weld line stays mainly inside of the upper belt away from the surface. But it exits at the upper surface of the belt and stays nearly diagonal in it. In this case the risk of pushing the reinforcement to the upper surface or even through exists.

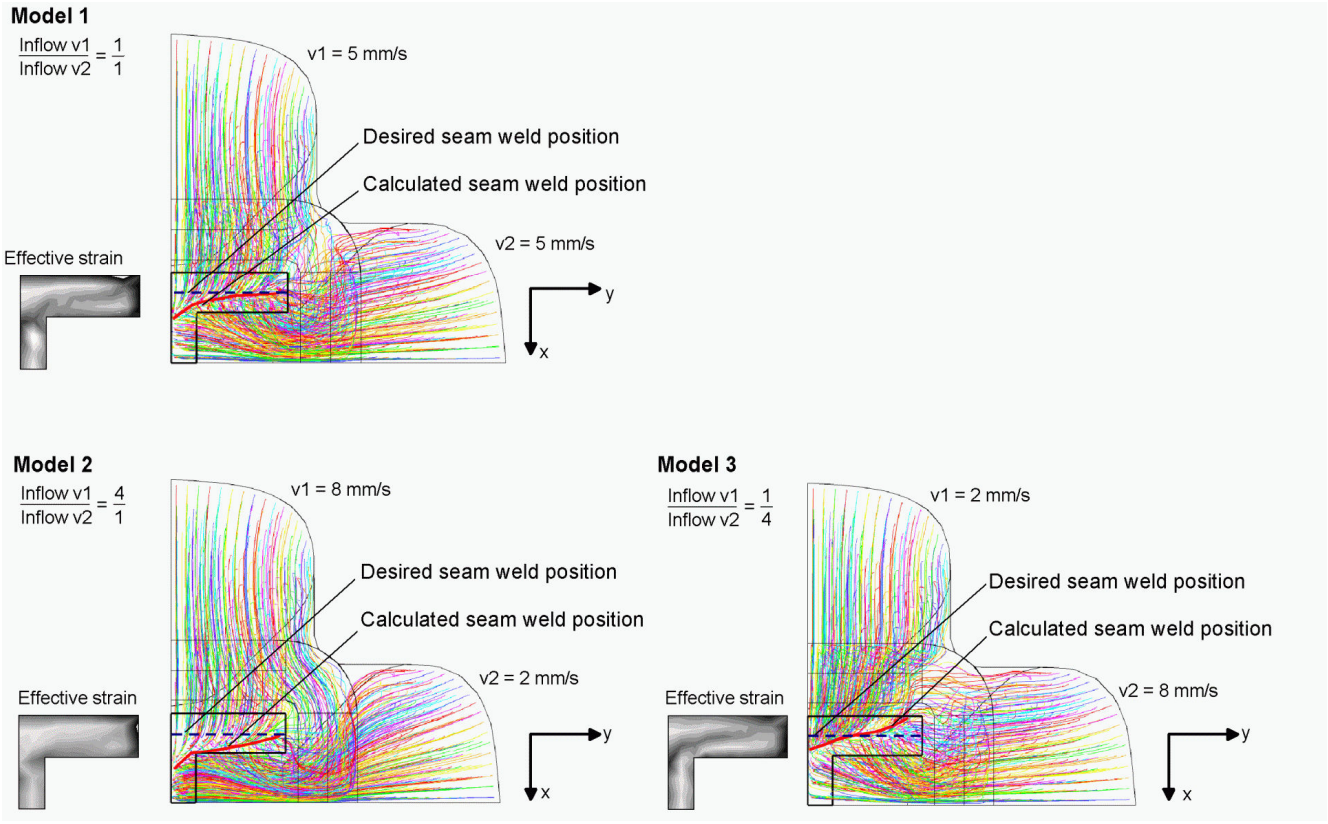

Figure 7: Prediction of seam weld position for different inflow velocities for the reduced model.

Concluding, the study showed that a manipulation of the material flow velocities in the channel region for this kind of tool geometry will not lead to an improvement in the material flow and seam weld position. The manipulation of the material flow in the channels will mainly result in a translative and partly rotative movement. But an adjustment of the seam weld curvature is not possible this way. In order to optimize the seam weld position, a complete new tool has to be set up based on a different die design concept: to avoid a v-shaped curvature of the seam weld geometry in the upper and lower belts, the new channel design should include a two-stage forming process. The first stage would be forming of the three profile sections based on a material flow through tree channels: half upper and half lower belt and the middle section of the profile. In the second stage the different material streams have to flow in the welding chamber. There, the reinforcement will first be introduced in between the three streams and, second, the independent flows have to undergo the welding process by compressive forming. This procedure offers the potential of an increasing

geometrical accuracy than usage of the four channel tool. Problems like reinforcement elements pushed to the profile's surface will not occur. A further improvement can be seen in the reduction of stress on the reinforcement. Due to the later introduction - when the main forming process is finished - the press ratio for the composite will be reduced. This results in a reduced hydrostatic pressure on the reinforcement and in a reduced velocity difference and in a reduced introduction of longitudinal stresses. Reduction of both components will lead to a decrease in failure by cracking of the reinforcement, as it was determined in experimental investigations.

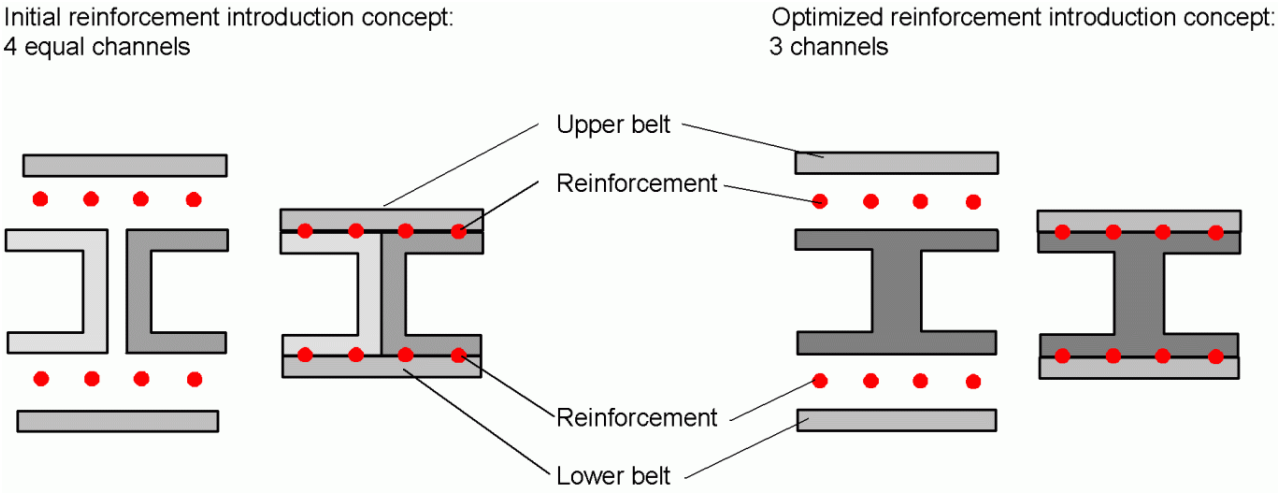

Figure 8: Initial and improved channel arrangement for seam weld position optimization.

Summary

The paper deals with the analysis of the seam weld positions regarding the inserting of reinforcement elements into the material flow for extrusion of composite profiles. For the numerical analysis of the material flow and the prediction of the seam weld position the commercial FE code HyperXtrude was used. A room-fixed FE mesh was set up for the analysis of the extrusion of a double-T profile. Regarding the positioning of the reinforcement elements in between two materials strands, the die geometry had four bridges and four channels.

1. It was possible to show that the process of composite extrusion is feasible by simulation with Eulerian formulation FE codes. The occurring stress components showed the expected qualitative and quantitative results for the reinforcement elements (orthogonal pressure, longitudinal tension) and for the base material, too.
2. The simulation of the complete model showed acceptable accordance regarding the weld line prediction with the experimental analysis. Two methods for weld line determination have been tested: the analysis of particle traces and analysis of effective strain distribution. Both show a sufficient agreement with each other as well as with the experimental results. Due to visual post processing for the seam weld position the results only have a qualitative character and the method of seam weld position determination has to be improved.
3. The influences of different inflow speeds on velocity, pressure and seam weld position have been studied for a quasi-static simulation. It could be shown that the chosen die geometry using four channels is not suitable to produce an acceptable seam weld geometry and position. For optimal positioning the complete tool geometry has to be changed. For a new design of the die a geometry with three channels will be suggested. This die should comprise two stage of extrusion: the first stage that includes the major press ration and forming of the section geometries and the second stage that deals with the introduction of the reinforcement and welding of the three strands to a composite profile.

Acknowledgement

This paper is based on investigations within scope of the Transregional Collaborative Research Center/ TR10 and is kindly supported by the German Research Foundation (DFG).

References

[1] H. Valberg: Metal flow in the direct axisymmetric extrusion of aluminium. Journal of Materials Processing Technology, Vol. 31 (1992), pp. 39-55

[2] I. Flitta, T. Sheppard: Material flow and prediction of extrusion pressure when extruding through bridge dies using FEM. Proc. of the 7th Int. Aluminium Extrusion Technology Seminar, Chicago, USA (2000), pp. 141-147

[3] L. Donati, L. Tomesani: Evaluation of a new FEM criterion for seam welds quality prediction in aluminium extruded profiles. Proc. of the 8th Int. Aluminium Extrusion Technology Seminar, Orlando, USA (2004), pp. 221-235

[4] J. Gasiorczyk, J. Richert: Application of FEM modelling to simulate metal flow through porthole dies. Proc. of the 7th Int. Aluminium Extrusion Technology Seminar, Chicago, USA (2000), pp. 195-202

[5] M. P. Reddy, H. E. Bertoni, W. Bob: HyperXtrude/Process – Extrusion process optimization software. Proc. of the 7th Int. Aluminium Extrusion Technology Seminar, Chicago, USA (2000), pp. 231-235

[6] I. Flitta, T. Sheppard: Nature of friction in extrusion process and its effect on material flow, Material Science and Technology, Vol. 19 (2003), pp. 837-846

[7] M. Schikorra, M. Schomäcker, M. Kleiner, A. Klaus: Numerical analysis of continuously reinforced extrusion processes, Annals of WGP, Vol. XI/2 (2004), pp. 143-146

[8] M. Kleiner, M. Schomäcker, M. Schikorra, A. Klaus: Manufacture of continuously reinforced profiles using standard 6060 billets, Proc. of the 8th Int. Aluminum Extrusion Technology Seminar, Orlando, USA (2004), pp. 461-469

[9] J. Theler, A. Wagner, A. Ames: Herstellung von Aluminium/Stahl-Verbundstromschienen mit metallurgischer Bindung zwischen Aluminium und Stahl durch Verbundstrangpressen. Metall, Vol. 30 (1976), pp. 223-227

[10] T. Sheppard, A. Jackson: Constitutive equation for use in prediction of flow stress during extrusion of aluminium alloys. Materials Science and Technology, Vol. 13 (2003), pp. 203-209

doi:10.4028/www.scientific.net/AMR.10.111

In-Process Simulation of Multi-Axis Milling in the Production of Lightweight Structures

Eduard Ungemach[1,a], Sven Odendahl[1,b], Marc Stautner[1,c], Jörn Mehnen[1,d]

[1] Department of Machining Technology, University of Dortmund,
Baroper Str. 301, 44227 Dortmund, Germany

[a]ungemach@isf.de, [b]odendahl@isf.de, [c]stautner@isf.de, [d]mehnen@isf.de

Keywords: Milling Simulation, Multi-Axis Milling, Lightweight Structures

Abstract. Lightweight structures are an important element in today's production industry. For the multi-axis milling of these structures some aspects have to be considered to achieve a good surface quality and to prevent damaging the milling machine during the machining process. In this article methods to determine suitable feed rates for the milling process, to identify parts of the workpiece with too much heat build-up, and to avoid collisions between workpiece and machine parts are presented. For this purpose a milling simulation based on a multi-dexel field workpiece model has been developed, in which two types of feed rate adaptation have been integrated. Work on a built-in temperature development simulation and collision control is in progress.

Introduction

Production of Lightweight Structures. There is an increasing demand for lightweight structures. The range of application includes the automobile production as well as production of airplanes and satellites. Rising energy costs and the desire for more comfort and better equipment lead to the need for lowering weight of vehicle parts. The main goal of development of lightweight structures is to increase the stability of the construction while at the same time maintaining a low weight. But there are several other reasons for the use of lightweight structures, which include reducing the environmental burden and saving production costs by using less material. Therefore, lightweight construction has economical and ecological advantages.

There are several common types of lightweight construction: differential construction methods, integral construction methods, integrating construction methods, composite construction methods, light hulls, and light frameworks. We aim at the flexible construction of lightweight frame structures, which can be bent unrestrictedly in space. Lightweight frames offer a high flexibility as it is often possible to produce different products from a set of similar basic parts, what allows to react faster on demands of the market. Additionally, it is possible to produce low quantities and thus filling niche markets [1].

Five-Axis Milling. Simultaneous five-axis milling offers two main advantages, which lead to various other positive aspects compared to three-axis milling. The first advantage is the possibility to reach the workpiece from various directions. This allows to avoid many otherwise required changes of the workpiece clamping, so that the number of steps in the process chain can often be reduced. The other main advantage is the prospect to use different tools. On the one hand, shorter tools become applicable. These are usually much stiffer and show less tendency of deflection. On the other hand, tools with different geometrical shapes can be used, for example a toroidal cutter instead of a ball cutter, what can imply a better surface quality due to less roughness. These two main advantages entail other positive side effects. The smaller number of reclampings allows to reduce time and labor costs as a lower amount of human intervention is necessary.

The use of shorter and stiffer tools also has various positive side effects: the process stability rises because of an increased service life of the tool and a reduced danger of tool fracture. The feed rate can be generally increased while maintaining a high surface quality, so that the cost

effectiveness grows. Another important aspect when using short tools is the higher geometrical accuracy, which reduces the need for time consuming and thus expensive manual finishing [2].

The described advantages have to compensate for some drawbacks. Five-axis machining centers demand higher investment costs, and additional costs emerge from the necessity to buy new, five-axis-capable CAM software and to train personnel on it. When generating NC paths, most CAM systems usually do not take the current shape of the workpiece into account. To avoid collisions between the workpiece and parts of the milling machine, they tend to generate quite conservative tool paths. Thus, they are often unable to make use of the five-axis advantages to the full extent and can still not assure a collision-free process. To avoid these problems while retaining as much advantages as possible, simulation of the milling operation represents a good solution.

Simulation of Five-Axis Milling. The main idea of simulating the milling process is to imitate the behavior of the real process with all relevant input values as accurately as possible to be able to transfer conclusions from the simulation to the real-world process. It should allow to identify all relevant problems of the actual process in advance of the real production. Therefore, it provides the possibility to save time and material costs without any risk of damaging the machining center or tools by collisions. An additional benefit is the ability to optimize the parameters of the process to gain higher product qualities at lower production costs. The production of lightweight structures is especially challenging for the five-axis milling process. To avoid a bending of the workpiece, special chucks are necessary. Thus, the probability of collisions is even higher than during the production of other types of structures, like more massive dies or moulds. The collision detection can be accomplished by using the simulation as a regular in-process tool to verify and optimize NC paths generated by CAM systems.

An in-process simulation has to fulfill various needs. In order to provide a maximum of flexibility, the duration of a simulation run should be short. If a run took much longer than the real process, the path could be tested for collisions by simply milling replacement materials like ureol. Additionally, the results of the simulation must be reliable as it replaces other types of verification and will be the only step that prevents damage of the semi-finished product, the tools, and the milling machine.

There are several requirements for the model of the workpiece in five-axis milling. In contrast to three-axis milling, where high precision is needed only for one direction, it is important to offer a high accuracy in all three directions. Undercuts cannot be machined in a regular three-axis milling process. However, for five-axis milling such assumptions cannot be made. For this reason, there is a special need for the support of undercuts in the simulation without a significant impact on the running time in order to ensure an efficient simulation of a generic milling process.

Implemented Data Structures

There are several common data models for workpieces. Most show one or more disadvantages, which prevent their use for the desired purpose. Set operations on mathematically defined basic volumes are easy to implement and offer a very high accuracy, see JERARD [3]. The resulting object is usually stored in form of a binary tree, which defines set operations between the respective basic volume elements like cubes, spheres, and quadrics. But their usage is usually much too slow for long NC paths. Another example is the T-Buffer implementation by VAN HOOK [4], which offers a high calculating speed. But it does not allow collision detection as it works only in the image space by using an extended Z-Buffer and so does not contain further information. For usual three-axis milling a so-called nailboard data model has proven to be sufficient [5]. A nailboard consists of a 2-dimensional field of virtual ‘nails’, which are arranged on a regular grid. The end of each nail represents a point on the surface. The milling itself is simulated by positioning a CSG (Constructive Solid Geometry [6])-modeled cutter at the specified position and clip the nails at the point of

intersection with the cutter. As the length of the nails is stored as floating point value, there is one direction with higher accuracy.

This model can be easily enhanced to offer the capability of representing undercuts. Instead of a single value, a list of height values at every grid vertex gives the option to model gaps in the material. The resulting structure is called a dexel field. To achieve a high accuracy in all directions, the model can be further extended by using three different dexel fields, which are perpendicular to each other, so that the nails are parallel to the three axes of space. Especially steep walls, which are almost parallel to the nails, benefit from the additional two dexel fields with much higher accuracy. In Fig. 1 a schematic illustration of a toroidal sample workpiece is shown.

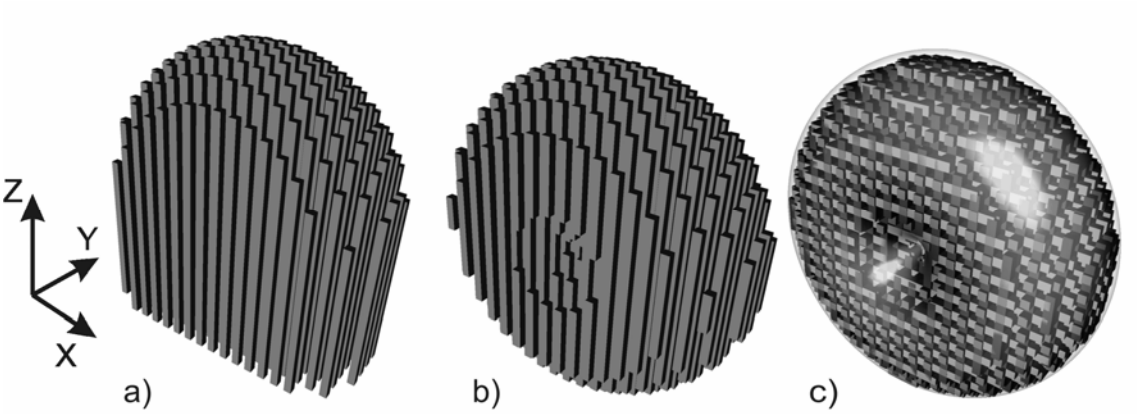

Fig. 1: Schematic illustration of a workpiece consisting of three dexel fields (c) compared to a single dexel field with undercuts (b) and without undercuts (a).

We use the prototype of a milling simulation, which implements a multi-dexel field for the workpiece and a CSG-based model for the definition of the cutter, the shank, and the tool holder [7],[8]. The other parts of the milling machine are modeled by triangle meshes. The simulation of the cutting process, as well as the test for collisions, is performed by calculating intersections between a ray starting on each dexel and the respective CSG primitives. The resulting intersection lists for each ray are combined according to the operators in the CSG tree into one intersection list, which represents the intersections between the workpiece and the combined CSG model. For further enhancement in calculating time the workpiece dexel field is stored in a hierarchical tree. The higher levels of the tree represent lower resolutions, but they are bounding volumes for the elements of the lower levels of the hierarchy. Therefore, if a CSG cutter has no intersection with the workpiece in the higher levels of the tree, there is no need to check the lower levels, which are more exact, but due to the higher number of nails are much slower to test.

Problem Cases

Feed Rate. The feed rate during a cut should be within a restricted range around the value the tool provider suggests for the material of the workpiece to achieve a good surface quality. Otherwise there could be more and/or deeper micro-cracks in the manufactured profile, which can lead to macro-cracks under load and finally to breakage of the whole structure. Additionally, a high deviation from the suggested feed rate could lead to heavy tool wear. However, in order to reduce the maximum force on the cutting edge during the milling process, to prevent tool breakage, and to decrease the material removal rate, which is another factor in relation to the surface quality because of the necessary chip disposal, the feed rate should be reduced at points of high tool load and high volume of the cut, respectively. On the other hand, the idle speed should be as high as possible to reduce the duration of the process and thus to increase the cost efficiency. Furthermore, at the points in between, the acceleration of the tool should be minimized in order to reduce the

probability of oscillations within the machine. Though in modern CAM systems it is possible to enter feed rate values and, thus, to integrate them in the NC-file, there is no adaptation with respect to forces on the cutting edge or acceleration of the tool. All feed rate changes have to be entered manually by the user based on experience.

Temperature. Lightweight structures are often manufactured from aluminum alloys or other materials with relatively low melting points (about 600° Celsius). Therefore, when the temperature increases during the milling process, the material becomes too soft. Normally, when the cutter enters the material, a chip is more or less cleanly separated from the workpiece. When the temperature increases, at first the cutting process is facilitated, but later the material starts to adhere to the cutting edge. With a further increase in temperature the material becomes smeary and a clean cut is no longer possible. This occurs especially at thin parts of the workpiece, where the heat energy accumulates because the heat transmission between the material and the ambient air is much lower than the heat flow within the material, or in cavities, in which the cutter is repeatedly moved over the same area. To avoid this effect, such tool paths have to be identified in advance to find out whether the milling strategy has to be changed or new paths have to be generated that prevent such an increase in temperature.

Kinematics deals with the mathematical description of the motion of points or geometrical objects in space without considering the forces that cause the motion. Therefore, it belongs to the branch of mechanics. In this article the focus is on the kinematics of milling machines. Milling machines can be divided into two main groups on the basis of their design: serial kinematic machines and parallel kinematic machines. Serial kinematic machines consist of actuators that are built like a chain. The position of an actuator depends on the state of the previous ones. Parallel kinematic machines consist of actuators that act directly on the tool holder or the workpiece holder. Especially during five-axis milling, the position of struts and other parts can be quite complex and often can not be easily derived from the position of the tool. For this reason it is very difficult to place clamps at a position where no collision can occur. As CAM systems in general do not have exact information on the milling machine layout, there is a risk that the generated NC paths lead to collisions between machine parts, workpiece, or clamps.

There is another difficulty that influences surface quality. Depending on the type of milling machine, rotations of the tool may lead to big rotations or movements of heavy machine parts, for example the spindle holder, although the tool center point does not move fast. Abrupt acceleration of such parts could result in oscillations and, therefore, in a lower surface quality.

Feed Rate Adaptation

There are several possible approaches to the problem of determining the most suitable feed rate at each point of the tool path. The adaptive control method, for example, uses a sensor technology to decrease or to increase the feed rate during the process depending on the measured force and/or volume of the cut. However, this means that the optimal feed rate is not determined until after each cut. In the following two approaches are presented, which adapt the feed rate prior to the machining process. Both are based on the engagement conditions determined by the simulation. The first one is an analytic approach, in which the optimal feed rate at each point is calculated relating to reduced cutting forces and decreased material removal rates. In this case a drawback of the dexel field model arises. Due to the raster of the workpiece, there are fluctuations in the calculated feed rate, which have to be counterbalanced. The second solution uses an artificial neural network to assess the conditions and to derive a suitable feed rate.

Analytic Approach. In this approach the feed rate is calculated from the engagement conditions so that the material removal rate and the force on the cutting edge remain within certain boundaries while at the same time keeping the feed rate in the optimal range given by the tool provider. For this

purpose not only the volume of the cut is taken into account, but also the geometry of the chip and differences between up and down milling and drill and draw cut (Fig. 2).

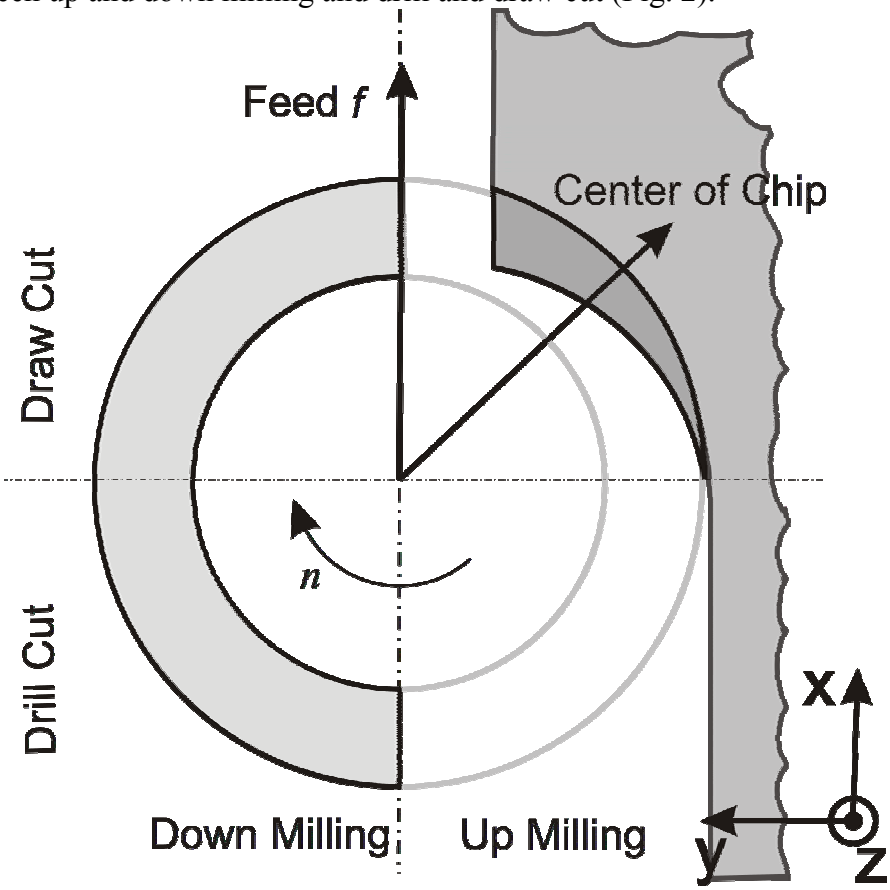

Fig. 2: Determination of the engagement conditions during the cut by the position of the current chip volume.

During feed motion, the feed rate is set to the maximum value possible for the used machine. However, in order to compensate for the model-induced fluctuations and to generally keep the acceleration of the tool to a minimum, the feed rate progression has to be smoothed. Therefore, the feed rate progression is converted from the time domain to the frequency domain by Fast Fourier Transform (FFT) [9]. Then the high frequencies are filtered out using a low-pass filter with a modified Blackman window function

$$\omega(f)=\begin{cases}1 & f<m\\ 0.42+0.5\cdot\cos[\pi\cdot(f-m)/(n-m)]+0.08\cdot\cos[2\pi\cdot(f-m)/(n-m)] & m\le f\le n,\\ 0 & n<f\end{cases} \qquad (1)$$

where m and n are variable parameters to position the window in the frequency spectrum and f is the frequency. In this way the transition between filtered and not filtered frequencies is softened, thus preventing ripples in the output. The window function is applied as a factor to the frequency values. Finally, the data is converted back to the time domain by Inverse Fast Fourier Transform (IFFT). A disadvantage of this method is that the feed rate adaptation cannot be performed until the simulation of the examined part of the tool path has been completed. The FFT and IFFT can both be efficiently calculated in O(n log n) time, where n is the number of considered feed rate values. The filtered and directly calculated feed rate progressions are shown in Fig. 3. For the purpose of comparison the moving average is displayed as well. As can be seen, the graph of the low-pass

filtered feed rate follows the calculated progression much better than the moving average graph, which is calculated from the previous ten values, without causing too high acceleration.

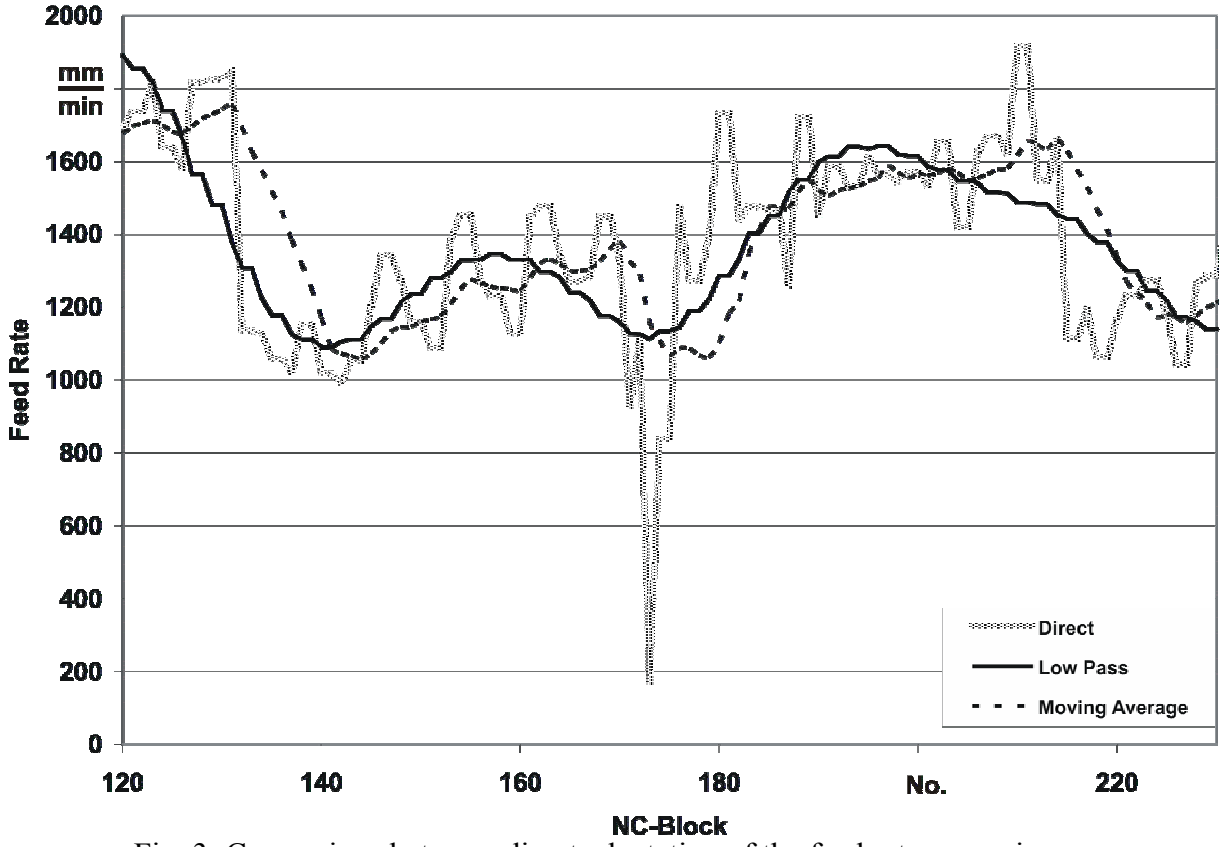

Fig. 3: Comparison between direct adaptation of the feed rate, a moving average approach, and a low pass filtered solution.

Neural Net Approach. This approach uses the same engagement condition data as the analytic solution. However, the feed rate is not directly calculated from this data, but the data is passed to a neural net. This neural net consists of a layer of input neurons, a layer of output neurons, and one or more intermediate layers (Fig. 4). It is a feed-forward net, which means that the value of a neuron depends only on the values of neurons from the previous layer and its own activation. The activation function applies a weight factor to each of the input values and takes the sum as activation value. To obtain the output of the neuron from this activation value, a sigmoid function is used. In this way, the whole net is evaluated from the input neurons up to the output neurons.

During the supervised learning process there is a feedback, whereby the activation function of the neurons is adjusted to compensate for deviations from the value, which is to be learned (backpropagation learning). In a forward pass the error is determined and in a backward pass the weights are modified accordingly. The set of learning data has to be chosen carefully so that all possible situations are recognized after the learning phase. Therefore, NC paths that have been proven to be particularly suitable relating to the feed rate for similar workpiece shapes are used to train the neural net. The more engagement condition data of one cut and the more cuts are to be input into the neural net for determining one feed rate output, the longer it takes to train the net and the more training data has to be provided.

Discussion. As a consequence, the two techniques for determining the adapted feed rate are useful for different purposes. The higher effort in the learning phase of the neural net suggests a usage in mostly constant milling situations like circular drilling. In other milling processes, where the engagement conditions frequently change, the filtering technique has some benefits due to the lower user effort required to get the resulting feed rates.

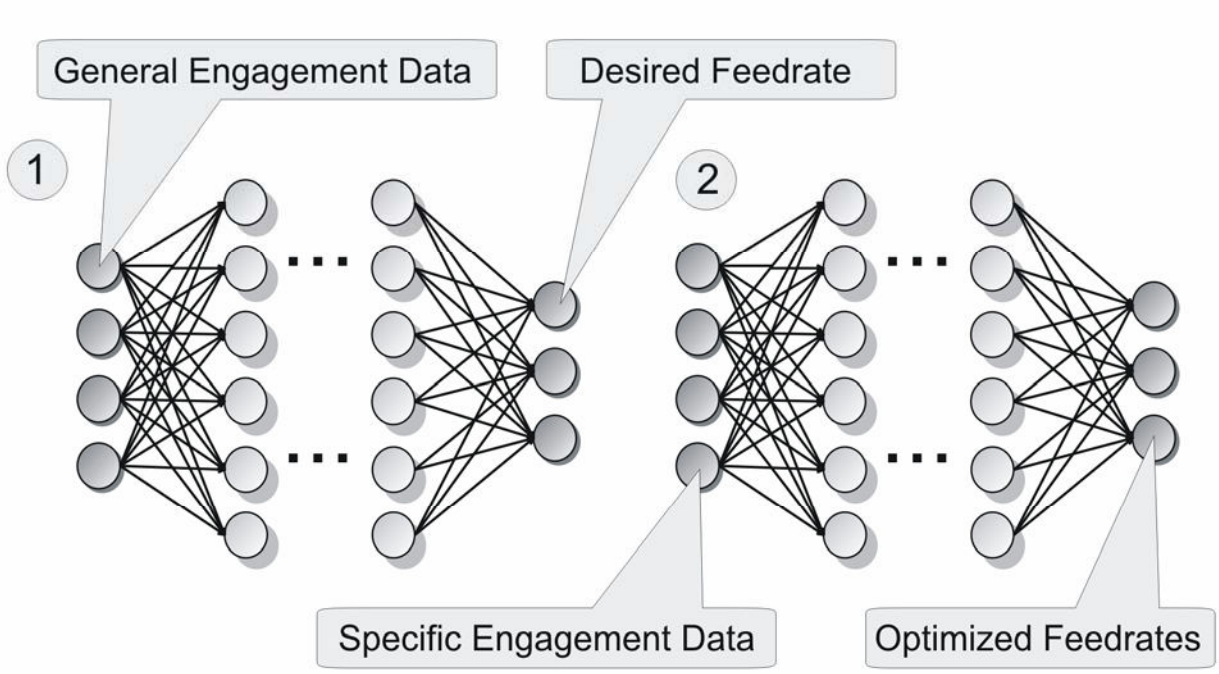

Fig. 4: Schematic of the neural net used for the feed rate adaptation

Temperature

In order to detect and to avoid situations in which areas of the workpiece surface become too hot and, consequently, too soft, a heat simulation is required that can be integrated into the milling simulation. It should be close to real-time so that the effect of changes in the milling strategy can be quickly determined. Therefore, an implementation employing the commonly used Finite Element Method (FEM) [10] is not practical. Finite Element Analysis (FEA) uses an element breakdown that, as solution for the partial differential equation, results in a system of linear equations, which gets more complex with each additional element. An implementation using a Finite Difference Method (FDM) [10], on the other hand, would be much more efficient. The proposed method is the FTCS-scheme (Forward in Time, Centered in Space). It uses a simple cube discretization technique, which can also be used in FEA, but the new heat distribution at a subsequent time step can be explicitly calculated from the previous values. In the one-dimensional case the scheme results in

$$T_x^{t+1} = \frac{\lambda}{c \cdot \rho} \cdot \frac{T_{x-1}^t - 2T_x^t + T_{x+1}^t}{\Delta x^2} \cdot \Delta t + T_x^t \tag{2}$$

where $T^t{}_x$ is the temperature at the grid point x during time step t, Δt is the duration of a time step, Δx is the grid width, and λ, c, and ρ are the material properties thermal conductivity, heat capacity, and density respectively. It is not as precise as a BTCS-scheme (Backward in Time, Centered in Space) or a FEM, but with sufficiently small time steps and elements

$$\Delta t \leq \frac{c \cdot \rho}{2 \cdot \lambda} \cdot \Delta x^2 \tag{3}$$

it is stable nevertheless.

To make the future implementation as efficient as possible, the discretization for the heat analysis should be aligned to the dexel field. This could be done by a fixed, three-dimensional grid

with each grid cube encompassing a specified number of dexel segments of each of the three dexel fields. Then it would be possible to efficiently update the grid whenever pieces are cut from the workpiece. In addition, a model is needed, which estimates the heat energy that is induced into the workpiece during a cut. The generated energy depends, for instance, on the cutting force and the chipping thickness. However, a fraction of this energy remains inside the tool and the chip, so that the energy fraction in the chip gets larger with increased cutting speed.

Kinematics

The two previously described problems can be counteracted via simulations of the milling process.

Collision Detection. To detect situations of potential collisions, the following two-step approach is a practical solution. In the first step, the positions of each part of the milling machine must be computed for certain points in time. If the time steps in-between are chosen to be small enough, the approximation for the resulting motion is sufficiently precise. In the second step, the various parts have to be checked against each other for possible collisions at each time step. The described scheme was chosen in an implementation of the kinematical simulation of the Mikromat 6X Hexa milling machine, using the free Library VCollide [11].

For the first step the position and orientation of all machine parts have to be calculated from the position of the tool center point. The solution to this problem is known as inverse kinematic transformation. As it is generally not unique, it is necessary to adjust the simulation to the actual controller of the milling machine. The software needs a description of the parts of the milling machine and a description of how the individual parts are joined. In the simulation, the surfaces of the parts are represented by sets of triangles. To reduce the number of collision tests, it can be specified which parts could collide; the other parts are not tested at all. To further enhance computing times, the triangles, which are tested against each other, are assigned to a hierarchy of bounding boxes. Triangles, which are located in different bounding boxes that do not overlap, cannot intersect and are therefore not tested.

Motion Harmonization. To prevent oscillation induced by sudden acceleration of machine parts, a software module has been implemented. When using ball cutters, the result of the milling operation is independent of the angle of the tool as long as only the radial part of the cutting edge is in engagement. This fact is used to circumvent one cause for oscillations. Furthermore, the developed software needs to be adapted to the respective machine layout. The input data required is a description of the moving parts including the limits for the motion and acceleration capability of the rotational axes. If a swivel motion is accelerated beyond a certain limit, the software adjusts this motion so that it starts earlier but with lower acceleration. The result is a much smoother overall movement of the milling machine. Another positive side effect is the possibility to increase the average feed rate, which might have been limited by the motion of the slowest axis.

Conclusions and Outlook

In this article an in-progress milling simulation has been presented, which addresses several problems that occur during the machining process. It includes two different methods for adjusting the feed rate in regard to process forces and acceleration. The neural net approach is particularly suitable when milling with only moderately changing engagement conditions. In this case, the learning phase of the neural net takes a reasonable amount of time, but the method provides good results nevertheless. In other cases, the analytic approach with a low-pass filter is more practical. It compensates model-induced fluctuations as well as variations that are caused by changing engagement conditions while still retaining the general calculated feed rate progression. The software modules, which were built to counteract the problems associated with the movement of the milling machines, provide suitable solutions: Collisions can be detected reliably and, therefore, the operational dependability of the whole process chain increases. The motion harmonization ensures

smooth machine and tool movements and also raises the performance of the process. In general, the surface quality of the machined part improves due to the applied procedures without a negative effect on the milling time.

However, there is still some work to be done to optimize the methods, which are described in this article. The two feed rate adaptation techniques already provide some good results, but some testing remains to be done to find the ideal position of the Blackman window in the frequency spectrum and to determine the optimal size and learning data for the neural net. The temperature simulation is not implemented yet, but the approach seems promising. The data model and mathematical details have already been developed except for the heat insertion model. However, this will be an important point for the simulation, which has to be worked on. After this part of the simulation has been implemented, it needs to be tested and calibrated with data gathered from FEM simulations and experiments. The test for collisions already works for the implemented milling machine. As the software structure has been designed to work with a general machine description, other milling machine types should be defined and tested for compliance with the controller of the machine. Additionally, further performance enhancements could be developed, and support for other data formats should be integrated to increase the usability of the simulation.

Acknowledgement

This paper is based on investigations of the collaborative research centre SFB/TR10 which is kindly supported by the German Research Foundation (DFG).

References

[1] *Kleiner, M.; Klaus, A.*: Forschung für die flexible Produktion leichter Rahmenstrukturen Aluminium, International Journal for Industry, Research and Application, Volume 80 12 / December 2004, pp. 1364-1366

[2] *Klocke, F.; Altmüller, S.*: Five-Axis Milling: Geometrical and Technological Benefits for High Efficiency Processes. Product Engineering – Research and Development in Germany, Annals of the WGP (Wissenschaftliche Gesellschaft für Produktionstechnik) Vol. V/1, pp. 1-5, Hanser-Verlag, München, 1998

[3] *Jerard, R.B.; Hussaini, S.Z.; Drysdale, R.L.; Schaudt, B.:* Approximate methods for simulation and verification of numerically controlled machining programs. The Visual Computer (1989) 5,6, pp. 329–348

[4] *v. Hook, T.:* Real-time shaded NC milling display. Proceedings ACM SIGGRAPH Conference (1986),Vol. 20, No. 4, pp. 15-20

[5] *Weinert, K.; Müller, H.; Friedhoff, J.:* Efficient discrete simulation of 3-axis milling. Product Engineering – Research and Development in Germany, Annals of the WGP (Wissenschaftliche Gesellschaft für Produktionstechnik) Vol. III/2, pp. 83-88, Hanser-Verlag, München, 1996

[6] *Foley, J. D.; Van Dam, A; Feiner, S.K.; Hughes, J. F.:* Computer Graphics, Principles and Practice. Addison-Wesley Professional, 1995

[7] *Weinert, K.; Guntermann, G.; Stautner, M.:* Effiziente Simulation der 5-Achsen-Simultan-Fräsbearbeitung. In: Begleitband zum 3D-Erfahrungsforum, WB Werkstatt und Betrieb, Darmstadt 2001, pp. 197-205

[8] *Müller, H.; Surmann, T; Stautner, M; Albersmann, F.; Weinert, K.:* Online Sculpting and Visualization of Multi-Dexel Volumes. In: Elber, G.; Shapiro, V. (publisher): SM'03, Eighth

ACM Symposium on Solid Modeling and Applications, Seattle, Washington, USA, ACM Press, NY, USA, 2003, pp. 258-261

[9] *Bluestein, L. I.*: A linear filtering approach to the computation of the discrete Fourier transform. Northeast Electronics Research and Engineering Meeting Record 10 ,1968 , pp. 218-219

[10] *Lewis, R.W.; Nithiarasu, P.; Seetharamu, K.:* Fundamentals of the Finite Element Method for Heat and Fluid Flow, J. Wiley & Sons, New York, 2004

[11] *Gottschalk, S., Lin, M.; Manocha, D.:* OBB-Tree: A Hierarchical Structure for Rapid Interference Detection. Proc. ACM Siggraph '96, 1996, pp. 171-180.

doi:10.4028/www.scientific.net/AMR.10.121

Analysis of cutting technologies for lightweight frame components

K. Weinert[a], S. Grünert[b], M. Kersting[c]

[1]Department of Machining Technology, University of Dortmund,
Baroper Str. 301, 44227 Dortmund, Germany

[a]weinert@isf.de, [b]gruenert@isf.de, [c]kersting@isf.de

Keywords: Computer Aided Engineering, Finite Element Analysis, Drilling, Circular Milling

Abstract. Most technical components applied in industrial practice are subjected to metal cutting operations during their production process. However, this leads to undesirable thermal and mechanical loads affecting the machined workpiece, which can result in an impairment of its serviceability. Due to their small wall thickness lightweight hollow profiles are highly susceptible to the inevitable machining loads and thermal stresses during drilling processes. For the virtual optimization of the machining process and in order to ensure a suitable process strategy, a finite element simulation of cutting operations for thin-walled light metal profiles is conducted. Due to the flexibility within creating drill holes of different diameters without tool changes circular milling represents a promising alternative to the application of conventional drilling tools for variable process strategies to handle batch sizes down to one piece efficiently. Hence, this article gives an insight into the investigations regarding the modeling concepts of the mechanical and thermal loads induced into the thin-walled lightweight frame structure during the circular milling process. Furthermore, process reliability aspects as well as the correlation of the calculated and the measured results will be discussed on the basis of experimental investigations. Finally, this article compares Finite Element Analysis aspects of circular milling processes with conventional drilling processes.

Introduction

The cutting process implies undesirable mechanical and thermal loads for the machined workpiece. Due to this load the peripheral zone of the bore hole can be negatively influenced. Because of this, the functionality and the quality of the workpiece might be affected. Moreover, the heat generated by the process can cause a deformation of the workpiece shape during machining, resulting in a permanent form deviation. Thus, the required workpiece quality may not be achieved. The extent of the damage depends on the parameters of the cutting process, the shape, and the material of the workpiece.

Regarding the aspects mentioned above, especially machining processes of thin-walled profiles require adapted procedures compared to full material workpieces. On the one hand, the low stiffness of a thin-walled profile aggravates the deformation caused by a machining process. On the other hand, the small cross-section leads to a minor transportation of the heat generated by the cutting process with the consequence of local heat accumulation. Therefore, the machining of thin-walled workpieces is examined at the Department of Machining Technology, University of Dortmund, within the 'Collaborative Research Center SFB/TR10'. In order to obtain detailed knowledge about the workpiece condition during the machining operation, a process simulation is carried out using the Finite Element Analysis (FEA). With this process simulation the stresses, deformations, temperatures, and their respective gradients in the workpiece can be calculated.

In comparison to conventional drilling using twist drills, the machining of holes by circular milling offers numerous advantages. In contrast to drilling processes in which the bore hole diameter is defined by the tool diameter, the circular milling, and thus the milling along a helix path, offers the possibility of machining different bore hole diameters with the same tool.

To attain detailed process knowledge, experimental studies concerning the circular milling and the conventional drilling process of holes as well as FEA simulations of the thermal and mechanical loads affecting the workpiece during the processes are presented in the following.

Mechanical Simulation of Conventional Drilling Processes

In order to supply feed force and drilling torque as realistic input parameters and strains as validation parameters for the mechanical simulation, according measurements were conducted. During the drilling tests performed on a three-axis machining center the standard twist drill (Ø 8mm, double-angle point 130°) was applied with machining parameters recommended by the manufacturer (v_c = 120 m/min, f = 0.25 mm). All machining loads were recorded with the measurement equipment consisting of a force plate for feed force and drilling torque detection, a signal conditioner to amplify the signals, and a PC for signal analysis. With the aid of thermocouples embedded in the wall of the aluminum profiles close to the bore hole the temperature progression at different distances from the drill hole surface can be investigated. These experimental results can additionally be used for the validation of future thermal simulation models [1].

The main aim of the FEA is to simulate the influence of the machining process on the workpiece. Hence, the appropriate process strategy can be acquired without experimental tests. Therefore, the workpiece behavior needs to be simulated as realistic as possible. The results can be utilized to evaluate and optimize the applied process strategy. It is obvious that complex simulation models with a high level of detail yield the best results. On the other hand, complex models require time consuming simulation runs. Therefore, different modeling concepts were developed and compared in order to find an approach leading to sufficiently accurate results in reasonable computation times. With the purpose of reducing the level of detail and the modeling effort, chip formation is not part of the simulations. This is possible since only the influence of the machining process on the workpiece is of interest and not the cutting process itself. The developed models basically differ in their level of detail in the area of load application and the assumed material behavior, i.e. linear and nonlinear material models. The workpiece, modeled as a square hollow section (40 x 40 x 2 mm), is fixed by constraints of those lines at which the profile is clamped during the experimental machining process. This assumption is reasonable since in the experimental setup the clamps consist of cylinder-shaped bodies fixing the bottom side of the profile and tongs pressing the web against the cylinders at a distance of 25 mm from each face side affecting only the investigated area. All simulation runs were performed with an implemented non-linear material model for aluminum with strain hardening (E = 70 kN/mm², υ = 0.34) [2,3,4].

First modeling concepts have been quite accurate with an exact replica of the cutting edge. These models were used for precise calculations, which have also been performed for the contact conditions of cutting edge and workpiece (**Fig. 1**).

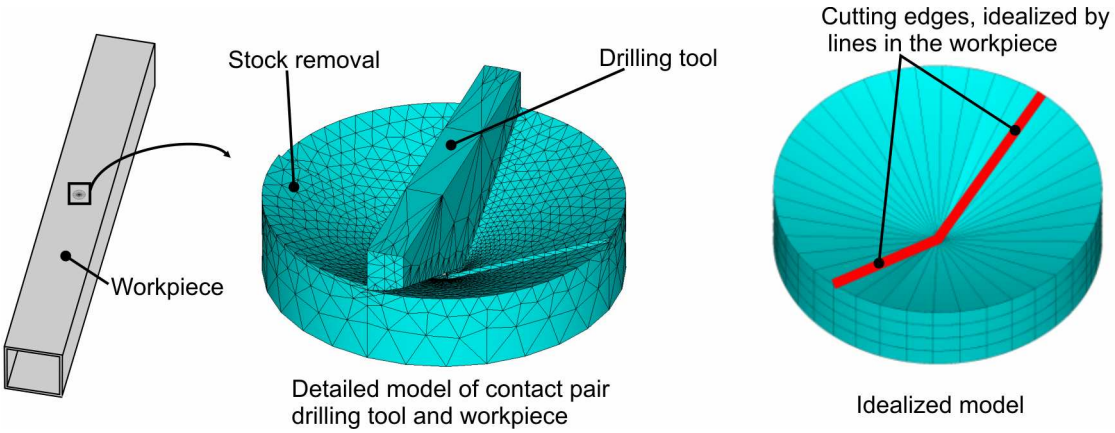

Fig. 1: Detailed and idealized model concept

According to only minimal deviations in the results, the investigations show that no further explicit modeling of the tool or the contact conditions is necessary. Those idealizations lead to a load application on the workpiece via nodes along lines which represent the cutting edges. The nodes on the lines are linked to a rigid body which transmits the feed force and the drilling torque (**Fig. 2**). At different points in time, different layers of the bore hole are machined according to process kinematics. The stock removal is idealized per Element-Death-Option in the FEA software because the model itself can not be modified during the solving process. With this option, the stiffness of selected elements is set to negligible small values, and therefore the elements have no influence on the workpiece [1,5,6].

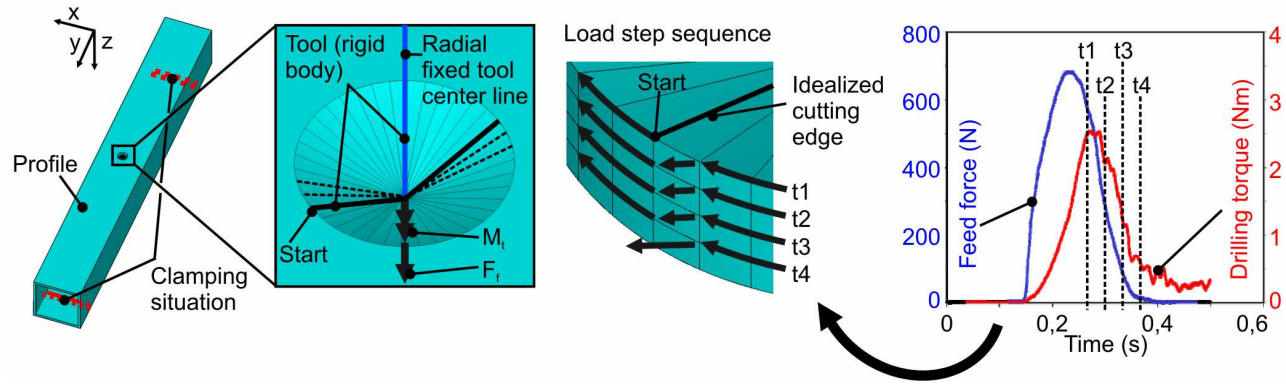

Fig. 2: Modeling concept for the mechanical simulation of the drilling process

Results of Mechanical Simulation and Comparison to Actual Drilling Processes

The analysis of the results of different idealization approaches lead to the conclusion that the level of simplification was suitable. The main focus is on the resulting stresses near the bore hole. It is obvious that the maximum values occur in the regions close to the cutting edge corner of the tool. As expected, the maximum values of the von Mises equivalent stresses when using the plastic material properties as more detailed simulation are significantly lower compared to the linear approaches. Considering the yield strength of 140 N/mm², it is obvious that the approximately semicircular-shaped computed plastic deformation zone has a radius of only a few millimeters (**Fig. 3**). Due to the plastic deformation the total strain in the respective region is comparatively high. As further analyses reveal, the total strain mainly consists of its plastic component. The macroscopic displacements calculated by different approaches are very similar to the results obtained by models, based on a linear material behavior. This could be expected since the plastic deformation only occurs inside and in a small region around the bore hole where the modeling concept provides larger deformations than the linear approaches. However, the distribution of the forces in the rest of the profile must be the same because the clamping situation is the same, which results in the observed similar macroscopic behavior [1].

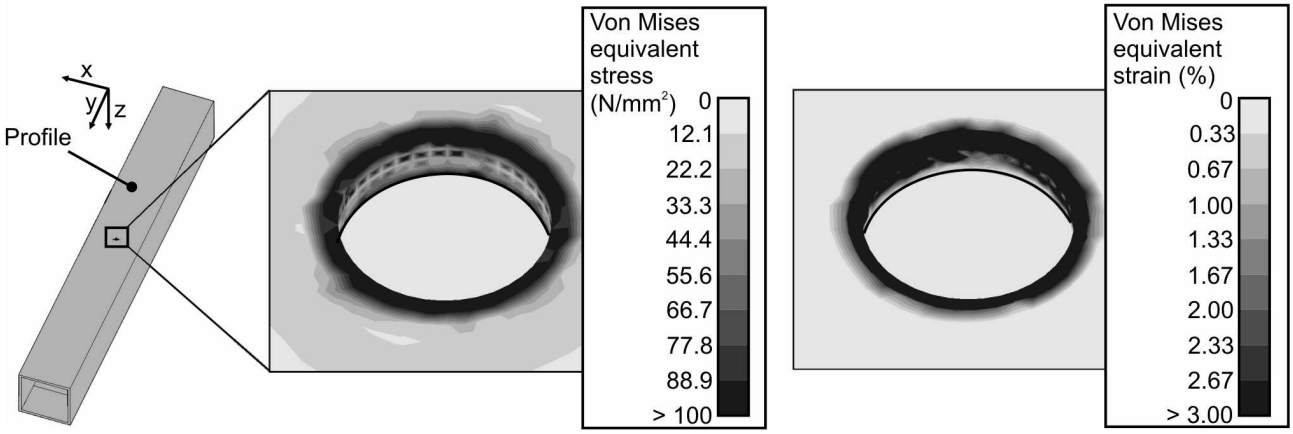

Fig. 3: Calculated von Mises stresses and strains after the conventional drilling process

Mechanical Simulation of Circular Milling Processes

For the determination of the input and validation parameters of the FEA simulation as well as to obtain detailed process knowledge, several experiments were accomplished to determine time series of forces and temperatures. To measure the cutting forces, a measuring setup was installed. With the aid of a dynamometer the three cutting force components F_x, F_y, and F_z could be detected. Hence, a very detailed study about the superposition between cutting, feed, and engagement motion and their resulting process forces was possible.

Because of the complex kinematics (helix-path), the process of circular milling requires extensive modeling. In addition to the rotation at the tool shaft, the milling tool moves into the workpiece along a helix path. The results of the drilling simulation show that the cutting edges of the tool can be idealized as lines in the workpiece [1]. The thin-walled profile, which is to be machined, is modeled as mentioned above. In the middle of the web a bore hole with a diameter of 8.5 mm is placed. In the experiments a single tooth milling cutter with a diameter of d = 5 mm and a rake angle of $\gamma = 13°$ has been used. The clamping situation is the same as in the drilling model. By means of the modeling restrictions on the machined workpiece the application of loads in the profile must be ensured. In the real process the cutting forces are applied by the milling tool along the major and minor cutting edge. During the milling process material is removed. In order to model the different applications of load and the continuous stock removal, the milling volume is divided into several segments to which the loads are applied. Therefore, the measured forces are inserted as cartesian forces on the idealized cutting edges at the appropriate segment. The application of loads is modeled when the minor cutting edge is orthogonal to the wall of the bore hole because at that moment the highest loads in the contact zone occur. The forces in z-direction are applied at the minor cutting edge, the forces in x- and y-direction are applied at the major cutting edge. To represent the movement of the cutting edges through the web, the forces are applied at different lines along the helix path. The minor cutting edge is represented by a line between two segments and its length amounts one half of the tool diameter (**Fig. 4**). The major cutting edge is represented by a line at the edge of a segment orthogonal to the bore hole wall. Furthermore, the contact length of the major cutting edge in the milling process increases during the process. After breaking through the web which is equivalent to 2/3 of the helix path the load situation is changed because only the major cutting edge is in contact. Accordingly, for the following load steps the loads are only applied along the major cutting edge. The material removal from the workpiece is modeled by deleting the elements of the appropriate volumes, as mentioned above [7].

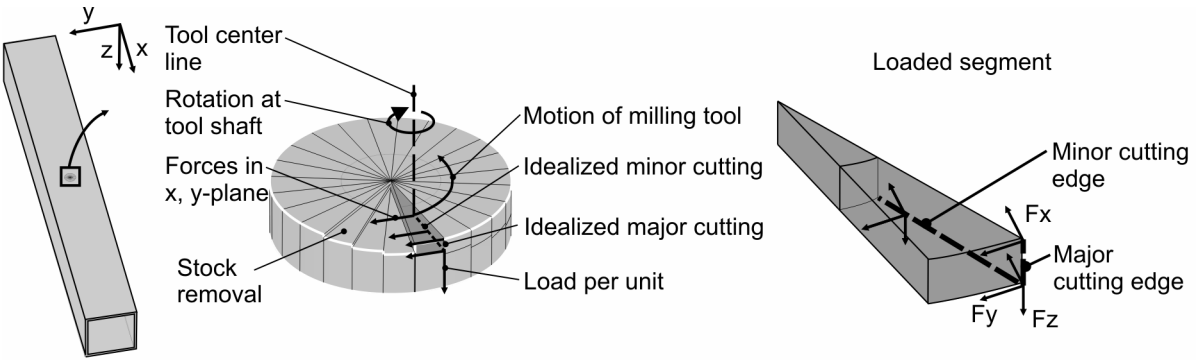

Fig. 4: Modeling concept for the mechanical circular milling process

Results of Mechanical Simulation and Comparison to Actual Circular Milling Processes

The FE analysis shows that at the beginning of the process the loads at the surface of the profile are considerably higher and the loaded area is larger than in the following load steps. The minor impression depth in the workpiece at the beginning of milling and the high forces in z-direction are decisive for this effect. The highest stresses occur until the milling tool breaks through the web. At this moment the force in z-direction disappears. In the following load steps the resulting stresses decrease at the surface and are exclusively limited to the area of the load application (**Fig. 5**). The applied collective of loads results in lower stresses of the surrounding areas. In total, the resulting stresses are, with 120 N/mm^2, lower compared to the yield point with 140 N/mm^2 [4].

In comparison to analyses of drilling processes with twist drills, the mechanical stresses of circular milling are lower regarding the magnitude of stress values and loaded areas [1]. But the lower resulting stresses in the workpiece are not only affected by the lower milling forces. In fact, the different contact conditions lead to lower stresses in comparison to conventional drilling in the workpiece. According to this, the circular milling is a mechanically sparing process compared to the drilling process in order to produce bore holes in thin-walled profiles.

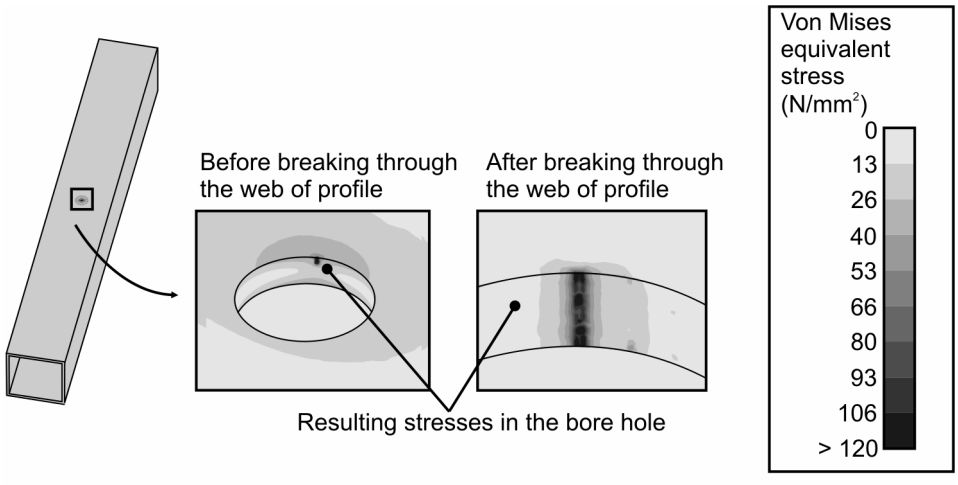

Fig. 5: Calculated von Mises stresses for the circular milling process [7]

Thermal Simulation of Conventional Drilling Operations

In order to simulate the thermal influences of the drilling process concerning the bore hole wall, different approaches have been developed. The first approach was to apply the heat, which is inserted by the machining process, as a heat flux density to the area actually touched by the tool according to the FE simulation approaches of grinding processes [8,9,10]. This approach was only suitable for the first half rotation of the tool. From this moment, the tool steeps into the material and

it is no longer possible to apply heat a flux density. This is due to the procedure of the material removal. All material properties are neutralized, but the volume of the neutralized segment still exists. However, a heat flux can only be applied at surfaces, so the areas under killed elements can not be applied. Therefore, this approach was not suitable for simulating the entire process [11].

Another approach of simulating the thermal influence on the lightweight structure is to idealize the cutting edges as lines of constant temperature (**Fig. 6**). Due to this approach it is possible to generate heat sources in lower levels of the profile wall. In experiments, the cutting edge shows different temperatures because of the different cutting speeds depending on the cutting edge sections. Because of the fact that the main interest of the investigation is the condition of the bore hole wall, the idealization with constant temperature is suitable. Because of the difficulties when measuring temperatures directly at the drilling tool, temperatures during machining aluminum by turning were taken [12]. This comparison is suitable because of the similarity of both processes with a continuous cut.

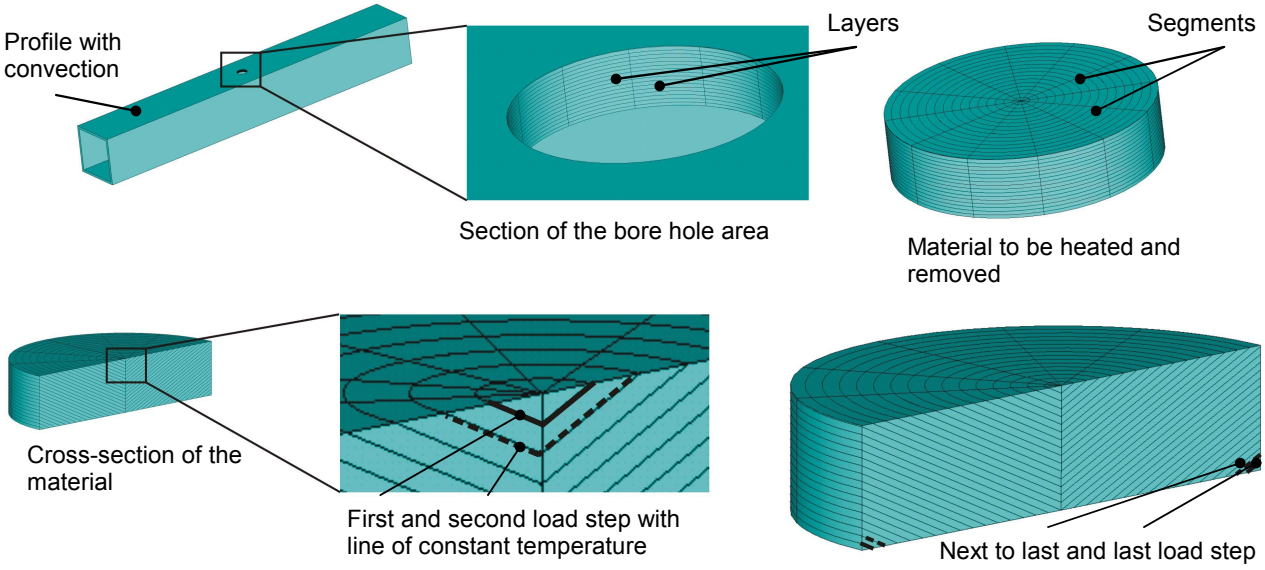

Fig. 6: Modeling concept for the thermal simulation of conventional drilling operations

In order to idealize the two cutting edges of the twist drill, the length of the lines of constant temperature amounts the radius of the bore hole and has a nose angle of 130°. According to the experiments, the heat source is moving through the profile wall in z-direction and rotates. The bore hole area is divided into segments and after a segment is touched by the heat source its properties are neutralized by the Element Death Option to simulate the material removal. After every half rotation the heat source steeps one level down because the complete material in the current layer is touched.

By this selection algorithm the transient manner experiment is applied for the simulation because the number of layers is equivalent to the number of half rotations the tool needs to move through the material. Furthermore, the rotation speed of the heat source in the simulation is equivalent to the revolutions per minute in the experiments [11].

Results of Thermal Drilling Simulation and Comparison to Actual Situation

In the area of the bore hole the material which is removed during the cutting process is modeled as layers in the remaining profile. The layers are arranged in the order they are cut off in the machining process. The shape of the layers is adapted to the tool's drill-point angle. Their thickness is equal to one half of the feed of $f = 0.25$ mm. Hereby, the geometrical dimension of the material that is continuously machined by the cutting edges is explicitly considered. In this modeling concept the thermal load is applied as a constant temperature on the nodes along the lines defining the cutting edge of the drill. Due to the different peripheral velocities along the real tool diameter a constant

temperature along cutting edges is very unlikely to occur. However, the simulation results obtained by this simplified approach close to the bore hole wall are sufficiently accurate. The temperature value chosen for this simulation has been derived from investigations regarding the temperature development during the turning process of aluminum [12]. These investigations delivered a range of cutting edge temperatures from 220°C to 370°C at a cutting speed of v_c = 120 m/min. In case of the modeling concept described in this paper, an average temperature of 350°C has proven to deliver the most accurate results.

Fig. 7 exemplarily shows the simulation results close to the bore hole wall. The displayed point in time is 0.12 s after the first contact of tool and workpiece, which is close to the end of the drilling process.

In this illustration only the remaining profile is displayed and not the rest of the bore hole ground to be machined in the next simulation steps. Animation sequences developed from the respective result files show the movement of the heat through the material. It is obvious that the thermal load induced by the tool only affects a very local region around the bore hole. As expected, the highest temperatures occur at the bore hole wall in the regions where the cutting edge corner contacts the material. However, the temperatures do not increase to critical values so that significant influences on the material strength should not be expected. Nevertheless, the computed heat distribution can be implemented in future mechanical finite element models in order to be able to consider temperature-depending material behavior. Moreover, the stresses induced by the different thermal expansion of the material can be included into the load distribution within the workpiece.

In order to validate the simulation model, the computed results are compared with experimental temperatures at discrete locations inside the workpiece. The thermocouples with a diameter of 0.6 mm were positioned at distances of < 1 mm, 10 mm, and 15 mm from the bore hole wall in the center of the machined web of the profile [1]. Fig. 6 shows two diagrams containing the respective temperature behavior over time. Obviously, the temperature progressions have the same characteristics. The maximum value reached at the thermocouple close to the bore hole wall is about 72°C (T1), which is equivalent to the computed temperature at this location. Slight differences can be observed during the cooling process of the workpiece. This might be due to the fact that the mesh was modeled fairly coarse in the regions farther away from the bore hole ground in order to save computing time. Thus, the interpolation algorithm of the software can only revert to relatively distant integration points. Further investigations revealed that the influence of the convection on the cooling rate of the profile can be neglected. A significant increase in the film coefficient only leads to a slightly steeper decrease of the temperatures inside the workpiece. Therefore, conduction must be considered to be the main heat transportation mechanism.

The high correlation of simulation results and validation parameters shows that the developed modeling concept is a helpful tool to estimate the temperature distribution in the workpiece during the machining process. Further enhancements regarding the mesh refinement and detailed material models delivered from the respective projects within the ‘Transregio 10’ will lead to more accurate results, especially regarding the cooling behavior.

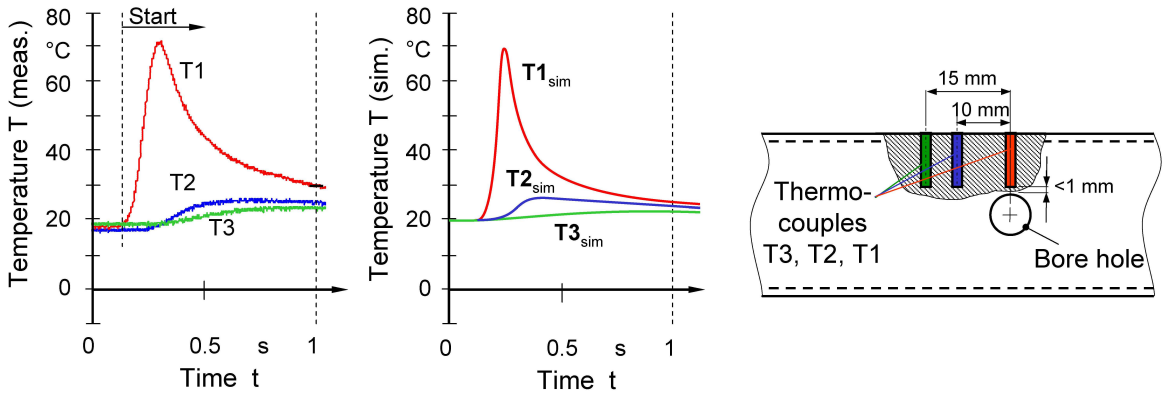

Fig. 7: Comparison of measured and calculated temperatures for the drilling process

Thermal Finite Element Modeling Concepts for Circular Milling Operations

In contrast to the already examined process of drilling with twist drills, not the entire area of the bore hole is loaded simultaneously. This results from the smaller diameter of the used milling tool in comparison to the machined hole. As previous investigations proved, it is a reasonable idealization to model the cutting edge of the tool as line loaded with a constant temperature [11]. The bore hole area is modeled in circle segments. In order to generate an algorithm to map the tool movement through the material, the circle segments have to be divided into an inner and an outer part. The inner circle has a radius of the difference between tool diameter and bore hole radius. The outer ring has the same diameter as the bore hole. The bore hole area was modeled in several layers, whose thickness accords with the number of circle segments (**Fig. 8**). This results from the helix the tool describes during the process. So, the increment in z-direction from each segment to another is defined by the feed of the helix path into z-direction divided by the number of segments. If a circle segment is passed, the tool also moves one layer deeper into the material. The more layers and segments the model consists of, the more detailed conclusions will be accomplished, but due to this the increase in calculating time is so high that a compromise needs to be found. For the investigations a model of 24 segments was chosen.

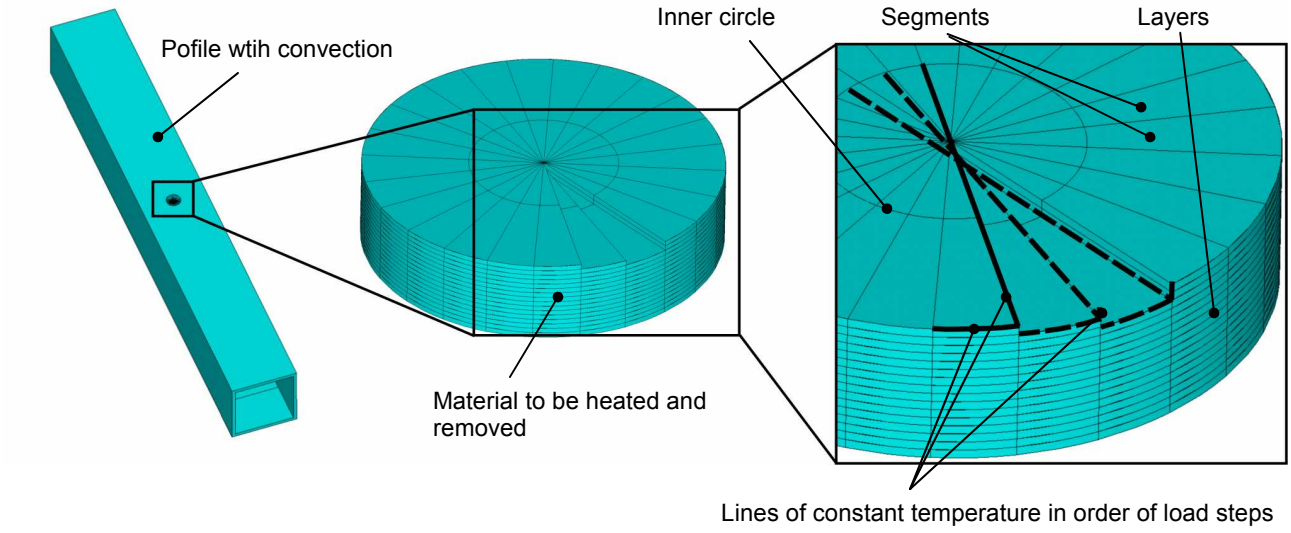

Fig. 8: Modeling concept for the thermal simulation of circular milling

The application of the single tooth milling cutter considers the tool`s minor and major cutting edge. In this case, the minor cutting edge is represented by one basic side of the affected circle segment, as it can be seen in fig. 8. The major cutting edge is twisted as the minor cutting edges of a

twist drill. It has a gradient of 30°. To represent this cutting edge, one of the two horizontal and vertical lines of the circle segment`s outer surface are selected, respectively. This is only an approximation, but it decreases the selection effort significantly. So these three lines are selected to represent the cutting edges and to approximate the process situation as exact as necessary.

The appropriate temperature depends, among other influences, on the cutting speed the material is machined with. A table of cutting edge temperatures while machining aluminum by turning subjected to cutting speed had to be extrapolated [12]. At the cutting speed of 375 m/min, as in the experimental investigations, cutting edge temperatures can be assumed to be 200°C to 400°C.

Results of Thermal Milling Simulation and Comparison to Actual Situation

After different simulation runs with varying temperatures on the idealized cutting edges, the most concordant temperature pattern is generated with a cutting edge temperature of 200°C. The results of the simulation in comparison to the experimental temperatures are shown in **Fig. 9**. It can be seen that the temperature of both the first and also the second peak correspond to the absolute values. Also the intervals at which the peaks occur are very concordant. This is due to the exact modeling of the segment at the process start. Otherwise the intervals would not be concordant or the relation between the first and the second peak would not match because of the length of the lines representing the major cutting edges. If the process starts at another segment, the length of the line is different when it covers the measuring point, and due to this there is more or less energy brought into the model.

On the one hand, there is a deeper temperature decrease between the peaks in the simulation as it is measured in the experiments. There are major values influencing the cooling, e. g. the convection which is set to $\alpha = 3.5$ W/m²K, and therefore equivalent to the convection at unmoved air. The ambient temperature is assumed to be 20°C [5]. This is the lowest possible value an increase will lead to more cooling, so this is not a possibility to increase the temperature between the peaks. On the other hand, there are material properties of heat conduction and heat capacity. These values are set by the machined material AlMgSi0.5. The values given for the material differ only in a small range depending on the references. Further simulations will obtain the variance of results subject to the variation of material properties.

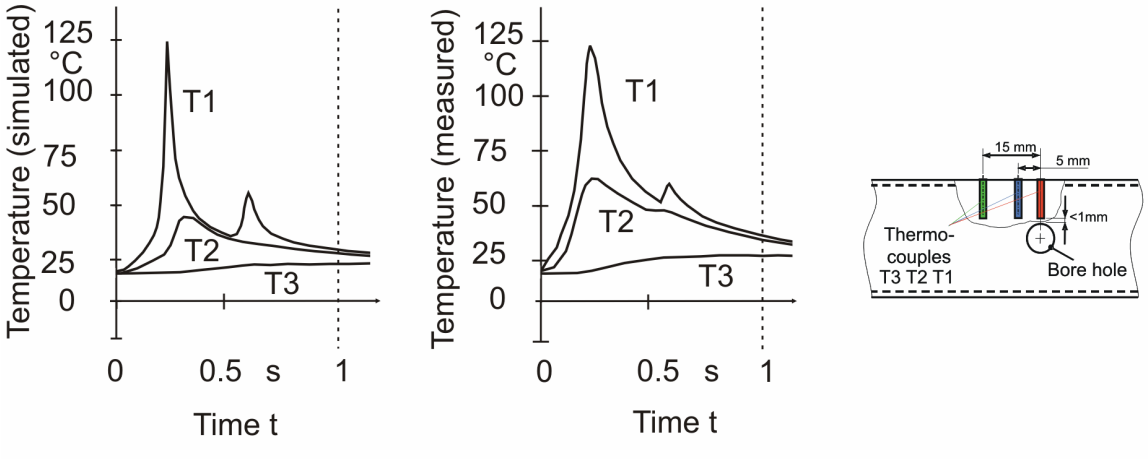

Fig. 9: Comparison of thermal simulation for the circular milling process

Summary and Outlook

For the validation and in order to achieve reasonable input parameters, the deformation of the profile and the occurring machining loads were determined in experimental setups. The results of the developed mechanical FE simulation concepts correspond quite well to the experiments. In addition to the experiments described in this paper further investigations with other tools and

different boundary conditions are scheduled. The basic finite element models described in this paper will then be adapted to these different machining conditions.

In comparison to conventional drilling processes for thin-walled lightweight structures, the circular milling process offers a high level of flexibility and machining quality, but it also requires detailed process knowledge. The complex kinematics of cutting, feed, and engagement movement in this special kind of milling process effect mutual force actions between tool and workpiece. These forces act, contrary to a drilling process, in all directions in space. During experimental investigations the mechanical and thermal complex of loads acting on the workpiece during the circular milling process has been determined. It could be shown that the effecting loads are significantly lower than in drilling processes. On the other hand, the thermal load due to the heat generation is higher.

In order to achieve a deeper understanding of the thermal mechanisms affecting the workpiece, finite element simulation concepts were developed for the computation of the thermal load inside the workpiece during and after the cutting operation. The transient modeling concept described in this paper featuring a reduction of the thermal load to lines of a constant temperature shows a good accordance with experimental validation parameters. The results of the thermal simulation runs can be used as input parameters for a thermo-mechanical finite element model for the drilling process leading to an integrated simulation approach.

Experimental investigations on the application of a circular milling process for the machining of thin-walled profiles showed promising results concerning burr formation and flexibility regarding different bore hole diameters. Additionally, in order to prepare them for the joining operation, front milling processes will be used for end machining of the thin-walled profiles. Therefore, future finite element simulation concepts must be developed for this kind of machining processes. Only by obtaining a reasonable compromise between an appropriate model complexity and the necessary computing time an economic simulation tool can be developed. The described approach to apply the occurring loads during the machining process as line-shaped boundary conditions will be used as a basis for the simulation of the accordant milling operations with their respective complex process kinematics.

The generation of a computable FEA model to apply the mechanical loads affecting the workpiece during the process was accomplished. Based on this concept, it was possible to calculate the resulting stresses surrounding the bore hole in the machined profile. In order to simulate the thermal loads affecting the workpiece, a computable model was generated by a modified model concept. The comparison with the temperatures measured during the experimental investigations resulted in a high concordance at the absolute temperature values. In consideration of the entire temperature pattern the concordance is in need of improvement.

Further investigations regarding the improvements of the FEA simulations aim at a higher detailedness of the model. A more detailed model is much more suitable to represent the real load application on the workpiece. Also the calculated results are to be validated by the stresses measured within the scope of the TR 10 project "correlation between microstructure and mechanical properties of joints made of lightweight construction materials". Current simulation runs verify the effect of a higher number of segments.

Based on the experimental results, further simulations need to be performed in order to calculate the consequences of different process parameters or tool variations. The obtained solutions will enlarge the knowledge of cutting processes and the correlation between the variations. The aim is to generate an FEA simulation to calculate the deviation of forces and temperatures subject to the conducted variations. These results can be used to decide on the appropriate process strategy in accordance with the machining task.

Acknowledgement

This paper is based on investigations of the Collaborative Research Center SFB/TR10 which is kindly supported by the German Research Foundation (DFG).

References

[1] Weinert, K.; Schulte, M.; Hammer, N.; Peters, C.: *Finite Element Modeling Concepts of the Load Application on Thin Walled Profiles During the Drilling*. Process Production Engineering – Research and Development, Annals of the German Academic Society for Production Engineering, XI (2004) 2, pp. 121-124

[2] Weinert, K.; Peters, C.; Schulte, M.: *Simulation der spanenden Bearbeitung dünnwandiger Profile.* ZWF Jahrg. 97 (2002) 12, Carl Hanser Verlag, München, pp. 649 – 651

[3] Zäh M. F.; Kleiner M.; Weinert K.; Roeren S.; Schikorra M.; Mehnen J.; Stautner M.; Peters C.; Schulte M.; Kersting M.: *Simulation von Prozessketten zur flexiblen Fertigung leichter Tragwerkstrukturen.* ZWF – Zeitschrift für wirtschaftlichen Fabrikbetrieb, Jahrgang 99 (2004) 5, pp. 248-252

[4] EN AW-6060: Werkstoff Datenblatt AlMgSi. Gesamtverband der Aluminiumindustrie e.V., Düsseldorf 2002

[5] Groth, C.; Müller, G.: FEM für Praktiker – Band 3: Temperaturfelder. 5th Ed., Expert,, Renningen, 2001

[6] Weinert, K.; Peters, C.; Kersting, M.: *FEM-Analyse der Bauteilbeeinflussung dünnwandiger Profile durch spanende Bearbeitung.* Aluminium, International Journal for Industry, Research and Application, 80 (2004) 12, pp. 1408-1412, Giesel-Verlag, Isernhagen

[7] Weinert, K.; Grünert, S.; Hammer, N.; Kersting, M.: *Analysis of Circular Milling Processes for Thin-Walled Space-Frame-Structures Applying FEA-Simulation*. Production Engineering – Research and Development, Annals of the German Academic Society for Production Engineering, submitted 2005, Status: in print

[8] Hoffmeister, H.-W.; Weber, T.: *Schleifprozesse simulieren mit der Finite-Elemente-Methode.* Maschinenmarkt 103 (1997) 33, pp. 20-25

[9] Westkämper, E.; Hoffmeister, H-W.; Weber, T.: *Grinding Process Simulation with FEM.* Production Engineering III (1996) 2, pp. 45-48

[10] Carslaw, H. S.; Jaeger, J. C.: *Conduction of Heat in Solids*. 2nd Ed. University Press, Oxford, 1959

[11] Weinert, K.; Kersting, M.; Schulte, M.; Peters, C.: *FEM-Simulation of Thermal Stresses During the Drilling Process of Thin-Walled Profiles.* Production Engineering – Research and Development, Annals of the German Academic Society for Production Engineering, XII (2005) 1, pp. 101-104

[12] Spur, G.: *Thermische Beanspruchung des Schneidkeils.* Zeitschrift für wirtschaftlichen Fabrikbetrieb 78 (1983) 10, Hanser, Munich, pp. 469-470

doi:10.4028/www.scientific.net/AMR.10.133

Structural Behavior of an EN AW-6060 Profile during and immediately after Welding by a Laser-Laser-Hybrid System

Michael F. Zaeh[1, a] and Sven Roeren[1,b]

[1] Institute for Machine Tools and Industrial Management *iwb*, Technische Universität München, Boltzmannstr. 15, 85748 Garching bei München, Germany

[a]michael.zaeh@iwb.tum.de, [b]sven.roeren@iwb.tum.de

Keywords: laser beam welding, FE-simulation, heat treatment, distortional behavior, residual stresses, joining of lightweight-structures

Abstract This paper describes the analysis of thermal and mechanical effects during welding and the following cooling-phase on a welded structure. An off-the-shelf aluminum-profile, as used in other simulation sub-projects of the research center, was chosen as a sample part for the simulation tests. Taking up an important production scenario of lightweight-production, the frontal closing of two profiles is modeled. The development of residual stresses and the distortion is investigated by a thermo-mechanical FE-simulation. The virtually examined process is provided by a hybrid, bifocal laser system consisting of both an Nd:YAG-laser and a high power diode laser (HPDL). For comparison, a single Nd:YAG-process was simulated, too. The theoretically different generation of residual stresses can be verified within the simulation.

Introduction

Simulation by means of the Finite Element Method (FEM) has become an outstanding part of engineering throughout all areas of planning and manufacturing components [1]. Both products and processes can be analyzed by FEM long before the real systems run. Therefore, a shorter time to market can be achieved, if costly machine-tests for the process-dimensioning can be decreased. The higher computational power and advanced systems for FEM-calculations allow the implementation of complex physical correlations. Therefore, not only static tasks can be solved but also highly dynamic, thermal, thermo-mechanical, electric, acoustic and fluid-dynamic problems can be investigated using recent software-systems. Moreover, the simulation task must be defined exactly before starting to model the scenario. Only that way a reasonable selection of programs and methods for simulation can be realized [2]. In this case, an aluminum-profile should be joined by welding two frontal ends together. The simulation task for this test should be the examination of the distortional behavior and the remaining stresses after welding (residual stresses) in the treated part. Therefore, the simulation-system SYSWELD/ESI was chosen to execute the calculations. Nevertheless, the developed methods described in this paper are universally valid and can be implemented in other common FEM-solvers as well.

Principal Aspects of Modeling of Weld Phenomena

For many years, efforts to simulate effects of welding have been made. Different requirements resulted in many approaches for the calculation of complex effects during and after welding [3]. At the authors´ institute the welding process itself is seen as a given input for the simulation. The intention is to predict the distortional behaviour of welded parts. Nevertheless, the effects of the process have to be included in the calculation for reasons of reliability of the results. Therefore, the simulation of the development of distortions and residual stresses is divided into two main parts.

Firstly, a thermal simulation contains the calculation of the transient temperature-field at every point of the calculated structure. Using the Finite Element Method (FEM), complex geometries are considered in the simulation. Input parameter for the thermal calculation is a moving heat

distribution δQ/δt (t,x,y,z). The principal physical relation of a thermal simulation is, with reference to [4],

$$\frac{\partial T}{\partial t} = \frac{\lambda}{\rho \cdot c_P}\left(\frac{\partial^2 T}{\partial x^2} + \frac{\partial^2 T}{\partial y^2} + \frac{\partial^2 T}{\partial z^2}\right) + \frac{1}{\rho \cdot c_P}\frac{\partial Q}{\partial t}, \tag{1}$$

with T the temperature [K], t the time [s], λ the heat conduction coefficient [J/Ksm], ρ the density [kg/m³], c_p the specific heat capacity [J/kgK] and Q [J] the energy input into the system. Heat transmission from the surface to the environment of the model is described by both radiation $\delta q_R/\delta t$ and convection $\delta q_C/\delta t$ in each case independent from the treated area represented as follows [5]:

$$\frac{\partial q_R}{\partial t} = \varepsilon C_0 \cdot T_S^4 \ , \tag{2}$$

where T_S [K] is the temperature on the surface and εC_0 [J/mm²sK^4] the Stephan-Boltzmann constant, and

$$\frac{\partial q_C}{\partial t} = \alpha_C \cdot (T_S - T_E), \tag{3}$$

with T_E [K] the temperature of the environmental atmosphere and α_C [J/mm²sK] the heat transfer coefficient.

Secondly, within the thermo-mechanical simulation the calculated temperature-field is considered for the computation of thermal strains. The development of these strains is mainly influenced by the mechanical boundaries of the modeled part. According to the elastoplasticity theory, strains lead to either residual stress or distortion [6, 7]. In this case, the strains are caused by a thermal load defined within the previous thermal calculation.

Following the fundamentals of mechanical engineering, every load on a system leads to certain effects. According to the model used, these effects can be acceleration, elastic and elastoplastic deformation or a mixture of the ones mentioned. It is assumed, that a commercial FEM-solver for welding simulation can process elastoplastic material behavior up to the melting temperature of the treated material. Therefore, two main influences can be defined for the criteria of transforming thermal strains into either residual stresses or distortion.

On the one hand, material data related to temperature describe the mechanical behavior. Strength and stiffness of the processed material are given by physical values such as Young´s modulus, tensile strength or Poisson´s ratio. The importance of a reliable set of material data in a welding simulation is obvious and exposed in [8].

On the other hand, clamping conditions have substantial influence on the effects of strain-stress reactions mentioned above. For the calculations described in this paper, nodes were fixed to model the clamping situation. Although several examinations [9] show the influence of different clamping strategies, the modeling of a rigid clamping device was chosen, due to similar scenarios in industry.

Generation of the FEM-model

A huge amount of errors concerning FEM-calculations are caused by insufficient mesh-modeling. Therefore, major efforts should be concentrated on correct modeling of a part-structure. In Fig. 1, one of two assembly components consisting of about 3000 elements and 4000 nodes is shown as an FEM-model, representing a rectangular hollow section of the dimensions 40 mm x 40 mm x 2 mm. For reasons of stability and representation of depth-effect of the laser, the model consists of three-dimensional elements [10]. In view of examining the thermo-mechanical effects of different heat inputs, the use of two-dimensional elements would lead to an insufficient abstraction of the melting zone.

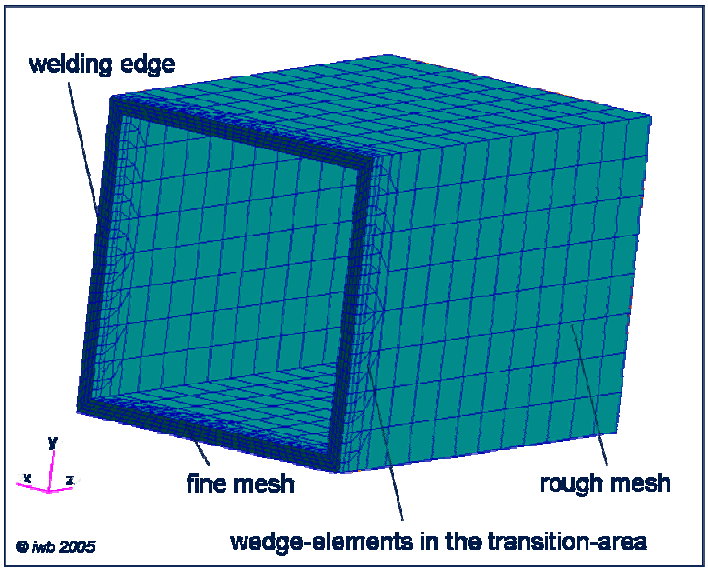

Figure 1: FEM-model of an aluminum-profile containing several refinement-zones

The refinement of areas where large gradients of both temperature and strains are expected was operated by generation of the so called wedge-elements in the transition-area between the detailed and the coarsely meshed zones. Thus, the result of having open nodes, influencing the stability of calculation can be avoided [11]. The maximum edge length of an element should be chosen so that the calculated melting zone corresponds to the real shape. Various tests in simulation provide a sufficient dimension of elements describing meshed zone. For the FE-models treated in this paper, the maximum edge length of elements in the welding zone was defined as 0.5 mm. Therefore, the temperature-field can be described in a sufficient accuracy and the high gradients of thermal strains can be taken into account without interrupting the calculation. Due to the comparatively short weld seams, an adaptive mesh to increase efficiency was not implemented. Following symmetrical conditions, the part shown in Fig. 1 was mirrored at the front-plane with keeping the original elements. Thereby, the joining-gap was reduced to zero and the merging of geometrically identical nodes leads to neglecting of mechanical effects concerning the gap-behavior. The results of former studies [9,12] defining air-elements in the joining-gap demonstrate the minor importance of these effects, mainly if the structure is highly restricted in its degrees of freedom by a rigid clamping situation.

For the consideration of thermal effects on the surface, such as radiation and convection, two dimensional elements were defined. Merged with the three-dimensional elements of the welded structure, the thermal balance can be modeled with regard to the real effects. This is important for an accurate description of the cooling phase, which strongly influences the remaining thermal effects.

Thermal Calculation

As mentioned above, the process is the major input for a distortional simulation of welded structures. The process-structure-interface used in the presented approach is a defined heat-distribution. Regarding the simulated process, the heat distributions are modeled by varying their geometrical dimensions and the power led into the model. These so called heat sources cause a reaction only in case of an intersection with the FE-part. This intersection on the surface can be achieved by defining a two-dimensional heat source on the surface nodes or within the borders of the material by a three-dimensional body moved through the model. In Fig. 2, two types of heat sources considered in this research work are shown, representing a two-dimensional surface heat source and a three-dimensional conical heat source.

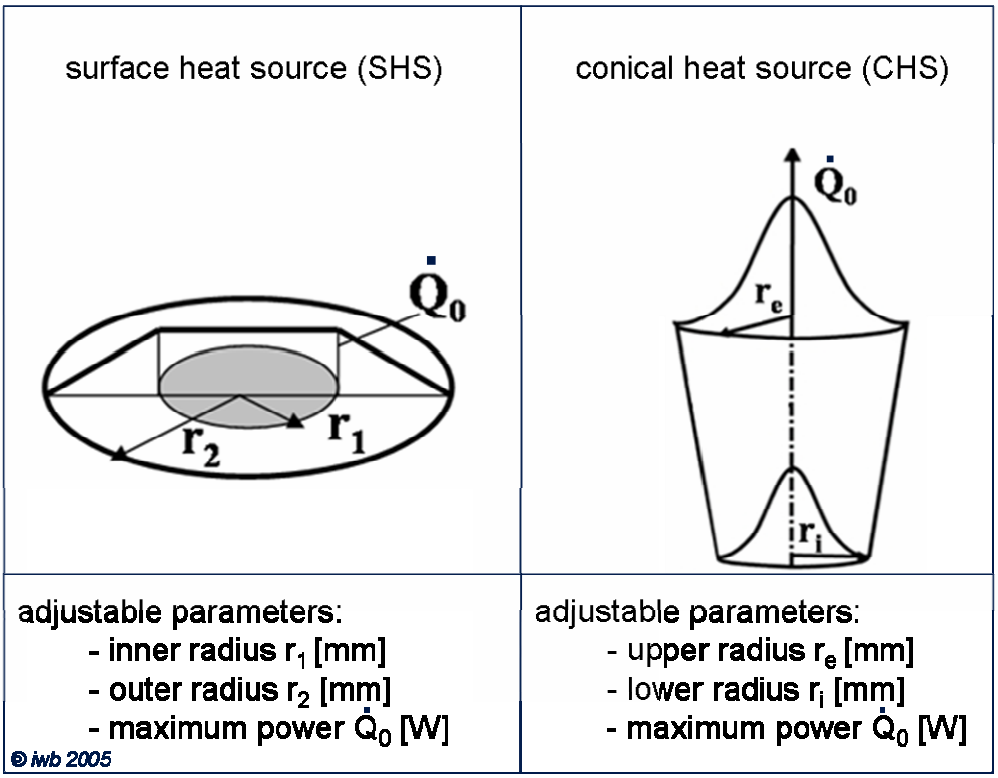

Figure 2: Heat sources for the simulation of hybrid bifocal laser beam welding

For the simulation of the hybrid, bifocal laser beam welding, the described two heat sources have to be combined and activated synchronously. Thereby, the thermal behavior of the laser-laser-hybrid-process can be seen. The adjustment of the heat source parameters is put into practice iteratively. The parameters have to be adjusted until the calculated temperature field corresponds to the real thermal behavior in a sufficient way. Due to the complexity of the process, the implementation of physical laws representing the laser distribution and the beam-material interaction into a global structural analysis is still not feasible. Therefore, a high level of abstraction is needed for the macroscopic simulation of the welded part. For the determination of the real behavior, two indicators of the process enable a comparison between reality and calculation.

On the one hand, a metallographic cross section of the welded structure gives a conclusion for the maximum dimension of the melting zone and the heat affected zone. Iteratively, the parameters of the heat sources can be adjusted until the calculated melting pool is nearly identical to the dimensions of the welded cross section.

On the other hand, additional information is needed. Due to the two-dimensional character of a cross section, more information about the length of the melting pool is required for the adjustment of the three-dimensional heat distribution. In principle, two approaches enable such an interpretation. Firstly, a costly measurement of the transient temperature during the welding process by thermal sensors provides an established dataset for a three-dimensional comparison. In addition, the theoretical examination of the thermal balance in a welded part and further assumption concerning all efficiency-losses during the beam-material interaction allows useful predictions. Former measurements of welding experiments based on an EN AW-6060 material indicated an energy transfer efficiency η_{ET} of 0.55 for both an Nd:YAG-laser-process and a process using a hybrid bifocal laser system consisting of an Nd:YAG and a HPDL [13]. At this, η_{ET} describes the ratio of energy irradiated by the laser onto the surface and energy absorbed by the workpiece. Assuming that the three main thermal effects within the workpiece (conduction, convection and radiation) are defined correctly, the heat input intensity can be estimated by considering the nominal output of the laser systems adjusted by the energy transfer efficiency. This assumption is

valid for the specific material EN AW-6060 and the laser system described based on measurements and theoretical considerations. Both the conical and the surface heat source presented in Fig. 2 enable an evaluation of the total energy put into the FEM-model, so that a comparison between the assumed energy input and the calculated one can be done.

Related to the sample presented within this paper, Fig. 3 illustrates the shapes of the melting pools provided by metallurgical measurements and theoretical assumptions regarding to energy transfer efficiency.

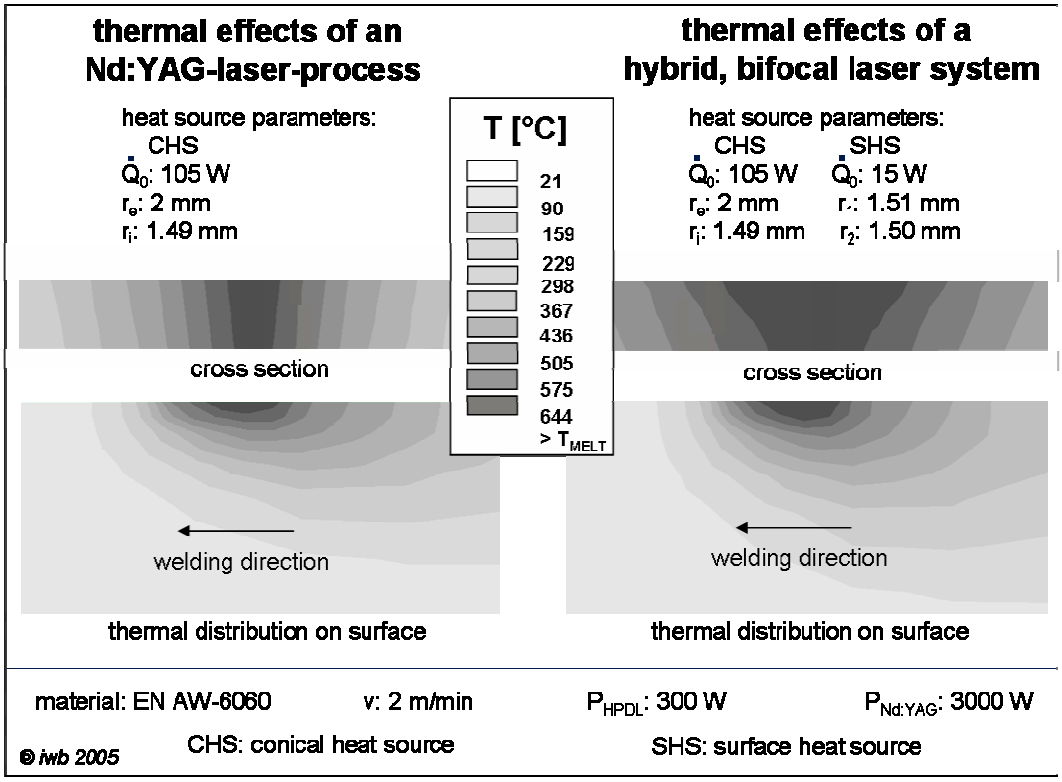

Fig. 3: Calculated temperature in an aluminum profile concerning an Nd:YAG and a hybrid, bifocal laser system

On the left side, the thermal effects of an Nd:YAG-laser-process are illustrated. Therefore, a conical heat source is used to represent the specific impact of the depth penetration into the material. On the right side of Fig. 3, the thermal effects of a hybrid, bifocal laser system are shown. The only difference to the simulation shown on the left side is the consideration of a supporting HPDL-process reproduced by the energy input of a surface heat source.

The definition of a heat distribution is treated as load within a thermal simulation. Furthermore, thermal boundary conditions as mentioned above have to be taken into account for the calculation of a transient temperature field. The implementation of radiation and convection at the surface of the component is state-of-the-art in the area of FEM-calculation [14]. Standard routines are defined in most commercial FE-solvers, but the consideration of material data is still an element of uncertainty. Within the collaborative research center SFB/TR10 of the DFG a research group consisting of the sub-projects related to simulation was created for an integration of their developed models and approaches. One of the intentions, as described in [15], is the universal definition of directives, consistently provided for all sub-projects. Therefore, a common material dataset for EN AW-6060 was defined. The use of this dataset across all sub-projects facilitates a comparison between the particular simulation results. Thus, the following thermal material data, were taken into account. Values above melting temperature support to avoid numerical instabilities during the calculation, because then only interpolated values are taken into account. 644 °C defines the

liquidus-transition, while 570 °C determines the solidus-point. The effects of latent heat during the change of the physical aggregate states were considered in c_P data, as seen in Table 1.

Temperature T	Density ρ	Heat conduction coefficient λ	Heat capacity c_P
[°C]	[g/cm³]	[W/mK]	[kJ/kgK]
20	2.7	187	898
100	2.68	190	945
200	2.67	194	995
300	2.66	198	1042
350	2.65	200	1069
400	2.64	202	1099
450	2.63	203	1120
500	2.62	205	1148
550	2.62	207	1170
610	2.61	210	1195
630	2.51	160	13000
655	2.41	110	1165
800	2.35	200	1165

Table 1: Thermal material data for EN AW-6060, used within the SFB/TR10

Following a joining scenario relevant to industrial tasks, the simulated sample describes the frontal closing of the above described aluminum profile. Therefore, the welding process is divided into four parts corresponding to the edges of the structure. In simulation, the heat input onto the four weldlines was interrupted three times for 0.5 s each at the end of every edge to consider the adjustment of a handling system onto the new welding direction. In Fig. 4 the calculated temperature distribution of both the Nd:YAG-process and the hybrid, bifocal laser process described above is shown at time 6 s, when the last side of the structure is welded.

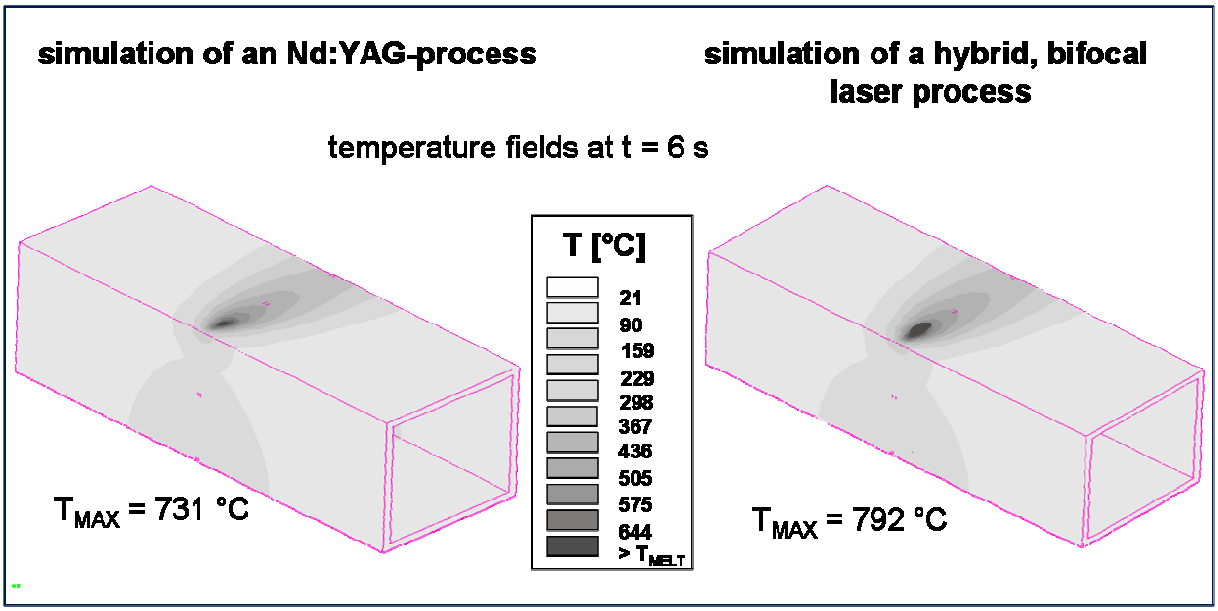

Fig. 4: Calculated temperature at 6 s of a Nd:YAG laser process and a hybrid, bifocal laser system

Implementing an additional heat source for the modeling of the hybrid, bifocal laser beam welding causes two major effects. On the one hand, as seen in Fig. 3, the size of the melting zone increases. On the other hand, the maximum temperature rises about 60 °C. These effects are caused by the additional energy defined by the surface heat source. Leaving the center of the melting zone, these different effects seem to decrease, as noticed by the isotones representing lower temperature.

The thermal calculation contains the cooling phase of the component, so that the last time step of the simulation is 290 s, when room temperature is nearly reached again.

Thermo-mechanical Calculation

Following the intention of the simulation described within this paper, the calculation of the transient temperature field is sine qua non for further steps. In conclusion, an industrial application of welding simulation requires mainly the prediction of the distortional behavior and the calculation of the residual stresses remaining in a treated structure.

Within the scope of the sample described above, the development of stresses caused by thermal strains is examined within the thermo-mechanical simulation. After cooling these stresses remain as residual stresses in the part. At this time, the thermo-mechanical behavior of the two processes simulated within simulation is analyzed by comparison. On the lines of the thermal calculation, mechanical boundary conditions affect the results of the calculation related to the thermal load. This load is given as a transient temperature field by implementing the results of the previous thermal simulation.

The clamping condition of the welded structure is realized by fixing two groups of nodes, being located at both ends of the profile. Every degree of freedom is frozen, whereby a very rigid clamping condition is modeled. In the automotive industry, workpieces to be welded are clamped close to the weld seam and as rigid as possible in order to avoid the development of joining gaps during welding. Furthermore, the resulting distortion can be minimized and component tolerances can be held down.

Due to the clamping of the nodes, the length of the profile beyond these areas is not relevant. The fixing of the nodes blocks the mechanical effects and the thermal flow is insignificant in both simulation and reality.

Relevant material data for the thermo-mechanical simulation are Young´s modulus E [MPa], Poission´s ratio ν [1], yield strength $R_{P\ 0.2}$ [MPa], tensile strength R_M [MPa] and the thermal expansion coefficient α [1/K]. Assuming the used material can be described by an isotropic behavior, the set of material data described in Table 2 was defined and implemented into the calculation.

Fig. 5 shows the results of the thermo-mechanical calculations. The residual stresses, generated by the different laser processes described above, are compared at the time 290s. Analyzing the results of the comparison, the following aspects can be recognized. Firstly, the residual stress distributions of the two processes differ from each other both in quantitative and qualitative form. Hereby, the stresses caused by the hybrid, bifocal laser process are lower, although the maximum temperature of this process is higher, as seen in Fig. 4. But assuming an elastoplastic material behavior as considered within the calculations [16], the local temperature gradients cause the major part of the remaining stresses due to latent heat effects and plastification. For example, when heating up a part in an oven, the material behavior during the process and the remaining stresses are mainly affected by the heating and cooling rate. Therefore, the amplitude of the heat is not the only effect to be considered for thermo-mechanical calculation. Similar samples for these effects are established in the area of engineering mechanics, for example relating to crash scenarios, as well [17].

Temperature T	Young´s modulus E	Yield strength $R_{P\,0.2}$	Tensile strength R_M	Thermal expansion coefficient α
[°C]	[MPa]	[MPa]	[MPa]	[1/K]
20	69000	95	178	0
100	64844	72	158	0.001912
200	52075	66	138	0.0045
300	52549	64	88	0.007252
350	46071	67	70	0.008523
400	40076	46	49	0.010032
450	35227	33	36	0.01205
500	15467	12	13	0.013296
550	7000	5	6	0.01423
610	500	0	0	0.0157
630	0	0	0	0.0157
655	0	0	0	0.0157
800	0	0	0	0.0157

Table 2: Thermal material data for EN AW-6060, used within the SFB/TR10

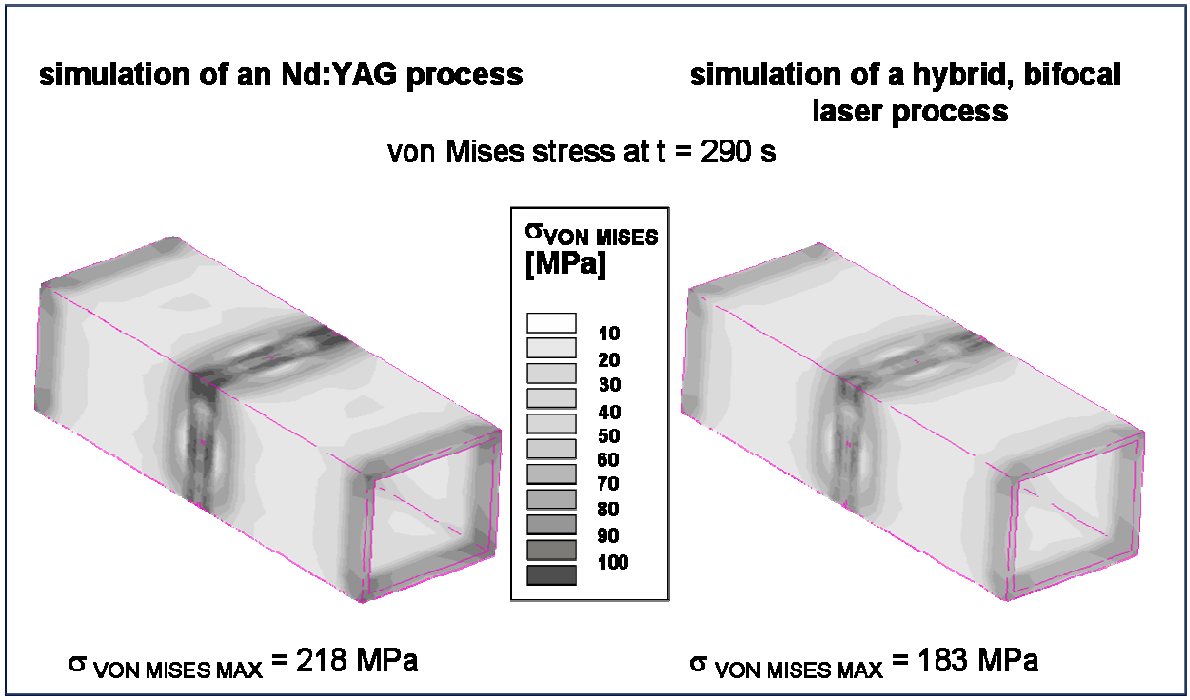

Fig. 5: Calculated von Mises stress at 290 s of a Nd:YAG-laser-process and a hybrid, bifocal laser system

Relating to the aluminum profile described in this paper, it can be remarked, that the high temperature gradients of an Nd:YAG-laser-process can be weakened by an additional energy input, e.g. by a HPDL. Therefore, the recently published advantages of the hybrid, bifocal laser beam welding [18] can be extended considering the decrease of residual stresses related to a single Nd:YAG-laser-process.

Concluding Remarks

In this paper, the thermal and the thermo-mechanical effects of two different laser processes were calculated by FEM-simulation. A single Nd:YAG-laser-process was compared to a hybrid, bifocal laser system, consisting of both an Nd:YAG and a HPDL.

For the modeling of the Nd:YAG-process a conical heat source was used to reproduce the deep penetration effect. To characterize the hybrid, bifocal laser beam welding an additional two-dimensional surface heat source was defined. The parameters of the heat sources were adjusted iteratively, based on metallographic examinations and theoretical assumptions of the beam material interactions. The results of corresponding thermal and thermo-mechanical simulations differ. The higher total energy of the hybrid process leads to a higher maximum temperature but to less residual stresses after cooling as well. This effect is caused by a decrease of the high temperature gradients characterizing the Nd:YAG-process. The additional HPDL process leads to a degradation of stresses although a higher insert of energy into the part is given. Theoretical assumptions of thermo-mechanics support the calculated results.

One further step will be the validation of the calculated results by real measurements of residual stresses after treatment on the surface of the welded part. The effects of different clamping conditions on the behavior of residual stresses are planned to be considered, too. In the last year of the sub-project, more complex profiles will be simulated. Furthermore, first investigations on an implementation of flexible heat sources depending on time and temperature should be undertaken. Thus, a possibility for the conjunction of structural analysis of a welded part with physical process simulation can be achieved.

Acknowledgement

This paper is based on investigations within the scope of the Transregional Collaborative Research Center/ TR10 and is kindly supported by the German Research Foundation (DFG).

References

[1] K.-J. Bathe: *Finite-Elemente-Methoden,* 2nd edition (Springer, Berlin, 2002).

[2] V. R Davé, J. H. Cowles, D. S. Lindland, G. C. Shubert, W. Lin and D. A. Hartman: The Financial Impact of Weld Process Modeling, Welding Journal, December 2004, pp. 24-27.

[3] H. Cerjak and H. K. D. H. Bhadeshia: Mathematical Modelling of Weld Phenomena 1-7, (Materials Modelling Series, Maney Publishing, London, 1993-2004).

[4] H. D. Baehr and K. Stephan: Waerme- und Stoffuebertragung, 3rd edition (Springer, Berlin, 1998).

[5] N. N. Rykalin: Berechnung der Waermevorgaenge beim Schweißen (VEB Verlag Technik, Berlin, 1957).

[6] D. Radaj: Heat Effects of Welding: Temperature Field, Residual Stress and Distortion, (Springer, Berlin, 1992).

[7] V. A. Lubarda: Elastoplasticity Theory, (CRC Press, Boca Raton, 2002).

[8] M. F. Zaeh, F. Auer and S. Roeren: Simulation of Laser Beam Welding Production Processes, in: Proc. of the 3rd international CIMTEC Conference, (Technagroup, Acireale, 2004), pp. 575-586.

[9] S. Roeren, A. Trautmann and M. F. Zaeh: Modelling of Transient Clamping Conditions during Laser Beam Welding, in: Proceedings of the Third International WLT-Conference on Lasers in Manufacturing 2005, Munich, June 2005, edited by E. Beyer, F. Dausinger, A. Ostendorf, A. Otto, pp. 95-100.

[10] C. Hackmeier: Messung und numerische Simulation der Schweißverzuege an Aluminium-Fahrwerkskomponenten. PhD-Thesis, Technische Universität München, 2003.

[11] F. Auer: Methode zur Simulation des Laserstrahlschweißens unter Beruecksichtigung der Ergebnisse vorangegangener Umformsimulationen. PhD-Thesis, Technische Universität München, 2004.

[12] L. Papadakis and S. Roeren: *Anwendungsnahe Modelle zur FEM-Berechnung des Verhaltens gefuegter Bauteile beim Laserstrahlschweißen*, in: Proc. of the SYSWELD-Userforum 2005, Weimar, pp. 37-47.

[13] Trautmann, A.; Zaeh, M. F.: *Hybrid Bifocal Laser Welding of Aluminum*, in: Proc. of ICALEO 2005, Miami, USA 31.10.-3.11.2005, pp. 153-162.

[14] O. C. Zienkiewicz: Finite Element Methods in Thermal Problems, in: Numerical Methods in heat transfer, edited by R. W. Lewis, K. Morgan and O. C. Zienkiewicz, Wiley and sons, NY, 1981, pp. 1-26.

[15] M. F. Zäh, M. Kleiner, K. Weinert, S. Roeren, M. Schikorra, J. Mehnen, M. Stautner, C. Peters, M. Schulte, M. Kersting: *Simulation von Prozessketten zur flexiblen Fertigung leichter Tragwerkstrukturen*,. ZWF Zeitschrift für wirtschaftlichen Fabrikbetrieb Vol. 99 (2004) 5, pp. 248 ff.

[16] SYSTUS Analysis Reference Manual, (ESI-Group, Paris, 2002).

[17] I. Szabo: *Hoehere Technische Mechanik*, 6th edition, (Springer, Berlin, 2001).

[18] M. F. Zäh, A. Trautmann: *Vergleich des hybirden, bifokalen Laserschutzgasschweißens mit Laser-MIG-Hybridverfahren*, in: Aluminium Vol. 12 (2004) 80, pp. 1287-1391.

doi:10.4028/www.scientific.net/AMR.10.143

Qualitative Knowledge and Manufacturing Considerations in Multidisciplinary Structural Optimization of Hybrid Material Structures

M. Huber[1,a], H. Baier[1,b]

[1] Institute for Lightweight Structures (LLB) – Technische Universität München

Boltzmannstraße 15, 85748 Garching, Germany

[a]huber@llb.mw.tum.de, [b]baier@llb.mw.tum.de

Keywords: Hybrid Material Structures, Design Optimization, Manufacturing Constraints, Fuzzy Knowledge, Genetic Algorithm

Abstract. An optimization approach is derived from typical design problems of hybrid material structures, which provides the engineer with optimal designs. Complex geometries, different materials and manufacturing aspects are handled as design parameters using a genetic algorithm. To take qualitative information into account, fuzzy rule based systems are utilized in order to consider all relevant aspects in the optimization problem. This paper shows results for optimization tasks on component and structural level.

Introduction

Material hybrid structures and components extend the achievable operating range compared to single material designs with regard to functional, structural mechanic, thermal and economic requirements. Affordable manufacturing processes have increased the number of applications of metal matrix composites (MMC's) during the last years. Chemical and possible thermo-mechanical mismatches have to be considered in an optimal design. For example, the difference in the thermal expansion coefficients generates thermal stresses in the two material components. This results in a reduced mechanical load carrying capability if the volume ratio of the reinforcement exceeds a certain limit under a given temperature load.

In addition, the manufacturing process of the reinforced part has to be taken into account since this determines the placement of the reinforcing elements and therefore the achievable volume ratio [1]. This combination of influences leads to a complex engineering task. To provide the engineer with optimal designs, a multidisciplinary, multi-objective optimization approach generates a set of optimal solutions from which the preferred design can be chosen.

Two typical structural optimization design tasks will be presented. The first is the optimization of a reinforced, extruded profile in a cantilever configuration. The second is the optimization of a car space frame composed of such profiles. Not all manufacturing aspects of these examples are yet available as numerical or analytical models. Therefore the experience and knowledge of the respective manufacturing domain expert is utilized to build fuzzy models in order to consider these influences at least in a coarse way. The overall optimization approach is described focusing on the modeling of qualitative and fuzzy knowledge. The results of the optimization tasks are presented and the performance of the approach is discussed.

Optimization of Hybrid Material Components and Structures

The first optimization problem considers an extruded aluminum or magnesium profile, which is reinforced during the extrusion process with steel wires or carbon fiber ropes (Fig. 1 left side). The goals are to minimize the weight and the deflection of a 1000 mm long, clamped - free, I-section beam under structural and thermal load. These are conflicting goals, in other words: Higher mass results in smaller deflection. The design variables are the geometric properties of the cross section, the number, size and material of the reinforcing elements and the matrix material. As a structural

constraint, a sufficient margin of safety against failure has to be ensured. The manufacturing effort should also be restricted. In the example application, this effort is assumed to be a function of the wall thickness ratio t_f/t_w, the circumscribed diameter d_B and the number of reinforcing elements.

Space frames are common concepts for vehicle structures and they are used, for example, in sports and micro cars, ultra light helicopters and aircraft. The main components are the beam profiles (straight as well as curved) and the joints. The complete space frame of a micro car (Fig. 1 right hand side) is optimized with regard to the structural mass and the torsional stiffness. A lower structural mass allows additional safety equipment because the overall weight of the car is restricted. The handling and the comfort of the car, however, is enhanced by a higher torsional stiffness (typical values for today's cars are in the range of 5000 Nm/° to 15000 Nm/°).

The space frame consists of forty hollow profiles of different cross sections, most of them following a 3d contour. To meet the strict mass restriction without a significant loss in torsional stiffness reinforced profiles and their manufacturing aspects should be considered. The aim is to provide the engineer with information about the most effective application of reinforced profiles and the optimal material combination(s).

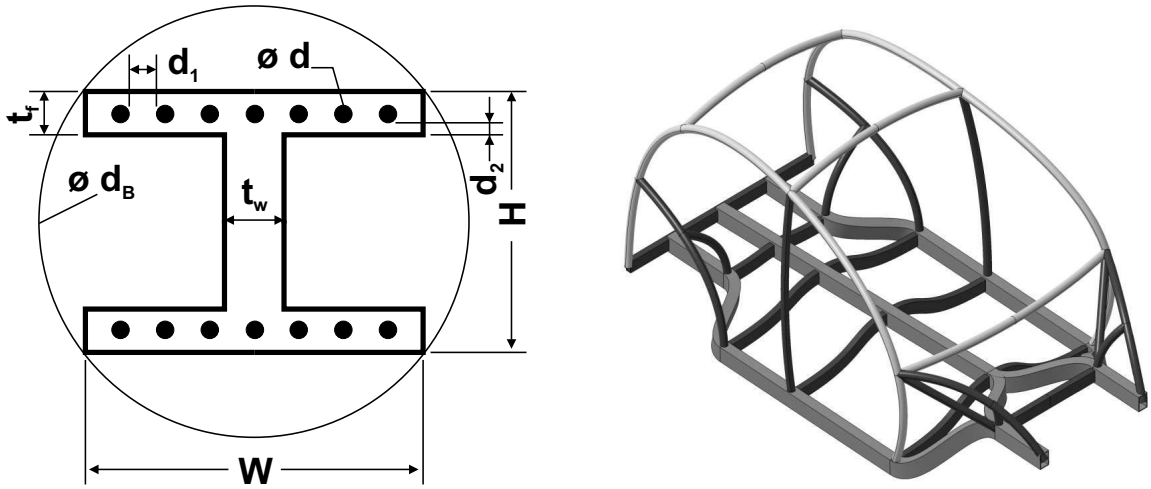

Fig. 1: Two typical optimization tasks – left: reinforced profile; right: car space frame

Manufacturing Aspects on Component and Structural Level

Basically each manufacturing step determines the structural properties of the corresponding part. In the presented cases the primary forming process – extrusion molding – has the greatest influence on the design. Generally the manufacturing aspects can be classified into two groups.

Geometrical restrictions limit the range of geometric design parameters. Some dimensions of the construction also depend on each other. An example is displayed in Fig. 2. The minimum wall thickness for an extruded profile without reinforcements is a function of the circumscribed diameter d_B (see Fig. 1 for definition) and the matrix material. Reinforcements increase the minimum wall thickness because the reinforcing elements have to be pulled by the matrix material during the extrusion process.

Some geometric restrictions and dependencies are well known and can be found in the literature whereas others have not been described explicitly. For the influence of the reinforcing elements, neither enough test data is available nor does the simulation model developed in a parallel project provide enough parametric information to build corresponding models [2]. Therefore experienced extrusion-molding engineers are used to establish the necessary knowledge base for fuzzy models.

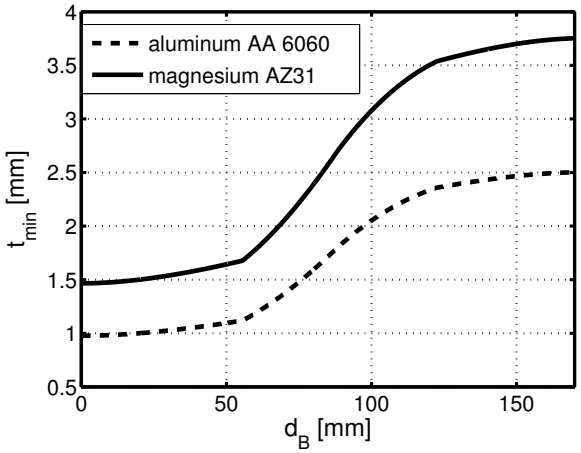

Fig. 2: Minimum wall thickness for complex, hollow section aluminum and magnesium profiles as a function of the circumscribed diameter d_B

The second class of manufacturing aspects concerns the manufacturing effort. For structures, the manufacturing effort of all components has to be taken into account. Therefore rough cost estimations are made, approximating the estimated process time for the manufacturing steps of each part and additional effort such as tooling cost. For example, the extrusion speed for an aluminum profile is about twice the extrusion speed of a magnesium profile, which influences the operating time and therefore the operating cost of the extrusion press. Also, the so-called down time (tool and material replacement) must be considered in certain cases. For the estimation of the manufacturing effort of structures not only the primary forming process is crucial, but also the following manufacturing steps. In the case of reinforced profiles, cutting and milling processes are important because tool wear is much higher for hybrid materials [3]. These manufacturing aspects can change the optimal designs drastically [4].

Because of this complex interaction between structural mechanics and manufacturing, the presented design problems are formulated as nonlinear optimization problems, which contain discrete design variables, multiple objectives and fuzzy influences.

Mathematical Design Optimization Formulation

The general mathematical formulation for a restricted optimization with several goals [5] is given in (1) – (5):

$$\min \mathbf{z} = \mathbf{f}(\mathbf{x}), \quad \mathbf{f} = [f_1(\mathbf{x}), f_2(\mathbf{x}), ..., f_{nob}(\mathbf{x})]. \tag{1}$$

$$\text{with:} \quad \mathbf{x} = [x_1, x_2, ..., x_{dv}]' \in \mathbf{R}^{dv}. \tag{2}$$

subject to:

$$\mathbf{g}(\mathbf{x}) \leq 0, \quad \mathbf{g} = [g_1(\mathbf{x}), g_2(\mathbf{x}), ..., g_{nic}(\mathbf{x})]. \tag{3}$$

$$\mathbf{h}(\mathbf{x}) = 0, \quad \mathbf{h} = [h_1(\mathbf{x}), h_2(\mathbf{x}), ..., h_{nec}(\mathbf{x})]. \tag{4}$$

$$x_{ilb} \leq x_i \leq x_{iub}, \quad i = 1, 2, ..., n_{dv}, i \in \mathbf{N}. \tag{5}$$

The functions $f_i(\mathbf{x})$ are called objective functions. Conventionally different objectives are combined into a scalar measure with certain methods, e.g. the weighted sum approach, turning the

problem into a single objective task. In this case, the decision about the relative importance of each objective is taken a priori without any knowledge about the tradeoff between the different objectives and only a *single* solution is attained.

The goal of a multi-objective optimization is to generate a *set* of optimal solutions (here optimal designs). The non-dominated set of the entire feasible search space is the Pareto-optimal set. The Pareto-optimal set in the objective space is called the Pareto-optimal front. These solutions have in common that no other solutions exist in the design space that are simultaneously better in all objectives. Only by having the Pareto front at hand the interactions between the different objectives become apparent to the decision maker, enabling better design decisions. For the vehicle space frame the objectives are to minimize the mass and maximize the torsional stiffness.

The geometric parameters, the wall thicknesses of the cross section and the material combination are the design variables $\mathbf{x}$ for the space frame profiles. Aluminum and magnesium are considered as possible matrix materials, steel wires and carbon fiber ropes as reinforcing elements. The volume ratio of the reinforcement is between 0 and 30 percent, which is assumed to be the maximum volume ratio achievable with the described extrusion molding process. The forty profiles are subdivided into four groups with reference to functional considerations (floor pan longitudinal and cross beams, pillars and roof beams). Each profile in one group has the same design, which leads to 16 continuous and 5 discrete design parameters.

Constraints, $\mathbf{g}(\mathbf{x})$ and $\mathbf{h}(\mathbf{x})$, arise from the manufacturing effort, the material cost and geometric restrictions of the extrusion molding process. In this optimization, no additional restrictions (stress, eigenfrequency…) are introduced in order to ease interpretation of the results with regard to the manufacturing aspects. To get further information on the influence of the manufacturing effort, the optimization is repeated with increasing restriction on this constraint, leading do different Pareto fronts.

Integration of the Different Disciplines in the System Equations

The models which relate the design variables to the relevant system behavior (structural, thermal …) are called system equations. Depending on the relevant system behavior, different models can be used such as finite element models (FEM) for structural, dynamic and crash analyses, computer aided design (CAD) models for the geometric representation of the structure, center of gravity and clash computation [6] or detailed numerical simulations of manufacturing processes. Often results from theses models or real test data are approximated in order to reduce the computation time (the system equations have to be computed repeatedly during the optimization run). At the Institute of Lightweight Structures response surface approximation methods are utilized for this task [7].

The properties and behavior of the cantilever profile are modeled with simple analytical equations i.e. the material properties are calculated with the rule-of-mixture, which shows good correlation with test data of a reinforced tensile specimen.

Complex structures like the space frame are designed in parametric CAD programs. The 3d contour lines of the space frame are created in CATIA V5 and they are exported to IGES files (Initial Graphics Exchange Specification), which can be interpreted in the FEM tool ANSYS. In ANSYS, the structural behavior is simulated using beam elements which support cross section data.

The models described above, such as detailed manufacturing effort estimations, are not always available in time. In order to consider all relevant influences on a design, at least in a roughly and approximated way, the experience, knowledge and forecasts of the respective domain expert are the only source of information. This knowledge is qualitative and fuzzy, but it can be utilized to formulate parameterized coherences. The transformation into mathematical models is done with the help of fuzzy rule based systems.

Modeling of Qualitative and Fuzzy Knowledge with Fuzzy Rule Based Systems

To integrate fuzzy and uncertain information at least in a roughly estimated way Hajela suggests the use of fuzzy models to utilize expert knowledge [8]. Fuzzy logic provides the basics for fuzzy modeling and it was introduced as a method of formally describing linguistic information. So-called fuzzy rule based systems (FRBS) have the ability to model complex behavior. The most important task is to build the knowledge base, which includes the *j* rules describing the relationship between inputs and outputs. The framework for the problem considered here is a system with n inputs $[x_1,\ldots, x_n]$ and one output y. These rules R_j have the following structure:

$$R_j : \text{if } x_{j1} \text{ is } A_{j1} \text{ and } x_{j2} \text{ is } A_{j2} \text{ and ... and } x_{jn} \text{ is } A_{jn} \text{ then } y_j \text{ is } B_j. \quad (6)$$

where $x_{j1},\ldots, x_{jn} \in [x_1,\ldots, x_n]$ and A_{ji}, B_j are fuzzy sets on the respective domains of the variables. The degree to which an input or output belongs to a fuzzy set is defined by a membership value between zero and one. A membership function μ_A associated with a given fuzzy set maps a value to its appropriate membership value. Gaussian, triangle, trapezoidal and monotonically in-/decreasing membership functions are used. In fuzzy logic, a certain crisp value does not belong to one set or another but can belong partly to different sets. For example, a profile with a length of 1250 mm would have a 0.5 degree of membership in the "short" set and a 0.5 degree of membership in the "medium" set in Fig. 3 on the left side.

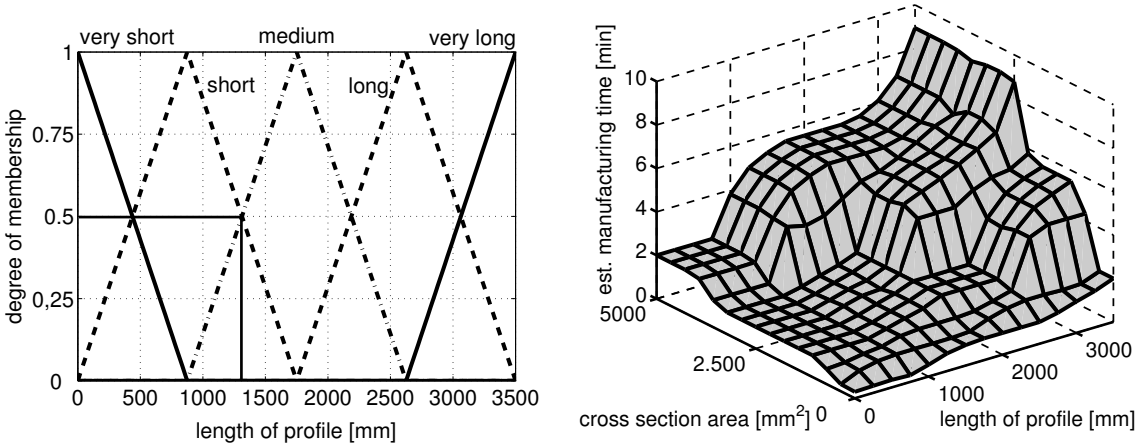

Fig. 3: Membership functions for parameter profile length on the left and output of a manufacturing time estimation model for extrusion molding on the right

The following steps are necessary to transform linguistic information into a mathematical model [9]. This is done together with the knowledge carrier:

- identify the input- and output variables and their respective domains
- define the fuzzy membership functions for each input and output variable to cover the respective domains
- transform the description of the system behavior into fuzzy rules stating the relations between the variables
- evaluation of the model

For aluminum a model for the estimated extrusion molding time (0-10 minutes; fuzzy sets: very short time, short time, medium, long time, very long time) is generated with the two inputs "length of profile" (0-3500 mm; fuzzy sets: very short, short, medium, long, very long) and "cross section

area" (0-5000 mm²; fuzzy sets: very small, small, medium, big, very big). For constant extrusion molding parameters the manufacturing time for a profile increases with increasing length and cross section. The billet refill must also be taken into account as downtime, this occurs more often for long and big profiles. The resulting output is shown in Fig. 3 on the right side.

For the I-section beam the geometric dependency between the circumscribed diameter, the material and the minimum wall thickness is modeled as shown in Fig. 2. The ratio between web and flange thickness and the number of reinforcing elements are input parameters for the manufacturing effort model for extrusion molding. The output of this model is a nondimensional effort value between zero (very low manufacturing effort) and one (high manufacturing effort).

The same models are used for the description of the geometric manufacturing aspects of the space frame. Effort estimations are based on manufacturing time approximations of four manufacturing steps. Altogether seven fuzzy rule based system models are utilized.

To solve the described optimization problems an optimization system has been established at the Institute of Lightweight Structures, which will be presented in the following section.

Main Elements of the Optimization Approach

The optimization system is composed of the following main elements:

- an application management system (MOSES: Multidisciplinary Optimization of Structures and Electro-mechanical Systems), guiding the automated conceptual design process, maintaining the optimization database and controlling the execution of the different software tools, as well as the parallel software execution on a computer cluster.
- the genetic optimization algorithm GAME (Genetic Algorithm for Multicriteria Engineering) capable of handling disjunctive and "rugged" design spaces (Fig. 4, [6]).
- a CAD tool (CATIA V5, Pro/Engineer) for appropriate geometrical description, representation and parameterization.
- the parameterized simulation models, including closed form solutions, response surface approximations, fuzzy logic models and finite element and/or finite difference methods.

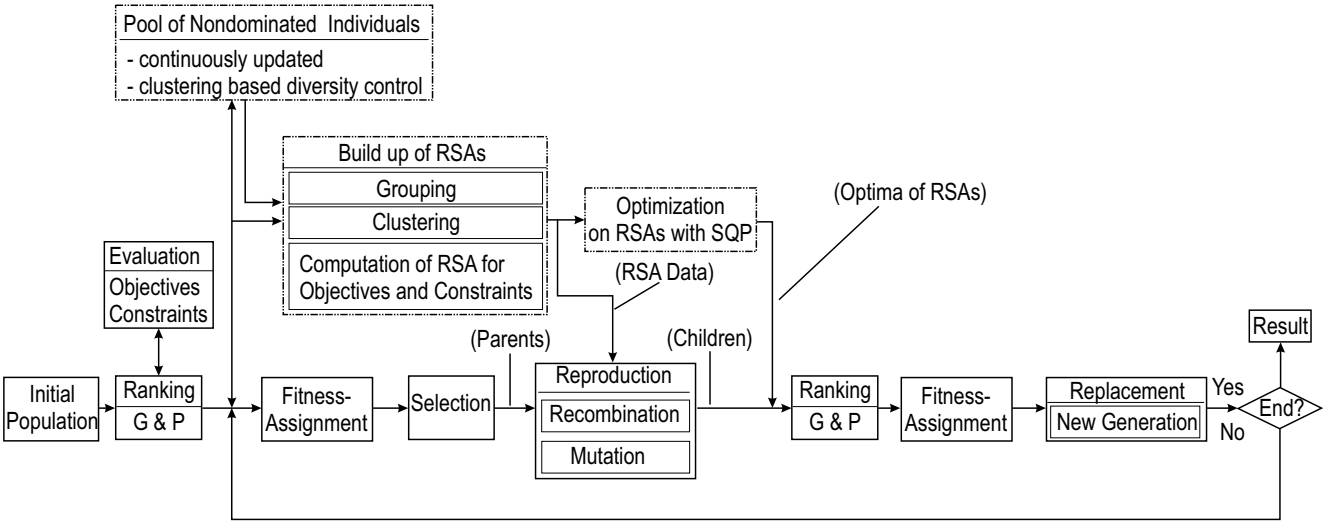

Fig. 4: Flowchart of the genetic algorithm GAME including response surface approximation (RSA) branch

The genetic algorithm GAME offers the possibility to provide a so-called Pareto front of optimal solutions for multi criteria problems to the engineer from which he can choose the preferred design without prior weighting of the optimization goals. A drawback of genetic algorithms is their high number of function evaluations. Especially when close to the constraint limits, these evaluations might quite often belong to infeasible designs. Such problems have been efficiently addressed by parallelizing the function evaluation (i.e. finite element computation) on a Linux cluster. The utilization of the information at hand for each design during the optimization run with the help of response surface functionalities increases the computational efficiency further.

For the presented examples, the population size is between 100 and 200 individuals, the number of children is twice the population size. The number of generations is limited to 35, no other stop criteria is used. The possibility of mutation is high with linearly decreasing standard deviations for the design variables. The possibility of crossover is small and remainder sampling is used for the parent selection process.

Results of the I-Section Profile Optimization

In Fig. 5 three Pareto fronts (set of all optimal compromises between conflicting objectives) for different optimizations with altering manufacturing effort restrictions are shown. Each point is an optimal design, which means, that no design with a lower mass can be found for a given deformation. The 'ultimate' design would be placed at the lower left corner of the diagram. If high manufacturing effort is tolerated (□, ■ in Fig. 5) aluminum profiles with carbon fiber reinforcements are optimal (material costs are neglected). Parts with less then 2 kg mass can be achieved with magnesium - carbon fiber combinations. Four to six reinforcing elements are located in the flanges, the web and flange thicknesses are quite different (Fig. 5 a). With higher restrictions on the manufacturing effort (○,● in Fig. 5) less reinforcing elements are used and the web thickness is four times higher than before (Fig. 5 b). With very strict restrictions on the manufacturing effort (× and + in Fig. 5) no reinforcement can be used and the web and flange have the same thickness (Fig. 5 c). For the same deformation of ~16 mm the three designs have weights of 2.8 kg (a), 3.2 kg (b) and 4.1 kg (c).

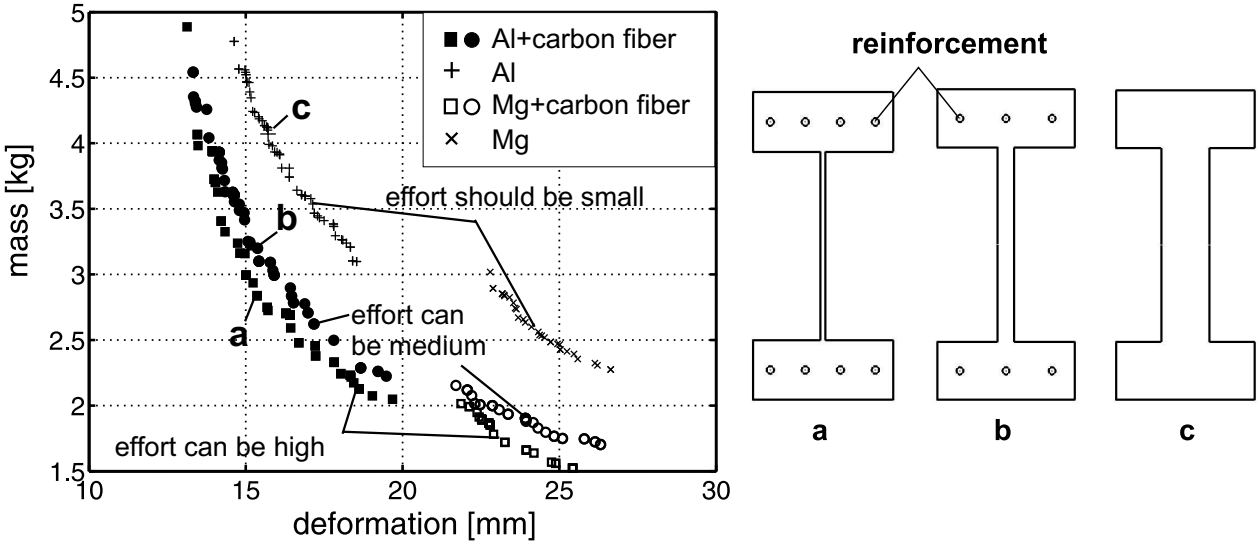

Fig. 5: Optimization results for the I-section beam: on the left side Pareto fronts for different manufacturing effort restrictions; resulting different designs on the right side

Results of the Space Frame Optimization

For the car space frame, multiple optimization runs were performed with different manufacturing effort restriction settings to determine the manufacturing effort influence on the optimal design. The results are plotted in Fig. 6 in the interesting range for micro cars. First, the manufacturing restrictions are neglected (O), then only the geometric manufacturing restrictions are added (+) and finally the manufacturing effort restriction is introduced (□). The 'ultimate' design would be located in the lower right corner in this diagram (high stiffness with low mass).

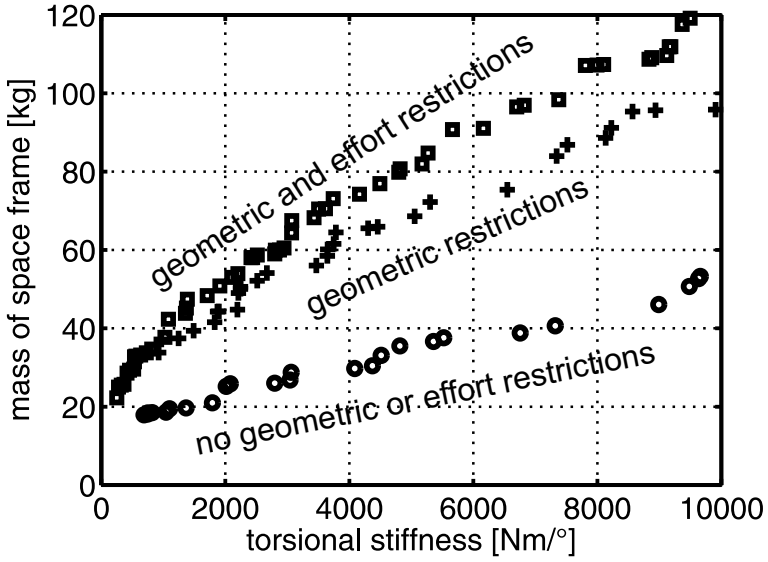

Fig. 6: Optimal solutions for car space-frame with varied manufacturing constraints

For the first run (O), most designs have magnesium profiles with a high carbon fiber volume ratio (≥25%). The mass is nearly doubled by introducing the geometric manufacturing constraints (+). This is mainly caused by much higher wall thicknesses for reinforced, extruded profiles and the limitation of the maximum dimensions of the rectangular cross sections (d_B!). Between the optimization with geometric manufacturing constraints (+) and the optimization with additional effort restrictions (□) relatively small differences can be seen for the goals, but the high percentage of magnesium profiles shifts to an even distribution for both matrix materials. Aluminum profiles can be manufactured with thinner wall thicknesses for the same outer dimensions and therefore the increase in mass is very small. Simultaneously the average volume ratio for carbon fibers (steel wires are ruled out for nearly every design) decreases. This affects the manufacturing effort for extrusion molding and machining positively.

	Al [%]	Al+steel [%]	Al+carbon [%]	Mg [%]	Mg+steel [%]	Mg+carbon [%]	mean volume ratio [%]
O	1.0	0.0	30.0	7.5	0.0	61.5	25.0
+	0.0	1.0	24.8	2.2	0.0	72.0	25.5
□	28.8	0.0	25.0	42.5	0.0	3.7	19.0

Table 1: Material distribution of floor pan profiles and mean volume ratio of reinforced profiles

In Table 1 the averaged material distribution of the floor pan profiles is shown. The absence of steel reinforced profiles is the result of two circumstances. First of all, no stress related restrictions were considered so the increased strength of reinforced profiles has no advantage. Only the increase

in stiffness together with the minimization of mass is important. Secondly, the higher material price of carbon did not provide a strong enough advantage for steel wires.

With further increasing manufacturing effort restrictions (not displayed in Fig. 6), it is better to use magnesium and aluminum profiles without reinforcement in one structure than to switch to an aluminum/carbon fiber combination for the whole space frame. The geometric dimensions of the profiles also change and provide insight into optimal design strategies.

The influence of the manufacturing constraints (geometric as well as effort) on the optimal designs is complex when they are all taken into account together. However, they can be described, or at least approximated with relatively few and easy to build fuzzy models. The result of the optimization is also interesting for the manufacturing processes. For example, the optimal designs depend highly on the minimum wall thicknesses for reinforced profiles. With an optimization introducing a 'desirable' minimum wall thickness, the potential gain from such designs should be communicated to the extrusion molding expert and possible research directions can be identified.

Conclusions

The combination of relatively cheap metal matrix materials with high performance reinforcing materials in hybrid structural members will change design philosophies in the next years. This development is enhanced by the adaptation of known manufacturing processes such as extrusion molding to produce reinforced parts with little additional effort.

To utilize the full potential of such components and structures, the basic design has to consider the possible chemical and thermo-mechanical incompatibilities, restrictions arising from the manufacturing processes itself (limiting geometric influences, but also consideration of manufacturing effort) and structural requirements. The presented optimization approach efficiently solves these problems and provides the engineer with optimal solutions. Fuzzy rule based systems are used to model qualitative knowledge in order to consider all important aspects even in early design stages, when no, or only few test and simulation data are available. They can be integrated into the optimization process like any other model and replaced if more accurate models become available. A limitation of the fuzzy rule based approach is the restricted complexity of the approximation models. The number of inputs for each model has to be small in order to evaluate the model output using human judgment.

The presented optimization problems show the potential of the utilized methods, clearly indicating the necessity to include the manufacturing aspects.

Acknowledgement

This paper is based on investigations of the collaborative research center SFB/TR10 which is kindly supported by the German Research Foundation (DFG).

References

[1] A. Klaus, M. Schomäcker, M. Kleiner: First Advances in the Manufacture of Composite Extrusions for Lightweight Constructions, Light Metal Age, Vol. 62 No. 8, pp 12-21, 2004

[2] M. Schikorra, M. Kleiner: Simulation of Aluminium-Steel Composite Extrusion, Proceedings of the NAFEMS World Conference, 17.05.-20.05. Malta, 2005

[3] K. Weinert, M. Lange: Machining of Magnesium Matrix Composites, Advanced Engineering Materials, Vol. 3 No. 12, pp 975-979, 2001

[4] M. Rais-Rohani: Manufacturing and Cost Considerations in Multidisciplinary Aircraft Design, NASA Grant NAG-1-1716, NASA Technical Reports Server, NASA, 1996

[5] B. Baier, C. Seeßelberg, B. Specht: Optimierung in der Strukturmechanik, Vieweg, Wiesbaden, 1994

[6] H. Langer, T. Pühlhofer, H. Baier: A Multiobjective Evolutionary Algorithm with Integrated Response Surface Functionalities for Configuration Optimization with Discrete Variables; Proceedings 10th AIAA/ISSMO Multidisciplinary Analysis and Optimization Conference 2004; 30.08. - 01.09. Albany, New York, USA, 2004

[7] R. Gleichmar: Approximationen und paralleles Rechnen bei der multidisziplinären Strukturoptimierung, PhD Thesis Technische Universität München, Institute of Lightweight Structures (LLB), 2004

[8] P. Hajela: Soft computing in multidisciplinary aerospace design - new directions for research, Progress in Aerospace Science, Vol. 38 No. 1, pp 1-21, 2002

[9] J. Durkin: Expert Systems: Design and Development, Macmillan, New York, 1994

doi:10.4028/www.scientific.net/AMR.10.153

Flexible and intelligent gripping technology for machining and handling of spatially curved extruded aluminum profiles

J. Fleischer[1, a], D. Ruch[1, b]

[1]wbk Institute of Production Science, Universität Karlsruhe (TH),

Kaiserstraße 12, 76128 Karlsruhe, Germany

[a]fleischer@wbk.uka.de, [b]ruch@wbk.uka.de

Keywords: Research, Clamping, Gripping, Flexible Production Systems

Abstract

With a novel extrusion process which is investigated in the Collaborative Research Center Transregio 10 (SFB/TR10), it is possible to manufacture spatially curved aluminum profiles. This process is the base for an automated small and medium size batch production of light-weight frame structures. For the handling and machining of the spatially curved profiles, highly flexible machines and manufacturing equipment are needed. Today's automated process chains do not reach a sufficient flexibility.

This article introduces a new approach to handle and machine spatially curved profiles using a flexible gripping and clamping system. Firstly, the requirements concerning the process comprehensive gripping technology, which have to be fulfilled for a flexible small and medium batch production of light-weight frame structures, are specified. Subsequently, the function and design of a flexible gripping and clamping system are described. Furthermore, metrological processes to maintain a once reached condition of order during the entire process chain are depicted.

Introduction

The wbk Institute of Production Science at the Universität Karlsruhe (TH) researches the fundamentals and technical possibilities to clamp and handle spatially curved profiles, with special regard to a flexible small and medium size batch production. The process chain for the flexible manufacturing is subdivided into the following process steps: Firstly, the spatially curved aluminum profiles are extruded with an innovative extrusion process [1]. During this process, the profiles are cut off by a buzz saw [2]. A combined handling and machining kinematics has the task to take over the extrusions after the cutting off and to machine them [3]. In a next step, the profiles are joined to a complete frame structure using laser beam welding or electromagnetic recasting [4].

The scientific scope of the research within the sub-project "flexible and intelligent gripping technology" is to maintain a once reached condition of order of the workpiece during the entire process chain. A novel gripping and clamping system is developed, which allows the automatic positioning and alignment of the spatially curved profiles without any manual intervention.

Requirements and state-of-the-art

The new extrusion method allows producing geometrically variable extrusion profiles with a minimum radius of up to 500 mm. The profile length may vary between 450 mm and 2,000 mm. Open profile cross-sections as well as closed profile cross-sections can be produced. These constraints demand for a clamping system that is able to adapt itself to the different geometries. In order to be suitable for an automated and flexible small batch production, this must be done automatically. To perform a precise machining, the profile has to be clamped with a high stiffness and a high accuracy. Because of the relative low stiffness of the extruded profiles, the clamping

system has to be able to clamp the workpiece near the tool contact. In addition it is aspired to maintain a once reached condition of order of the workpiece during the entire process chain.

Basically, today there are two different methods used for clamping and machining complex workpieces. The first and common method in the industry is to use rigid clamping fixtures, which fix the workpiece over the entire length to the machine table. The machining can then be performed for instance with a portal milling machine. This way of clamping and machining allows a well-defined positioning of the workpieces and thus makes it possible to machine the workpieces in a high accuracy. Such clamping fixtures are normally adapted to one special geometry. The disadvantages of this clamping method are the high production costs of the rigid clamping fixtures and the low degree of flexibility.

An alternative solution is the application of a flexible clamping fixture (Figure 1). These are built up out of several clamping units, which have the ability to adapt to the workpiece over its entire length [5]. These flexible clamping systems are used for example in the aircraft industry. However, such clamping fixtures are very complex with regard to design and control because of their large number of numerically controlled axes. Furthermore, the workspace of the machine kinematics has to be at least as large as the workpiece itself, in order to allow the machining over the entire length.

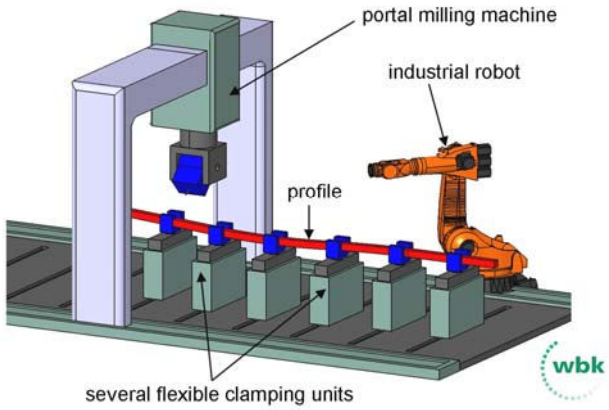

Figure 1: Machining with current machine technology

To allow an automated workpiece handling additional devices, for example industrial robots or special purpose machines, are used (Figure 1). These machines are normally adapted to one special product. For this reason the loading and unloading is often carried out manually within small and medium size batch production.

Design of the gripping and clamping system

In order to fulfill the above mentioned requirements, a novel clamping concept has been developed within this research project (Figure 2). In contrast to conventional ways of machining, the profile is not clamped over the entire length of the workpiece but is locally fixed with a major gripper (close to the machining tool). For a flexible handling of the workpieces, a secondary gripper is mounted to an industrial robot. The robot is also used to move and orientate the profile within the major gripper. By this, it is possible to machine the profile over its entire length. The complexity of the constructive design and the control can be reduced clearly using this novel machining concept, as the number of actuated degrees of freedom is kept to a minimum. Beyond that, the machining space needed for the machining kinematics is small in contrast to the solution with flexible clamping systems.

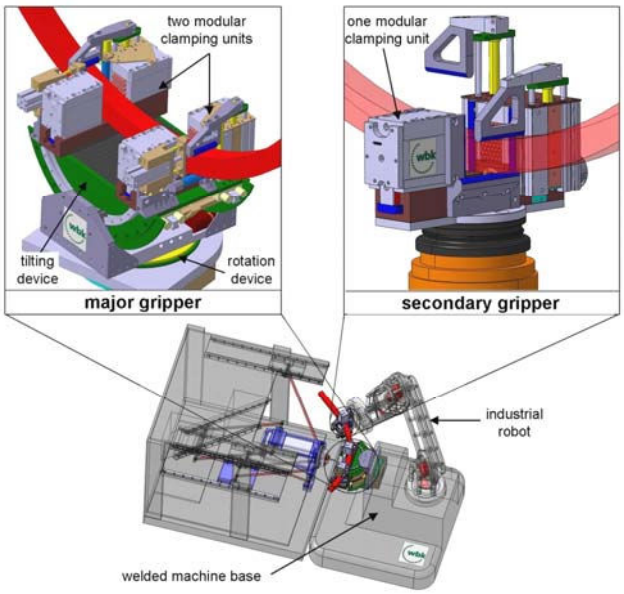

Figure 2: Machining strategy with major gripper and secondary gripper

In order to realize a comprehensive gripping system for clamping and handling of the profiles, a highly flexible modular clamping unit has been developed which enables to fix profiles with different cross-sections and orientations definitely (Figure 3). The major gripper comprises two clamping units, the secondary gripper comprises one clamping unit. The clamping unit basically exists out of the following four elements: The clamping jaw base, one fixed and one moveable clamping jaw and of a guiding unit. Different kind of actuators can be adapted to the clamping unit, so that the required clamping force is available for the respective application. The required clamping force of the major gripper is applied with a hydraulic cylinder due to the high energy density of hydraulic systems. The clamping force of the secondary gripper is applied to the profile pneumatically, as in this case the required forces are obviously smaller than in the major gripper.

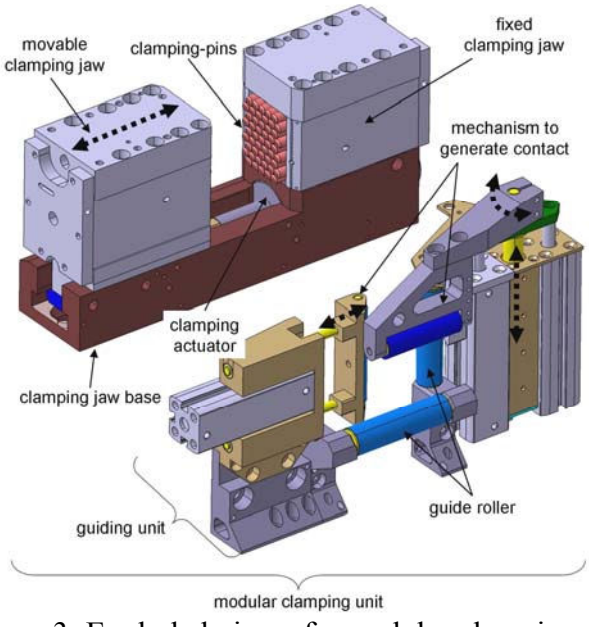

Figure 3: Exploded view of a modular clamping unit

The two clamping units of the major gripper are positioned in such a way, that it is possible to move the profile within the gripper along the longitudinal axis of the profile (Figure 4). During the machining process, the profile is securely clamped by the two clamping units. The clamping units are fixed on top of a tilting and rotation device, which allows the alignment of the profile for the machining. The tilting and rotation device is firmly connected to the welded machine base (Figure 2). The two main functions “clamping of the profile” and “guiding of the profile” are separated constructively (Figure 3). The guiding units of the major gripper are located directly besides the clamping units (Figure 4). At the secondary gripper, similar units are used, which are simplified due to the lower requirements (Figure 5).

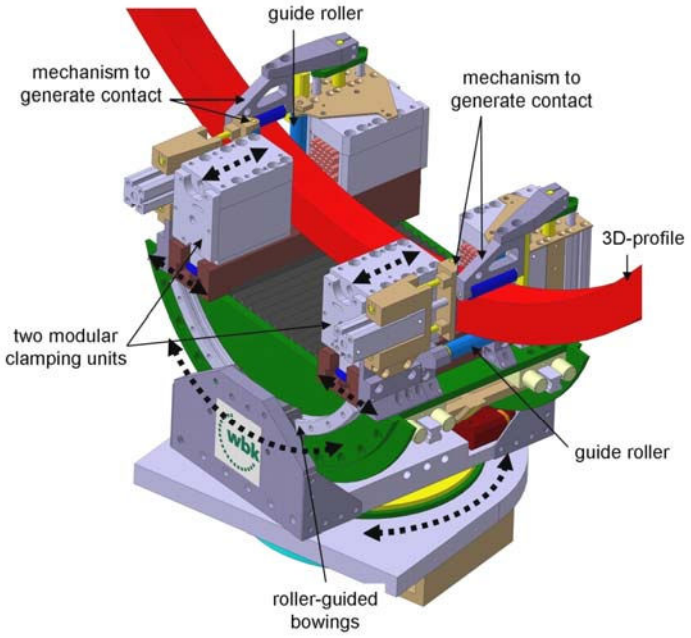

Figure 4: CAD-model of the major gripper

The two clamping units of the major gripper can be pivoted by the tilting device by ±30°. Therefore, it is guaranteed that drilling and milling can always be executed orthogonally to the profile surface. The tilting device is constructed in such a way, that the Tool Center Point (TCP) of the machine is always in the centre of the tilting device. This is realized with two roller-guided bowings. The guide rails of the roller-guided bowings move around the TCP, when the gripper is executing a tilting movement (Figure 6). The guiding carriages of the roller-guided bowings are firmly screwed to the rotation device. The two rotational axes of the rotation device and the tilting device have to intersect in the TCP, so that the centre of the rotational movement is close to the TCP. The rotational axis enables the pivot of the profile by more than 180°. Therefore it is possible to machine the back side of the profile with a milling cutter spindle. Both, the tilting axis and the rotational axis are passive axes which are positioned through the movement of the profiles. The angle position of the axes is hereby adjusted by the profile with the secondary gripper and the industrial robot. For the machining of the profile, both axes are being fixed. This enables a direct force flow from the cutting tool over the profile to the machine base. Additionally, the free end of the profile is supported by the secondary gripper in order to avoid free oscillations.

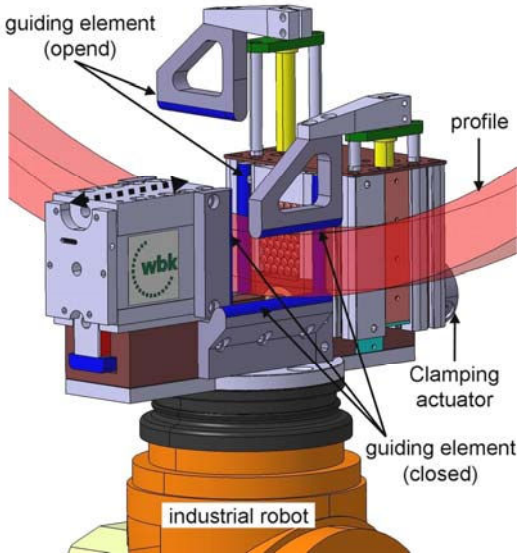

Figure 5: CAD-model of the handling gripper (secondary gripper)

In order to allow different machining processes, the two clamping units can be positioned independently. Drilling, for example, is executed in the middle of two separated clamping units. Moving both clamping units to one side, end milling of the profiles gets possible. For this, the two clamping units are connected to the tilting and rotation device by linear guides. The driving motors of the belt drive are integrated inside the tilting device. The positions of the clamping units are measured with directly operating linear measuring devices. Therefore, it is possible to vary the distance of the clamping units in such a way, that the profile can be clamped optimally for each possible machining process. During machining both clamping units are fixed.

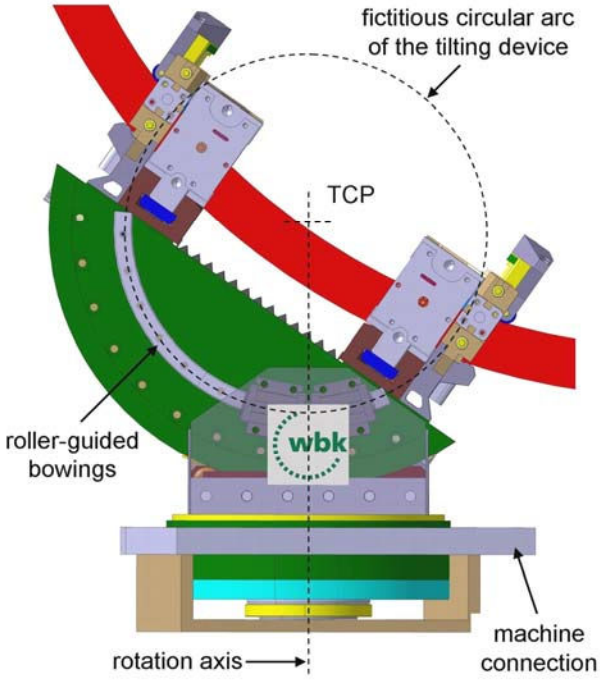

Figure 6: Tilting axis and rotation axis

The intrinsically clamping of the profile is done by multipoint-grippers, also called omni-grippers. This permits the clamping of different profile cross-sections with different alignments [6]. Multipoint-grippers are capable of casting nearly any workpiece contour in a reversible way. With

the multipoint-grippers, a combination of form fit and force closure is obtained between the profiles and the clamping units. The generated form matching between the clamping unit and the workpiece minimizes the mechanical strain [7].

The fixing of the profile can be illustrated with three process steps. At first, the clamping-pins of the multipoint-grippers are adapted to the surface contour of the profile using compressed air. After casting of the profile contour, the clamping-pins are arrest to the enclosure. After the fixing of the pins, a clamping force can be applied to the profile. In order to prevent plastic deformation or slipping of the profile, the hydraulic pressure of the clamping actuator can be controlled continuously. Figure 6 shows the prototype of the clamping units of the major gripper, fixing a spatially curved profile.

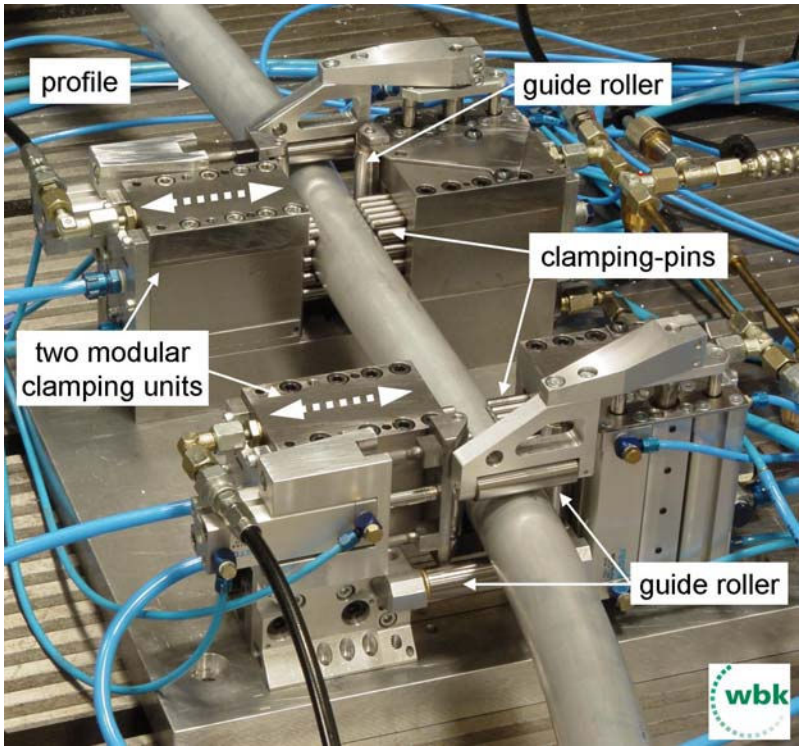

Figure 7: Clamped profile in the major gripper
(without tilting and rotation device)

In order to move the profile within the clamping fixture, the multipoint gripper has to be released. In doing so, it has to be avoided that the spatially curved profile gets stuck between the pins. It is required that all pins of the multipoint gripper are fetched back automatically. Therefore, the interior of the multipoint gripper consists of two pressure chambers. The front and the back chambers are separated by a moveable cutting-off plunger (Figure 8). Once a pneumatic excess pressure in the back chamber is generated, the cutting-off plunger moves forward. Simultaneously, the single pins of the clamping fixture move forward until they are connected either to the profile or to the cutting-off plunger. For the automated fetching back of the single pins an excess inside the front chamber is generated. Due to the excess the cutting-off plunger is moved backwards into its initial position. Thereby, the single pins are picked up by the cutting off-plunger and are also moved back into their initial position. The clamping of the single pins is realized with a hydraulic clamping element integrated into the top cover of the clamping jaw (Figure 8). The pins are arranged in such a way, that the clamping force is distributed uniformly to all pins. Thus, a reciprocal clamping of the single pins inside the enclosure is achieved.

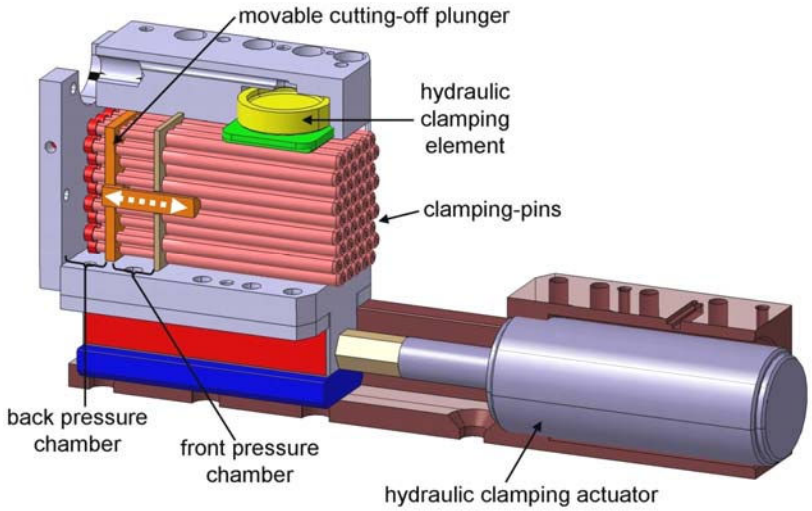

Figure 8: Sectional view of the movable clamping jaw and the clamping jaw base

The axial forces to the clamping-pins, which are generated during the gripping process, can be transmitted to the enclosure by frictional forces. Using a clamping force of 20 kN an axial clamping force of 6 kN can be achieved, when a constant static friction coefficient of μ=0.1 is assumed. Calculations with abstract finite element models result in maximal equivalent stresses of 310 N/mm^2 at the contact area of the clamping-pins (Figure 9).

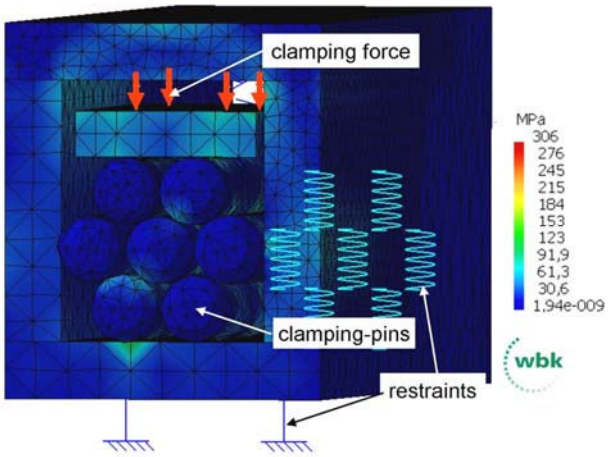

Figure 9: FEM-calculation of the contacts of the pins

Strategies for measuring the profile position

The profile guiding and profile positioning is realized by four guide rollers which are fixed to the clamping units in pairs (Figure 8). The profile is clamped to the guiding rolls during the whole process with a mechanism to generate contact between the profile and the guiding rolls. The guiding mechanism is actuated pneumatically. The rolls of the mechanism for generating a contact can be swung outwards in an angle of 90° (see Figure 2, 3). Thus, the profiles can be inserted easily into the clamping system before machining and can be removed afterwards.

Using rectangular profiles, the profile and the guiding rollers are in a linear contact. This enables to define five degrees of freedom of the profile position. The sixth degree of freedom describes the displacement of the profile along the longitudinal axis. As long as the profile is not clamped it is indefinite in one degree of freedom. Using circular profile cross-sections only four degrees of freedom can be defined. The displacement of the profile along the longitudinal axis and the

rotational motion around the longitudinal axis itself are indefinite. It is necessary to use an adequate metrological process for defining the lacking degrees of freedom. At present, several approaches of measurement techniques are investigated. The longitudinal displacement of the profile can, for instance, be measured by friction rolls, by Reflection Light Scanners, by Laser Surface Velocimeters or by using the principle of an optical mouse, which utilizes the surface structure of the profile and calculates the displacement by correlation. For all methods a reference mark is required in order to reference the systems after inserting the profiles. For instance the reference mark can be placed on the profile during the extrusion process and afterwards be detected by a Laser Reflection Light Scanner (Figure 10, right). In the first instance the achievable preciseness was acquired by measuring linear profiles. Within the experiments with an optical mouse several parameters including the process velocity, the measured length, the structure of the surface, the sampling rate or the type of lightning have been varied. With an optical mouse a minimal deviation of 0.2% was reached using a color sprinkled profile, which was scanned with a process velocity of 320mm/min. In this case the profile surface was lighted by a laser-mouse. Using a friction roll, deviations between 0.015% and 0.2% have been obtained. In this case, stop-and-go trials, which appear in reality, showed the largest deviations. Within the experiments with the friction roll, the contact pressing force, the process velocity, the material of the friction roll and the length to be measured have been varied.

Slight marks with a gage of about 70 µm which were engraved on the profile surface with a laser reached good results in conducted measurements. With a Reflection Light Scanner it was possible to detect these marks certainly. With multiple marks it is imaginable that the profile position can be determined incrementally if the reference marks are placed on the profile in well-defined distances (Figure 10). This process works in analogy to the gaging process of an incremental measuring system. The rotary motion around the longitudinal axis of profiles with round profile cross-sections can be detected in the same way by an additional mark, which is displaced on the surface in a 90° angle relatively to the other marks. First experiments with this method on a straight profile achieved a repeat accuracy of ±5 µm, for a measured length of 1,600 mm. Thereby, the sensor has been moved instead of the profile. As reference, the linear measuring scale of a serial machining device has been utilized for the experimental setup. However, tests with two-dimensionally curved profiles showed, that the intensity of the reflected laser beam is not sufficient when the surface of the workpiece is inclined thus resulting in errors of measurements. Furthermore, the system shows a sensitive towards scratches on the surface of the workpiece.

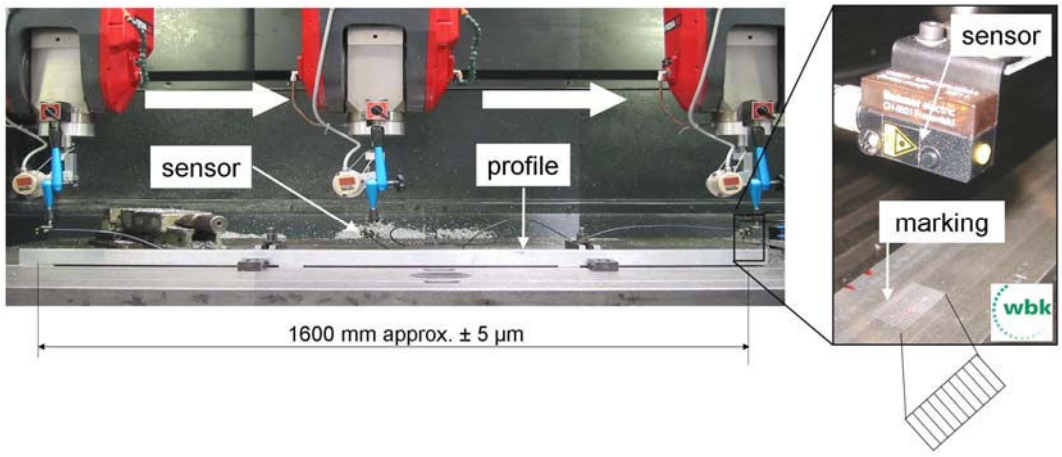

Figure 10: Position measurements with marks

In order to definitely identify the markings, the reflection light scanner shall be replaced by an image processing system. This system is insensitive towards an obliquely positioned profile surface

and capable to distinguish between markings and scratches. First tests showed promising results. An image processing system is a promising method to acquire the position of the profile within the major gripper.

Summary and perspective

For the automated small and medium size batch production of light-weight frame structures with spatially curved profiles, highly flexible machines and manufacturing equipment are needed. Today's automated process chains do not meet these requirements sufficiently. The presented highly flexible clamping concept permits to grip and clamp profiles, which may vary in geometry and quantity, without a specially adapted clamping fixture or clamping system. With the combination of a major and a secondary gripper it is possible to machine profiles and to handle the profiles continuously with a once reached condition of order over the entire length of the process chain. For an exact positioning of the profiles, several metrological processes have been tested. With multiple marks in well-defined distances on a linear profile it was possible to determine the position of the profiles incrementally in a high accuracy. Tests with two-dimensionally curved profiles showed, that the detection of the marks with a Reflection Light Scanner is not sufficient. The application of an image processing system is a promising approach for the detection of the marks. Further tests with an image processing systems take place in future.

Acknowledgment

This paper is based on investigations of the collaborative research centre SFB/TR10 which is kindly supported by the German Research Foundation (DFG).

References

[1] Klaus, A.; Kleiner, M.: Developments in the Manufacture of Curved Extruded Profiles – Past, Present, and Future, Light Metal Age Vol. 62 (2004), No. 7, pp. 22-32

[2] Fleischer, J.; Stengel, G.: Bahngenerierung für eine robotergeführte Abtrenneinheit für räumlich gekrümmte Strangpressprofile. Einsatz eines CAD-Systems zur Programmierung einer fliegenden Säge, wt Werkstattstechnik online Jahrgang 94 (2004), H. 9, S. 457-461

[3] Fleischer, J.; Schmidt-Ewig, J.P.: Innovative Machine Kinematics for Combined Handling and Machining of Three-Dimensional Curved Lightweight Extrusion Structures, Annals of the CIRP Volume 54/1, S. 317-320, 2005

[4] Trautmann, A.; Roeren, S.; Zäh, M.F.: Welding of Extruded Aluminium Profiles by a Hybrid Bifocal Laser System, Lane, 2004

[5] Homepage Fa. Fooke GmbH, http://www.fooke.de, 10.2005

[6] Homepage Fa. Matrix GmbH, http://www.matrix-innovations.com, 10.2005

[7] Hesse, S.: Greifer Praxis: Greifer in der Handhabungstechnik, Vogel Buchverlag, 1. Auflage, Würzburg, 1991

doi:10.4028/www.scientific.net/AMR.10.163

Design and Optimization of an Innovative Machine Kinematics for Combined Handling and Machining

J. Fleischer[1, a], J. P. Schmidt-Ewig[1, b]

[1]wbk Institute of Production Science, Universität Karlsruhe (TH),

Kaiserstraße 12, 76128 Karlsruhe, Germany

[a]Fleischer@wbk.uka.de, [b]SchmidtEwig@wbk.uka.de

Keywords: kinematics, handling, machining

Abstract The importance of rigid and self supporting space frame structures for the automotive and aerospace industry continually increases. To meet the market requirements for a flexible and competitive small batch production, innovative machine concepts must be investigated. By integrating handling and machining capabilities into one machine structure, redundant degrees of freedom can be reduced and a former idle economic potential can be made use of.

This paper introduces a systematic approach to reveal synergetic potentials that emerge by integrating two different fields of function, the handling and the machining. Therewith a matrix with technical solutions for a combination of handling and machining is generated. These solutions are the base for new machine concepts that fulfill both tasks with a minimal number of machine axes. The authors present a machine concept which is combined out of a four-axes parallel kinematics and a conventional serial kinematics. The two kinematic structures collaborate and allow the product flexible handling and machining of three dimensional rounded extrusions with a minimal technical effort. The machine concept is dimensioned and optimized for a maximal stiffness by the coupling of a multi body simulation to an external parameter optimization software. The optimization results show that the stiffness of the machine concept could be explicitly improved.

This paper is based on investigations of the collaborative research centre SFB/TR10 which is kindly supported by the German Research Foundation (DFG).

Introduction

The aim of the collaborative research center SFB/TR10 is to investigate the scientific fundamentals and methods for arranging integrated process chains that allow a product flexible and automated small and medium batch production of space frame structures. In principle, the process chain can be realized on the basis of current machine technology. Yet, current solutions for automation are too expensive for an economic small batch production. In order to minimize this disadvantage, innovative machine concepts for the machining and handling of three-dimensional curved extrusions are investigated in this paper. The work focuses on the integration of these former separately regarded tasks into a single machine structure. This offers new potentials for an automated and economic production: Time-consuming clamping and alignment procedures between the different processes can be reduced. In addition, redundant machine axes can be eliminated by integrating the two different fields of function, handling and machining.

Requirements

To specify the requirements of the machine structure for handling and machining, initially both cases are regarded separately. A machine kinematics that is only used for handling has to take over the cut-off extrusions and to supply the machining centre. After machining, the extrusions must be positioned for the different joining processes. In order to fulfil this task, the kinematics must

possess three translational and three rotational degrees of freedom. The required workspace approximately corresponds to the workspace of a common industrial robot with a range of 2,000 mm. For a precise positioning of the profiles a repeat accuracy of about 0.1 mm is needed. In order to allow flexible offline programming, the highest possible absolute accuracy is aspired. High accelerations are of minor importance for handling.

A kinematic structure for machining must be able to carry out all translational and rotational movements needed for the metal cutting (3+2 axes milling). Further, it must be possible to machine five sides of the extrusions without a new clamping procedure. To perform a precise machining, the kinematic structure requires high stiffness and accuracy. In order to reach a close shape tolerance while performing processes like circular milling, a high acceleration of the tool center point is needed. The three last-mentioned requirements are not necessary continuously within the entire workspace as they are only needed for the single machining steps (drilling a borehole, machining the extrusion end).

A further requirement for a successful milling process is having the extrusion clamped near the tool contact. This primarily affects the flexible and intelligent clamping unit which is also developed within this collaborative research center. However, there are strong interdependencies between the design of the clamping unit and the kinematic structure resulting in additional restrictions for the kinematics.

State of the Art

Regarding the state of the art, it can be seen that technical solutions already exist for the separated fields of function: An articulated robot with six degrees of freedom and an appropriate workspace can be used for handling. The machining of long extrusions can be performed with a portal milling machine. The clamping of extrusions is generally done with the help of fixtures that allow fixing the workpiece over the entire length to the machine table. The disadvantages of this solution are the high production costs of the fixtures and a low degree of flexibility. An alternative for the product flexible clamping of extrusions is the application of flexible clamping fixtures which are capable for fixing the workpiece over the entire length at variable locations. However, such clamping fixtures are very complex with regard to design and control because of their large number of numerically controlled axes.

The realization of the production system based on current technology is only possible with a high economic and technical effort due to the high number of NC-axes and the large workspace of the machining kinematics.

Integration of Handling and Machining

This disadvantage can be eliminated by integrating handling and machining. Theoretically all movements and rotations needed for the two tasks can be realized with the minimal number of six machine axes. The necessary machine proprieties can be derived from the requirements mentioned above: A kinematic structure is needed that allows three translational and three rotational movements and possesses a high stiffness, accuracy, and acceleration within a large workspace. These high requirements cause the realisation of such a structure to be very costly again. Especially the demand for a high stiffness and accuracy within a large workspace determines that a realistic economization is hardly possible with this approach.

This raises the question which degrees of freedom can be used for both tasks without a considerable additional technical effort. In order to go further into the question for an appropriate integration of functions, a methodical approach helps to come closer to a cost efficient solution (Figure 1). In analogy to well-known design methods (e.g. the design method of Pahl and Beitz [1] and the axiomatic design approach of Suh [2]) the system is decomposed into independent sub-functions and the respective requirements are determined. In this case, the sub-functions for

integration are regarded as the different machine axes that are needed for carrying out the translational and rotational movements of the workpiece. At this point, the handling and machining are still regarded separately, so that in total twelve different degrees of freedom occur.

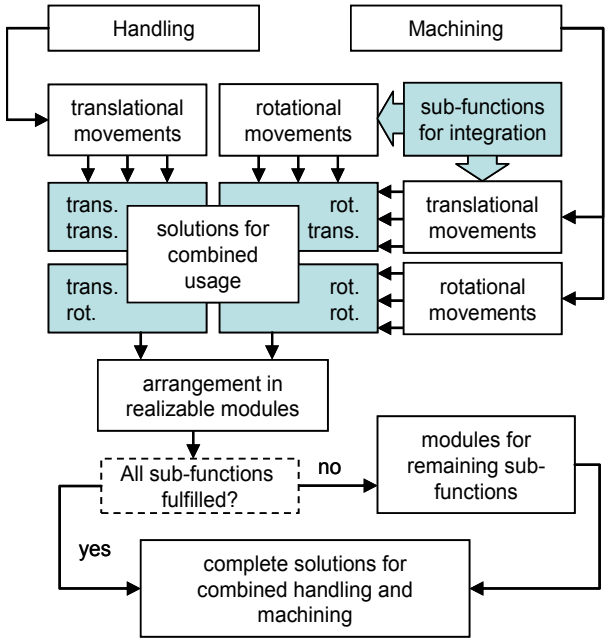

Figure 1: Methodical approach for integrating functions.

In order to find possibilities for integrating the fields of function, the sub-functions and their requirements are combined within a morphological structure. The combinations reveal different solutions for a concerted use of machine axes together with the requirements that have to be kept for a realization:

- Solution 1: Translational movements are concertedly used for handling and machining.
- Solution 2: Rotational movements are concertedly used for handling and machining.
- Solution 3: Translational movements are additionally used for rotating.
- Solution 4: Rotational movements are additionally used for translation.

Regarding the first solution, it can be seen that a machine axis which is used for translational handling and machining motions needs a high stiffness, accuracy, and acceleration within a large workspace. Again, the high requirements cause the realisation to be very costly. However, if these requirements are not needed continuously within the entire workspace, a further possibility for a combined usage is given. The handling kinematics can be used to position the extrusion within the workspace for a subsequent machining operation. By this, the workspace of the machining axes can significantly be reduced. The conditions for this solution are that a measurement device detects the exact position of the workpiece and a clamping unit absorbs the machining forces.

If rotational movements are used for both fields of function (Solution 2) a stiff kinematic structure is needed that allows three rotations with high accuracy and acceleration. Because the regarded axes are only used for rotating the workpiece, the large workspace needed for handling does not affect the requirements negatively. Technical solutions that meet the necessary requirements already exist, like the pivoted milling head of a five-axis machine tool. Thus, the direct combined usage of rotational movements is possible with an acceptable technical effort.

In the third solution, translational movements are additionally used for rotating the workpiece. This is possible with the principle shown in Figure 2.

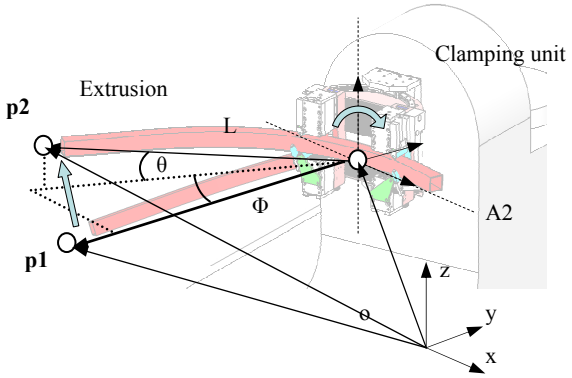

Figure 2: Transforming translational movements into rotations.

The front end of the extrusion (**p1**) is fixed in a pivoted clamping unit with two rotational degrees of freedom that are not driven, but can rotate freely. The angle can be adjusted by moving the rear end of the extrusion (**p2**). The orientation of the extrusion can be described with help of the three Eulerian angles Φ, θ und ψ [3]. For a rotation around two axes, the third angle ψ is always equal to zero. The following relation exists between the rotation and the position of the rear extrusion end:

$$\mathbf{p2} = \mathbf{p1} + \mathrm{L} \cdot \begin{bmatrix} \cos\theta \cdot \sin\phi \\ -\cos\theta \cdot \cos\phi \\ -\sin\theta \end{bmatrix} \tag{1}$$

Thus, an accurate rotation can be achieved by a relatively imprecise translational movement.
If this principle is reversed, precise rotations can be transformed into large but rather imprecise translational movements (Solution 4).

Based on the different solutions for eliminating redundant machine axes, realizable modules can be constructed which accomplish multiple sub-functions. For sub-functions that can not be fulfilled by a synergetic usage, separate modules have to be developed. With the various modules several machine concepts were composed which are able to perform both fields of function. In a next step the concepts were benchmarked based on the following criteria:

- Flexibility with respect to the extrusion geometry
- Technical effort for realization
- Attainable accelerations
- Complexity of the clamping unit

A detailed presentation of the best rated machine concept is given in the following section.

Machine Concept For combined Handling And Machining

Figure 3 schematically shows a machine concept that allows the automated machining of curved extrusions by concertedly using handling and machining axes. The concept is built up out of a serial kinematic structure based on an articulated robot and a parallel kinematic structure. In order to guarantee effective machining, a flexible clamping unit has the task to fix the extrusion near the tool center point.

The serial part of the machine structure is used for flexible handling of the extrusions. In addition, it is used for adjusting two machining angles as described in solution 3. For this, the clamping unit is pivoted and possesses two rotational degrees of freedom allowing a rotation around the tool center point (Figure 4).

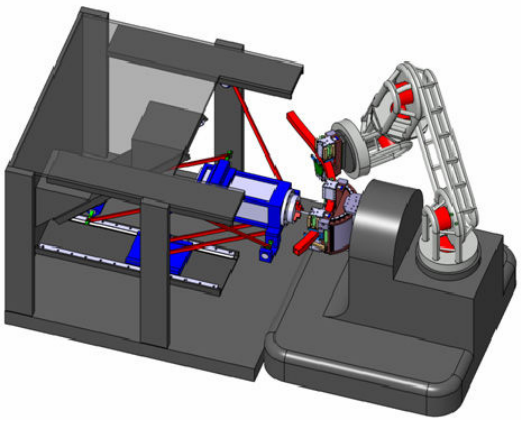

Figure 3: Concept for integrated handling and machining.

After having adjusted the desired angle, the rotation axes can be locked to reach a high stiffness. This way, the serial kinematics does not bear any machining forces, but only damps possible vibrations of the free extrusion end. A second synergetic advantage results from integrating solution 1 into the machine concept. For this the extrusion is moved through the clamping unit so that the part of the extrusion which is to be machined is located near the tool center point. Thus, the required workspace of the machining axes and the complexity of the clamping unit can clearly be reduced.

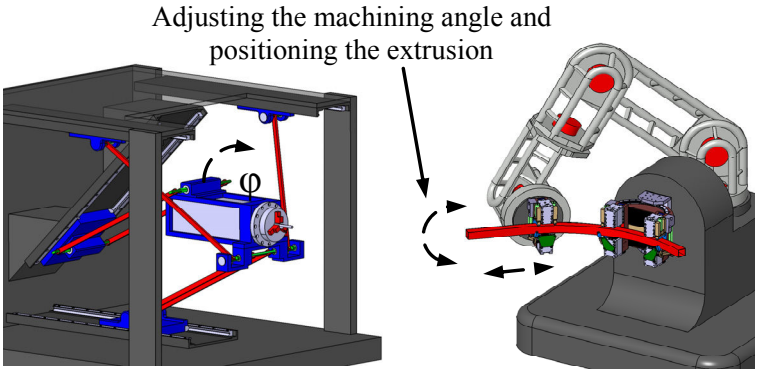

Figure 4: Components of the machine concept.

The entire procedure for machining extrusions with this machine concept is described in the following:

Step 1: Extrusion is positioned in the clamping unit.
Step 2: Machining angle is adjusted.
Step 3: Rotation axes are locked.
Step 4: Extrusion is machined.

The steps are repeated until the machining process is completed.

The translational motions required for machining are not executed by the extrusion but by the spindle unit. For this, three further degrees of freedom with high stiffness, accuracy, and acceleration are needed within a rather small workspace of about 250 mm x 250 mm x 150 mm. These requirements match the characteristics of parallel kinematic structures. Parallel kinematics feature a rather poor ratio between installation size and workspace, but offer high accelerations due

to the small moving mass. For five-sided machining, an additional rotation axis is needed which allows a 90° tilting of the spindle unit.

While a standard industrial robot can be used for the serial kinematics, no suitable concept could be found for the parallel kinematics within a literature survey. Most activities in this domain regard either three- or six-axis solutions [4] [5]. In addition, the most parallel kinematic structures perform only small tilting angles or need additional actuators to eliminate singularities [6]. The existing four-axes parallel kinematic concepts are not directly applicable for the task because of a none sufficient accessibility of the workspace [7] or too small tilting abilities [8].

For this reason, a novel parallel kinematic structure with 4 axes has been developed on the basis of existing concepts. A prototype of this kinematics will be implemented within the collaborative research center. The design is dimensioned and optimized with the help of a methodology for simulating and optimizing machine tools during the concept and design stadium [9].

Simulation and Optimization of the machine concept

Figure 5 shows the first design approach of the parallel kinematics. The geometry was chosen so that the basic requirement of a collision-free movement through the desired workspace is possible. The spindle unit is driven by four slides and is fixed by six links. The four links that are attached at the front side of the spindle unit completely determine its translational position, but still allow one rotational motion. The rotation angle is adjusted by the remaining slide which is tilted by 45°. This arrangement features an almost linear behavior between the motion of the rear slide and the angle of the spindle unit.

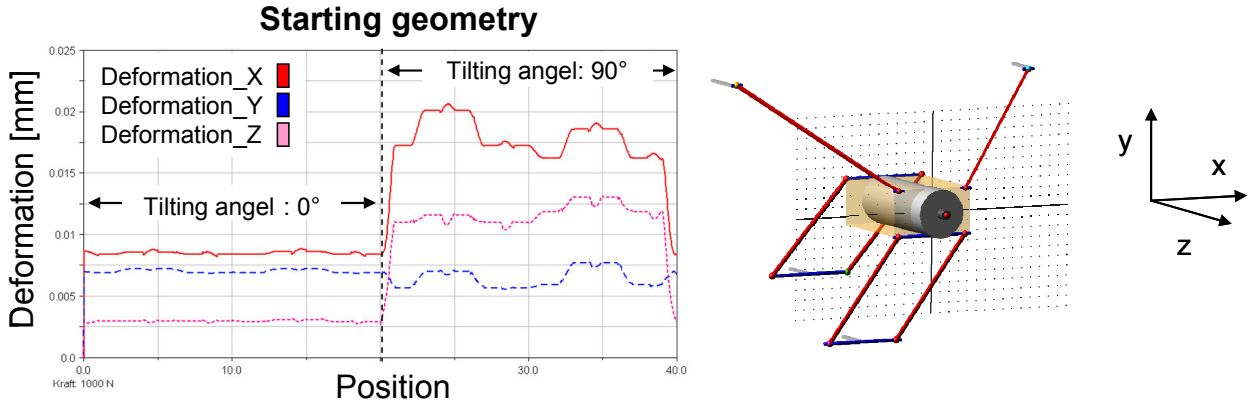

Figure 5: Deformation characteristics of the first design approach

For the determination of the machine proprieties for different positions of the tool centre point (TCP) a multi-body-simulation (MBS) model of the first design approach is built up. In order to simulate the deformation behavior, the stiffness of the twelve joints and the six links is integrated into the model by bushing elements. A simulation sequence is set up, during which the TCP is moved along the edges of a workspace with a size of 250 mm x 250 mm x 150 mm. This is done with a tilting angle around the x-axis of 0° and 90°. The sequence is repeated three times, whereas a force of 1000 N in X-, Y-, and Z-direction is applied to the TCP, respectively.

An investigation that was performed with this simulation sequence has shown that the first design approach is generally meets the requirements for machining. Yet, its static deformation characteristics still has potentials for improvement. The minimal stiffness of 50 N/µm is sufficient for the machining of aluminum extrusions, yet a higher value is aspired in order to raise the machining quality and accuracy. The deformation characteristics of the structure also is highly inhomogeneous because the stiffness varies within the range of 50 N/µm within the workspace. A further negative aspect is the torsion strain that occurs in the links. Aim is to have only tensile and

compression loadings, so that a construction with a small cross section and a small mass of the links is possible.

In order to improve the machine characteristics, an optimization of the design approach is performed, by coupling the MBS-model to an external parameter optimization software. A prerequisite for the optimization is the possibility to investigate the characteristics of different design geometries in a short period of time. For this, the MBS-model is parameterized. Overall 14 geometry parameters can be varied which consider the slide positions, the length of the links, the joint positions at the spindle units and the tilting angle of the rear slide. Due to the fact, that the link stiffness is a function of the length, this value also is parameterized. In order to consider different workspace positions during the optimization, the simulation sequence described above is used. The movements of the sliders, that are needed for the specified movement of the tool centre point are also dependent on the geometry parameters. Thus, a parametric description of the inverse kinematics problem is implemented in the model, which allows to calculate the required slider movements.

The basic sequence of the parameter optimization is shown in figure 6. The geometry parameters are included in the optimization software and can be varied by it. The new parameters are passed over to the MBS-Software by an ASCII-File. The Solver of the multi-body-simulation calculates the characteristics of the according machine geometry and writes the results into a second ASCII-File. The optimization software accesses the results and compares them to a predefined objective and restrictions.

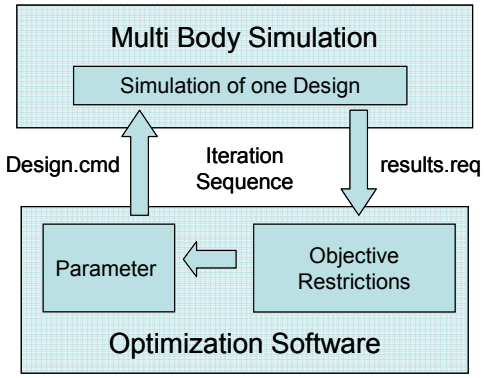

Figure 6: Optimization sequence

In this case the objective is to minimize the maximal deformation occurring during the simulation sequence. In order to reduce the torsion strain in the links, their torsion stiffness is highly reduced. Thus, an occurring torsion strain leads to a large overall deformation, causing the optimization software to discard the according design. In order to avoid collisions, different additional restrictions are specified. For example, the distance between the rear links must be smaller than the distance of the front links. If this criteria is not met, again the design is discarded.

The optimization sequence is controlled by a genetic algorithm, which are comparatively robust and also provide good results if many parameters are varied at the same time [10]. A starting population of 60 designs is optimized within 12 generations. The maximal deformation of 0,0212 mm could be gradually reduced. After 9 generations the maximal deformation value constituted 54% of the initial value. The last three iterations did not improve the deformation anymore. This indicates that a minimum was found an a further variation of parameters does not result in further improvements. The deformation characteristics of the optimized geometry is shown in figure 7.

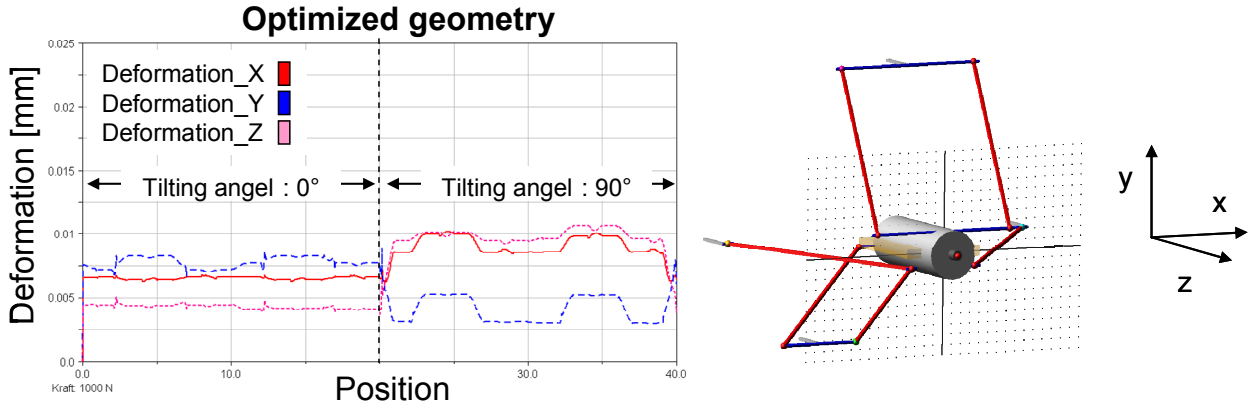

Figure 7: Deformation characteristics of the first optimized design

The stiffness of the machine structure could be improved to approximately 100 N/µm. In addition the deformation characteristics could clearly be homogenized. Further investigations have shown, that the links in the new geometry are only loaded in their longitudinal direction and no torsion stresses occur any more.

The consideration of all interdependencies within the optimization model is very extensive. Thus, the structure normally has to be modified slightly during the further design work. For this reason a design study of the optimized geometry was performed which gives helpful information on which parameter can be varied, without influencing the machine characteristics significantly.

The optimization results show, that the parallel kinematic design is well suitable for the machining operations. In combination with the serial kinematics, an automated 3+5 axes machining of extrusions with a length of up to 2000 mm can be realized. In addition the extrusion can be handled within a circular working area with a diameter of approximately 4000 mm. The integration of handling and machining makes it possible, to perform both tasks with a reduced number of machine axes and an minimal technical and economic effort.

Summary

The combination of handling and machining offers high economic potential by reducing redundant degrees of freedom. In order to find a suitable kinematic structure, the requirements were specified and different solutions for the integration of the two fields of function were systematically investigated. Based on this, a machine concept was created that allows an integration of handling and machining. The first design approach of the concept was simulated and optimized regarding its stiffness. The optimization results show that the stiffness of the machine concept could be explicitly improved. A prototype of the machine concept will be implemented within the further course of the activities.

References

[1] Pahl, G., Beitz, W., 1996, Engineering Design: Systematic Approach, Springer-Verlag, Berlin, 2. revised edition edited by Wallace, K.

[2] Suh, N. P., 2001, Axiomatic Design, advances and applications, Oxford University Press, Oxford, New York.

[3] Shabana, A.A., 2001, Computational Dynamics, John Wiley & Sons, Inc., New York.

[4] Merlet, J.-P., 200, Parallel Robots, Kluwer Academic Publishers.

[5] Weck, M., Staimer, D., 2002, Parallel Kinematic Machine Tools - Current State and Future Potentials, Annals of the CIRP, 51/2:671-683.

[6] Neugebauer, R., Schwaar, M., Ihlenfeldt, S., Pritschow, G., Eppler, C., Garber, T., 2002, New Approaches to Machine Structures to overcome the Limits of Classical Parallel Structures, Annals of the CIRP, 51/1:293-296.

[7] Pierrot, F. et al.: H4 parallel robot: modeling, design and preliminary experiments, IEEE Int. Conf. on Robotics and Automation, Seoul, 23-25 Mai 2001:3256-3261

[8] Clavel, R. et al.: A new parallel kinematics able to machine 5 sides of a cube-shaped object: Hita STT, 1st Int. Colloquium, Collaborative Research Centre 562, Braunschweig, 29-30 Mai 2002: 107-118

[9] Neithardt, W.: Methodik zur Simulation und Optimierung von Werkzeugmaschinen in der Konzept- und Entwurfsphase auf Basis der Mehrkörpersimulation. Dissertation, Universität Karlsruhe (TH), 2004

[10] Pohlheim, H.: Evolutionäre Algorithmen. Springer Verlag, Berlin, Heidelberg, New York 2000

Keywords Index

Authors Index